2020

Gait entrainment in coupled oscillator systems: Clarifying the role of energy optimization in human walking

Ryan T. Schroeder
Edith Cowan University

Edith Cowan University

Copyright Warning

Gait entrainment in coupled oscillator systems:

Clarifying the role of energy optimization in human walking

This thesis is presented for the degree of

Doctor of Philosophy

Ryan T. Schroeder

Edith Cowan University

School of Medical and Health Sciences

and

University of Calgary

Graduate Program in Biomedical Engineering

2020

Abstract

Empirical evidence suggests that parameters of human gait (e.g. step frequency, step length) tend to minimize energy expenditure. However, it is unclear if individuals can adapt to dynamic environments in real time, i.e. continuously optimize energy expenditure, and to what extent. Two coupled oscillator systems were used to test the learned interactions of individuals within dynamic environments: (1) experienced farmworkers carrying oscillating loads on a flexible bamboo pole and (2) individuals walking on a treadmill while strapped to a mechatronics oscillator system providing periodic forces to the body. Reductionist trajectory optimization models predicted energy-minimizing gait interactions within the coupled oscillator systems and were compared to experimental data assessed with linear mixed models. On average, pole carriers significantly adjusted step frequency by 3.3% (0.067 Hz, p=0.014) to accommodate the bamboo pole – consistent with model predictions of energy savings. Novice subjects entrained (i.e. synchronized) their step frequency with machine oscillations up to ±10% of preferred step frequency and at amplitudes as low as 5% body weight (or ~33 N). Still, some subjects rarely entrained at all, and many exhibited transient entrainment, i.e. they drifted in and out of step frequencies matching the machine oscillations. Overall, subject entrainment was more robust and consistent with lower frequencies and higher amplitudes (20-30% of body weight). Although no systematic difference was found between the metabolic consumption of subjects during and not during entrainment, the net mechanical work done on subjects by the force oscillations had a strong effect on metabolic output (p<0.0001). Net work was largely determined by the alignment of oscillation forces within the gait cycle. Both the optimization model and subjects aligned force oscillations with their body velocity to increase positive power. All in all, it seems that subjects prefer entrainment with environmental oscillations under certain circumstances. However, entrainment does not appear to be motivated by energetic cost, at least not directly and not as a first priority. It is possible that individuals stabilize interactions with the environment (e.g. entrainment) as a prerequisite for effective feedforward and/or feedback gait control.

Preface

Chapter 2 of this thesis has been published as R. T. Schroeder & J. E. A. Bertram, “Minimally Actuated Walking: Identifying Core Challenges to Economical Legged Locomotion Reveals Novel Solutions”. Frontiers in Robotics and AI, vol. 5, issue 58.

Chapter 3 of this thesis has been published as R. T. Schroeder, J. L. Croft, G. D. Ngo, & J. E. A. Bertram, “Properties of Traditional Bamboo Carrying Poles have Implications for User Interactions”. PLoS ONE, vol. 13, issue 5.

Chapter 4 of this thesis has been published as R. T. Schroeder, J. E. A. Bertram, V. S. Nguyen, V. V. Hac, & J. L. Croft, “Load Carrying with Flexible Bamboo Poles: Optimization of a Coupled Oscillator System”. Journal of Experimental Biology, vol. 222, issue 23.

Acknowledgements

I am incredibly grateful for the help and support I have received over the past several years while completing my PhD degree. Although I could not possibly list the names of every individual who contributed to my experience along the way, I would like to highlight a few who I am particularly thankful to for their efforts.

First, I would like to acknowledge my co-supervisors—Dr. James L. Croft and Dr. John E.A. Bertram—without whom, my successes would not be possible. I cannot thank you enough for your encouragement, your support, and your patience during my growth as a student. To my PhD committee, I am incredibly grateful for the intellectual freedom you have given me to explore new ideas, even when you likely knew that they would fail. It is because of those failures, that I feel I have grown as an academic. Furthermore, you were always there to help guide me back toward the correct path when I wandered too far astray. You have always challenged me to think more deeply about my topic and to expand beyond the confines of my own intellectual limitations. Thank you for all the hard work and time you have contributed to helping me succeed at my goals. To my colleagues and lab mates (there are too many to mention by name!): Thank you for all your help and intriguing conversations that have kept me inspired over the last several years. I have gathered insights from each and everyone of you, and I will always remember you, even if it's from afar one day.

I cannot express how thankful I am to my family for always supporting me throughout all my endeavours. To my parents: you both have always been there for me, and I cannot thank you enough for your perpetual love and support. To my brother: you are truly one of my best friends, and I will always look to you for advice and perspective. To my sister: I appreciate your love and friendship and am so glad to have you in my life. To my family-in-law: thank you so much for welcoming me into your home, only to work hours on end on my degree! Your interest and support in my endeavours is truly endearing. Lastly, to my wife: I cannot begin to properly express my appreciation for your love and support. You have taught me so much, and I have benefited from your years of hard work. I appreciate your patience and thoughtful responses when I ask for your wisdom. You have truly been a guiding star, and I would not have achieved the same heights without you.

Table of Contents

List of Tables

List of Figures

CHAPTER 1

Introduction

1.1 Human Locomotion as an Oscillating System

Human locomotion is fundamentally an oscillatory system. Footfalls mark repeating movement patterns characterized by various gaits (e.g. walking, running, skipping, etc.). For example, during walking, the body rises and falls over a strut-like stance leg as the contralateral leg swings forward to contact the ground at heel strike. In the next step, the pattern repeats itself but with the legs performing opposite actions, until the body is configured at the end of the stride as it was in the beginning of the stride. The time duration of these actions is referred to as the stride time and is composed of two approximately equal periods called step time (e.g. the time period between consecutive left and right heel strikes). The inverse of step time is step frequency, and the distance travelled by the centre of mass during step time is called step length – thus, giving fundamental parameters characterizing the oscillation (i.e. frequency and amplitude). The product of step length and step frequency equals the average forward velocity of the body during locomotion and is intrinsically linked to the primary task goal: transporting the body from some starting point A to some ending point B, in the desired amount of time.

1.2 Optimization of the Locomotion Task

Some have argued that a more useful definition of the task should incorporate optimization of the centre of mass trajectory over the substrate (Croft et al., 2017). However, this poses the question: what is the cost function that humans (and other animals) are attempting to optimize? Energy consumption is one such candidate that has garnered much attention and success in a wide range of studies (particularly with regards to gait) (Donelan et al., 2001; Bertram, 2005; Srinivasan & Ruina, 2006; Hasaneini et al., 2013; Selinger et al., 2015; Darici, 2018; Abram et al., 2019; Selinger et al., 2019; Simha et al., 2019). It is often expressed as the mass-specific cost of transport, or energy consumption per unit body mass per unit distance travelled (Margaria et al., 1963; Taylor, 1970; Tucker, 1970; Alexander, 1976; Strang & Steudel, 1990; Minetti & Alexander, 1997; Cunningham et al., 2010).

Undoubtedly, there are many other candidates that likely contribute to the overall cost function of humans performing gait (e.g. stability, time, accuracy, comfort, avoiding injury, etc.) and the weighting of these terms probably varies depending on the specific task circumstances.[1] Nonetheless, energy consumption appears to provide a reasonable first approximation of the real cost function under a diverse set of circumstances (Donelan et al., 2001; Selinger et al., 2015; Polet et al., 2018; Croft et al., 2019A; Simha et al., 2019). For example, individuals choose very different speed-step-frequency combinations depending on whether they walk on a treadmill (speed constraint), over ground while matching steps to a metronome (step frequency constraint) or on stepping stones placed at set distances (step length constraint) (Bertram & Ruina, 2001). Although all three relationships differ substantially in response to the applied constraint, they intersect near the set of gait parameters subjects choose when no constraints are present (e.g. walking freely over ground), and these parameters coincide with the point of minimum cost of transport (Bertram, 2005). Within the total solution space available (boundaries determined by constraints: e.g. physiological or physical), every combination of parameters has a cost associated with it. If the goal is to minimize cost, then the individual must learn to navigate the relevant parameters until they have successfully converged on the minimum-cost solution. This parameter space is sometimes referred to as a "cost landscape" (Croft et al., 2019B).

It is currently unclear what factors determine how individuals navigate cost landscapes. If the optimization goal is to minimize energy, then one might expect the motor control system to adjust movement patterns based on a sensitivity to oxygen consumption, for example. However, previous studies have shown that individuals do not adjust gait in exchange for increased levels of oxygen concentration fed to them through an air tube (Wong et al., 2017). It is possible that mechanosensors play a role in determining gait adaptations that lead to energy-optimality. In this scenario, mechanical variables such as muscle tension or proprioception could provide quick feedback for the nervous system to incorporate in a feedforward model, whereby energy consumption is only estimated and then fine-tuned later on with additional information more directly indicating metabolic

[1]Energy seems to have a synergistic relationship with other important variables (e.g. if an individual falls from instability, it costs additional energy to pick themselves up and accelerate back to the desired speed)

states. O'Connor and Donelan (2012) suggested a similar gait control based on experiments manipulating visual flow in a virtual environment. In the experiment, subjects responded to a sudden increase in visual flow by adjusting walking speed in the opposite direction of the perturbation. Subjects made these adjustments within a few steps, but then slowly returned to their original preferred speed over time. The authors interpreted their findings as evidence of a rapid, predictive process (i.e. feedforward model) followed by a slower, more subtle process, perhaps using direct information from energy cost (assuming that preferred walking speed occurs at the cost minimum). Other studies have shown evidence of a similar, two-part optimization process (Snaterse et al., 2011; Pagliara et al., 2014).

1.3 Coupled Oscillator Systems

It is possible that fast-response, feedforward models of gait are first developed early in life, when individuals still exhibit high levels of plasticity, and are continuously updated to more accurately represent changes in the body and the environment over time. Thus, when adults are fully grown, these models are likely well-established. It may be difficult to disentangle the development of feedforward models from such a deep-rooted foundation. An alternative is to place individuals in uncertain or unusual environments, which may stimulate new development of feedforward models (i.e. motor learning). Given the oscillatory nature of gait discussed previous, this thesis explores inexperienced and experienced subject interactions within coupled oscillator systems, where the human subject represents one oscillator and the environment, another. Standard gait studies tend to neglect interactions with the environment, perhaps since humans most often interact with static environments in daily life (e.g. a sidewalk, a staircase, etc.). However, human locomotion is not a static system. Experimental protocols that employ dynamic environments as a means for probing human locomotor control may represent a new avenue for research on the topic.

In general, coupled oscillators are dynamic systems that include at least two independent oscillators which have a meaningful interaction with one another. Examples include: two pendulums connected by a spring (Dilão, 2009), the relationship between cardiovascular and respiratory oscillations (Schäfer et al., 1998; Lotrič & Stefanovska, 2000; Stefanovska et al., 2000; Stefanovska, 2007), neurons firing in cortical networks

(Buzsáki & Draguhn, 2004), individuals walking on a swaying pedestrian bridge (Dallard et al., 2001), and many other such systems.

In this thesis, individuals were placed into two complimentary oscillation environments (one passive, one active) to explore rich gait interactions guided by the individuals as part of the coupled oscillator system. The first considers an age-old Asian tradition of carrying heavy loads on flexible bamboo poles (Kram, 1991; Castillo et al., 2014). As the person walks along a path, they bear the pole on a shoulder and the load oscillations provide dynamic reaction forces to the body. Here, the phase and amplitude of the oscillations depend on the frequency of the stimulation (i.e. step frequency). In the second environment, a mechatronics system provides controlled oscillatory force perturbations to the trunks of human subjects in the vertical dimension, as they walk on a treadmill. In this system, frequency, amplitude and phase are all controlled and monitored such that any change in the interaction can be attributed to the individual, and not the machine.

1.4 Entrainment

Entrainment is an important concept relevant to coupled oscillator systems. It refers to a special case interaction where both oscillators operate at a matched frequency. During entrainment, the interaction is generally more stable from one cycle to the next, however variation in amplitude is still possible. When carrying a loaded bamboo pole, entrainment is somewhat given, since the frequency of the forcing function (step frequency) drives motion of the load under most circumstances. Instead, it is important to consider stimulations to the pole-load system at step frequencies relative to the passive system's damped resonant frequency, where load oscillations spike in amplitude and phase is transient. In contrast, the mechatronics oscillator system described in this thesis is controlled to be relatively independent from the subject's oscillations; thus, the ratio of step frequency to motor frequency is an important parameter describing the entrainment condition when it equals one.

When entrainment does not occur in a coupled oscillator system, interactions can become unstable and flux from cycle to cycle. This is true even when the frequency of each oscillator is stable. For example, assume metronomes A and B are set to independent frequencies – e.g. time periods lasting 3 and 2 s, respectively. If both

metronomes begin beating at the exact same moment (in phase, or $\phi = 0^{\circ}$ where ϕ is the phase of B relative to A), then this necessarily means that the following cycle of B will occur at $\phi = 240^{\circ}$ ($\Delta\phi = \frac{2\ s}{3\ s} * \frac{360^{\circ}}{cyc}$). After another cycle, B now occurs at $\phi = 120^{\circ}$ (or 480° from the original reference point), and back to $\phi = 0^{\circ}$ (in phase again). In this simple example, phase is constantly changing in every new cycle, even though both frequencies are independently stable. At the same time, the two different frequencies create an interaction that occurs at a lower frequency; both metronomes pulse in phase after every three cycles of B and after every two cycles of A. The relatively low frequency of the interaction occurs such that its time period is equal to the lowest common multiple of the two time periods: 6 s in the example given. The frequency of the phase interaction is always less than the individual frequencies making up the system but is *equal* to the individual frequencies during entrainment, resulting in stable phase – sometimes referred to as "phase-locking."

Entrainment is not always a binary feature of coupled oscillators. Oscillators often move in and out of entrainment in either predictable or unpredictable ways: for example, audience members clapping in synch with one another (Néda et al., 2000). In some cases, the basin of entrainment (i.e. the region of frequencies where entrainment occurs) can be quite narrow. For example, previous studies used an ankle exoskeleton providing periodic torque pulses to show that a neuro-mechanical oscillator contributes to the locomotor control of healthy human walking (Ahn & Hogan, 2012). The authors reported a narrow basin of entrainment and slow phase-locking (i.e. subjects took a long time before entraining at their preferred phase). These observations were cited as part of the rationale for a weakly attracting nonlinear oscillator in human locomotor control. However, the authors also noted that the magnitude of the perturbation (about 10% of maximum ankle push-off) likely influences both the basin of entrainment as well as the time period before convergence on phase-locking. In this thesis, the basin of entrainment is explored by systematically varying oscillation magnitudes and frequencies, in order to evaluate sensitivity and limits on human entrainment to oscillation environments. Perturbations are applied close to the centre of mass (the trunk) to characterize a more generalized response since different perturbation magnitudes may be relevant to entrainment when applied at different joints (perhaps even after normalization).

1.5 Objective

The objective of this thesis is to test theories of energy optimization in human walking, by utilizing novel oscillation environments to illicit gait adaptations in both naïve and practiced individuals. The following are specific aims of the studies detailed here.

1. Use optimization models to predict energetic cost over a range of interactions with the oscillator systems (i.e. loaded bamboo pole, mechatronics oscillator system) and compare to metabolic expenditure measurements in humans
2. Identify energy-minimizing interactions (i.e. hypotheses) predicted by the optimization models and test if humans comply with the predicted interactions
3. Test the sensitivity and limits of humans adopting preferred interactions

1.6 General Approach

In this thesis, simple reductionist trajectory optimization models are used to make testable predictions (i.e. hypotheses) regarding how an individual should interact with an oscillating system in order to minimize energetic cost. Although the specifics of each model depend on the oscillator system relevant to the chapter, generally speaking, each model utilizes a simple point mass to represent the centre of mass of a human subject and two telescoping legs that can actively extend (positive work) or resist compression (negative work) over the course of a step. Various constraints are placed on the model – e.g. maximum allowable leg length, keeping the body above ground, non-slip contacts, etc. Similar bipedal walking models have been utilized in previous studies (Srinivasan & Ruina, 2006; Srinivasan, 2011; Hasaneini et al., 2013; Croft et al., 2019A). In addition, the external oscillator is modeled with a spring-mass-damper mechanism for the bamboo pole, and an oscillating force impulse for the mechatronics system. Realistic constraints are modeled for this system as appropriate – e.g. peak force, power output, voltage capacity, etc. Leg forces are implemented in the model as control variables for the trajectory optimization to modulate with the explicit goal of minimizing work done over the course of a step. Since positive and negative muscle work scale to metabolic energy differently (Margaria, 1976), this fact was implemented in models when it was deemed relevant. Only steady gaits were considered (i.e. positive work must equal negative work over the course of a step). Analyses of the model outputs focused on trends in cost over the parameter space rather than exact numbers. Many of the models presented in this thesis also place a cost on the rate of leg force squared and integrated

over the step. This cost was utilized in order to penalize unrealistically impulsive forces that are not within the force-producing capabilities of biological muscle. Such cost functions have been implemented in various models to similar effect (Kuo, 2001; Rebula & Kuo, 2015; Handford & Srinivasan, 2016). Furthermore, empirical studies have shown that increasing force rate induces a metabolic penalty even when work is kept constant (Doke & Kuo, 2007).

Once the models are formulated, they are optimized over a range of parameters describing various interactions (step frequency, phase, motor oscillation amplitude, etc.). This procedure outputs trends of predicted cost over the selected parameter space, which can then be validated with empirical measurements of human metabolic expenditure via respirometry. Unguided gait adaptation is also tested, in order to observe if subjects prefer the predicted and measured optimal interactions after sufficient exploration with the oscillator system for a given experiment. A positive result implies the internal cost function of human subjects is sensitive to energetic cost consequences of the solution space present in the experiment. Although causality is difficult to prove explicitly, observations of subjects converging upon energy-optimal solutions provides strong evidence that the system has some representation of this cost and is responsive in real time. On the other hand, a negative result implies the internal cost function of human subjects is *not* primarily sensitive to energetic cost, at least in the context of the experiment conducted and over the time scale tested. Either result provides important insight regarding the variables relevant to successful locomotor control.

1.7 Significance

Although there is ample evidence that parameters of natural walking tend to coincide with energy minima of their associated cost landscapes (Bertram & Ruina, 2001; Bertram, 2005; Donelan et al., 2001; Kuo, 2001), much less is known regarding the extent to which humans actively adapt to cost landscapes in real time, in what circumstances this occurs and how the process is coordinated. This thesis explores various aspects of human gait and its control that may contribute to this process. Such insights may inform the design of wearable machines, such as prostheses, exoskeletons, or other ambulation-assistive devices. For example, one challenge to wearable machine design is that individuals exhibit different levels of performance during

adaptation and learning (Selinger et al., 2019). Some researchers have developed real-time optimization protocols designed to adjust parameters suited to individual needs (Zhang et al., 2017).

Another field that may benefit from the studies presented in this thesis is gait rehabilitation. A common goal of rehabilitation work is to return patient function back to a "normal" state, where normal is sometimes defined by what an average healthy human does (Johnstone, 1995). Often this involves a characterization of internal aspects such as joint angles, torques or muscle activation, which may change depending on the particular circumstance at the time they are measured (Prentice et al., 2004; Cikajlo & Matjačić, 2007) However, by considering the fundamental interaction of an individual with their external environment, explicit cost functions may be uncovered that are more principally relevant to the intended task goal (Croft et al., 2017). Given such a goal (e.g. to minimize energy consumption), it is conceivable that achieving "normal" gait may actually be suboptimal, given the constraints placed on the system by the impairment. An alternative is to determine the optimal solution based on constraints of the condition and to train individuals on the appropriate solution (Handford & Srinivasan, 2016).

Mechanical perturbations have the potential for retraining gait in disabled individuals and those rehabilitating from injuries such as stroke (Mansfield et al., 2017). Perturbations can be used to stabilize and destabilize gait (Wu et al., 2017) or prompt dynamic entrainment with an external oscillator (Ahn & Hogan, 2010). However, it is currently unclear what range of parameters (e.g. perturbation magnitude, frequency) form a meaningful basin of entrainment that individuals will respond to. Indeed, this is also unknown for healthy individuals, but could help to inform the extent of locomotor control regimes including nonlinear oscillators such as rhythmic central pattern generators. As such, the current thesis sets out to thoroughly define parameter ranges where entrainment occurs, both in terms of perturbation magnitude (i.e. sensitivity) and frequency (i.e. limits). In this thesis, perturbations are focused at the body level in order to tease apart the fundamental interaction of the individual's mass with the environment (loaded bamboo pole, mechatronics oscillator system, etc.) as a means to test energy optimization during gait.

1.8 Thesis Structure

This thesis discusses healthy human locomotion and its response to dynamic oscillating environments. Chapter 2 introduces some key background on the mechanics of human walking, as well as the motor control system's tendency to exploit energetically optimal conditions available in the cost landscape. Reductionist trajectory optimization models are used to explore bipedal walking gaits with minimal actuation, and the principles learned thereof are applied in the design of a simple exoskeleton actuation strategy which assists motion of the trunk directly, thus neglecting the more common strategy of assisting the legs (Sawicki & Ferris, 2008; Lewis & Ferris, 2011; Mooney et al., 2014; Takahashi et al., 2015; Witte et al., 2017; Zhang et al., 2017). This chapter is published in the special research topic "Advances in Mechatronics and Biomechanics towards Efficient Robot Actuation" for the journal Frontiers in Robotics and AI, Bionics and Biomimetics (Schroeder & Bertram, 2018).

Chapter 3 provides data and analysis on bamboo poles used as tools for load carrying in an oscillating environment. Four poles were purchased from local craftspeople in northern Vietnam and brought back to the laboratory to thoroughly test properties associated with compliance, damping, and resilience. A simple model based on classical beam theory was used to compare the damped resonant frequency of poles during free vibration to those predicted by the model. Ten additional poles used by individuals at a farm site in Vietnam were also tested, however property measurements were coarser due to equipment access and logistics in the field. Pole properties and their subsequent analyses are discussed in the context of conflicting measurements of energy consumption when carrying load on a compliant pole versus a rigid pole. This chapter is published in the journal PLoS ONE (Schroeder et al., 2018).

Chapter 4 follows up on Chapter 3 with data from individuals with years of experience carrying loads on compliant bamboo poles, where the interaction between the loaded pole and the person is treated as a coupled oscillator system. A trajectory optimization model is used to predict the energetic cost of carrying a load on a compliant pole versus a rigid pole, over a range of step frequencies and spring constants in order to explore the effect of these variables on cost. The local cost landscape is then simulated for individual subjects in order to predict changes in step frequency as a means of reducing the predicted cost. These predictions are then compared to the actual adjustments made

by subjects, when switching from rigid to compliant bamboo poles during experiment trials. This chapter is published in the Journal of Experimental Biology (Schroeder et al., 2019).

In Chapter 5, a machine oscillator system is used to provide sinusoidal force profiles to individuals walking on a treadmill in a body harness. Three experiments are performed. In Experiment 1, constant oscillation amplitude and frequency are prescribed while the subject freely adapts for five minutes. In the next five minutes, the subject is constrained to walk with a metronome while oscillation forces continue. The metabolic cost of each phase of the experiment is compared and kinetics and kinematics during entrainment are evaluated to characterize the interaction strategy preferred by subjects. In Experiment 2, forces are slowly ramped up from zero to 30% body weight amplitude but at a frequency displaced from the subject's preferred step frequency. The amplitude at which individuals first begin to match their frequency to that of the motors is measured, as this marks the subject's sensitivity to entrainment in the experiment. Experiment 3 begins with the motors operating at a frequency matching that of the subject's preferred step frequency, so as to begin with entrainment. Then, the motor frequency slowly drifts away from preferred (either higher or lower) and then drifts back to the initial condition. The frequency where individuals first reject entrainment is a measure of the subject's limit to entrainment in the experiment. Asymmetries in the subjects' capacity to entrain at relatively low and high frequencies are discussed.

Chapter 6 provides a final discussion about the role of energy minimization in individuals adapting to dynamic environments. Limitations and future directions are discussed, as well as alternate hypotheses that may help to explain some of the data presented in this thesis.

In all chapters of this thesis, I conducted the following: development of all mechanical systems (oscillating backpack, oscillating harness system, etc.), design of experiments (partial contribution of experimental design in Ch. 2 and Ch. 3), all data analyses, all mathematical derivation, development of all models (e.g. trajectory optimization, etc.), majority of composition of manuscript first drafts, and editing of all manuscripts.

Chapters 2-5 were written as standalone publications (Chapters 2-4 currently published, Chapter 5 to be published). As such, there is some overlap between content in the

background, methodology and discussion sections of each chapter. Additional relevant information has been added to the Appendix of this thesis for the reader's benefit.

CHAPTER 2

Literature Review and Trajectory Optimization Models

2.1 Introduction

The movement patterns of humans and other animals have been described in remarkable detail (Bregler et al., 2004; Winter, 2009). However, why any given movement pattern is used, and not some other, is currently not thoroughly understood. Some of the machinery of biological systems (aspects of their morphology and internal organization) is inherited (involving inevitable evolutionary inertia). As a result, it becomes a challenge to distinguish true adaptive design modifications that improve locomotory capability from adaptations that simply accommodate functionally neutral, or even detrimental, anachronistic features. This makes it very difficult to interpret the actions used in locomotion, regardless of the technical detail in which it is analyzed. It would be beneficial to put the actions observed in locomotion in the context of what they accomplish and determine the advantages and limitations a particular strategy provides to the motor control system.

In this paper we describe our understanding of some key aspects regarding the dynamics of legged locomotion. This understanding has emerged largely from synthesizing the works of groups attempting to construct artificial walking machines. One advantage of trying to generate an original walking machine, rather than mimicking how humans or animals already move, is that it naturally identifies specific challenges and obstructions faced in legged locomotion without the biased expectations of an existing system. Identification of the challenges to be solved is one of the first steps in the design process and the discovery of new and different potential solutions.

There are two parts to this contribution. In the first part our intention is to describe an emerging perspective on legged locomotion dynamics. We use the context of human walking as a familiar example in which these ideas can be evaluated. The objective is to demonstrate how this perspective can aid in interpreting, and not just describing, observed movement strategies. In the second part of the contribution we explore the potential of simply actuated walking models to see how the identified challenges can be met most efficiently. Finally, we discuss the application of concepts on minimal actuation

as an external environment (i.e. exoskeleton) for human locomotion by applying a theoretical oscillating impulse acting at the torso of a walking human.

In this contribution we discuss two hypotheses: (I) the action of the legs in human walking optimizes (or nearly optimizes) the interaction of the body mass with the external environment, consequently specific movement strategies are selected based on taking advantage of energy saving opportunities while mitigating costlier alternatives; (II) external actuation applied directly to the centre of mass (as opposed to at specific joints or in tandem with muscle groups along the body) can reduce the optimized leg work required in a reductionist bipedal optimal control model during walking. We advocate for a reductionist approach in our modelling in order to more clearly isolate features that contribute to effective actuation and control strategies. The proposal is that details of within leg function and other such physiology-based features are secondary considerations relative to the more fundamental interaction between the body mass and its external environment that defines the task of locomotion.

2.2 Part I: Alternate Perspectives on the Task of Locomotion

One conventional definition of the task of locomotion might describe specific features observed in real-world examples (e.g. human walking can be distinguished from running because the latter has a non-contact phase during the stride cycle). However, in this case the solution to the problem is an observed feature without a clear definition of the problem being solved, so this approach mixes the task with the solutions implemented to accomplish the task. As such, it is nearly impossible to separate these two aspects of function, and this confuses the context of the observations and muddles our attempts to find and evaluate explanatory constructs.

Another common approach is to consider that locomotion simply seeks to transport the body from one location to another. However, this definition—fundamental though it may be—does not provide any real insight into how such a task should be managed. Indeed, one could imagine an infinite number of solutions to this formulation of the problem. In order to deal with this issue, we have recently proposed a reformulation of the fundamental task of legged locomotion (Croft et al., 2017). Briefly, any form of locomotion ultimately requires an interaction between the organism (more specifically, its mass) with its external environment. For example, steady level flight requires navigation of the body through the low-density fluid of our atmosphere, while simultaneously

balancing forces of lift and gravity, as well as thrust and drag. Given this fundamental task, there are a number of mechanisms potentially available to manage the body mass-environment interaction – fixed, rotary or flapping wings that can be powered by combustion engines, electric motors or muscles. In a similar manner, we contend that the fundamental task of legged locomotion should be considered the optimal dynamic interaction of the system mass with the external environment (e.g. in terrestrial locomotion, this is typically the substrate, gravitational force, etc.). An optimal (or near optimal) interaction allows for effective travel and must meet overarching goals determined by the priorities of the system (e.g. travelling some distance in a given amount of time, etc.) (Srinivasan & Ruina, 2006).

Similar to flight, terrestrial locomotion has its own set of mechanisms that constitute the locomotory apparatus, all of which can be used to mediate the mass-environment interaction. The available mechanisms are composed of the machinery of the system (supporting tissues and actuators, whether organic or artificial) and the control regime implemented on the machinery (Fig. 2.1). Still, the phrase optimal dynamic interaction remains ill-defined. In the following, we describe the role of energy minimization and analyze some basics of the human walking system while drawing on this perspective.

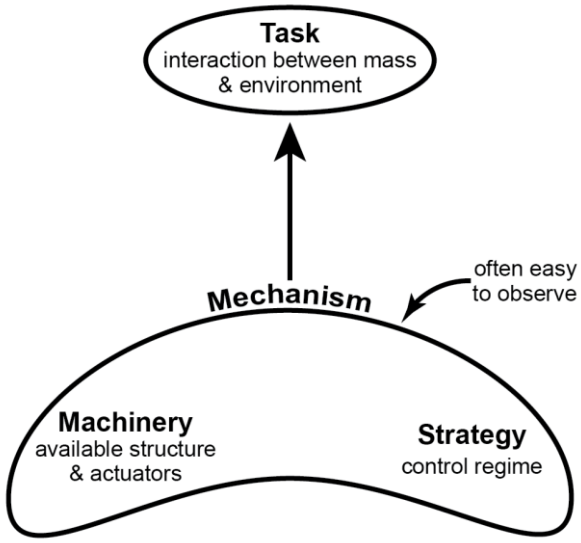

Figure 2.1. A diagram of the contextual hierarchy of locomotion

The task involves the fundamental optimal dynamic interaction of the body mass of the individual with the external environment through which they move. The task fulfills the goal of transportation

as specified (distance, direction, speed, etc.), and one of the defining features in biological systems appears to be a drive towards energetic minimization. Mechanism(s) of locomotion (e.g. leg actuation, generation of joint torques, adjustment of leg stiffness, etc.) manage the task. The mechanisms available are constructed from the machinery (physical structures/tissues such as motors/muscles/skeleton) and the control strategy implemented to the machinery. Mechanisms tend to attract the attention of observers since the kinematics of the limbs are often readily visible, but the implementation of those mechanisms are only understood in the context of the fundamental task they accomplish.

2.2.1 The energetic basis for gait parameter selection

In natural human walking there is a standard, repeatable relationship between overground speed and stride frequency (Grieve & Gear, 1966; Bonnard and Pailhous, 1993). In fact, this relationship is so standard that it is possible to determine the bounds of normal walking and use these to define abnormal locomotion (Schwartz et al., 2008; Lythgo et al., 2011; Dixon et al., 2014). A different, but equally consistent relationship exists for human running (Kurz et al. 2005; Perry & Burnfield, 2010; Hein et al., 2012; Floria et al., 2017). However, documenting the gait parameters used in a given circumstance does little to explain why these are the particular movement strategies (nearly) universally selected. Certainly, it is physically possible to walk (or run) with an extremely broad range of speeds, stride lengths or stride frequencies – so why is one set of solutions selected over others?

A hint at the basis for gait parameter selection (in this example, the parameters of interest are speed, step frequency and step length) and the natural constraints that determine the advantages of one strategy over another, can be drawn from the observation that individuals tend to choose a preferred walking speed when unburdened from explicit time constraints (e.g. rushing to catch the light at a crosswalk). Preferred walking speed tends to coincide with the global minimum cost of transport (CoT), or energy per distance traveled (Holt et al., 1995), although this observation continues to be challenged, (Godsiff et al., 2018). The CoT also appears to have an important influence on the selection of gait parameters over a range of walking speeds (Bertram & Ruina, 2001; Bertram, 2005). Since speed (v) is the product of step length (d_s) and step frequency (f_s), it is theoretically possible to manage any speed with an infinite number of step frequency-step length combinations. However, healthy humans tend to employ a generally standard relationship (Kuo, 2001).

As with the selection of preferred speed (and its step frequency-step length combination), the systematic change in these parameters from preferred speed can also

be explained based on CoT energetics. As speed changes, step parameters (d_s and f_s) are chosen to match the minimum solution for speed constraints on the objective function of CoT (Kuo, 2001). Although it may be suggested that speed change is a natural requirement of walking control, this result suggests that the control strategy is treated as a constrained optimization, where the optimization approaches the minimum cost combination available on the CoT surface.

Similarly, because speed is the product of step length and step frequency, it is also possible to demonstrate the constrained optimization response for the other two parameters (d_s, f_s) as well as for speed (v). When either step length or step frequency is constrained, the response of the other two parameters also tends to follow a minimum cost solution, but the solution differs based on the shape of the cost surface (Bertram, 2005). Optimizing the CoT surface as the objective function can explain a striking contrast in the speed-frequency relationship human subjects exhibit while walking with a constrained frequency (following a range of metronome beat frequencies), a constrained step length (walking in registry to a range of spaced floor markers) or a constrained speed (walking on a treadmill for a range of belt speeds) (Fig. 2.2). This result shows that the selection of gait parameters in humans is not stereotyped but is actually quite plastic, and specifics of the gait are chosen (or at least highly influenced by a pressure) to minimize the cost of moving over the substrate. It should be acknowledged that other influences (e.g. obstacles to be avoided at the substrate, slippery surfaces, etc.) certainly play a role in the selection of gait parameters as well, and in fact, there is often an interdependence between other considerations and energy consumption (e.g. avoiding a slippery surface or else recovering from a fall has an energetic cost associated with it; Brandão et al., 2015). Regardless, in addition to human walking, energetic cost has also been shown to have a dominant influence on step width in human walking (Donelan et al., 2001), human running (Gutmann et al., 2006), walking in cats (Bertram et al., 2014) and for direct, acute manipulations of the objective function (the CoT surface; Selinger et al., 2015).

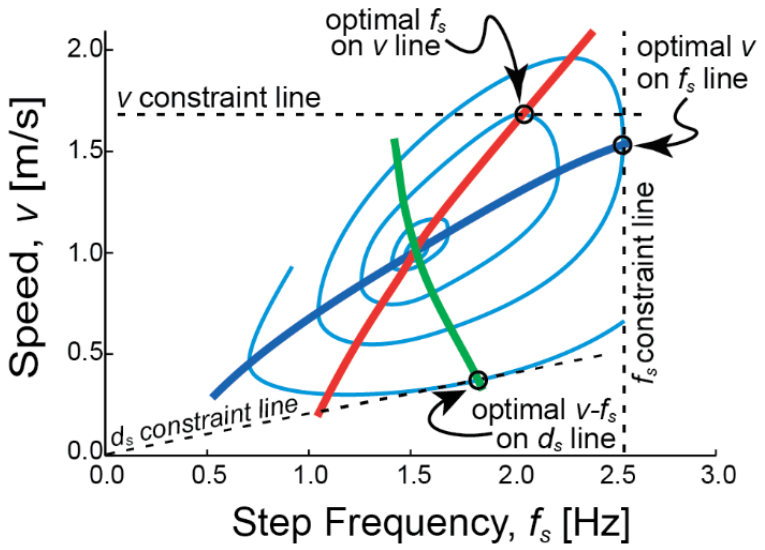

Figure 2.2. Constrained optimization of gait parameters in walking

Light blue contours represent equivalent cost combinations (iso-cost contours), where each contour is energetically less costly than the one residing outside it (minimum cost is central at the point where the red, blue and green lines intersect). For any constraint of speed (v), step frequency (f_s), or step length (d_s) the minimum cost solution features gait parameters where the constraint line is tangent to the cost contour (any other solution lies outside the contour, so is costlier). Constrained v relationship (red) is determined from horizontal tangents and the constrained f_s relationship (blue) is determined from vertical tangents. The constrained d_s relationship (green) is determined from sloped tangents (since $v = d_s f_s$).

2.2.2 Actuator performance

The evidence above indicates that minimizing energy expenditure is a key control factor in humans (and likely in other animals as well). It might be useful to consider *how* energy can be minimized. One option is to seek more efficient actuators. However, even if ideal efficiencies are possible, this approach has a yield limited by the cost of the strategy. However, the strategy itself can be modulated (adjusting the control regime, Fig. 2.1) and such modulation can have a substantial consequence for cost. Consider, for instance, that most high-fidelity legged robots, such as Honda Asimo, have motors that are at least 3-5 times more efficient than mammalian muscle, yet their CoT for walking on legs can be well over 10 times greater than that of humans (Collins et al., 2005). Understanding the subtleties of human walking control may have large payoffs in robotics.

In many engineering circumstances inadequate energy or power capabilities can be addressed with the implementation of more sophisticated actuators and/or larger power

supplies. However, state-of-the-art technology capable of maximizing performance potential is often very expensive. Furthermore, scaling up the power of actuator systems typically comes at a trade-off of increased volume and weight not particularly suitable for the mobility desired in locomotion systems. Thus, artificial design options may be informed by an understanding of how organic systems manage impressive performance despite efficiency limitations. In this, we contend that the goal of energy minimization directs attention to some important factors influencing general performance of legged locomotion systems and the effective movement strategies available to them.

2.2.3 Energy transduction in walking

The predominant conventional approach to analysis of walking gaits considers transduction of energy forms as it flows within the system (e.g. between potential and kinetic energy; Cavagna et al., 1977; Cavagna et al., 2002). However, we argue that a more comprehensive strategy should also track energy flow into and out of the system (Srinivasan & Ruina, 2007). This aspect is important because energy loss must be paid back in the form of mechanical work, and this imparts a metabolic cost on the organism, at least for the case of a steady state gait. Thus, assuming energy loss is undesirable, the manifestation of this loss must indicate either a limitation of the specific gait mechanism used and/or a constraint that restricts the strategy chosen. Understanding how the loss occurs (and why it occurs) allows for clear distinction of various strategies available to manage the interaction with the substrate. How does energy move through a legged walking system?

Walking is commonly described based on variations of an inverted pendulum model where potential (PE) and kinetic energy (KE) fluctuations are largely out of phase during the single stance portion of the stride. During this time, the centre of mass (CoM) rises to a maximum (PE increases as KE decreases) and then begins to fall (PE decreases as KE increases), and this passive redirection is largely managed by the acceleration of gravity. Direct exchange of PE and KE during single stance implies a near constant total mechanical energy and minimal energetic losses from the system (i.e. single stance represents a low-cost portion of the gait cycle; Fig. 2.3). Typically, the inverted pendulum model only considers the stance phase described, and as such, energy losses from the system are often neglected, even though they do occur in real-world locomotion.

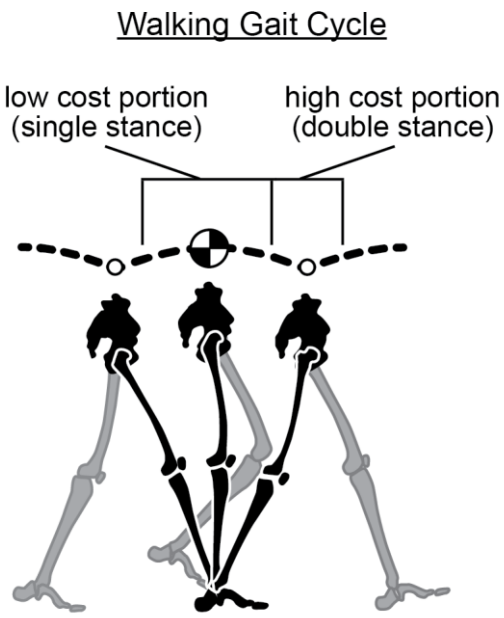

Figure 2.3. The walking gait cycle

The walking stride involves a low energetic cost portion where gravity redirects the centre of mass from upward to downward (a passive transition) – this occurs during single stance in the inverted pendulum phase of walking. The stride also involves a high cost portion where the centre of mass is redirected from downward to upward (active). This is costly because it must be mediated by action of the legs. Note vertical fluctuations in the trajectory are slightly exaggerated for clarity.

Specifically, redirection of the CoM (from down to up) incurs a cost that must be mediated by the action of the legs (Srinivasan & Ruina, 2007). This occurs during double stance in walking when the CoM reaches its lowest point in the gait cycle. Since this vertical redirection is largely active, it requires a high energetic cost (relative to the rest of the gait cycle; Fig. 2.3), which manifests as a loss of energy that must be repaid through leg work (to maintain steady state gait). It is informative to look more closely at the mechanisms through which this can occur in walking, and consider strategies implemented to minimize the energetic cost.

2.2.4 Collision dynamics and transition loss

An important, and often overlooked, cause of energy loss originates with collision dynamics. A collision involves an abrupt change in the momentum of a body when it interacts with an impulsive force, and this results in a loss of energy. In terrestrial locomotion the legs contact the substrate and alter the trajectory of the individual's mass. Although in biological systems these interactions may not appear particularly

impulsive in the classical dynamics sense, the trajectory change of the body mass from downward to upward during the step-to-step transition of walking can be viewed in terms of collision events (Kuo, 2002; Kuo et al., 2005; Ruina et al., 2005; Srinivasan & Ruina, 2006; Lee et al., 2013). The organism experiences a loss of kinetic energy as the ground reaction force does mechanical work on the CoM (in addition to the trunk, this also includes body segments with motion relative to the trunk). The energetic consequence on the organism can be quite meaningful and is quantified by the dot product of the ground reaction force (GRF) vector and the CoM velocity vector integrated over the duration of the impulse (Lee et al., 2011). The consequence of this relationship is such that a perpendicular vector orientation results in no work done by the impulse (no energy loss), since cosine of 90° (and 270°) equals zero. However, non-zero mechanical work is done with any other vector geometry.

Although in terrestrial locomotion the limbs act primarily as struts, the inherent compliance of the jointed limb means that force application is not purely impulsive but is instead distributed over the duration of the step. Nevertheless, the basic principles that govern redirection of colliding objects can be applied to the redirection of the CoM during locomotion. This results in an energy loss that forms the basis of legged locomotion costs in gaits such as walking and running. An alternative view is that at least some energy is retained and recovered by elastic structures in the leg. Elastic energy recovery is undoubtedly useful, but it is not essential to gait (Srinivasan & Ruina, 2006). The optimal CoM path appears to be identical whether the supporting legs have elasticity or not (Ruina et al., 2005). In reality, it is likely that collision mitigation and elastic energy recovery occur – with both being complimentary (Bertram & Hasaneini, 2013).

2.2.5 Minimizing energy loss at the step-to-step transition

The reader may recall that the high cost portion of walking occurs when the CoM is redirected from moving downward to upward at the step-to-step transition during double stance (Fig. 2.3) and forward momentum is maintained over the stride cycle. Since there are two legs contacting the substrate over the transition, various strategies exist to mitigate energy loss if the two limbs work together in a coordinated manner.

In fact, details of the step-to-step transition turn out to be critically important in determining the overall CoT of bipedal walking (Donelan and Kuo, 2002). One option is to use heel contact at the beginning of stance to redirect the CoM, where it is simply vaulted over the strut-like leg (Fig. 2.4A). However, this vaulting action inevitably results in energy loss as the strut redirects the path of the CoM. This loss can be replaced by push-off work from the trailing (former) stance leg, which momentarily maintains ground contact during the transition period.

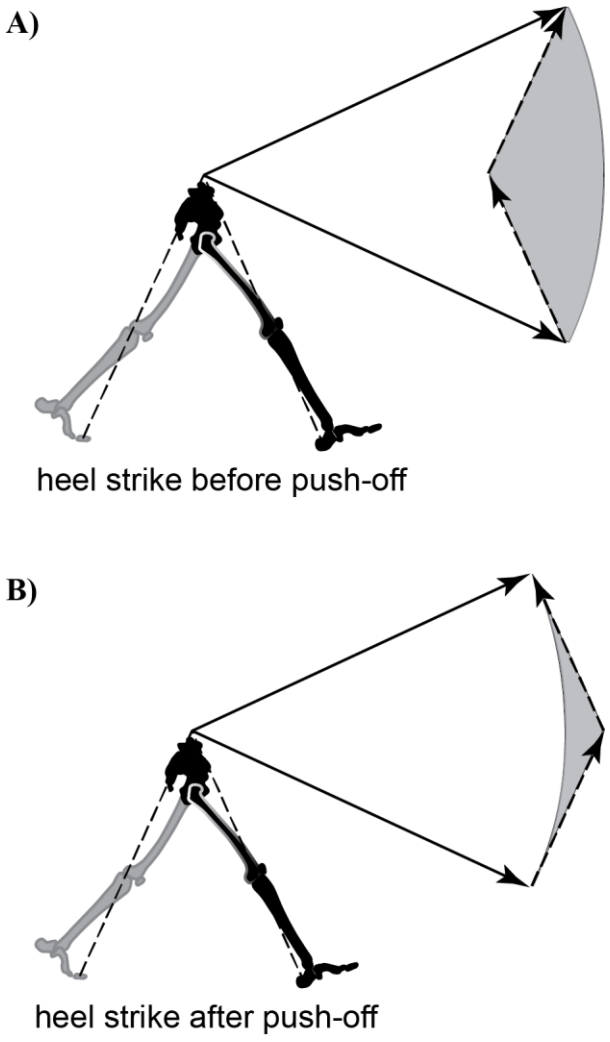

Figure 2.4. Sequencing during the step-to-step transition

Reorientation of the centre of mass velocity vector during the step-to-step transition (double stance) in walking. **A)** Energy inefficient walking – the leading leg makes contact (heel strike) and the velocity vector magnitude decreases along a path parallel to the contact leg (collision loss). The trailing leg then applies a push-off force accelerating the velocity vector back to its

original magnitude. The circular arc connecting the tips of the velocity vectors indicates a change in vector orientation without change in magnitude (constant kinetic energy). The area between the arc and the vector path during the step-to-step transition (shaded grey) is proportional to the work required for the transition. **B)** Energy efficient walking – a preemptive push-off occurs from the trailing leg prior to heel strike of the leading leg. The push-off shifts the velocity vector to a more horizontal orientation making the interaction between the new stance leg and velocity vector much more favorable (less work required in the transition is indicated by the reduced size of the grey shaded area). Note leg and velocity vector angles are exaggerated for clarity.

Although a strategy utilizing heel strike *before* push-off is a viable solution, it is not the most effective strategy for managing the step-to-step transition. Instead, it is highly advantageous to initiate heel strike just *after* push-off from the trailing leg (Donelan et al., 2002A; Kuo, 2002; Kuo et al., 2005). This particular sequencing allows the previous stance limb to begin redirecting the CoM with a forward and upward impulse (commonly referred to as preemptive push-off) before the collision occurs. The preemptive push-off helps to orient the CoM velocity vector more perpendicular relative to the force vector resulting from heel strike (Fig. 2.4B). Ultimately, this allows for substantial reduction of momentum (and energy) loss due to the collision (Ruina et al., 2005).

It is possible to eliminate collision loss at the step-to-step transition with a gait sometimes referred to as Groucho walking. To accomplish this, the substrate is contacted with a relatively straight leg that initially flexes and then extends over stance. This allows the CoM to maintain its vertical position as it passes over the contact point in a straight horizontal path. Although this can eliminate the collision-based loss, it turns out that the leg work required (extending and flexing under the load) is greater than the collision loss it prevents. This has been shown both analytically (Ruina et al., 2005; Gordon et al., 2009) and empirically (Ortega & Farley, 2005; Gordon et al., 2009).

Another feature of an energy effective step-to-step transition involves swing leg retraction. In swing leg retraction the impending next stance leg is accelerated opposite the direction of travel just prior to it contacting the ground (heel strike). Due to mechanical coupling of both legs at the pelvis, rearward acceleration of the leading leg results in a reaction force (at the hip) that accelerates the rest of the body forward, and this aids push-off of the trailing leg. As such, impulses from push-off can be partially down regulated. However, the relative magnitude and timing of stance leg preemptive push-off and swing leg retraction requires coordination to optimize energetic cost (Hasaneini et al., 2015).

In natural human gait, an optimal step-to-step transition strategy comprises a trade-off between collision loss reduction and leg work associated with flexion and extension at the joints. (Bertram & Hasaneini, 2013). It should be emphasized, however, that an effective step-to-step transition in walking requires coordination between both legs in the approach up to and during the transition. This coordination is indicated by the distinctive double hump vertical GRF of human walking. Whereas this pattern is generally interpreted with regard to function of each leg individually, it occurs largely because the second vertical maxima in stance is associated with the critical preemptive push-off while the first indicates the transfer of load to the new stance leg (i.e. heel strike). Each portion of the contact should be functionally interpreted with respect to its role in the transition, rather than as an aspect of the force sequence an individual leg generates over stance (Usherwood, 2016; Bertram, 2016C).

Given some insight into the subtle strategies available to manage the energetic cost of the step-to-step transition in human walking as described above, how can this be applied to alternative designs in legged robots? Passive dynamic walking machines (no actuators nor controllers, as the name implies) are equipped with legs that spontaneously swing in an appropriate manner to stabilize forward progress (McGeer, 1990) while moving down a slightly sloped ramp. With each step, a small amount of PE is converted to KE as the machine falls forward, however this extra energy is soon lost due to collision interactions with the ramp's surface at the step-to-step transition (Garcia et al., 1998). Ultimately, this allows for a near steady state gait pattern that qualitatively looks remarkably like human walking (Bertram, 2016A).

Variations on the passive dynamic walker incorporate simple actuators that can provide small impulses at each leg to allow for level surface walking (Collins et al., 2005). As discussed above, the preemptive push-off impulse of the actuator plays an important role in overcoming energetic losses due to collisions while redirecting the CoM from a downward trajectory to upward.

There is also a secondary role of the active (preemptive) push-off in that helps facilitate the leg's forward swing in order to set up the next step. Ankle plantar flexion just prior to heel strike has been associated with preparing the leg for the swing portion of the step (Winter and Robertson, 1978; Meinders et al., 1998). It is likely that the push-off does indeed fulfill this functional role, but the swing preparation and preemptive, collision

mitigating push-off are not mutually exclusive, so it is likely that both roles are satisfied by this single action (Zelik & Adamczyk, 2016).

2.3 Part II: Simply Actuated Walking Models

In this part of the contribution, we outline various options for reductionist bipedal designs that rely (to varying degrees) on many of the concepts discussed in Part I. We begin with single actuator mechanisms and progress to multi-actuator mechanisms, in order to alleviate some of the restrictive dynamics inherent in simpler designs. Finally, we discuss an application of similar concepts to an exoskeleton strapped to the trunk of a walking human. For most of the models presented, control optimization software is used to determine energetically minimal solutions. These solutions are then analyzed post-hoc in order to isolate important features that either support or violate expectations of what economical locomotion should look like based on an understanding of established theory. This section is organized with specifically chosen models to invoke a discussion about important dynamic restrictions and the consequences of different actuation patterns on the energetics of effective locomotion during bipedal walking. A primary objective of the models is to explore the limit of reducing the number of actuators necessary to allow active bipedal locomotion (at least in the planar case).

2.3.1 Single actuator designs

2.3.1.1 Constant force single actuator inverted pendulum

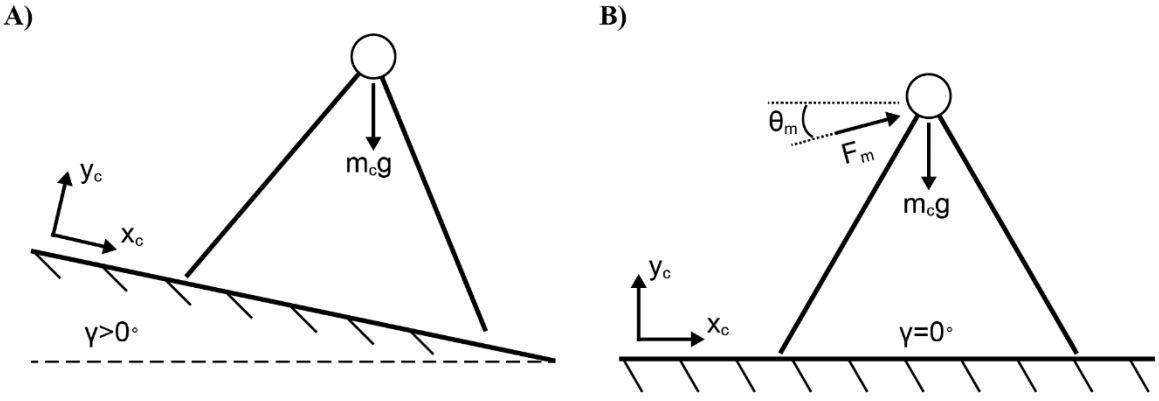

Figure 2.5. Constant force actuator drives a quasi-passive dynamic walker

A) Passive dynamic walker on sloped ground. **B)** Quasi-passive dynamic walker equivalent to A) with a constant force actuator on flat ground.

The placement of an actuator at each leg to power foot extension is one means by which to add work and replace energy lost from collisions and other inefficiencies (Collins et al., 2005). This may be considered a bioinspired design, but it is likely that much of the energetic benefit is achievable merely with a single actuator acting directly at the CoM. In fact, it is possible to mathematically replicate the constant gravitational forces acting on the passive dynamic walker on a sloped surface with a single actuator (constant orientation and force magnitude) acting directly on the CoM for a walker on a level surface (Fig. 2.5). To solve for the actuator orientation and magnitude, the gravitational force (acting on a reference frame of an elevated slope, $\gamma > 0°$) is set equal to a constant actuator force plus a gravitational force (acting on a reference frame of no slope, $\gamma = 0°$). Two equations are formulated for the forces in the horizontal and vertical directions (left side of the equations: gravitational force acting on a sloped surface, right side of the equations: gravitational and actuator forces acting on a flat surface).

$$\text{Horizontal: } m_c g cos(1.5\pi + \gamma) = 0 + F_m \cos(\theta_m) \tag{2.1}$$

$$\text{Vertical: } m_c g sin(1.5\pi + \gamma) = -m_c g + F_m \sin(\theta_m) \tag{2.2}$$

where m_c is the body mass, g is gravitational acceleration (e.g. $9.81\ m\ s^{-2}$), F_m is a constant actuator force, θ_m is the angle of the actuator and γ is the angle of the ground's slope. When equations [1,2] are solved simultaneously, F_m and θ_m are analytically determined.

$$F_m = m_c g \sqrt{2 + 2\sin(1.5\pi + \gamma)} \tag{2.3}$$

$$\theta_m = \frac{\gamma}{2} \tag{2.4}$$

The strategy of powering a walking machine purely with gravitational forces means that no batteries are necessary, and the work done by gravity is essentially free. Furthermore, only a very subtle slope is needed to overcome the energy losses due to collisions if the system is constructed properly. However, the constant-force actuator alternative must do work to mitigate gravitational forces as well as overcome collision losses. Although this actuation strategy may exist as a viable solution, the constant force profile can likely be improved upon. For example, more sophisticated strategies might leverage dynamic force production as a means for reducing the mechanical work done by the actuator.

2.3.1.2 Optimized single actuator (horizontal) inverted pendulum

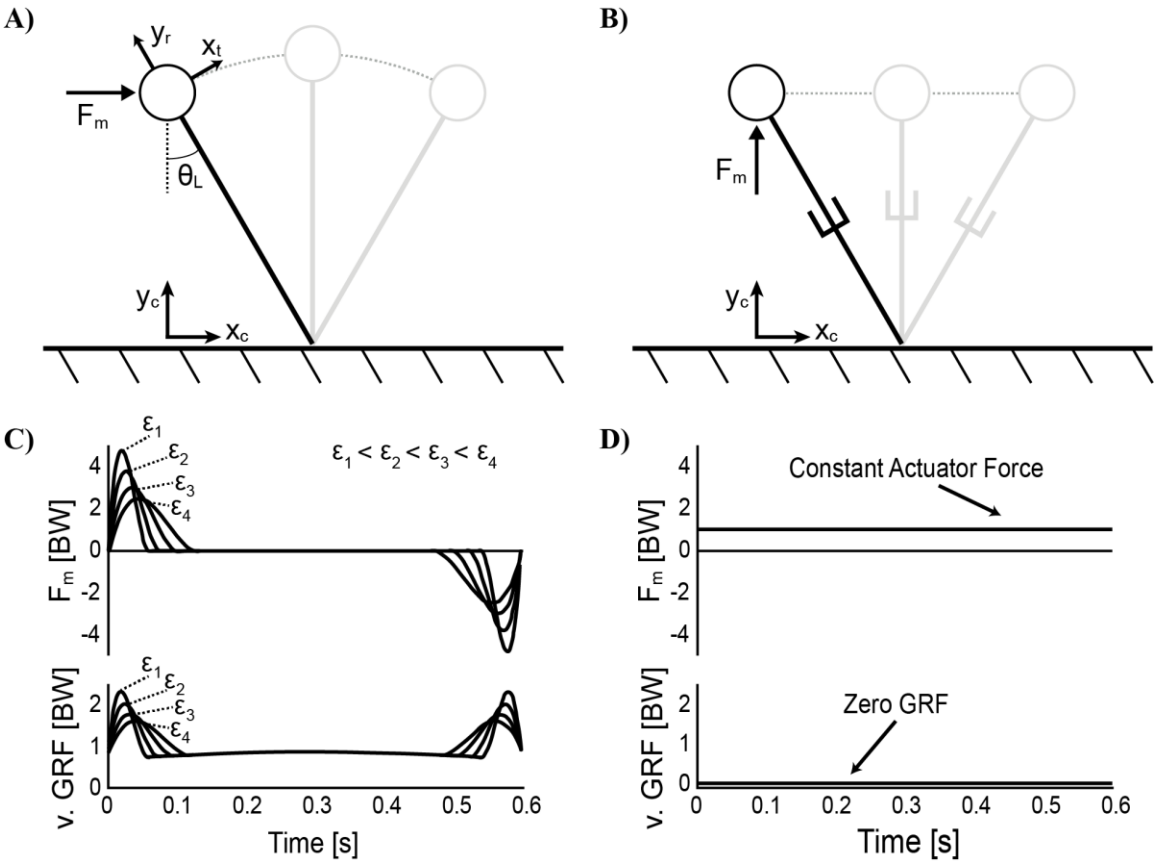

Figure 2.6. Single actuator walking models

A) Inverted pendulum control optimization model with a horizontal actuator and rigid legs. **B)** Groucho walker with a vertical actuator and collapsible legs. **C)** Vertical ground reaction force (v. GRF) and actuator force (F_m) plotted over time, in units of body weights (BW) for the optimal solution of the inverted pendulum model with a horizontal actuator (multiple force rate scaling constants are shown: $\epsilon_1 = 3x10^{-6}$, $\epsilon_2 = 9x10^{-6}$, $\epsilon_3 = 3x10^{-5}$ and $\epsilon_4 = 9x10^{-5}$). **D)** The Groucho walker with a vertical actuator has zero vertical GRF and a constant F_m that defaults to supporting body weight.

Assuming that ideal actuation strategies are unknown a priori, control optimization procedures can be used to determine the actuator force profile that minimizes mechanical work over a step. Although a specific actuator angle ($\theta_m = \frac{\gamma}{2}$) was necessary to replicate the gravitational forces acting on a passive-dynamic walker down a slope, this angle is not required for a non-constant actuator force profile. Instead, a fixed horizontal orientation ($\theta_m = 0°$) was chosen somewhat arbitrarily (Fig. 2.6a), although this configuration does allow for symmetrical force profiles mirrored about mid-stance (i.e. when the CoM is directly above the foot-ground contact). The equation of motion for

a standard inverted pendulum model is expanded to reflect the influence of a fixed horizontal actuator.

$$m_c\ddot{x}_t = m_c g cos(1.5\pi - \theta_L) + F_m \cos(-\theta_L)$$

$$-m_c\ddot{\theta}_L L = m_c g cos(1.5\pi - \theta_L) + F_m \cos(-\theta_L) \quad (2.5)$$

where $\ddot{x}_t$ is the tangential acceleration of the CoM motion and θ_L is the leg angle relative to vertical. Note, the actuator force, F_m, is not constant as in Eq. (2.3), however it is a control variable optimized in the control optimization process. The reaction force of the rigid leg is also shown for the inverted pendulum.

$$R_r = \quad m_c\ddot{y}_r - m_c g sin(1.5\pi - \theta_L) - F_m \sin(-\theta_L)$$

$$R_r = -m_c\dot{\theta}_L^2 L - m_c g sin(1.5\pi - \theta_L) - F_m \sin(-\theta_L) \quad (2.6)$$

where L is a constant leg length used in the model. Gait parameters such as average forward velocity (v), step frequency (f_s) and step length (d_s) are all pre-determined constraints in the model. Specifically, time is constrained from initial point $t_o = 0$ to final point $t_f = T_s$ where $T_s = \frac{d_s}{v}$. Step length was enforced by constraining CoM position at the initial point $x_c = 0$ and at the final point $x_c = d_s$. A biologically realistic step length was chosen (Alexander, 1992) for an average forward velocity of $v = 1\ m\ s^{-1}$.

$$d_s = 1.25\left(\frac{L_{max}^{0.7}}{g^{0.3}}\right) v^{0.6} \quad (2.7)$$

A path constraint was applied to the optimization in order to ensure that only solutions requiring reaction forces greater than or equal to zero (i.e. $R_r \geq 0$) throughout the step were considered (tension leg forces were not allowed since this would require the foot to actively stick to the ground). Endpoint constraints were also applied such that only periodic force profiles and CoM kinematics (i.e. steady state patterns) were considered.

Finally, the objective function, or cost function, was chosen to minimize the summation of a mechanical work-based cost and a force-rate-squared term (scaled by an arbitrarily small number, ϵ_1). The force-rate-squared term was employed in order to avoid extreme impulsive actuator forces (a theoretical, but unrealistic optimum). This allows for

smoother force profiles and a quicker optimization with more reliable results. The cost function is explicitly stated.

$$C = \int_{t_o}^{t_f} \left(\dot{W}_m^+ - \dot{W}_m^- + \epsilon_1 \dot{F}_m^2 \right) dt \tag{2.8}$$

where $\dot{W}_m^+$ is the positive mechanical power of the actuator, $\dot{W}_m^-$ is the negative mechanical power of the actuator and $\dot{F}_m$ is a time-rate of the actuator force. Mechanical power is calculated.

$$\dot{W}_m = \quad F_m \dot{x}_t \cos(-\theta_L) = \dot{W}_m^+ - \dot{W}_m^-$$

$$\dot{W}_m = F_m \dot{\theta}_{\mathrm{L}} \mathrm{L} \cos(-\theta_L) = \dot{W}_m^+ - \dot{W}_m^- \tag{2.9}$$

Orthogonality of $\dot{W}_m^+$ and $\dot{W}_m^-$ was ensured by augmenting the cost function with an additional cost term scaled by a small number: $\epsilon_o \dot{W}_m^+ \dot{W}_m^-$. The cost of this term was always driven to zero in all optimizations, and therefore it did not contribute to the overall cost of the solution. However, its implementation ensures that the actuator can never produce both positive and negative work simultaneously.

A sparse nonlinear optimizer program (SNOPT) (Gill et al., 2005) was used to solve for the optimization problem and the MATLAB (The MathWorks Inc. in Natick, Massachusetts) software GPOPS-II (Patterson & Rao, 2014) was used for problem discretization and setup. A duel part optimization process was employed. In the first part, multiple solutions (n=15) were determined with random initial guesses in order to reduce the likelihood of settling at a local optimum in the cost function. The lowest cost solution of the 15 random initial guesses (i.e. seed) was then put through a perturbation phase where initial guesses were supplied by the seed solution plus random noise scaled to 12.5%, or one eighth, of each variable's overall range. Multiple perturbation solutions (n=15) were determined, and the seed solution was only considered optimal if its cost remained lower than the outcome of all perturbation iterations. In the case that a perturbation iteration resulted in a lower cost solution, it was chosen as the new seed, and an additional round of perturbation iterations was conducted. This process was reiterated until the seed's cost was found to be lower than all perturbation solutions. The perturbation phase was conducted in order to fine tune the optimal solution.

The solution resulting from the optimization is characterized by an actuation strategy similar to what optimal control theorists often refer to as bang-coast-bang (Athans & Falb, 1969). Specifically, near impulsive forces mark the beginning and end of the step, with a quiet period of inactivation toward mid-stance ($t_o = 0$ is associated with the beginning of stance, essentially heel strike). The first bang (impulse), toward the beginning of the step, is positive (i.e. in the direction of travel) and accelerates the body's tangential motion from rest. The second bang, toward the end of the step, is negative (i.e. opposite the direction of travel) and decelerates the body's tangential motion back to rest (Fig. 2.6C). It should be noted that a true bang-coast-bang pattern more commonly exhibits instantaneous discontinuities of state, however this kind of solution is penalized with the force-rate-squared term. Nevertheless, the near impulsive forces (high magnitude, short duration) can still be considered an approximation of a more literal bang-coast-bang pattern. To illustrate the smoothing effect of the force rate cost, the optimization was run with force rate scaling constants over a broad range of values ($\epsilon_1 = 3x10^{-6}$, $\epsilon_2 = 9x10^{-6}$, $\epsilon_3 = 3x10^{-5}$ and $\epsilon_4 = 9x10^{-5}$). As the scaling constant increases, the force magnitudes decrease and are spread out over a longer period of time in order to achieve the impulse required by the solution (Fig. 2.6C).

One can compare the dynamic function of the optimization's near impulsive forces to similar actions in human walking: push-off and heel strike, respectively. In efficient bipedal locomotion, the preemptive push-off earns its name by initiating the impulse just before heel strike. As a result of adding energy into the system first, the CoM velocity vector is redirected upwards (and forwards). This serves to orient the angle relating force and velocity vectors more perpendicularly, and ultimately results in a reduction of collision losses imparted by the heel strike impulse (Fig. 2.4B).

However, the current walker utilizes a reversed strategy with a heel strike-like impulse toward the end of the step to slow to a stop and then a push-off-like impulse toward the beginning of the next step to accelerate back to speed again. This strategy is particularly expensive and re-emphasizes the benefit of optimal sequencing of leg forces during human walking. The reason the walker cannot utilize the alternate beneficial sequencing is because it must satisfy constraints of periodicity. The result is that the CoM is required to begin and end with zero velocity at the stepping transition, as a direct result of the inverted pendulum beginning with a rising arc and ending with a falling arc. As such, a unique continuous periodic solution exists where the CoM begins and ends with zero

velocity (note the option of a collisional impulse at the transition is excluded since it creates a discontinuity in the CoM trajectory).

2.3.1.3 Single actuator Groucho walker

An alternative system which allows for radial deviations in the CoM (e.g. telescopic legs) could potentially achieve continuous periodic gaits. Such a system might rely on a vertically oriented actuator in order to effectively support the weight of the body, since the legs are not actuated and cannot bear load (Fig. 2.6B,D). In this case, it is easy to imagine that a trivial solution would be optimal. Specifically, the solution could utilize a constant force actuator to consistently support body weight along a straight path. Further, because no vertical oscillation is necessary, zero mechanical work is required of the actuator.

It should be noted that the analogous gait in human walking—referred to earlier in Part I as Groucho walking (Bertram et al., 2002)—imparts a much greater cost on the person relative to natural walking (Ortega & Farley, 2005; Gordon et al., 2009). This has a very different energetic consequence compared to that of the isometric force actuator, simply because the actuator is supporting body weight from an ideal orientation underneath the body. Essentially, this solution represents the dynamic equivalent of a wheel, which allows for continuous support even as it rolls in a straight path along the ground. Another example of such a system is the gliding of an ice skater. The legs simply bear the weight of the body but do no work to displace the body.

Perhaps a system utilizing a vertically oriented actuator might take advantage of the rigid strut-like leg in the inverted pendulum and use the actuator to provide impulses at the stepping transition. Although such a walking mechanism is theoretically possible, there is little the actuator could do without requiring a tension force in the leg to keep it grounded, or else launch itself into the air during actuation.

In the following section, we discuss the potential of walking robots that require multiple actuators to accomplish efficient walking gaits.

2.3.2 Multiple-actuator designs

2.3.2.1 Inverted pendulum with telescopic leg actuators

The fully passive inverted pendulum model has been used to characterize the fundamentals of human walking for many decades (Cavagna & Margaria, 1966;

Alexander, 1980). Although it remains a successful model for describing aspects of natural gait, it is limited by its capacity to predict motor responses during atypical walking gaits. Here, the word atypical specifies any such gait where the inverted pendulum is not naturally selected (e.g. Groucho walking, running, skipping, etc.). This is somewhat peculiar given that all forms of typical *and* atypical gaits still utilize the same morphological leg. Thus, an alternative way to think about the inverted pendulum is as a motor control strategy for effective bipedal walking. Specifically, it is the minimal energetic cost associated with the distinctive arced trajectory of the inverted pendulum that allows for efficient bipedal walking. Although focus is generally on the minimal work required for the inverted pendulum during single stance, a bipedal system *does* require an instantaneous impulse to redirect the CoM from downward to upward at the step-to-step transition (assuming a steady, periodic gait), and this impulse *does* impart a quantifiable cost on the system. Of course, in reality, the biological biped does not utilize ideal impulses (instantaneous with infinite magnitude), but rather, it imparts impulse-like forces (high magnitude, relatively short burst duration) to manage CoM redirection. These impulsive forces largely align with the orientation of the legs in the form of a push-off and a heel strike force, which both contribute to the characteristic double-humped profile of the vertical ground reaction force, as discussed in Part I (Fig. 2.7B).

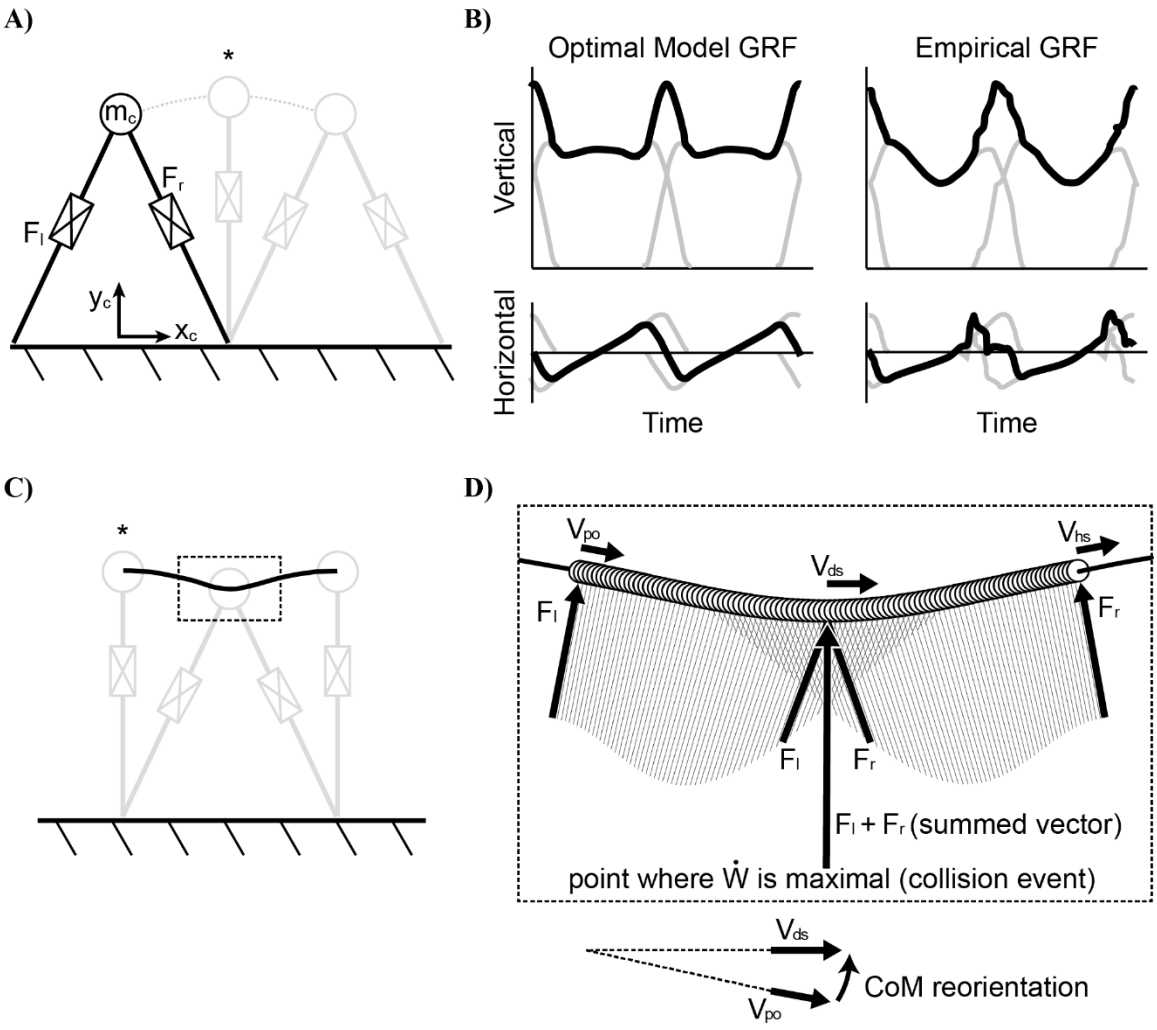

Figure 2.7. Inverted pendulum model with telescopic leg actuators

A) Kinematics of centre of mass (CoM) trajectory and legs shown for double stance, mid-stance (asterisk) and double stance again. **B)** Two consecutive cycles of vertical and horizontal ground reaction forces (GRF) are shown as outputs of the optimization model alongside empirical force plate data of human walking (unfiltered force record, after Bertram, 2016B). Force data from individual legs are shown in grey whilst the total force is shown in black. **C)** Kinematics of CoM trajectory are shown for mid-stance [asterisk notes mid-stance as a common point in the gait cycle between panes A) and C)], double stance and mid-stance again. The dashed box indicates the step-to-step transition region shown in **D)** where the CoM velocity vector is reoriented from the beginning of push-off (V_{po}) through to the middle of double stance (V_{ds}) and to the end of heel strike (V_{hs}). Force vectors of both legs (F_L and F_r) and the CoM are shown for multiple snapshots over the transition (thin lines are sequential vectors over the transition). The point of maximal mechanical power is shown at the middle of double stance where the legs do positive and negative work simultaneously, even though the summed vector appears perpendicular to the CoM velocity vector (misleadingly implies zero work).

To test whether these dynamics are optimal without explicitly constraining them (such as with the inverted pendulum model), two telescopic legs with linear actuators are utilized to provide optimized force profiles that manage the CoM trajectory with minimal mechanical work. A similar model was utilized by Srinivasan & Ruina (2006). Even though the model used the same mechanism (telescopic leg actuators) for all conditions, it spontaneously discovered an optimal walking gait at slow speeds and an optimal running gait at high speeds. It also discovered a hybrid pendular-running gait at intermediate speeds. Although humans do not naturally employ pendular-running locomotion, evidence that various avian species use a similar pattern have since been described (Usherwood, 2010).

Here we employ a similar model, also with two massless telescopic leg actuators and a point mass body (Fig. 2.7A). The equations of motion are detailed.

$$m_c \ddot{x}_c = \sum_{(l,r)} F_i \left(\frac{x_c - x_{fi}}{L_i}\right) \tag{2.10}$$

$$m_c \ddot{y}_c = \sum_{(l,r)} F_i \left(\frac{y_c}{L_i}\right) - m_c g \tag{2.11}$$

where $\ddot{x}_c$ is the horizontal acceleration of the CoM, F_i is the leg actuator force for both left (l) and right (r) legs, x_f is the position of the foot contact (where the force vector originates from; the foot contact is a constant parameter since a non-slip contact is assumed) for both legs and L is the effective leg length of each limb, as formulated below.

$$L = \sqrt{\left(x_c - x_f\right)^2 + {y_c}^2} \tag{2.12}$$

In order to ensure the model does not take advantage of unreasonable leg length values (e.g. $L \gg d_s$), a path constraint was applied to the optimization. The constraint mandates that a leg actuator cannot produce force if the CoM is further away from the foot contact than the maximum leg length indicates.

$$F_{Leg}(L_{max} - L) > 0 \tag{2.13}$$

A control optimization protocol was applied (as described in the single actuator methods) that included a work-based cost and a force-rate-squared cost for each leg actuator

[Eq. (2.8)]. The force-rate-squared term serves to penalize highly impulsive forces in favor of more realistic, smooth leg forces. The mechanical power of the leg actuators ($\dot{W}_{Leg}$) utilized in the cost function is shown as a function of leg force (F_{Leg}) and leg length velocity ($\dot{L}$).

$$\dot{W}_{Leg} = F_{Leg}\dot{L} \tag{2.14}$$

$$\dot{L} = \frac{(x_c - x_f)\dot{x}_c + y_c\dot{y}_c}{L} \tag{2.15}$$

GRF of this model are shown in comparison to empirical data (Fig. 2.7B). Many key features of human walking are reflected in the vertical GRF of the model. For example, the model oscillates between periods of single stance (a single leg provides force) and double stance (both legs provide simultaneous force). The characteristic double-humped profile is also notable in the optimal solution of the model. The hump towards the end of stance occurs due to active extension of the trailing leg and replicates the preemptive push-off found in human walking. Recall, the preemptive push-off does positive work to reorient the CoM velocity vector more perpendicularly to the force vector of the coming collisional impulse at heel strike (Fig. 2.4B, Fig. 2.7C,D). This impulse manifests in the signal as the hump at the beginning of the next stance leg and occurs due to extension forces of the forward leg resisting compression. Similar to human walking, this sequencing helps to maintain momentum with minimal loss at the step-to-step transition. Horizontal GRF are also similar—both showing a deceleration phase towards the beginning of stance and an acceleration phase towards the end of stance. Finally, the point of zero horizontal acceleration occurs approximately at mid-stance (CoM is above the foot contact position).

Overall, the optimal solution of this model takes advantage of the passive dynamics of the inverted pendulum during the majority of single stance by holding a rigid leg (constant radius trajectory means the leg does not extend, and this has no work-based cost since leg velocity is zero). However, the model deviates from this pattern at the step-to-step transition and relies on impulsive forces by both legs simultaneously in order to manage the redirection of the CoM from down to up. The majority of the model's work-based cost is accumulated at this transition, however, it is managed as efficiently as possible, short of using ideal impulses (recall these solutions are penalized by a force-rate-squared cost for more realistic force profiles).

2.3.2.2 Forced coupled oscillator model (no actuator cost)

The inverted pendulum with telescopic leg actuators is arguably the most realistic model for human walking, as compared to other walking mechanisms described in the contribution thus far. This is because previous models considered rigid strut-like legs (as well as, in one case, collapsible legs) and relied on a fixed-orientation actuator to provide force directly to the CoM. However, humans use legs themselves as actuators (non-fixed orientation) to apply force to the body. Still, it may be useful to consider a composite of the two strategies, where a total of three actuators are available to the model: two telescopic legs plus an additional vertical force applied directly to the CoM. Essentially, this allows the model to deconstruct the GRF into distinct signals that are distributed among the different actuators, thereby implying optimal function based on the orientation and magnitude of the resulting force vectors.

Specifically, a coupled oscillator mechanism is used to consider a more specific form of actuator force applied to the CoM. The coupled oscillator mechanism consists of a linear actuator that drives a point mass (m_L) in vertical oscillations off the body (Fig. 2.8A). The influence of these forces is manifested through the reaction force of the actuator on the body CoM (m_c). In this model, the added point mass of the coupled oscillator mechanism can be thought of in two ways: (1) as an additional load that the walking mechanism carries or (2) as a portion of the existing CoM now split into two pieces (in either case, $m_L < m_c$). Although this distinction does affect force magnitudes, we account for this by reporting forces in units of body weight, where $1\ BW = g(m_L + m_c)$. This is analogous to a horse's head bobbing up and down during locomotion. The mass of the head is a portion of the total body weight and the neck muscles are the actuator to help drive (and control) this load, although in this case much of this oscillation is likely passively managed by the complex nuchal ligament (Gellman and Bertram, 2002). Regardless, the oscillation of the head is thought to have an impact on the whole-body locomotion of the animal, as the head typically makes up about 10% body mass.

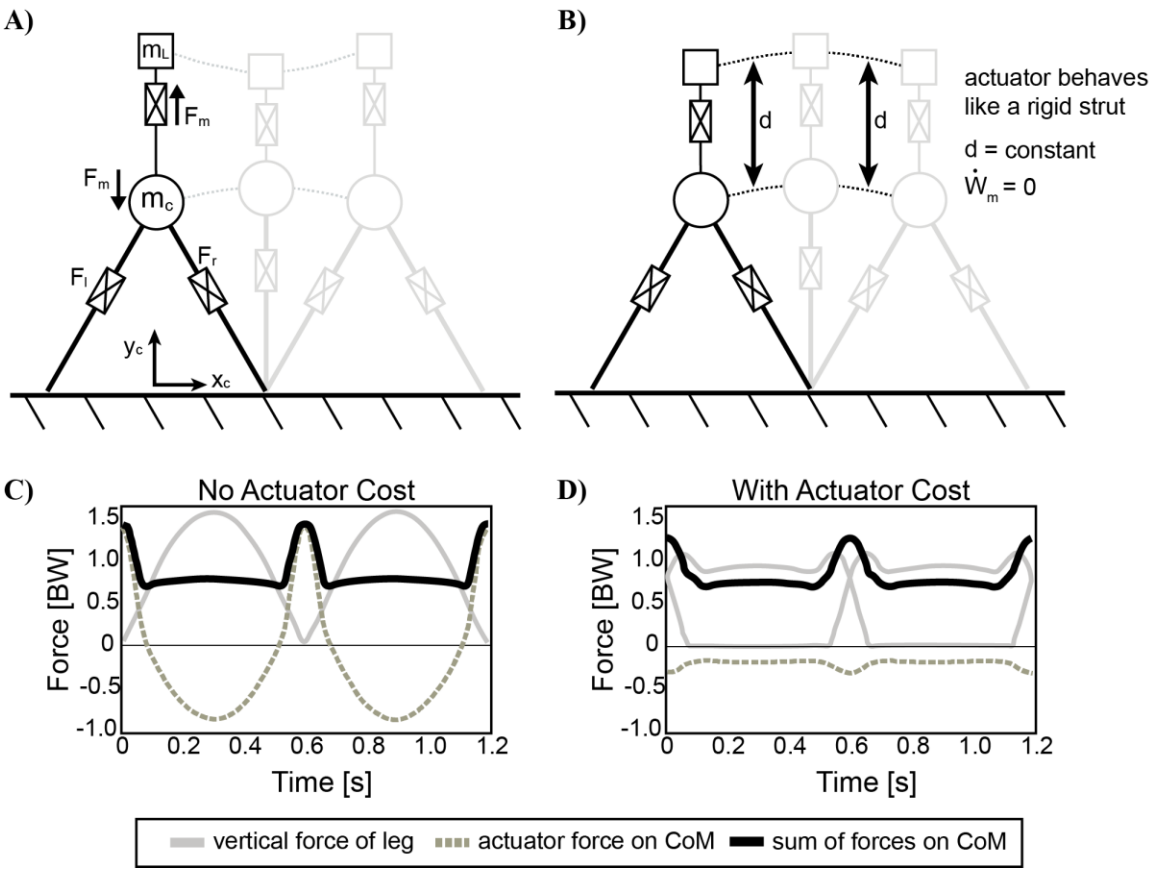

Figure 2.8. Inverted pendulum model with telescopic leg actuators and a coupled oscillator at the body centre of mass

Point mass trajectories of body (m_c) and load (m_L) are shown for the optimal solution where **A)** actuator cost *is not* considered and **B)** actuator cost *is* considered. **C)** Ground reaction forces are shown for the solution when actuator cost *is not* considered and **D)** for when actuator cost *is* considered. The sum of forces on m_c are similar, but its components are distributed over all three actuators.

Additional constraints are modeled such that the load is driven with a continuous periodic motion—the consequence of which is an average actuator force equivalent to the load's weight. With these constraints, the actuator is prohibited from merely performing Groucho patterns (constant vertical force to the CoM) like the single actuator design described previously. This is because the constant reaction force required to bear CoM weight would result in an equal and opposite force accelerating the coupled load in the downward direction for the duration of the step, making a periodic pattern infeasible. Instead, the actuator force must provide equal amounts of positive and negative work to maintain steady state kinematics of the load. Since an average upward force is required for the actuator to maintain full support of the load's weight, a constant loading effect is

felt (in the downward direction) at the CoM of the walker, in addition to the dynamic oscillation force.

The equations of motion of the previous model are expanded to include the forces imparted by the coupled oscillator mechanism.

$$m_t \ddot{x}_c = \sum_{(l,r)} F_i \left(\frac{x_c - x_{fi}}{L_i}\right) \tag{2.16}$$

$$m_c \ddot{y}_c = \sum_{(l,r)} F_i \left(\frac{y_c}{L_i}\right) - F_m - m_c g \tag{2.17}$$

where m_t is the total system mass ($m_c = 0.8m_t$ and $m_L = 0.2m_t$) and F_m is the optimized force of the coupled oscillator actuator. Equations describing motion for the added point mass, m_L, are shown below.

$$m_L \ddot{x}_L = m_L \ddot{x}_c \tag{2.18}$$

$$m_L \ddot{y}_L = F_m - m_L g \tag{2.19}$$

Furthermore, leg length and mechanical power of the leg actuators (as well as the maximum leg length constraint) are implemented per equations [12-15].

First we consider the optimal solution for the model described with no actuator cost (i.e. work done by the coupled oscillator actuator imparts no cost influence on the optimal solution, however work done by the leg actuators is considered) (Fig. 2.8A,C). In this case, the GRF shows a prominent single hump, as opposed to the more typical double-humped profile observed in the model without the coupled oscillator. Essentially, the legs provide isometric, weight-bearing forces (body plus average loading of coupled oscillator) during the stance phase of the gait while the third actuator takes over forces that facilitate mechanical work done to redirect the CoM near the step transition. The summation of the leg actuator and the coupled oscillator force profiles replicates the summed forces of the familiar double-humped pattern, which is responsible for bearing body weight and oscillating the body (inertial force) (Fig. 2.8C). In many ways the solution is unsurprising given that the double-humped profile is already known to be an optimal pattern. The only difference is that the optimization spontaneously seizes on a strategy that delegates the energetically expensive work-based portion of the force profile to the actuator (since there is no cost penalty to do so) and the legs maintain the

inverted pendulum portion of stance since these forces are largely isometric (i.e. constant leg length with zero work done).

2.3.2.3 Including actuator cost

The coupled oscillator model described above requires essentially no work of the telescopic leg actuators. As such, it is a passive gait, from the perspective of the biped since the leg actuators are used mostly as rigid struts. However, it is useful to consider whether there is any utility in the coupled oscillator strategy beyond the supplementation of free mechanical work available via the coupled oscillator actuator. Therefore, the same model is used to consider an optimal solution that seeks to minimize actuator work in the coupled oscillator as well as work done by the legs. Additionally, a force rate penalty is utilized for all three actuators to avoid unrealistic impulsive forces. The equation for actuator work is listed below, and the resulting optimal solution is shown in Figure 2.8B,D.

$$\dot{W}_m = F_m \dot{d} \tag{2.20}$$

$$\dot{d} = \dot{y}_L - \dot{y}_c \tag{2.21}$$

The solution looks quite different from that which neglected the coupled oscillator actuator cost. Instead of the actuator providing dramatic sweeping impulses to the load/CoM system, it acts like a rigid strut. The force oscillations observable in Figure 2.8D facilitate a kinematic trajectory that changes in tandem with the body point mass. As a result, the displacement between the two point masses (d) is constant, and the relative velocity ($\dot{d}$) is zero. Thus, the actuator is not used to perform mechanical work (Fig. 2.8B). Indeed, the cost of this solution is the same as the model with no coupled oscillator (Table 2.1). Ultimately, this result suggests that the coupled oscillator actuator cannot reduce the cost of the overall system, even though it has already been shown capable of reducing leg work. In order to understand why this mechanism cannot reduce the cost overall, the apparent cost of the actuator was manipulated. Specifically, a weighting coefficient, $C_m$was introduced in order to discount the cost of the coupled oscillator actuator's mechanical power in the objective function during optimization.

$$C_m \dot{W}_m = C_m F_m \dot{d} \tag{2.22}$$

$$0 < C_m < 1$$

By implementing a weighting coefficient, the energetic benefit of the actuator's force oscillations is less obscured by its diminished cost, allowing suboptimal solutions to be evaluated. Figure 2.9 shows the full work (i.e. no discount) done by the actuator, as well as the leg work and total work of the legs plus the actuator over a range of weighting coefficients. Force profiles for optimization solutions are also shown (same format as in Fig. 2.8C,D) for the following weighting coefficients: $C_m = 0.05, 0.35, 0.65\ and\ 0.95$. As expected, the force profiles are very similar to the case of no actuator work considered when $C_m = 0.05$. However, the force oscillations become less pronounced at higher C_m values, until they begin to converge on a rigid strut solution when $C_m = 0.95$ (Fig. 2.9).

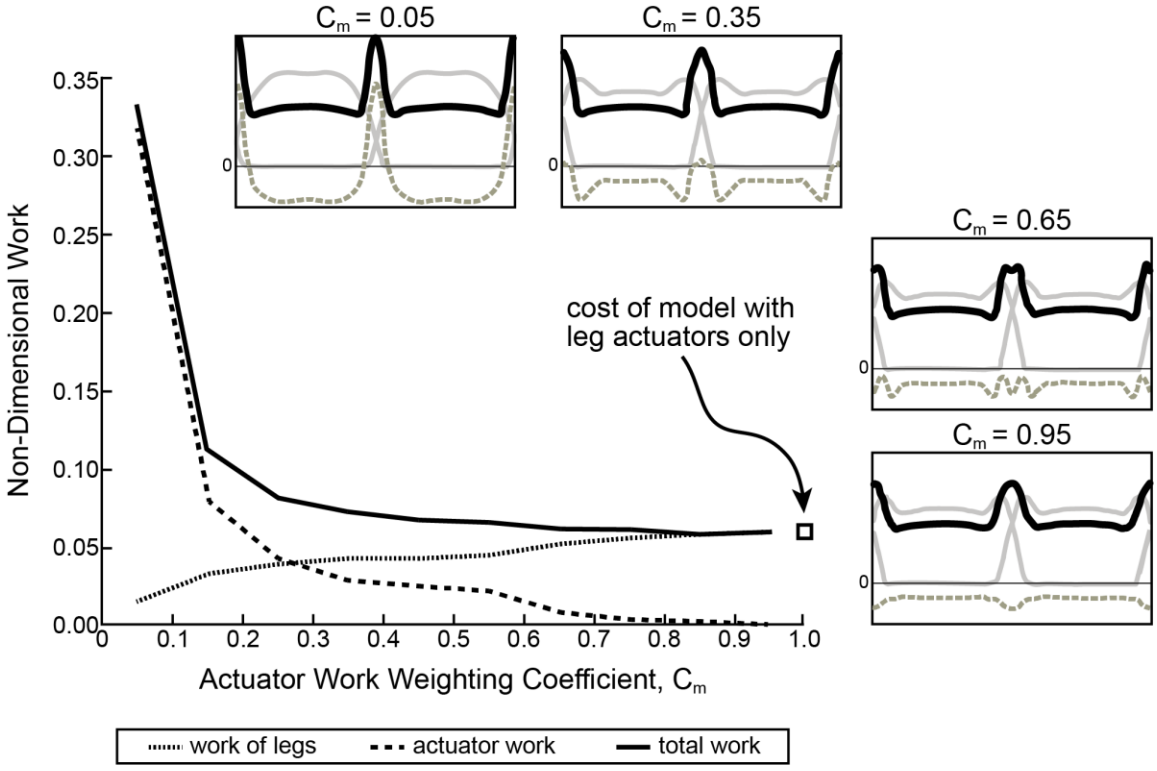

Figure 2.9. Weighted actuator work

Non-dimensional mechanical work is shown for contribution of legs and coupled oscillator actuator, as well as total work over a range of weighting coefficients ($0 < C_m < 1$). This reduces the apparent cost of the actuator and thus, alters the optimization solution. Actuator work contributes most of the work for a low coefficient and almost no work for a high coefficient. The opposite is true of the legs. Ground reaction force profiles are shown for four different weighting coefficients (solid grey lines are single leg forces, dashed grey lines are actuator reaction forces and solid black lines are a summation of both). The total work of the model approaches the work done by the model with no couple oscillator actuator at higher coefficients.

At very high discounts ($C_m = 0.05$) the full actuator work increases drastically, although leg work is greatly reduced. At low discounts ($C_m = 0.95$) and even moderate discounts, total work plateaus to the cost of the model with no coupled oscillator, while actuator work diminishes and the legs take up more and more of the cost. Essentially, the energetic advantage that the coupled oscillator actuator provides to the legs is overshadowed by its full cost, and as a result, the optimal solution uses the actuator as a rigid strut (no work), unless its cost is artificially discounted.

It is perhaps surprising that the addition of a coupled oscillator actuator cannot improve upon the energetics of a bipedal mechanism without it. Indeed, the step-to-step transition is costly in part because the orientation of the legs during double stance means that both positive and negative work must be done simultaneously on the body in order to redirect the CoM trajectory (Donelan et al., 2002A; Donelan et al., 2002B). The non-vertical orientation of the legs (in contrast to the vertical actuator) means that a larger force magnitude—and consequently, more work—is required to alter the body trajectory from downward to upward.

Although it is unclear exactly why work of the actuator is more expensive than the work it saves the legs, there are a few identifiable factors that contribute to its cost. First, in order to offload the legs during their high mechanical power at double stance, the load must be accelerated downward to incite a positive reaction on the body, and this incurs a cost. Next, this action must be paid back with positive acceleration in order to maintain a positive/negative net work balance (this is required to have a steady state, repeatable pattern). Ideally, the positive acceleration (negative reaction force) can be supported by the legs with isometric force during single stance (i.e. no extra energetic cost to the legs), however actuator work is still required to brake the load from its acceleration and then lift it up against gravity. The consequence of these factors and their interactions is such that any use of the actuator (beyond isometric force) costs more than it saves.

Ultimately these results indicate that the economy of a walking machine would not benefit from the implementation of a coupled oscillator mechanism as described. Still, the concept may retain its utility in a system where reducing leg work (rather than work overall) is desirable.

2.3.2.4 Applying realistic actuator constraints

One way to translate the coupled oscillator model into a real-world context is to imagine a human walking with such a mechanism mounted to a body harness. Although this design concept would not benefit the energetics of the whole system (person plus machine), it could still prove a useful strategy for reducing leg work and mechanical power required by the person to walk.

In this example, two linear shaft motors (model: S320T, Nippon Pulse America Inc., Radford, Virginia) are used. The two motors are controlled to act in unison and with a parallel configuration (one mounted anterior to the torso and the other mounted posterior to the torso). The summed effect of the two motors embodies the theoretical actuator allowing known loads with vertical oscillations to apply impulses to the CoM (front and back actuators are used to minimize pitch moments since the harness can only be mounted at the surface of the torso, a small moment arm distance from the true CoM). Similar to the model, reaction forces of the permanent magnets (mounted to the frames) are felt by the user's body through the attaching harness. It is hypothesized that an individual will choose motor patterns based on the principle of energy minimization, in which, the optimal work-based solutions discovered by the optimal control problem reflect the coupled oscillator interaction chosen. Although current literature suggests that humans sometimes adapt gait patterns to accommodate elastic load oscillations to reduce metabolic exertion (Rome et al., 2005; Rome et al., 2006; Ackerman & Seipel, 2014; Castillo et al., 2014), more evidence is needed to show that humans can employ energy minimization strategies consistent with the interactions proposed by the forced coupled oscillator mechanism described. Still, realistic system constraints and considerations can be implemented for the applied problem.

In order to consider the dynamics of the actuators in this applied system, the variable F_m is updated.

$$F_m = K_F i_a - c_d \dot{d} \tag{2.23}$$

where i_a is the armature current, K_F is the motor force constant that relates current and force and c_d is the damping coefficient that characterizes viscous damping of the motor.

Three additional constraints are implemented to simulate a more realistic system: (1) motor/load kinematic oscillation range is limited by stroke; (2) maximum force

capacity is limited by the motors; (3) maximum voltage is limited by a direct current power supply (model: PS16L80, Advanced Motion Controls, Camarillo, California). These constraints are described mathematically.

$$-\frac{S}{2} \leq d \leq \frac{S}{2} \tag{2.24}$$

$$-F_{m,max} \leq F_m \leq F_{m,max} \tag{2.25}$$

$$-V_{PS,rms} \leq V \leq V_{PS,rms} \tag{2.26}$$

where d is the displacement of the load relative to the body point mass ($d = y_L - y_c$), S is the motor stroke, $F_{m,max}$ is the maximum acceleration force, $V_{PS,rms}$ is the root-mean-square voltage available from the power supply and V is the total voltage draw, determined from Kirchhoff's Voltage Law.

$$V = V_{Ri} + V_{emf} + V_{ind}$$

where V_{Ri} is the voltage at the armature resistance, V_{emf} is the voltage due to back electromotive force (emf) and V_{ind} is the voltage due to inductance. By assuming that force is proportional to current and noting Ohm's Law, we derive:

$$V = \frac{R_a}{K_F} F_m + K_{emf}\dot{d} + \frac{L_{ind}}{K_F}\dot{F}_m \tag{2.27}$$

where R_a is the armature resistance, K_{emf} is the motor back emf constant, and L_{ind} is inductance. Note that a motor controller is chosen specifically for this system (model: DMC4123, Galil Motion Control, Inc., Rocklin, California) with sinusoidal amplifiers (D3520), however actuation performance is not further limited since constraints of the other equipment are more restrictive.

When the actuator dynamics and constraints are implemented, the optimization converges on a solution that utilizes a positive pulse of motor reaction force applied to the body (negative force on the load) near the middle of double stance (where maximal leg power is produced; Fig. 2.7D, Fig. 2.10B,C). Essentially, this allows for redirection of the CoM while the load is effectively weightless (i.e. $F_m \approx 0$), from the perspective of the legs. However, this offloading must be paid back in order to maintain a steady state pattern and so a negative reaction soon follows. The sequencing is beneficial overall

since the positive pulse helps to offload the legs during a time of high mechanical power output (near the middle of double stance) and the negative pulse hinders the legs during a time of diminished mechanical power (closer toward single stance). It should also be noted that much of the negative pulse is provided by damping force (and some armature current) since load velocity peaks shortly after the positive pulse (~90° phase delay; Fig. 2.10C).

During single stance, the total reaction force of the motor is near the weight of the load, due mostly to the armature current (although some damping force is present). The effect of this force during single stance does not contribute much to the cost of the solution since mechanical power is largely zero due to the constant leg length (inverted pendulum strategy). However, leg force decreases slightly over stance in an asymmetrical pattern as it provides isometric weight-bearing force that is offloaded slightly by an increasing damping force (Fig. 2.10B,C). This damping occurs due to the body CoM slowing its vertical motion relative to the load as it rises to mid-stance and then begins to fall away from the load. This pattern of reaction force continues into the beginning of push-off and helps to unload the legs slightly during this time. Eventually the positive pulse of reaction force occurs again at the next step and the cycle repeats.

Given that the actuator system provides beneficial offloading to the legs at a time when total motor voltage is not nearly saturated (~67% $V_{PS,rms}$; Fig. 2.10D), it is fair to question why higher force magnitudes are not used. However, the positive pulse must be paid back with negative reaction force (positive force on the load) and the maximum voltage becomes saturated at forces just beyond the weight of the load (Fig. 2.10D), leaving little room for additional oscillation. In fact, the maximum force allowed by the system can be calculated as follows (assuming $\dot{d} = 0$, $\dot{F}_m = 0$):

$$F_m\left(V = V_{PS,rms}\right) = \frac{K_F}{R_a} V_{PS,rms} \tag{2.28}$$

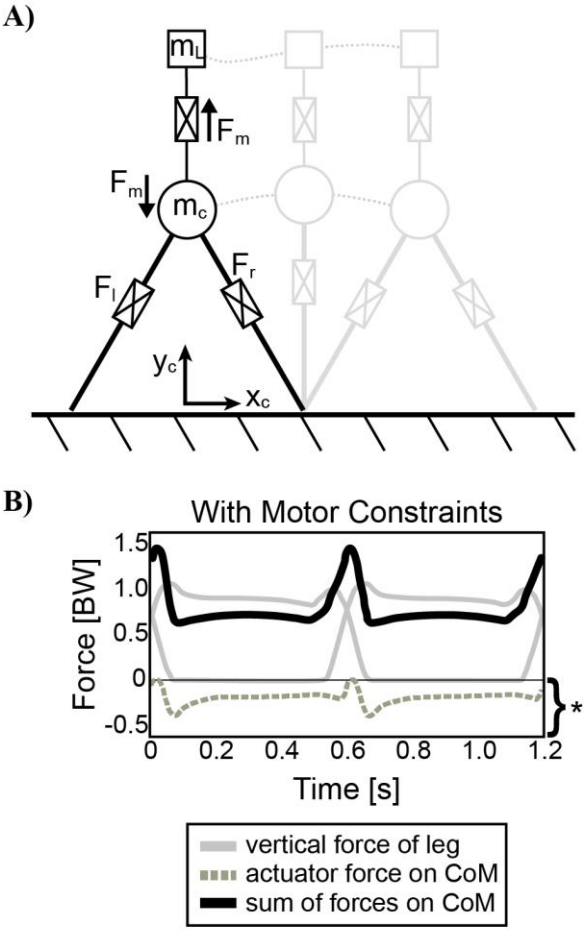
A)
m_L
F_m
F_m
m_c
F_l
F_r
y_c
x_c
B)
With Motor Constraints
Force [BW]
1.5
1.0
0.5
0
-0.5
0
0.2
0.4
0.6
0.8
1.0
1.2
Time [s]
*
vertical force of leg
actuator force on CoM
sum of forces on CoM
C)
Actuator Force on CoM ($-F_m$)
$c_d\dot{d}$ (damping)
$-K_F i_a$ (current)
Force [BW]
0
-0.5
$-F_m$ (sum)
0
0.2
0.4
0.6
0.8
1.0
1.2
Time [s]
*
D)
Motor Voltage
$V/V_{PS,rms}$
1.0
0.5
0
-0.5
voltage saturation
0
0.2
0.4
0.6
0.8
1.0
1.2
Time [s]

Figure 2.10. Oscillating impulse with a "realistic" actuator

Inverted pendulum model with telescopic leg actuators and a coupled oscillator at the body centre of mass. **A)** Point mass trajectories of body (m_c) and (m_L) are shown for the optimal solution where the actuator cost is not considered. However realistic actuator dynamics (damping) and constraints (e.g. stroke, motor force capacity, peak voltage available from power supply) are implemented. **B)** Vertical ground reaction forces are shown for individual legs, the total actuator reaction force on the centre of mass (damping plus force due to armature current) and the summation of forces. Note that the grey dashed line is the same as in **C)** where both terms of actuator reaction force are shown (damping and force due to armature current). Note, the actuator reaction force and its components are scaled by the bracket and asterisk indicated at the bottom right of pane B) **D)** Armature voltage normalized to maximum voltage available from the power supply is shown since this is the only restricting actuator constraint affecting the solution.

With the parameters of the system selected, maximum force production is limited to approximately 115% the weight of the load. This limitation comes from the voltage available from the power supply rather than the force capacity of the motors themselves. In fact, the motor force itself only ever approaches about 33% of the motor force capacity, and as such, this constraint does not limit the solution. Likewise, the maximum stroke range used in the solution is around 22% of that available, and so this constraint also does not limit the solution.

Given that the actuator system is heavily restricted in its ability to pay positive reaction forces back with negative forces beyond the weight of the load, it must rely heavily on the damping force that dominates immediately following the positive pulse. As well, the motor can provide some additional negative force beyond the voltage limitation at this time since the back emf voltage reduces the overall voltage draw.

The strategy just outlined reduces the leg work accumulated over a step, even with the limitations of the actuator constraints. However, the overall system expends more work in total, since the actuator strategy is more expensive than the savings it provides to the legs (Table 2.1). Still, if the design goal of such a device is to offload the leg work done by a human wearing an exoskeleton, then the solution presents this potential.

2.4. Other Considerations

2.4.1 Leg swing dynamics

The reader may have noticed that the complication of leg swing dynamics has not played a formative role in the development of walking models discussed here. Although this is an important aspect of locomotion that ultimately cannot be ignored, we have chosen to focus on the underlying mechanisms that have a dominant influence on the energetics of whole-body trajectory management (Donelan et al., 2002B; Kuo et al., 2005). There is some evidence that swinging the leg consumes approximately 10-33% of metabolic expenditure during bipedal walking (Doke et al., 2005; Gottschall & Kram, 2005; Umberger, 2010), however the dynamics of a pendular leg (or more specifically, a double pendulum) can likely be facilitated with mostly passive dynamics.

For example, a slightly more complex and more thoroughly actuated model replicating human gait (Hasaneini et al., 2013) spontaneously employs a bang-coast-bang strategy to power leg swing in walking. Specifically, a quick burst impulse is used to accelerate the leg forward (first bang), then the leg swings with mostly passive dynamics (coast) and another quick burst impulse is used to decelerate the leg before the next touchdown (second bang). It has previously been recognized that similar activation patterns govern natural leg swing in humans (Mochon & McMahon, 1980; Doke et al., 2005; Doke & Kuo, 2007). Furthermore, the bang-coast-bang strategy has generally been demonstrated an optimal mode of movement control when initial and final conditions require a similar state (e.g. initial velocity equals final velocity) (Srinivasan & Ruina, 2006; Srinivasan, 2010).

The mechanical cost of a bang-coast-bang leg swing is proportional to the leg's rotational velocity squared, given that the impulse must do work to impart kinetic energy ($W = \frac{1}{2} I\omega^2$) for a desired travel of the leg over the duration of swing (Srinivasan, 2010). Ultimately, the rotational velocity of the leg is related to the stride length that the foot must sweep through and the time duration of the swing. Assuming that double stance is relatively short, it then follows that the time duration of swing is approximately equal to step frequency. Thus, step length and step frequency should play an important role in determining the energetic cost of leg swing. Walking is associated with relatively low speeds (i.e. low step frequency and step length), and so it is predicted that the leg swing cost should also be low, as compared to other gaits such as running. In addition, step frequency and step length were constrained to the same values in all models [see Eq.

(2.7)], and as such, there is likely a general increase of the cost surface for solutions presented here. However, the unaccounted cost of leg swing should not change the optimal solutions presented, since a global shift in the cost surface does not change its shape nor the location of the minimum.

It should be noted that this speculation assumes a decoupling between the leg dynamics and the rest of the body. However, it is easy to imagine that oscillations from a coupled oscillator mechanism, for example, may have an influence on the passive nature of the double pendulum leg, and thus, a more complicated energetic interaction. More detailed and thorough models should be developed to answer such questions about the energetics of leg swing and determining interactions.

2.4.2 Mechanical work, metabolic energy and electrical power consumption

All of the models presented here utilize a mechanical work-based cost for optimization. Although it is ultimately the metabolic energy that most likely influences motor control choices regarding movement patterns in humans, a work-based cost was chosen instead. For one, work is easily quantifiable as a mechanical variable, whereas metabolic energy requires the consideration of a more complicated physiological interaction. For example, the metabolic energy associated with isometric contraction (no work) is costlier for force generation than it is for force maintenance (Russ et al., 2002).

A simple approximation of the metabolic energy associated with work done by the muscles is determined by considering the differential efficiency of muscle contraction (25% for concentric contraction and -125% for eccentric contraction). However, given that only steady state gaits were considered by the optimizations, equal amounts of positive and negative work must be done over a step. Thus, the differential conversion from work to metabolic energy should not change any of the optimal results, other than the overall value associated with cost.

Also, since the models are meant to represent theoretical walking mechanisms that can be thought of as either robots or simple abstractions of human bipeds, it is unclear that metabolic cost is even the most appropriate cost to consider. Given that different actuators consume energy in different ways, it seems appropriate to consider mechanical work, since it is a physical requirement that all actuators must consume at least this energy (biological or artificial). An electromagnetic shaft motor was considered

for implementation in the coupled oscillator mechanism, and as such, electrical power could have been used for the optimization. However, this cost scales somewhat differently from simple mechanical work, and so this changes the cost scaling comparisons of the leg actuators relative to the oscillator motor. Consequently, mechanical work was used as a more generally comparable energetic cost.

2.5 Cost Results Summary

In this contribution, we have outlined multiple reductionist walking mechanisms. Although each model is limited by the inherent physics of its individual makeup, they all test the employment of strategies reflecting one or more principles important to efficient bipedal locomotion. Although the single actuator Groucho design allows for zero work to be done over a step, this mechanism represents a trivial solution, which is already epitomized by wheeled mechanisms, and these systems have their own considerations less relevant to truly legged machines (e.g. typically requires some form of infrastructure, such as a road, since the effective radius is invariant). The horizontal actuator inverted pendulum model utilizes a bang-coast-bang approach in order to ensure continuous periodic motion of the CoM, however this model imparts a large cost on the actuator, since it must provide impulses to slow the CoM to a full stop and reaccelerate up to speed with every step. The sequencing of positive and negative work is restricted to operate suboptimally (effective heel strike before push-off) simply because a resting motion is necessary at the step-to-step transition. The energetic cost of this model is unnecessarily excessive relative to more economic designs discussed thereafter ($cost \cong 22.05x10^{-2}$; Table 2.1).

The inverted pendulum with telescopic legs represents a model that can replicate dynamics more similar to human walking. The total cost of the leg actuators is approximately 3.5 times less than the fixed-horizontal actuator model ($cost \cong 6.25x10^{-2}$; Table 2.1), even though it has twice the number of actuators. This result is largely due to the extra degree of freedom given to the CoM so it can deviate from a constant radius profile. This is important because it allows for a continuous periodic gait pattern that maintains momentum (minimizes leg work) at the step-to-step transition rather than bringing the system to rest with every step. Still, the orientation of the legs at this transition (non-vertical) also exists as a limitation to what is possible for energy

minimization, since positive and negative work of each leg must be done simultaneously, and this is somewhat wasteful.

The coupled oscillator mechanism is used to take advantage of inverted pendulum motion during stance and vertical actuation at the step-to-step transition. When the cost of the coupled oscillator actuator is not considered, it completely takes over the expensive portion of the gait required for redirecting the CoM motion from downward to upward, and only uses the legs to bear isometric loads with mostly zero leg deflection during single stance (almost no work in this portion). The cost of the legs is essentially null in this model however the work done by the coupled oscillator actuator is prohibitive ($cost \cong 301.25x10^{-2}$; Table 2.1).

When the cost of the coupled oscillator actuator is considered, the optimization converges on a strategy that uses the actuator for isometric force production only. This is the dynamic equivalent of returning the load mass back to the CoM and exists essentially as a null result. The optimal pattern exists as it does because the cost of using the actuator to perform work is costlier than not using it at all. The resulting cost is equivalent to the model with no coupled oscillator actuator ($cost \cong 6.25x10^{-2}$; Table 2.1).

Finally, the coupled oscillator model is optimized with no actuator cost, but with more realistic system dynamics and constraints deemed potentially restricting from data sheets of commercially available equipment. The resulting optimal pattern utilizes impulsive forces to reduce the weight of the load at costly double stance. It also takes advantage of damping forces to help oppose the relative acceleration of the load over the duration of single stance. This results in a ground reaction force, which is somewhat asymmetrical. The overall cost of the model is approximately 18.9% higher than with no coupled oscillator ($cost \cong 7.43x10^{-2}$; Table 2.1), however leg work is still reduced by about 16.6% ($leg\ work \cong 5.21x10^{-2}$; Table 2.1).

Table 2.1. Cost summary for models

Model Description	Leg Work ($x10^{-2}$)	Actuator Work ($x10^{-2}$)	Total Work ($x10^{-2}$)
Horizontal Force	na	22.05	**22.05**
Telescopic Legs	6.25	na	**6.25**
Telescopic Legs + Coupled Oscillator	0.29	301.25*	**301.54**
Telescopic Legs + Coupled Oscillator	6.25	0	**6.25**
Telescopic Legs + Coupled Oscillator	5.21	2.32**	**7.53**

Non-dimensional work is shown for all relevant actuators (legs, actuator at the centre of mass and total). Work is indicated with not applicable (na) if the model does not include such an actuator. *cost of actuator work is not considered for this optimal solution. **cost of actuator work is not considered for this optimal solution but actuator constraints on stroke, force capacity and voltage supply are implemented.

2.6 Models and their Solutions in Context

We began this contribution by recognizing an alternate definition for the fundamental task of locomotion as the optimal dynamic interaction between the system mass and the external environment as mediated by mechanisms available to the organism (Fig. 2.1). Most exoskeleton designs tend to focus on principles directed at specific mechanisms of gait. For example, a variety of active ankle exoskeletons have been developed in recent years with the strategy of providing mechanical power directly at the ankle joint during push-off, and have achieved successful reductions in metabolic consumption ranging from 6-24% the cost of unassisted walking (Sawicki & Ferris, 2008; Malcolm et al., 2013; Mooney et al., 2014; Zhang et al., 2017). Although this approach clearly has potential for success when the mechanism of focus is well understood in the context of its role in whole-body energetics, a different approach is to consider strategies that influence the interaction between the organism and its environment more directly.

Indeed, we began this discussion by entertaining the notion that the leg actuators in Collins et al.'s variation on the passive dynamic walker (2005) could mostly be replaced with a single actuator at the CoM. The dialogue that followed eventually culminated in the coupled oscillator exoskeleton as a more elaborate manifestation of this approach to control an optimal interaction at the body more directly. Even though the resulting optimal strategy turned out to be similar (apply impulsive forces to the body near push-

off), we have shown that this type of actuation does not necessarily need to be applied at the ankle joint, at least in theory. This is an important insight given that carrying loads (e.g. actuator, transmission, battery, etc.) at the foot can result in a cost increase 4.4 times greater than carrying the same load at the waist and 1.7 times greater at the shank or thigh (Browning et al., 2007). Furthermore, the coupled oscillator strategy does not seek to minimize loading (as an ankle exoskeleton might), but rather *requires* some loading to operate. As such, the weight of the actuator, transmission, battery, etc. actually helps to generate the reaction forces that benefit leg work. In fact, increased loading could potentially minimize the necessary stroke required, assuming that voltage constraints are improved over the power supply currently suggested in the model. Of course, empirical studies are still needed to verify the theoretical potential of a coupled oscillator exoskeleton in practice.

Overall, we view the control optimization models discussed here as a direct exploration of how the interaction (system mass and external environment) can be optimized and to what extent. Although focus is directed at the optimal interaction and not at the mechanism, it is impossible to facilitate the interaction in the absence of a mechanism. As such, we rely on reductionist abstractions of real mechanisms. For example, biological legs with sophisticated musculature and joint spaces are collapsed into simple telescopic actuators that can actively extend. Electrical windings and ferrous shafts mounted to body harnesses are replaced with an extensive actuator driving a point mass load. Although some may view these simplifications as inaccurate depictions that do a disservice to complex systems in real life, the reductionist nature of such mechanisms allows for clearer interpretation of what makes an interaction optimal in the first place (i.e. fewer moving parts).

This is not to say that the details of a mechanism are not important. To the contrary, appropriate tuning of mechanisms (e.g. spring stiffness), for example, can greatly affect the performance of an exoskeleton (Sawicki & Khan, 2016). However, the design process of such devices is well-served by a prior understanding of its effect on energetic exertion at the whole-body level (assuming this is the goal), before focusing on such details as tuning. This is arguably validated by the fact that ankle exoskeletons have likely benefitted from the prior understanding of the importance of push-off on the energetics of human walking.

To some degree, the practice of reductionist actuation modelling may be interpreted as an arbitrary thought experiment. However, we maintain that each variation of the bipedal walker is a new opportunity to gather insight on the fundamental barriers to efficient actuation in locomotion. The results of such practice—if interpreted carefully—can lead to important advances in the perspective that roboticists and biologists hold on the science of animal and machine locomotion.

CHAPTER 3

Mechanical Properties of Bamboo Poles: A Tool for Load Carriage

3.1 Introduction

Human load carriage remains an important part of working life in various cultures around the world, and this has led to the development of diverse carrying strategies. One notable example is the use of flexible bamboo poles in Southeast Asia. These resilient tools are typically placed on the shoulder to facilitate carrying of substantial loads (often as much as body weight or more) as well as awkward or bulky loads for farm work and transportation to the marketplace (Fig. 3.1). This is of particular interest in locomotion research because the flexible pole may influence the metabolic expenditure required to transport loads. However, there is conflicting evidence supporting this hypothesis. Specifically, some researchers have found a slight increase in metabolic cost (+3%) whilst others have found a decrease (-5%) for carrying with a compliant pole (Kram, 1991; Castillo et al., 2014). Although it is not the focus of this paper we highlight these studies to show how material/structural properties of the pole may have an effect on locomotion energetics.

Figure 3.1. Pole carrying technique and example poles

Top: A farm worker carries a bamboo pole in northern Vietnam. The pole is supported at the shoulder with the hand (same side as the supporting shoulder) resting on top of the forward end to steady the system. Growth nodes are also indicated (Bottom Left: poles used in the study; Bottom Right: CT scan of pole C). These nodes are characterized by a thickening of the cross-section from a portion of a hollow tube to a portion of a solid cylinder.

Kram (1991) described a dynamic interaction in which the pole's deflection allows the load to travel in a relatively flat trajectory compared to the carrier's body mass during locomotion, thus reducing the mechanical work (proportionate to the load's oscillation amplitude) required to lift the load with each step. He used polyvinyl chloride (i.e. PVC) pipes as a proxy for bamboo poles to explore whether general flexibility might have this effect on human subjects performing a running gait. Although the relatively low stiffness of the plastic poles (approximately 523 N m^{-1} in Kram's study) reduced peak forces acting on the shoulder, increases in metabolic expenditure (+22% for a 19%-of-body-weight load) were mostly in line with studies showing that metabolic cost increases approximately proportionately to the mass of a load carried with a backpack or waist harness (Griffin et al., 2003; Bastien et al., 2005). In other words, the plastic poles used in Kram's study did not save energy and metabolic cost was similar to the expected cost of carrying the load in a standard backpack, despite differences in stiffness and other influential parameters, such as damping.

In a subsequent study, Castillo et al. (2014) compared the metabolic cost of transport for carrying a total load of 170 N (17.3 kg) using rigid steel poles and bamboo poles (that they fabricated themselves). In contrast to the previous study, the cost was reduced by approximately 5% when using the bamboo pole compared to the steel pole over a defined range of walking step frequencies. The authors performed a basic vibration analysis to show that resonance (i.e. the fundamental oscillation frequency at which the flexible pole vibrates freely) can influence the energetics of locomotion. This is because the magnitude (and phase) of the vibrations—as well as reaction forces felt by the individual—occur as a function of oscillation frequency, and this is largely determined by the step frequency of the user (Kram, 1991; Dallard et al., 2001; Rome et al., 2005; Ackerman & Seipel, 2011B; Castillo et al., 2014; Cavagna & Legramandi, 2015; Joshi & Srinivasan, 2015).

More specifically, Castillo et al. (2014) implied that a carrier should walk with a step frequency slightly higher than the resonant frequency of the pole-load system in order to receive an energetic benefit. At this relative frequency, the pole and load oscillate at a relatively high magnitude while out of phase with the vertical body oscillation of the carrier. Ultimately, it is theorized that this interaction should require less leg work by the carrier, since the summed mass of the system stays relatively flat (the load is low when the body is high and vice versa, where motion cancels when summed). The apparent

contradiction in results of studies by Kram and Castillo et al. may be due to a variety of factors (e.g. walking versus running gaits, pain or discomfort carrying with a steel pole, etc.). However, the type of pole (e.g. material, structure, etc.) and, consequently, its properties can likely have an important influence on the energetics of load carriage.

Potwar et al. (2015) recognized the importance of pole properties in a study that described a design parameter optimization model constraining stiffness, weight of the pole, and strength (in order to mitigate mechanical failure). The explicit intent of this model was to identify a range of pole dimensions minimizing peak forces on the shoulder for both walking and running gaits. Although this theoretical analysis successfully determined optimal design parameters for load carrying, the structural and material properties of authentic bamboo poles (i.e. fashioned by individuals using them daily) have not been rigorously evaluated within the context of locomotion energetics and load carrying.

The purpose of this study was to characterize the design parameters of authentic bamboo poles used in traditional load carrying by Vietnamese farmworkers. Although multiple considerations are likely to influence the fabrication of a carrying pole, two specific design outcomes were evaluated: reduction of both (1) peak forces to the body and (2) energetic expenditure of the carrier. The former was evaluated by comparing pole properties in this study to those determined as optimal by Potwar et al. (2015). The latter was evaluated by comparing resonant frequencies measured in this study to those associated with a reduced metabolic cost of the carrier (Castillo et al., 2014).

To accomplish this analysis, we performed testing in rural northern Vietnam (farm site) as well as in the lab. Conditions at the farm site meant we were only able to make simple evaluations (10 poles). However, four additional poles were fabricated by a local craftsperson at the farm site with local materials, and these were subsequently brought back to the lab for more thorough evaluation. The data from the lab-tested poles (LPs) were used to determine detailed mechanical and structural properties and validate a theoretical model describing dynamic pole behaviors. This model was then used to determine the same set of properties and design parameters—albeit indirectly, through the model's outputs—for the 10 farm-tested poles (FPs).

Specifically, Euler-Bernoulli equations (i.e. classical beam theory) were used to characterize stiffness of a mass-spring-damper system describing load oscillations. The purpose of this model was to characterize a relationship between resonance behaviors and fundamental properties of the bamboo poles in order to assess potential influence on human locomotion. Insights from this study should prove useful to the understanding of load carriage with a flexible apparatus. In particular, the implications of design strategies on reaction forces and energetics are discussed. While many potential benefits have previously been identified for the implementation of such devices, authentic bamboo poles fabricated with traditional techniques have not been evaluated. Design attributes are inferred from empirical and theoretical analysis described further in the following sections.

3.2 Methods

Two experiments (resonance and load-deflection) were performed in order to test relevant mechanical and structural properties. These data were used in a theoretical model describing the relationship of resonance and other dynamic behaviors. Furthermore, computed tomography (CT) scans were used to image the LPs and measure basic geometric parameters associated with cross-sectional profiles along the length of each pole.

The physical properties explored in this study can be grouped into two categories: (1) *base* and (2) *derived*. The *base* group comprises Young's modulus (i.e. E, modulus of elasticity), hysteresis (*hys*), damping ratio (ζ), basic geometric parameters, and second moment of area (I). The *derived* group includes spring constant (k) and damping coefficient (c). A flowchart describing testing and analysis of the two pole groups is shown in Fig. 3.2.

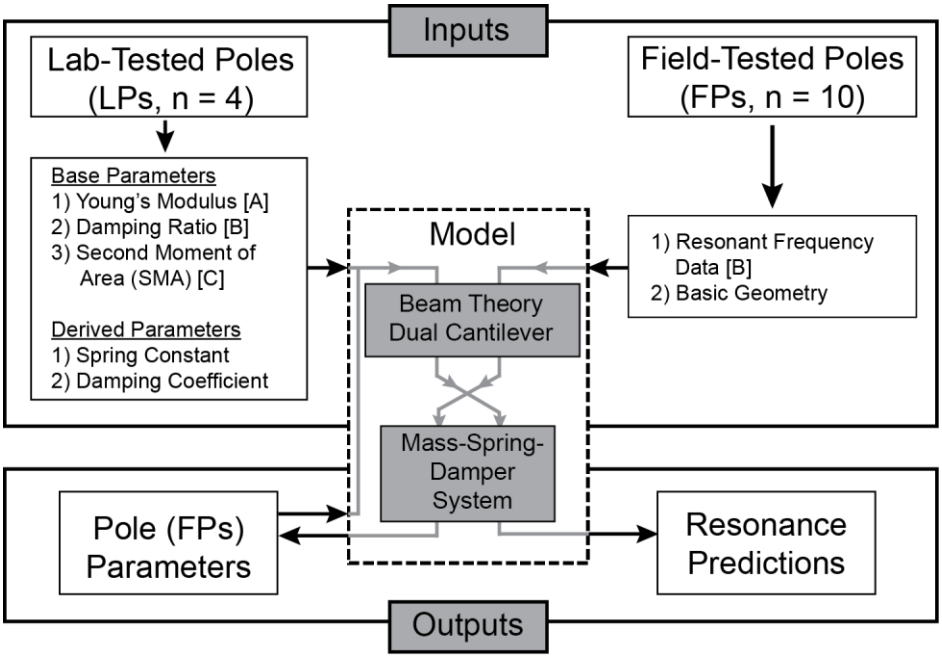

Figure 3.2. Methods flowchart

The flowchart indicates experimental data/results used in the model to quantify pole parameters and resonance predictions for the lab- and field-tested poles. Note: properties labeled with [A], [B], or [C] were determined from the corresponding test indicated at the bottom of the flowchart.

3.2.1 Resonance test

In the first test, resonant frequencies were measured for the poles oscillating during free vibration over a range of loads. To accomplish this, a rigid testing frame was constructed. Two aluminum I-beams (S 3 in X 7.5 in, ASTM A6) were clamped across a steel frame solidly connected to both the floor and ceiling in a reinforced concrete building. Each pole was tightly clamped at a single attachment point at its functional centre, which was determined by balancing the pole on the shoulder (with an arbitrary but equal load at each end of the pole). The functional centre often did not coincide with the geometric centre of the pole due to variance in density as well as an extra moment created by the weight of the carrier's hand laying over the top of the pole, in the natural carrying style used by the indigenous Vietnamese farmworkers (see Fig. 3.1). Because of this imbalance, functional centres tended to lie closer to the front of each pole. The functional centre was chosen in order to more closely replicate pole loading as it would be seen in practice.

When mounted to the frame, two limit stops (wooden pegs) were placed just above the neutral height of each end of the pole (i.e. the height of the pole ends while under no load). This served to ensure that the resonant frequencies only characterized the stiffness of the pole bending in its functional direction - downward. Next, the testing pole was loaded with lead weights (21.82-201.09 N or 2.225-20.505 kg applied equally to each end of the pole, in intervals of 21.82 N or 2.225 kg). Baskets and wire supports (commonly used and purchased in Vietnam) were used to cradle the weights (Fig. 3.1) and added an additional 4.71 N (0.480 kg) to each end. With each loading level, the pole ends were held up by hand until they lightly touched the limit stops (neutral position). Data collection was synchronized to the release of the pole from its neutral position. The loaded pole was allowed to oscillate under free vibration for 30 seconds (this duration was adequate to allow all poles to come to rest under any of the applied loads). Throughout all tests, the pole ends did not touch the limit stops, thus ensuring the correct direction of bending.

Inertial sensors (Xsens MTw, Xsens Technologies, Enschede, The Netherlands) were used to measure the vertical acceleration of the loads during free vibration (one at each end of the pole) and displacement was subsequently calculated by double integration with initial conditions. Mean values and standard deviations of the oscillation frequency were calculated for all poles and under a range of loading. Furthermore, the decay of the displacement signal was determined via:

$$\varphi = \ln\left(\frac{y_i}{y_{i+1}}\right), y_i > y_{i+1} \tag{3.1}$$

where φ is the logarithmic decrement; y_i and y_{i+1} are the magnitudes of two consecutive signal peaks. The logarithmic decrement was noted for each cycle until the signal decayed completely and the median value was chosen to characterize the signal. This median value was then used in Eq. (3.2) to calculate the damping ratio—signal decay relative to a critically damped system.

$$\zeta = \frac{\varphi}{\sqrt{(2\pi)^2+\varphi^2}} \tag{3.2}$$

3.2.2 Load-deflection test

Stiffness and hysteresis properties of the poles were characterized using a load-deflection test. Each pole was fixed to the rigid frame at its functional centre. High contrast markers were placed along the length of each pole (at each growth node and intermediate between each node, see Fig. 3.1). A total of 12-13 points were measured, depending on the number of nodes per pole.

A digital camera (Casio EX-ZR700) was placed perpendicular to the pole at a distance of 10 m (to minimize parallax and lens distortions). Continuous video (30 Hz) recorded pole deflection under a series of loads placed in the baskets attached at each end of the pole. Starting from a zero-load position, successive weights of 21.82 N (2.225 kg) were added to both baskets until a total of 201.09 N (20.505 kg) was applied (nine weights in each basket, overall pole load 402.17 N or 41.010 kg). The pole was allowed to settle to a constant deflection following the addition of each weight. These weights were then removed in succession so the pole's relaxation could be recorded. The images were calibrated, and a marker on the frame was used to verify that support frame deflection was negligible. For all test videos, the support frame's deflection was measured as less than a pixel, and thus, the frame was considered to be ideally fixed and rigid. All marker videos were digitized in MATLAB (The MathWorks Inc., Natick, Massachusetts) using the DLTdv5 software program (Hedrick, 2008).

Displacements were determined by subtracting the initial (i.e. zero-load) positions from the deflection positions for each load. All positions were measured by averaging the data over each ten-second interval (after any basket sway was brought to rest). The standard deviation of each position was also determined for each load increment.

Load-deflection curves were used to depict deflection at the load attachment peg for a full cycle of loading and unloading. The area between the curves was calculated in order to quantify strain energy lost to hysteresis, defined as:

$$hys = \frac{\int_0^{\delta \max} F^+(\delta)d\delta - \int_0^{\delta \max} F^-(\delta)d\delta}{\int_0^{\delta \max} F^+(\delta)d\delta} \tag{3.3}$$

where δ is deflection, F^+ is the curve for loading and F^- is the curve for unloading. The concept of resilience as strain energy returned by the system can also be defined as $res = 1 - hys$.

3.2.3 Model

Simple beam theory was used to determine the Young's modulus of the bamboo. Specifically, two cantilever beams were considered—one for each end of the pole—with a single concentrated load applied at the load attachment peg. Note this model assumes that no net translational or rotational motion should occur about the contact point at the carrier's shoulder. Although this assumption is likely violated in practice, experienced users typically maintain a balance of forces at the shoulder (a technique facilitated by the hand resting on the front end of the pole, see Fig. 3.1) for increased system stability.

In order to assess pole compliance, a deflection surface was mapped over two parameters: distance from the fixed functional centre to each marker along the pole and weight of the load. A least squares non-linear regression was fit to this surface via the following model, derived from simple beam theory for a cantilever beam:

$$\delta = a(3mgx_L x^2 - mgx^3), a = \frac{1}{6EI} \tag{3.4}$$

where δ is the deflection, m is mass of the load, g is gravitational acceleration (9.81 m s^{-1}), x is the distance from the fixed functional centre of the pole to a given marker, x_L is the distance from the fixed functional centre of the pole to the load attachment point, E is the Young's modulus of the bamboo and I is the second moment of area of the pole's cross-section at the marker of interest. From this model, the flexural rigidity ($E*I$) was determined for each pole.

Next, a mass-spring-damper model was used to determine a theoretical relationship for the damped resonant frequency of the system. The equation of motion for this one degree of freedom system is:

$$m\ddot{y} + c\dot{y} + ky = mg \tag{3.5}$$

where y describes motion of the load along a vertical axis (positive is defined downward – the assumed direction of the pole's deflection under load), c is the damping coefficient, equivalent to the expression $2\zeta\omega_n m$ where ω_n is the natural frequency of the oscillating system during free vibration when no damping is present and k is the spring constant describing the relationship between force and deflection. A cantilever beam model was used to show this relationship in Eq. (3.4). Here however, the spring constant influencing the load is only relevant for the case when $x=x_L$. Also, since deflection is

equivalent to the displacement of the load, δ is substituted with the spatial variable *y.* A further adaptation allows for a dynamic point load, *P(y)*, that can change as a function of the load's displacement. Note that in the static form, *P* is simply the weight of the load, as in Eq. (3.4). After these adjustments, the spring constant can be defined as:

$$P = \frac{3EI}{x_L^3} y = ky \tag{3.6}$$

With the mass-spring-damper system described, a damped resonant frequency (ω_{DR}) is calculated from the expression in Eq. (3.7), where $\frac{3EI}{x_L^3}$ is substituted for *k* via Eq. (3.6):

$$\omega_{DR} = \sqrt{1-\zeta^2} * \sqrt{\frac{k}{m}}$$

$$= \sqrt{1-\zeta^2} * \sqrt{\frac{3EI}{mx_L^3}} \tag{3.7}$$

Eq. (3.7) provides a theoretical prediction of the pole-load's damped resonant frequency via a mass-spring-damper system and simple beam theory. This model was used to compare the frequencies measured in the resonance test with the theoretical frequencies predicted by basic pole properties measured directly in the load-deflection test.

3.2.4 CT scans and geometric model

Three-dimensional images of the bamboo LPs were acquired using computed tomography (GE Revolution GSI, General Electric, Milwaukee, WI, USA). Scan parameters were selected (120 kVp, 99 mA, pitch 1:1) to produce images with a voxel size of 0.625 mm x 0.625 mm x 5 mm (width x height x length). Slices of the images were analyzed at 5 mm intervals along the longitudinal axis of each pole. This analysis included a determination of width, height, cross-sectional area, centroid, and second moment of area for each slice. To calculate these parameters, linear interpolation was used to consider the culmination of vertices as a polygon in a given slice. Because the resolution of the scanner is sufficiently high, errors introduced by the linear interpolation are negligible. The calculations for centroid, area, and second moment of area for a polygon are shown in Eq. (3.8-3.10) (Bourke, 1988):

$$C_z = \frac{1}{6A}\sum_{i=0}^{n-1}(z_i + z_{i+1})(z_i y_{i+1} - z_{i+1} y_i)$$

$$C_y = \frac{1}{6A}\sum_{i=0}^{n-1}(y_i + y_{i+1})(z_i y_{i+1} - z_{i+1} y_i)$$

$$C = (C_z, C_y) \tag{3.8}$$

where *C* is the centroid of the shape, *z* and *y* are the horizontal and vertical components of the coordinate system, respectively, *n* is the total number of vertices in a cross-sectional slice and *i* represents a particular vertex being processed by the algorithm. Also, *A* is the area of the defined shape (Bourke, 1988):

$$A = \frac{1}{2}\sum_{i=0}^{n-1}(z_i y_{i+1} - z_{i+1} y_i) \tag{3.9}$$

Further, the second moment of area was determined for the polygon-shaped section of each CT slice using the following algorithm (Bourke, 1988):

$$I_{zz} = \frac{1}{12}\sum_{i=0}^{n-1}\left(y_i^2 + y_i y_{i+1} + y_{i+1}^2\right)(z_i y_{i+1} - z_{i+1} y_i) \tag{3.10}$$

Mean values of the second moment of area were recorded for all LP measurements within the centre region bordered by the nearest growth nodes (bamboo grows to form a hollow stem that is fairly uniform between horizontally thickened nodes). The FPs were measured (by hand) at the functional centre only, and a geometric model was used to approximate the second moment of area along the length of the pole. This model is essentially a horizontal portion of a tubular cross-section (see Fig. 3.3A) and requires two simple parameters as inputs: (i) height (while the pole lays flat) and (ii) width. The outer radius *R* and other important parameters were calculated from the input values. Since the inner radius *r* is not available from this model, it was scaled in direct proportion to the outer radius. This proportionality constant ranged from 0.69 to 0.78 for a variety of poles and a mean value 0.73 was used as an approximation in the model.

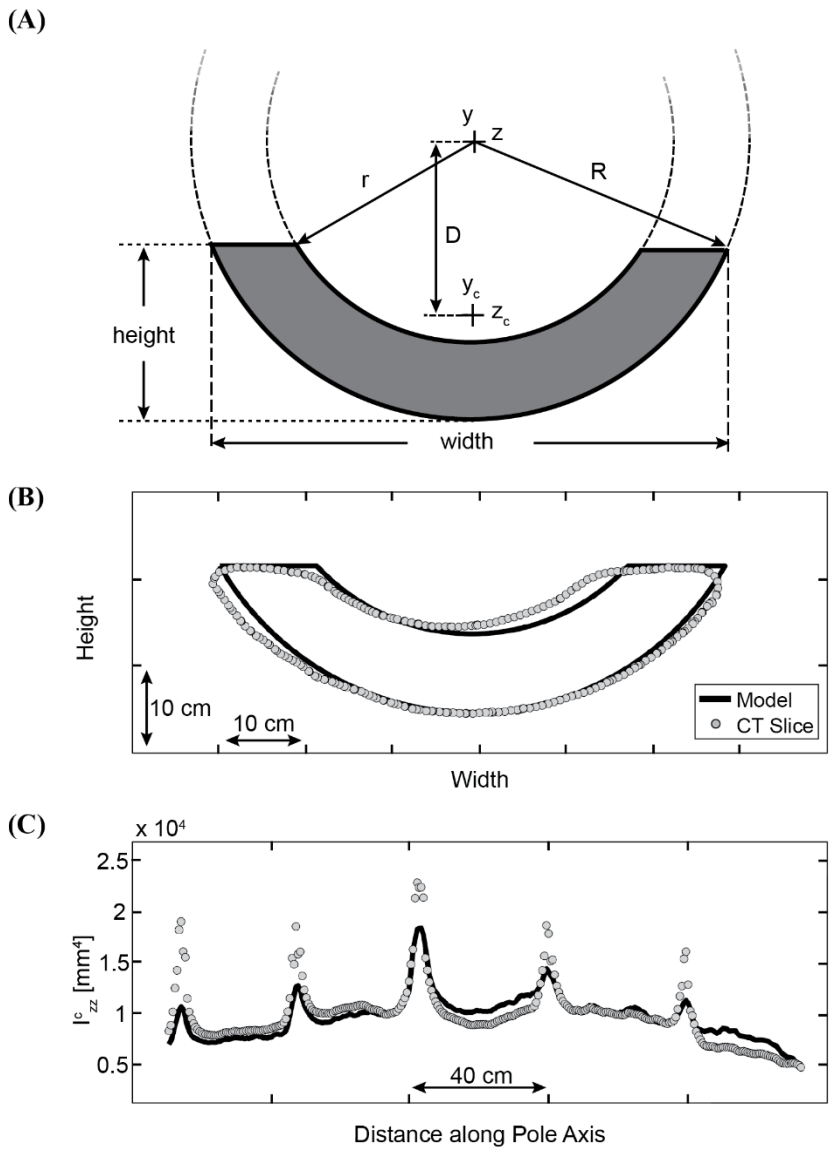

Figure 3.3. Geometric data and model outputs

(A) The pole model geometry is shown in the shaded portion at the bottom of a tubular cross-section. **(B)** An example slice from a CT scan of Pole C (LP) is shown. **(C)** The second moment of area for all slices of the example Pole C) are plotted. Gray circles indicate empirical data and solid black lines are the model's outputs.

The second moment of area of the geometric model (see Fig. 3.3A) was calculated for the FPs by subtracting the inner circle from the outer circle. Horizontal elements were integrated over the vertical range (i.e. height) of the shape relative to a coordinate system located at the centre of the concentric circles.

$$I_{zz} = \int y^2 \, dA = 2\int_{-R}^{-R+h}\left(y^2\sqrt{R^2 - y^2}\right) dy - 2\int_{-R}^{-R+h}\left(y^2\sqrt{r^2 - y^2}\right) dy \tag{3.11}$$

where I_{zz} is the second moment of area about the horizontal axis passing through the centre of the concentric circles, *y* is the vertical coordinate relative to this centre, *R* is the outer radius, *r* is the inner radius, and *h* is the height of the tubular portion. The parallel axis theorem was used to determine the second moment of area relative to the centroid of the cross-sectional shape.

$$I_{zz}^{c} = I_{zz} - AD^2 \tag{3.12}$$

where I_{zz}^{c} is the second moment of area relative to the centre of the cross-sectional shape, *A* is the area of the shape and *D* is the distance from the centre of the concentric circles to the centroid of the tubular portion. Eq. (3.12) was used to calculate the second moment of area for both LPs and FPs.

3.3 Results

3.3.1 Stiffness and hysteresis

The stiffness of a linear system is commonly characterized by the slope of its load-deflection curve where a steeper slope implies a structurally stiffer system. These curves describe the deformation at the load attachment point for a full cycle of loading/unloading and are shown for each of the LPs (see Fig. 3.4). It should be noted that

the different slopes in each pair of curves is primarily due to a functional centre that is biased towards the front of the pole. As a result, the curves representing the front end of each pole (shorter length) tend to be stiffer. The average hysteresis [see Eq. (3.3); Fig. 3.4] and resilience are also listed for each pole. Hysteresis values ranged from 2.9% in Pole F to 9.9% in Pole E. These values indicate relatively modest energy losses due to damping.

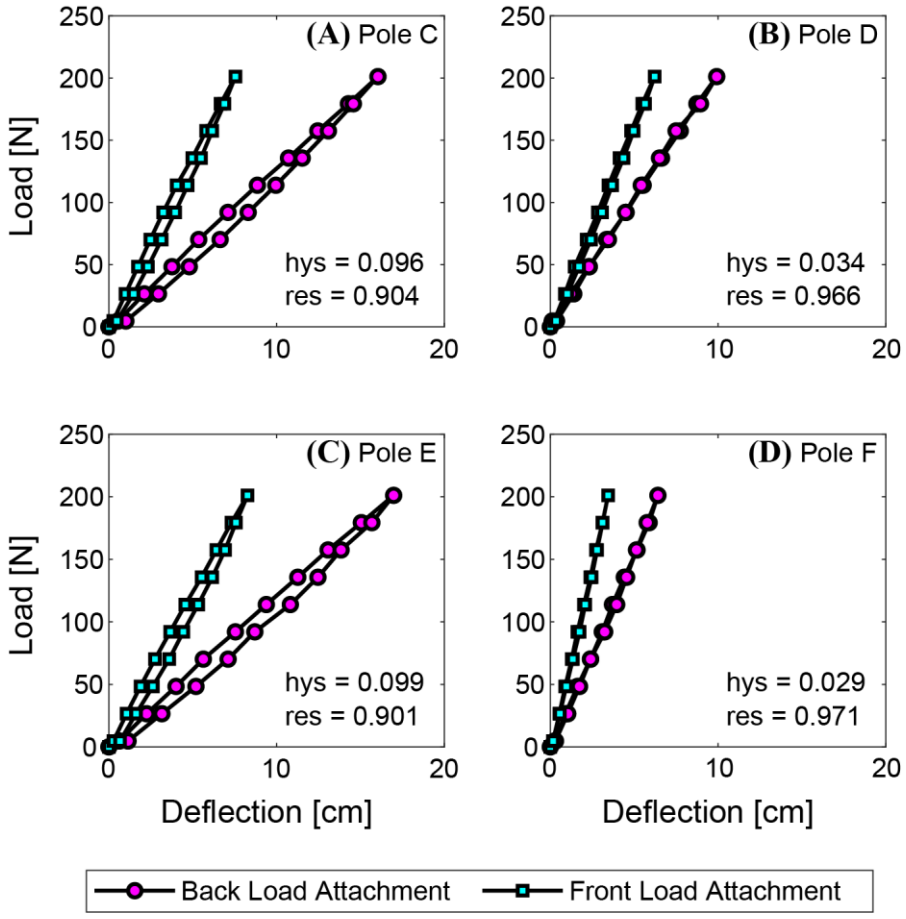

Figure 3.4. Load-deflection curves for the LPs

A full cycle of loading and unloading is shown for each end of each LP: **(A)** Pole C, **(B)** Pole D, **(C)** Pole E, **(D)** Pole F. Note that standard deviation of all deflection measurements are well below ±0.01 cm and cannot be viewed in these plots.

3.3.2 Young's modulus

Although the plots shown in Fig. 3.4 illustrate pole stiffness over a range of loads, each pair of curves only indicates deflection for two discrete points at the basket attachment points near the ends of the pole. However, multiple points were measured along each pole's axis during the stiffness test. Thus, in order to more thoroughly characterize stiffness of the LPs, a surface was plotted where the vertical axis indicates deflection and the horizontal axes are load and distance (from the fixed centre to the point of deformation along the pole's axis). A least-squares non-linear regression was used to fit the data to a theoretical surface derived from classical beam theory for a cantilever beam [see Eq. (3.4); Fig. 3.5A,B]. The coefficient *a*—defined in Eq. (3.4)—was

determined from these regressions in order to solve for the Young's modulus, *E*, of the bamboo material.

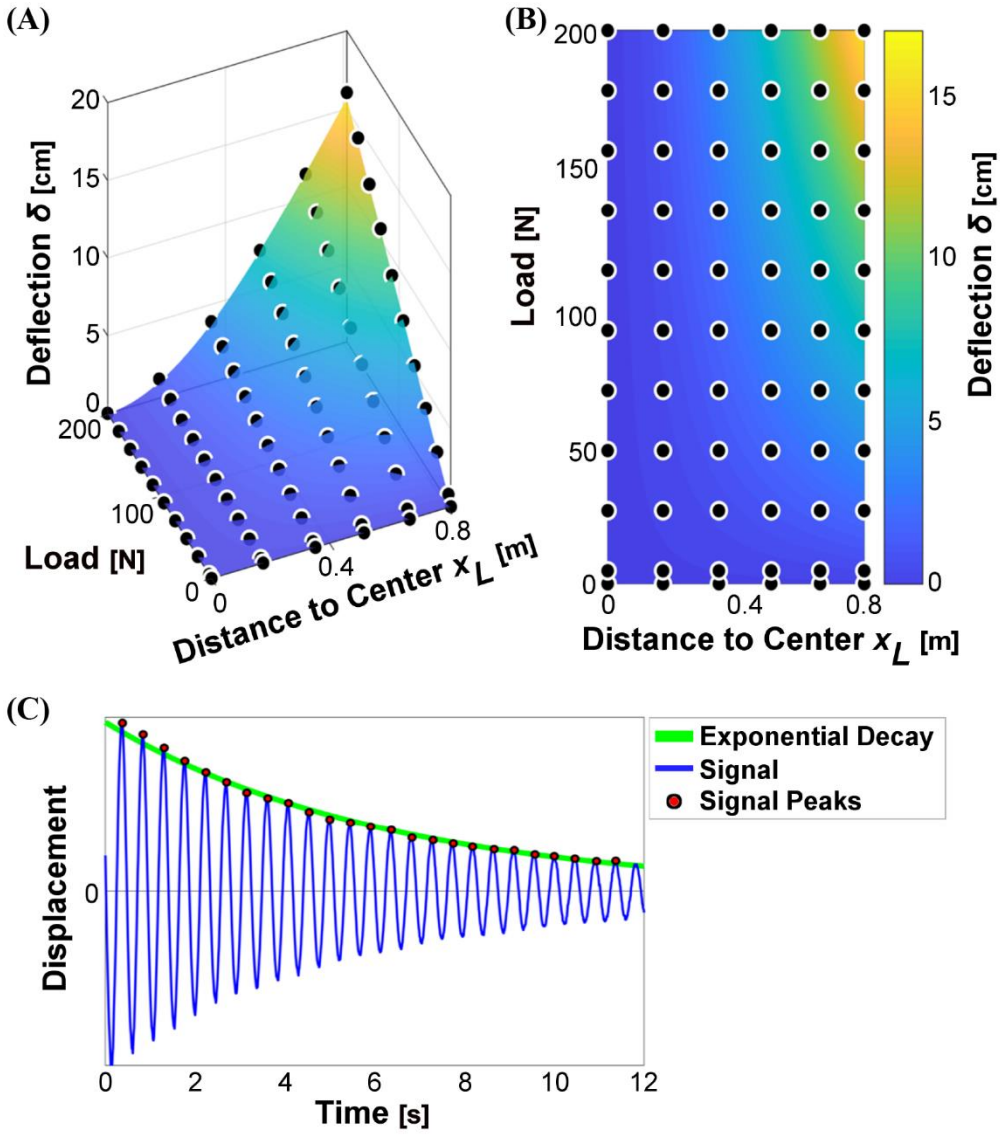

Figure 3.5. Examples of load-deflection surface and resonance testing data

(A) An example of the least-squares non-linear regression model fit to data from Pole C (LP) is shown. Note that the surface is linear with respect to load and nonlinear with respect to distance of the loading point from the centre. **(B)** The contour map shows the curvature of the surface with yellow shades indicating more deflection and blue shades less deflection. **(C)** An example of signal decay for a pole and load under free vibration is shown. The thick green line follows the exponential decay of peak signal magnitude while the thin blue line shows the vertical oscillations measured with inertial sensors placed at the load attachment points. Note that scaling of the vertical plot axis is not labeled since absolute magnitude is irrelevant for this test.

The resulting regression coefficients, *a*, are reported for poles labeled *C-F* (LPs) as best estimate (95% confidence intervals) ($x10^{-4}$ s^2 kg^{-1} m^{-3}): 7.29 (7.25-7.34), 5.14 (5.12-5.16), 8.56 (8.53-8.60) and 3.98 (3.94-4.02), respectively. Upon measuring the second moment of area (see section 3.3.4) the Young's Moduli were calculated from the best fit regression coefficient and ranged from 14.7-22.2 GPa for the LPs. Furthermore, the spring constant, *k*, was determined for the load acting at the basket attachment point on the pole via the relationship given in Eq. (3.6). The resulting values ranged from 1.31-3.59 kN m^{-1} for the LPs.

The spring constant was also determined for the FPs. However, instead of calculating this parameter from its relationship to Young's modulus, it was determined from the coefficient of a least-squares non-linear regression applied to resonance test data. The non-linear model used for this regression is given by Eq. (3.7). The spring constant values determined from this regression ranged from 1.83-4.18 kN m^{-1} for the FPs. After calculating the second moment of area, the Young's modulus was determined for all of the FPs using the best estimate of the spring constant. These values ranged from 10.1-21.0 GPa for the FPs.

3.3.3 Damping ratio and damping coefficient

The damping ratio was calculated from resonance behavior by characterizing the exponential decay of signal peaks over time (see Fig. 3.5C). Damping ratio results ranged in value from 0.010-0.013 for the LPs and 0.011-0.018 for the FPs. The average damping coefficients were calculated from these results: 2.77-3.56 N s m^{-1} for the LPs and 3.45-7.28 N s m^{-1} for the FPs.

3.3.4 Second moment of area

Figs. 3.3b and 3.3c show a comparison of the dimensional measurements of an example pole (LP-C) from the CT scan with the corresponding model geometry. The middle panel (*b*) shows an overlay of the model and the CT scan while the bottom panel (*c*) shows the second moment of area data calculated from both the model and the CT scan for all slices of Pole C. Although there are subtle differences between the scans and the model, it gives a reasonable representation of the pole geometry.

Although the second moment of area tapers slightly toward the ends of the pole (the form cut by the Vietnamese craftsperson who fabricated each pole), these systematic

trends are modest, confirming that the cross-sectional geometry is relatively consistent along the pole's axis. More prominent fluctuations are found at fairly regular intervals where the second moment of area spikes. These spikes occur at the pole's growth nodes, however their influence on the deflection of the structure is likely modest given their small contribution to the total length—essentially brief interruptions to an otherwise consistent cross-section. Mean values for geometric parameters—determined from the middle section bordered by the nearest bamboo nodes—were used to characterize the entire pole. The widths of the poles range from 55.7-61.4 mm for the LPs (measured with the CT scans) and 48.0-62.0 mm for the FPs (measured by hand at the farm site). The heights of the poles range from 17.9-25.0 mm for the LPs (CT scans) and 18.0-24.0 mm for the FPs (hand measurements). Finally, the second moment of area measurements are reported as follows: 1.028-2.740x10^4 mm^4 for the LPs and 1.078-2.254x10^4 mm^4 for the FPs.

3.3.5 Model predictions and empirical resonant frequency

The predictive capacity of the mass-spring-damper model was assessed by comparing it to empirical data of free vibration under various loads. Resonant frequencies associated with the lowest load were approximately 3-5 Hz while frequencies at the highest load were approximately 1-2 Hz. Standard error (SE) of the model ranged from ±0.099-0.177 Hz (or 5.11-7.54% of the frequency range over all tested loads) for the LPs (see Fig. 3.6).

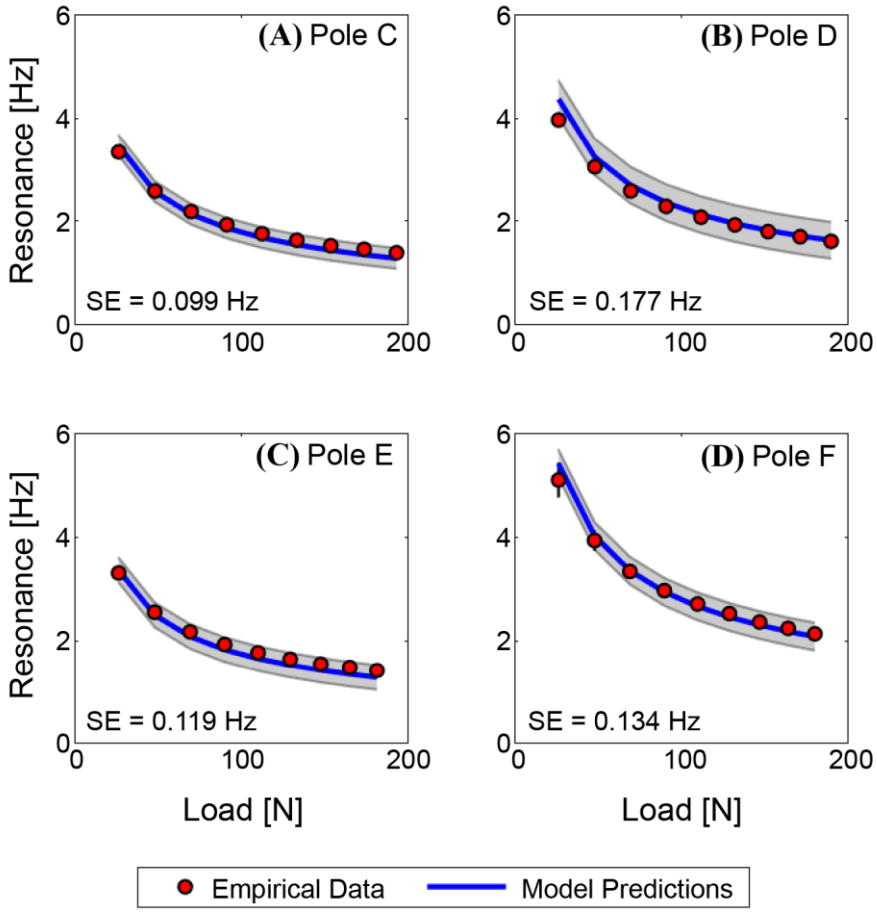

Figure 3.6. Resonant frequency curves for the LPs

The relationship between resonant frequency and load is shown for each of the LPs. Circles are mean frequencies measured empirically during free vibration, and the solid line indicates resonant frequencies predicted by the mass-spring-damper model. Two standard errors of each model approximate 95% confidence intervals and is indicated by the grey shaded region. Standard deviations of the empirical means are also shown by the error bars of individual data points. Note, much of this error is too small to be visible at the scale of these plots. **(A)** Pole C **(B)** Pole D **(C)** Pole E **(D)** Pole F.

Model predictions were also compared to data gathered in the field (FPs) where the standard error ranged from ±0.163-0.482 Hz (or 8.61-23.64% of the frequency range over all tested loads). For this sample, resonant frequencies for the lowest load were approximately 3.0-5.0 Hz while frequencies at the highest load were approximately 1.5-2.5 Hz (see Fig. 3.7).

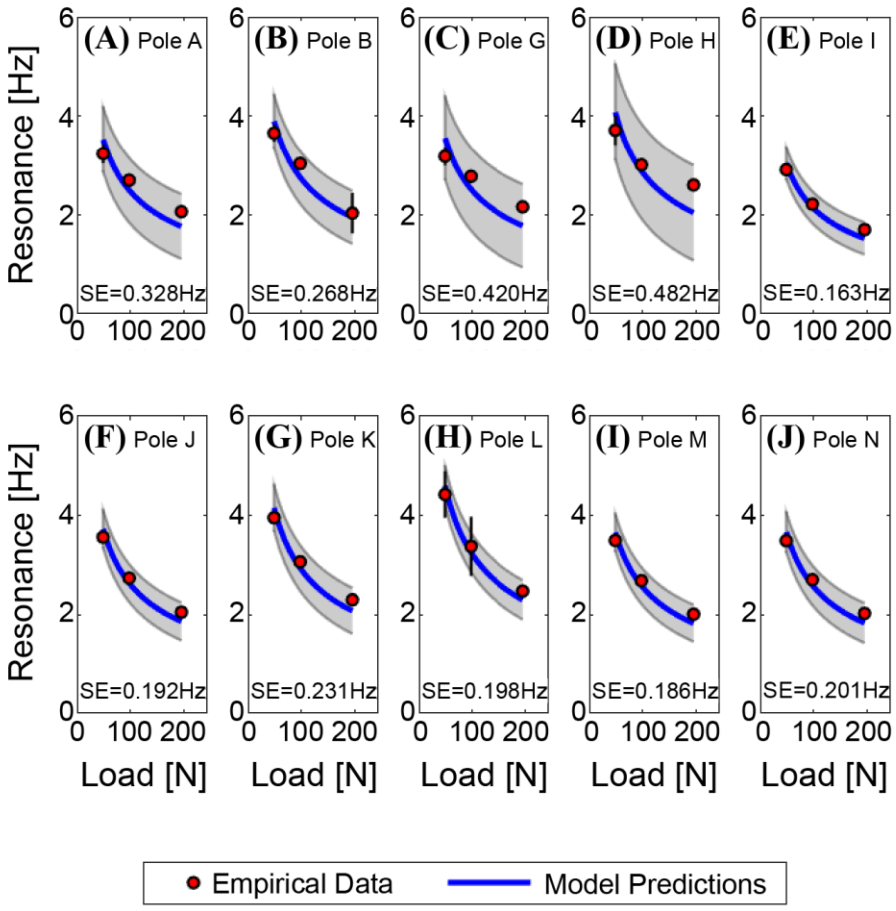

Figure 3.7. Resonant frequency curves for the FPs

The relationship between resonant frequency and load is shown for each of the FPs. Circles are mean frequencies measured empirically during free vibration, and the solid line indicates resonant frequencies predicted by the mass-spring-damper model. Two standard errors of each model approximate 95% confidence intervals and is indicated by the grey shaded region. Standard deviations of the empirical means are also shown by the error bars of individual data points. Note, much of this error is too small to be visible at the scale of these plots. **(A)** Pole A, **(B)** Pole B, **(C)** Pole G, **(D)** Pole H, **(E)** Pole I, **(F)** Pole J, **(G)** Pole K, **(H)** Pole L, **(I)** Pole M, **(J)** Pole N.

3.3.6 Summary of pole properties

One important function of the model is as a tool to predict fundamental pole properties without explicit measurements. Thorough assessment and characterization of the four LPs verified the resonance predictions of the model. Assuming that the LPs are a representative sample of the larger bamboo pole population, properties of the FPs were

also estimated from the model. The results of these properties are summarized in Tables 3.1 and 3.2, as well as the properties that were measured directly for the LPs.

Table 3.1. Summary of pole geometry and inertia

Testing location	Pole	Mass [kg]	Second Moment of Area [10^4 mm^4] mean (±SD)	Width [mm] mean (±SD)	Height [mm] mean (±SD)	Outer Radius [mm]	Length [m]
Lab	C	0.70	1.028 (0.059)	61.4 (0.8)	17.9 (0.5)	35.3	1.550
lab	D	0.83	1.538 (0.058)	60.6 (0.6)	22.5 (0.3)	31.7	1.573
lab	E	0.73	1.322 (0.052)	58.2 (0.2)	19.4 (0.2)	31.5	1.527
lab	F	0.98	2.740 (0.117)	55.7 (0.6)	25.0 (0.7)	28.0	1.409
field	A	0.85	1.862	60.0	22.0	31.5	1.297
field	B	0.85	1.422	59.0	20.0	31.8	1.256
field	G	0.90	1.191	62.0	18.0	35.7	1.237
field	H	0.94	1.689	61.0	21.0	32.7	1.272
field	I	0.94	1.650	60.0	21.0	31.9	1.424
field	J	0.76	1.078	48.0	20.0	24.4	1.255
field	K	0.81	1.905	61.0	22.0	32.1	1.305
field	L	1.00	2.254	58.0	24.0	29.5	1.348
field	M	0.90	1.698	56.0	22.0	28.8	1.395
field	N	0.93	1.318	61.0	19.0	34.0	1.296

Values of inertial and geometric properties are listed for both the lab- and field-tested poles. Note that standard deviation (SD) is listed for some properties of the lab poles but not for the field poles. This is due to the nature of the measurements made (basic hand measurements for the latter).

Table 3.2. Summary of pole properties

Testing location	Pole	Spring Constant [kN m^{-1}] (95% CI)	Young's Modulus [GPa]	Damping Coefficient [N s m^{-1}]	Damping Ratio Median (±SD)	Hysteresis [%]
lab	C	1.47	22.2	2.77	0.011 (0.019)	9.4
lab	D	2.00	21.1	2.77	0.010 (0.016)	3.2
lab	E	1.31	14.7	3.41	0.013 (0.032)	9.6
lab	F	3.59	15.3	3.56	0.010 (0.022)	2.9
field	A	2.46 (1.20-4.16)	11.2	3.92	0.012 (0.012)	…….
field	B	2.99 (1.80-4.48)	10.1	4.24	0.012 (0.010)	…….
field	G	2.50 (0.95-4.78)	16.5	3.45	0.011 (0.034)	…….
field	H	3.28 (1.25-6.29)	16.7	5.51	0.014 (0.020)	…….
field	I	1.83 (1.25-2.52)	13.3	4.02	0.015 (0.015)	…….
field	J	2.75 (1.91-3.75)	21.0	5.23	0.015 (0.011)	…….
field	K	3.42 (2.29-4.76)	16.6	4.63	0.012 (0.010)	…….
field	L	4.18 (3.09-5.44)	18.9	7.28	0.018 (0.042)	…….
field	M	2.65 (1.84-3.59)	17.6	3.68	0.011 (0.010)	…….
field	N	2.66 (1.80-3.69)	18.3	4.34	0.013 (0.040)	…….

Values for stiffness and damping parameters are listed for both the lab- and field-tested poles. Note that 95% confidence intervals (CI) are listed for spring constant of the field poles but not for the lab poles, since varying methods of analyses were used for each sample. Hysteresis values are not reported for the field poles since this test was not conducted at the farm site.

The average Young's modulus (mean±SD) was 18.3±3.9 GPa for the lab tested poles (LPs) and 16.8±2.6 GPa for the field-tested poles (FPs), an 8.1% difference. Comparisons of the average spring constant of the LPs and the FPs are as follows: 2.09±1.04 and 2.87±0.64 kN m^{-1} a difference of 37.1%. Damping ratios were 0.011±0.001 for the LPs and 0.013±0.002 for the FPs, a difference of 20.2%. Damping coefficient results were 3.13±0.42 and 4.63±1.13 N s m^{-1}, 48.1% different. Finally, the second moment of area for the LPs and the FPs were 1.66±0.75 and 1.61±0.36 x10^4 mm^4, a 3.0% difference.

3.4 Discussion

Despite the different methods used to determine properties of LP and FP samples (direct testing versus inference from the model), the mean values of the two groups are

comparable. Damping coefficient differs the most between the two groups (48.1%). As damping coefficient was not measured directly, this is likely due to differences between these poles and the assumptions made in the model. Furthermore, damping coefficient is calculated from both damping ratio and spring constant – each of which contribute their own sources of variance and error. Damping ratio differs by 20.2% between the groups, however the absolute values are all very low (0.010-0.018). That is, this variance is largely irrelevant (from a dynamics standpoint) given that the lowest and the highest values still suggest the poles are quite resilient. There is also a difference between the mean spring constants of both groups (37.1%), though this difference is less than a standard deviation of the LP sample. Variance in the poles' spring constants can be attributed to a number of factors including cross-sectional geometry, Young's modulus of the bamboo, and pole length. In particular, the LPs tended to be longer than the FPs on average, contributing to lower spring constants even as Young's moduli were mostly similar. The testing location may have also influenced some of the properties (e.g. Young's modulus, mass, etc.). In particular, the FPs were tested in the humid, subtropical climate of northern Vietnam while the LPs were tested indoors in the relatively dry and moderate climate of Calgary, Alberta. The effects of acclimatization were monitored every two weeks for a three-month period after the LPs were first brought to the lab. During this time, only one property value changed meaningfully; the average mass of the LPs dropped from 0.90 to 0.81 kg. This compares to an average mass of 0.89 kg for the FPs (measured in Vietnam). It seems likely that this loss of mass can be attributed to a decreased moisture content associated with the drier testing climate of the LPs. It is likely that this contrast in moisture content may help to explain differences in damping properties of the two pole types (recall, the FPs had a 48.1% higher damping coefficient on average when compared to the LPs).

Regardless of the variation in properties and parameters between the two groups of poles, the average values tend to agree with previous literature describing bamboo properties. For example, the average Young's modulus of all the poles (17.3 GPa) is consistent with values published in various studies: Lakkad and Patel (1981) measured the Young's modulus of bamboo (Kao Zhu and Mao Zhu species) in the orientation of individual fibers as 20.6 GPa; Amada and Lakes (1997) tested multiple samples of bamboo (species not specified) with different moisture content and found a Young's modulus for transverse bending ranging from 7.31-14.80 GPa. In the same study, loss

tangent values indicated extremely low levels of damping ($\tan \delta \approx 0.01$). However, the loss tangent values were slightly increased when the bamboo samples were subjected to thorough wetting (up to $\tan \delta \approx 0.015$ after wetting). These findings align with the results of our study showing generally very low values for damping ratio and hysteresis, however slightly more damping with the humid FPs compared to the relatively dry LPs.

Although measured low levels of damping are consistent with previous studies, one limitation remains a lack of knowledge about the specific mechanism(s) for energy loss (e.g. viscous, structural, etc.). We chose viscous damping for our model primarily due to its extensive consideration in previous literature—for engineering and biological structures and materials (Baker et al., 1967; Banks & Inman, 1991; Miller, 2005; de Langre, 2008)—as well as its ability to predict energy losses driven by various physical mechanisms (including viscous and non-viscous mechanisms). In many systems, different models for energy loss are relatively insensitive to the effect they have on the ultimate output of the model: in our case, resonance. Although a discussion of energy loss mechanisms is important, we opted for a more pragmatic approach to our modelling: namely, to predict the most dominant influences on system resonance.

Another limitation of the model involves the assumption of a constant cross-sectional geometry. Clearly, the CT data show that this is not precisely the case (see Fig. 3.3C). However, cross-sectional fluctuations are modest when considering trends over the length of the pole (tapering at the ends) and abbreviated when considering localized inconsistencies such as thickening at the nodes. Thus, we argue that introducing model complications to incorporate these variations are unlikely to be worth the refined accuracy. Perhaps the most obvious approach to further evaluation is a finite element model derived from the CT scans. We rejected this approach because we felt it was not necessary for predicting fundamental resonance of the pole-load system. Furthermore, analysis of the FPs would not benefit from such a model, since CT scanners were not feasible on the farm site. Nonetheless, a future study looking to test our simple model and understand nuanced behaviors of the structure could certainly benefit from the finite element method.

In order to consider design parameters of the bamboo poles, their properties (either measured or calculated) are compared with optimized values suggested by the peak force minimization model developed by Potwar et al. (2015). The model predicted

shoulder forces based on a spring-loaded inverted pendulum locomotion model interacting with a beam-like pole (similar to the current study). They also took multiple constraints into consideration. A pole mass constraint was used to limit the mass of the pole to less than 10% of the total load, assuming published values of bamboo density and calculations of pole volume. A strength constraint was also applied by considering the theoretical mechanical stress required for failure (e.g. plastic deformation). A load clearance constraint was enforced by limiting pole stiffness (lower bound) to allow for a maximum of 0.4 m pole deflections. The optimal parameter space was further bounded by limiting pole stiffness (upper bound) in order to match peak shoulder forces expected of a rigid backpack carrying a similar load.

In Fig. 3.8, both the FPs (white circles) and LPs (grey diamonds) are plotted over the parameter space bounding the optimal range for pole design. This figure is a recreation of the model developed by Potwar et al. for a carrier walking at 1.34 m s^{-1} with Mao Zhu bamboo [note this species of bamboo (i.e. *Phyllostachys edulis*) is commonly found in northern regions of Vietnam (Tran, 2010) near the Thai Nguyen province where our poles were collected]. Although parameter optimizations were conducted for other conditions, this comparison was chosen simply because the optimal region is closest to the pole parameters measured in our study. Although all of the pole parameter combinations (pole length and outer radius) are clearly outside of the optimal range, there are a few reasons why this may be the case.

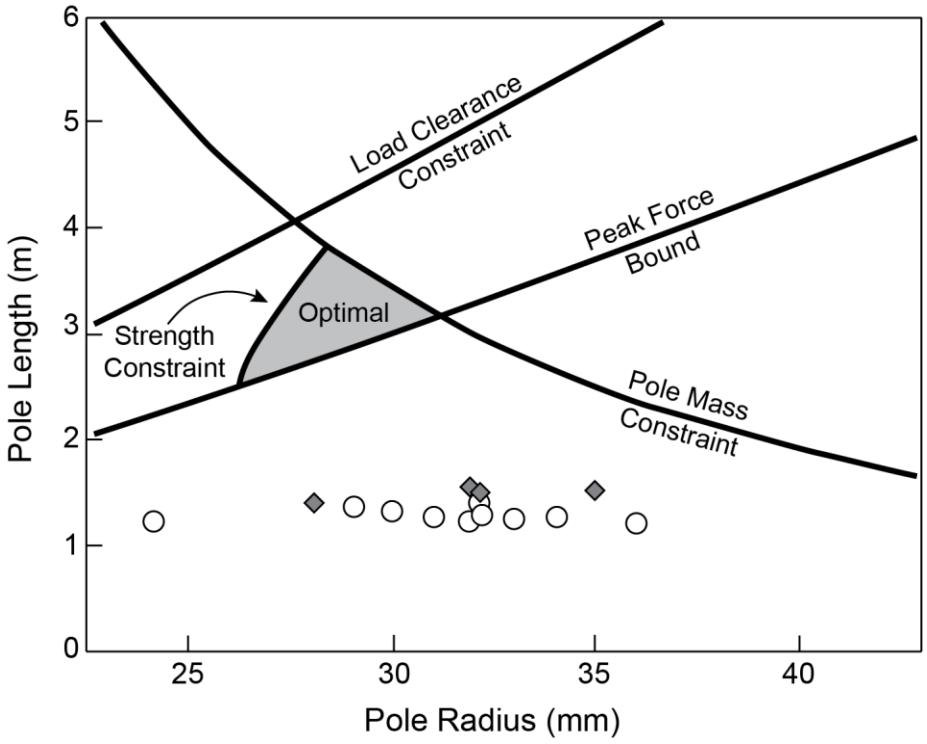

Figure 3.8. Measured pole parameters versus parameters of optimization model

Pole parameters (radius and length) are compared to the shoulder force optimization model developed by Potwar et al. (2015). Four constraints were used to determine a region of pole parameters that minimize forces felt at the shoulder. All 14 poles from the current study are also plotted (light circles are the FPs and dark diamonds are the LPs) for comparison.

Specifically, the optimal parameter range assumes a pole with a semi-circular cross-sectional geometry, which is thicker (greater cross-sectional height) than the pole geometries observed in CT scans. As a result, applying our height measures to the Potwar et al. model results in an erroneous stiffness estimate. Still, the suggested optimal pole length is likely too far off for cross-sectional geometry to account for this discrepancy alone.

Although the optimal parameter space considers multiple constraints/bounds, there is perhaps an additional consideration left unaddressed: the effect of pole length on practicality and maneuverability. The current model predicts an optimal pole length of around 3 m and often more, (depending on bamboo species, cross-sectional properties, and walking speed). While this length may not pose too much difficulty for an individual working alone in a field, it would make loading and handling of the pole difficult in a

crowded marketplace. It is possible that our poles were fabricated in part to facilitate maneuverability.

The model indicates optimal parameters that reduce forces distributed over the bearing surface of the shoulder. However, since our poles do not meet these optimality constraints, perhaps it is fair to conclude that they are manufactured to meet different design goals or optimize a different aspect of the interaction between the individual and the tool. Here, we consider an alternative: the resonant oscillation of the pole-load system is tuned to the cadence of the carrier, to exploit an energetic benefit.

A thorough consideration of how pole properties influence locomotion energetics likely requires a rigorous model validated through empirical data. However, it may be useful to consider the general range of resonant frequencies, since reaction forces (felt by the carrier) increase with larger oscillations of the load and oscillations typically spike at, and around, resonant modes. For example, Castillo et al. (2014) found that individuals received energetic benefits when they walked at a step frequency slightly above the resonant oscillations of the pole-load system. However, this is likely only feasible when the resonant frequencies are in the approximate range of a person's preferred step frequency.

Typical preferred walking conditions include a step frequency range of approximately 1.5-2.0 Hz and a velocity of 1.0-1.5 m s^{-1} (Bertram & Ruina, 2001; Bertram, 2005). While this range of frequencies approximately coincides with the resonant frequencies of the LPs at larger load levels (see Fig. 3.6), they are somewhat below the resonance curves for the FPs even at high loads (this difference is largely due to increased load stiffness resulting from the generally shorter lengths of these poles). Still, these comparisons are largely qualitative (i.e. non-rigorous) and do not take into consideration potential frequency responses associated with carrying rigid or oscillating loads.

For example, subtle increases of walking frequency tend to occur when a person carries a rigid load, although these changes are often insignificant (Charteris, 1998; Griffin et al., 2003). At the same time, increases in walking speed are associated with increases in step frequency (Cavagna & Franzetti, 1986; Bertram & Ruina, 2001). Therefore, the pole resonant frequencies may benefit the energetics of relatively fast walking, which may be appropriate for the increased pace of busy work on the farm or in the marketplace. In

summary, if there *is* indeed an energetic benefit to walking with these poles, they would likely exist with heavier loads, 200 N (20 kg) per pole end or more (common load levels during farm work) and at relatively fast walking speeds. Regardless, future research would benefit from investigating more sophisticated models capable of predicting the motor behavior of locomotion when interacting with the flexible oscillations of different loads. However, such models should be thoroughly validated with rigorous empirical studies assessing locomotion of experienced users under natural conditions.

3.5 Conclusions

A number of objectives were met by this study. We tested and assessed the mechanical properties of the four LPs (fabricated in a Vietnamese village according to traditional methods), which allowed us to describe basic dynamic behaviors inherent to their structure, material and design. Through this series of tests, we attained a set of fundamental parameters and properties. These included Young's modulus of the bamboo, hysteresis and resilience of static loading/unloading, the rate of energy loss due to viscous damping occurring during free vibration, the second moment of area of the pole cross-sections and the resonant behaviors of the poles vibrating under load.

We applied a theoretical model using classical beam theory (of a cantilever beam with a partial tubular cross-section) to a mass-spring-damper system to predict the resonant behavior of differing loads. This model was experimentally validated for the four LPs. Finally, we used the theoretical model to determine the same set of mechanical and structural properties for the other 10 FPs.

These measurements provide a foundation for models evaluating the role of pole use and function by traditional cultures using this technology. Although Western cultures rely on a fixed load attachment such as a strapped backpack, this solution may be less effective and less energetically economical than interacting with the dynamic oscillations of a flexible bamboo pole. However, if the mechanisms of such interactions are to be determined, then the poles themselves must be thoroughly evaluated and understood. With the results presented here, a thorough and rigorous human locomotion model can now be used to investigate such interactions.

Chapter 4 has been published as Schroeder, R. T., & Bertram, J. E., Nguyen, V.S. , Hac, V.V. & Croft, J.L. (2019). Load carrying with flexible bamboo poles: optimization of a coupled oscillator system. *Journal of Experimental Biology, 222*, jeb203760. doi:10.1242/jeb.203760

CHAPTER 4

Human-pole Coupled Oscillations: Interactions with a Passive Load Carrying Device

4.1 Introduction

Backpacks with non-compliant straps are commonly used in western nations when carrying moderate to heavy loads. Elastic suspension systems—such as spring-loaded backpacks (Rome et al., 2005; Rome et al., 2006) or flexible poles (Castillo et al., 2014)—can reduce energetic expenditure of load carriage. While spring-loaded backpacks are relatively new, individuals in Asia have been using flexible bamboo poles to transport loads for centuries. However, the potential benefits of carrying an oscillating load are still under debate. Some studies have shown that these systems can increase energy expenditure (Foissac et al., 2009; Martin & Li, 2018) or have little effect (Kram, 1991) compared to carrying loads in a conventional backpack. These discrepancies may be explained by key differences between the various studies – for example, gait type [walking (Rome et al., 2005; Rome et al., 2006; Castillo et al., 2014; Foissac et al., 2009; Martin & Li, 2018) versus running (Kram, 1991)], directionality of load oscillations [vertical (Rome et al., 2005; Rome et al., 2006; Castillo et al., 2014; Foissac et al., 2009; Kram, 1991) versus medial-lateral (Martin & Li, 2018)], or load suspension mechanism [spring-loaded backpack (Rome et al., 2005; Rome et al., 2006; Foissac et al., 2009; Martin & Li, 2018) versus compliant poles (Castillo et al., 2014; Kram, 1991)].

Dynamics models of compliant loading have demonstrated the effect of spring constant and damping on the energetic cost of human walking (Ackerman & Seipel, 2014; Li et al., 2016A). Such models assume leg length changes over stance (prescribed as a sinusoidal path) and parameter values (e.g. frequency, amplitude) scaled to empirical data but neglect an individual's capacity to adjust gait and optimize interactions with the load. A human walking with an oscillating load is essentially a coupled oscillator system: one oscillator passive (the flexing load), the other active (the person). An individual may experience and adapt to interactive effects, particularly if there is an advantage to do so. Such interactions are observed in various systems – e.g. while walking on a swaying pedestrian bridge, individuals spontaneously synchronize their steps with one another and entrain to the bridge's oscillations (Dallard et al., 2001). We hypothesize

entrainment exploits energy saving opportunities available when gait is coordinated with substrate motion. People also modify behavior to wearable devices; infants bounce in an elastic harness and learn to match frequency to the system's resonance (Goldfield et al., 1993). Individuals wearing a knee exoskeleton optimize step frequency over a range of available energetic cost options (i.e. cost "landscape") when naturally preferred frequencies are penalized with controlled resistance from the mechanical device (Selinger et al., 2015). These examples describe unusual circumstances that nonetheless illicit coherent gait adaptations over time. Modelling approaches that rely on fitting data from standard locomotion tasks (e.g. undisturbed treadmill walking) often fall short in predicting, and thus explaining, non-standard locomotion tasks (e.g. carrying load oscillating on a compliant bamboo pole).

Trajectory optimization is an alternative that has made accurate predictions about energy-minimizing gait solutions under a variety of standard and non-standard circumstances: walking/running at various step-length-velocity combinations (Srinivasan & Ruina, 2006), uphill/downhill locomotion (Hasaneini et al., 2013), navigating a shaking platform (Joshi & Srinivasan, 2015), walking with an oscillating impulse applied to the body (Schroeder & Bertram, 2018), and even manoeuvres associated with the urban sport of parkour (Croft et al., 2019A). Here, we used trajectory optimization to determine energy-minimizing solutions for humans carrying loads suspended from flexible poles of various stiffness and load. We then compared these results to empirical data from Vietnamese farmworkers highly experienced in this manner of load carriage. Perhaps these individuals are sensitized to functional advantages of this carrying mode and/or are capable of subtle adjustments that exploit those opportunities. Experience can profoundly influence the energetics of unusual load carrying. For example, women in some African tribes can carry loads on their heads for substantially less energetic cost than novice westerners carrying the same load in a backpack or on their heads (Maloiy et al., 1986; Cavagna et al., 2002). When inexperienced individuals are introduced to novel cost landscapes, they sometimes require guided "exploration" where a range of gait options are introduced before they can spontaneously locate the optimal solution (Selinger et al., 2015). When carrying loaded bamboo poles, unguided exploration through natural variation likely occurs with extensive practice – particularly when exposed to various loads, poles, and terrains. Past studies are largely limited by their exclusive use of naïve, inexperienced participants which may help explain inconsistent

findings. Thus, we studied Vietnamese farmworkers with years of experience carrying substantial loads on bamboo poles.

4.2 Methods

4.2.1 Study participants

Fourteen participants (eight males, six females) were recruited for the study after a local translator conducted a brief pre-participation interview to ensure that basic inclusion criteria were met (e.g. no recent injuries affecting gait and at least five years of experience, although many participants claimed lifelong experience). Of the fourteen participants, seven used a pole daily, three weekly, one monthly, and three seasonally. At the time of data collection, the average age (± standard deviation) was 45 ± 17 years, body mass was 50.2 ± 5.9 kg, and height was 1.56 ± 0.07 m. All participants provided informed consent to participate through a qualified interpreter, and these studies were approved by ethics review boards of Thái Nguyên University of Medicine and Pharmacy, Edith Cowan University (Human Ethics Review Board 15249), and the University of Calgary (REB16-0910).

4.2.2 Walking trials

Participants were asked to walk along a one-meter-wide path with a steady gait while carrying one of two pole types: (i) a rigid, season-dried bamboo pole with a full circular diameter (i.e. it was not split to make the characteristic flattened carrying pole, so remained rigid) or (ii) their own personal compliant bamboo pole (pre-fabricated and well-used)—property measurements of these poles were presented previously (Schroeder et al., 2018). Participants walked along a twenty-meter path at a steady preferred velocity and cadence while carrying loads (0, 30, and 50% body weight). For zero load, subjects carried their own pole unloaded on their shoulder in a casual manner. Otherwise, sandbags were used to load the pole to a proportion of the participant's body weight (BW). The sandbags were suspended from the pole in carrying baskets on wire frames (baskets/frames purchased from a local market in the region) and were evenly distributed between both ends of the pole in the standard manner employed in the region. The order of conditions (pole type and load) was randomized with five trial repetitions each. Participants were allowed practice trials to acclimate to each condition as needed. All instructions were communicated through a local guide and translator.

4.2.3 Instrumentation and measurements

Wireless inertial measurement units (Xsens Technologies B.V., Enschede, The Netherlands) captured acceleration and angular displacement in the vertical, lateral, and fore-aft directions (acquisition rate = 60 Hz). Three sensors were placed on subjects (above each ankle and at the lower lumbar region of the back) and three along the pole's length (directly above the shoulder contact point and at each end near the attachments of the loaded baskets). The ankle sensors were used to determine step frequency by calculating the time difference between acceleration peaks, and the remaining sensors were integrated to characterize fluctuations in centre of mass (CoM) and pole-load velocity and displacement over each step. All sensor signals were nulled between each trial to minimize drift error.

Although reaction forces between the pole and shoulder were not measured directly, an approximation was calculated from kinematics. Compliant pole spring force (F_s) was calculated via the product of the pole spring constant (k_p) and the vertical displacement between the body CoM (y_c) and the load (y_L): $R_{cmp} \approx F_s = k_p(y_c - y_L)$. Damping forces were neglected given the system's distinctly underdamped nature (Schroeder et al., 2018). For the rigid pole, reaction force was calculated as: $R_{rig} = m_L(\ddot{y}_c + g)$, where m_L is the load mass, $\ddot{y}_c$ is vertical acceleration of the body CoM, and g is gravitational acceleration ($9.81\ m\ s^{-2}$), assuming motion of the load and body are tightly coupled.

A GoPro Hero 4 camera (GoPro Inc., San Mateo, California, USA) recorded video in the sagittal and coronal planes (frame rate = 120 Hz), although only the sagittal data were analyzed. The sagittal camera was placed perpendicular to and approximately four meters away from the pathway to reduce parallax and lens distortion. Video calibrations were performed between participants by filming two markers at known vertical and horizontal distances in the sagittal plane. Average forward velocity was determined from the videos by converting pixels traveled to meters traveled and dividing by the time duration. A rough indication of leg length was determined by approximating a point at the subject's greater trochanter and measuring the vertical distance to the ground while the subject stood still. This method was used instead of a measuring tape to avoid potential cultural sensitivities as well as any misunderstanding due to language barriers. All video digitization was performed in MATLAB (MathWorks, Natick, Massachusetts, USA) using custom software DLTdv5 (Hedrick, 2008).

4.2.4 Optimization model

Trajectory optimization was used to make predictions about the cost of walking at various step frequencies relative to the damped resonant frequency (f_{DR}) of the pole-load system.

$$f_{DR} = \frac{1}{2\pi}\left[(1-\zeta^2)\frac{k_p}{m_L}\right]^{0.5} \tag{4.1}$$

where k_p and ζ are the pole spring constant and damping ratio, respectively, [property values from (Schroeder et al., 2018)] and m_L is the mass of the load. Here we define relative step frequency,

$$f_r = \frac{f_s}{f_{DR}} \tag{4.2}$$

where f_s is the participant's absolute step frequency. Relative step frequency has a profound influence on the magnitude and phase of the load's oscillation relative to the individual carrying the pole. The response is particularly transient near resonance (i.e. $f_r = 1$) where relative magnitude spikes and phase shifts dramatically from 0° (in phase) to 180° [out of phase, Fig. 4.1; comparable to analysis in (Castillo et al., 2014)].

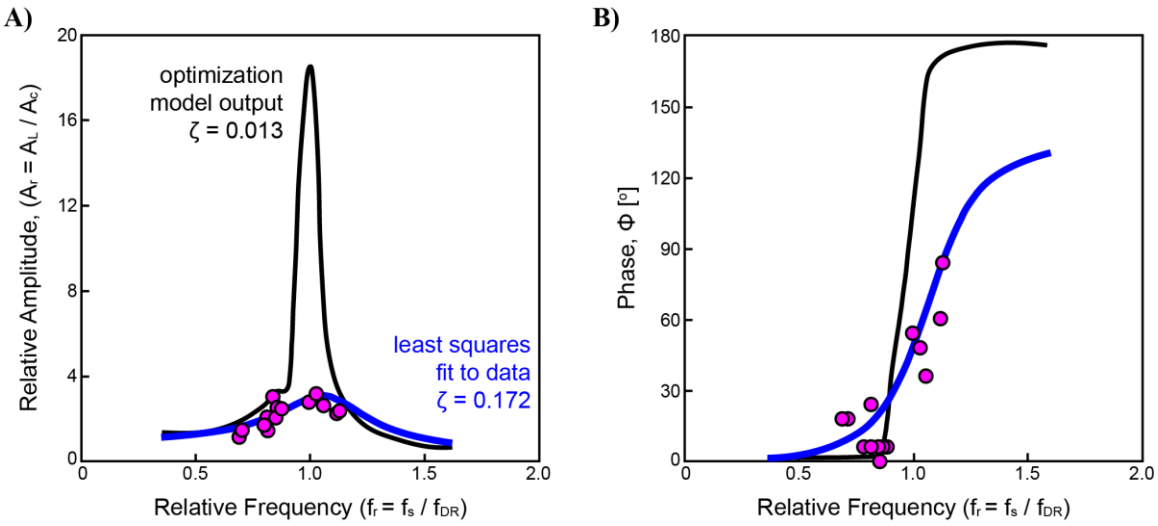

Figure 4.1. Relative amplitude and phase relationships over relative step frequency

A) Load oscillation amplitude relative to the body is shown for the optimization model using average pole properties (Schroeder et al., 2018) and a least squares non-linear regression fit to participant data (N=14). The fitted damping ratio is an order of magnitude higher than that determined by direct pole measurements, indicating higher damping levels during load

carriage. **B)** Phase relationship is shown for the optimization model and the data fit. Each data point represents the mean phase measured from individual subject data while carrying the compliant pole with a 50% body weight load.

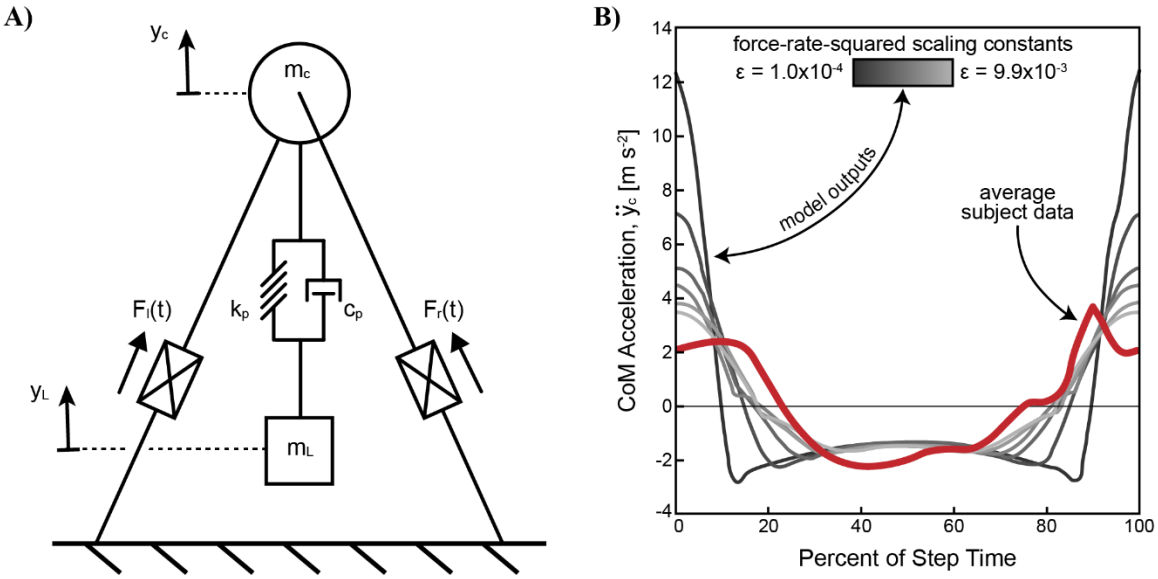

Figure 4.2. Bipedal model and force-rate-squared scaling constant

A) The bipedal model utilizes telescoping legs to provide extension forces that do positive and negative work on the body centre of mass (m_c). A mass-spring-damper mechanism simulates pole flexion under load (m_L). **B)** Optimization model outputs of the centre of mass acceleration are shown over a range of force-rate-squared scaling constants, where lower constants are associated with higher, narrower peaks of acceleration and higher constants are associated with lower, wider peaks. Average participant data are shown in red. The scaling constant used in the model was chosen to approximately match acceleration peaks in average participant data.

The optimization model consists of a point mass representing the body's centre of mass (CoM) and two massless telescopic legs that can actively extend (positive work) or resist compression (negative work). The model is reminiscent of earlier reductionist models (Srinivasan & Ruina, 2006; Schroeder & Bertram, 2018; Srinivasan, 2011), however it includes an additional mass-spring-damper mechanism that is supported by the CoM to simulate the pole-load system (see Fig. 4.2A). The optimization process modulates the leg forces and resulting trajectories of the system mass (unknown a priori) until the cost function is minimized. For the case of carrying a rigid (i.e. non-oscillating) load, the CoM experiences forces from the legs and from gravity, and the mass of the load (m_L) is added to the body point mass (m_c).

$$m_t = \begin{bmatrix} 1.0 \\ 1.3 \\ 1.5 \end{bmatrix} m_c \tag{4.3}$$

where m_t is the total system mass (body CoM plus load) for loading levels of 0, 30 and 50% body weight. The equations of motion are shown for the system below.

$$\begin{bmatrix} m_t \ddot{x}_c \\ m_t \ddot{y}_c \end{bmatrix} = \begin{bmatrix} \sum_{(l,r)} F_i \left(\frac{x_c - x_{fi}}{L_i} \right) \\ \sum_{(l,r)} F_i \left(\frac{y_c}{L_i} \right) - m_t g \end{bmatrix} \tag{4.4}$$

where x_c and y_c are the horizontal and vertical displacement of the body CoM, respectively, x_f is the foot contact point (i.e. the origin of the leg force vectors) for the left (l) and right (r) legs, and L and F are length and force magnitude, respectively, of the left and right legs. For the case of carrying a compliant load, Eqn. (4.4) is augmented.

$$\begin{bmatrix} m_t \ddot{x}_c \\ m_c \ddot{y}_c \\ m_L \ddot{x}_L \\ m_L \ddot{y}_L \end{bmatrix} = \begin{bmatrix} \sum_{(l,r)} F_i \left(\frac{x_c - x_{fi}}{L_i} \right) \\ -k_p (y_c - y_L) - c_p (\dot{y}_c - \dot{y}_L) + \sum_{(l,r)} F_i \left(\frac{y_c}{L_i} \right) - m_c g \\ m_L \ddot{x}_c \\ -k_p (y_L - y_c) - c_p (\dot{y}_L - \dot{y}_c) - m_L g \end{bmatrix} \tag{4.5}$$

where x_L and y_L are the horizontal and vertical displacement of the load point mass, respectively, k_p and c_p are the pole spring constant and damping coefficient ($c_p = 2\zeta\sqrt{k_p m_L}$), where ζ is the damping ratio and $m_L = \begin{bmatrix} 0.3 \\ 0.5 \end{bmatrix} m_c$ for the 30 and 50% body weight loading conditions. Leg length and velocity, used in Eqns. (4.4,4.5), are defined in terms of the body CoM position and the foot position for each leg.

$$L = \sqrt{\left(x_c - x_f\right)^2 + y_c^2} \tag{4.6}$$

$$\dot{L} = \frac{(x_c - x_f)\dot{x}_c + y_c \dot{y}_c}{L} \tag{4.7}$$

The model optimizes the leg forces over a single step (assuming left and right steps are symmetrical). The body begins at $x_c = 0\ m$ and ends at $x_c = d_s$, where step length is defined as the total distance the body CoM travels over a single step: $d_s = \frac{v}{f_s}$. Here, v is the average forward velocity and f_s is step frequency. To enforce a given velocity, time begins at $t = 0\ s$ and ends at $t = T_s$, where T_s is the inverse of step frequency. Foot

contact positions were defined for the left (l), the right (r), and the left leg again, for the next step (n): $\begin{bmatrix} x_{fl} \\ x_{fr} \\ x_{fn} \end{bmatrix} = \begin{bmatrix} -0.5 \\ 0.5 \\ 1.5 \end{bmatrix} d_s$. These foot contact positions define the initial position of the body CoM to begin at the middle of double stance (i.e. dual contact phase) at $t = 0\ s$.

In addition to initial and final conditions associated with the optimization of a step, multiple constraints were imposed on the model. For example, a path constraint was used to ensure that leg length never exceeded a maximal value while producing force.

$$F(L_{max} - L) \geq 0 \tag{4.8}$$

Additionally, leg forces were only allowed to be positive (i.e. extension forces only), however no constraints were placed on simultaneous leg forces (i.e. double stance was allowed). Other constraints were applied to enforce that final states (position, velocity, etc.) equaled initial states. This was done to ensure that only steady state gaits were considered. Boundaries were set for the vertical position of the load to prevent oscillations penetrating the ground or else pulling up on the pole (i.e. consistent with observations of pole bending in the downward direction only).

$$0 \leq y_L \leq y_c \tag{4.9}$$

The optimization's objective function (J, i.e. cost function) was composed of two terms associated with the absolute value of work due to leg extension (W_e) and a force-rate-squared term (FRS) summed for both legs.

$$J = \int_0^{T_s} \left(\dot{W}_e + FRS\right) dt \tag{4.10}$$

$$\dot{W}_e = F\dot{L} \tag{4.11}$$

$$FRS = \epsilon \dot{F}^2 \tag{4.12}$$

where $\dot{W}_e$ is the mechanical power of leg extension. The positive and negative components of leg extension were summed to get the absolute value of power ($\dot{W}_e = \dot{W}_e^+ - \dot{W}_e^-$), and $\epsilon_o \dot{W}_e^+ \dot{W}_e^-$ was added to the cost function, where ϵ_o is an arbitrarily small number. This additional cost term did not contribute to the overall cost since it was

always driven to zero in all optimizations; it was used to ensure that positive leg power could not occur unrealistically with simultaneous negative power from the same leg.

The force-rate-squared term is used as a smoothing factor to penalize extremely impulsive forces that are physiologically unrealistic and numerically challenging. Although the use of this cost is somewhat arbitrary, there is emerging evidence that metabolic consumption increases with frequency of muscle activation (and force rate) even as mechanical work remains constant (Doke & Kuo, 2007). Other gait optimization models have similarly incorporated force-rate terms in their cost functions (Rebula & Kuo, 2015; Handford & Srinivasan, 2018). Here, the scaling constant was adjusted until CoM acceleration peaks matched those from participants carrying zero load and was then held constant throughout all optimizations (Fig. 4.2B).

An additional cost was imposed on the optimization solution post hoc by considering work to swing the leg. This cost was modelled independent to the optimization under the assumption that leg swing costs are largely independent from the cost of leg extension work when carrying loads (Griffin et al., 2003). The leg swing cost was modelled after Doke et al. (2005), assuming a simple pendulum actuated with torque to achieve desired step frequencies.

$$W_s = \frac{\pi}{4} m_c C_s |f_s^2 - 4f_n^2| \tag{4.13}$$

where W_s is the mechanical work required to torque a pendulum at a given frequency, m_c is the mass of the body CoM, and f_n (0.64 Hz) is the natural frequency of the free-swinging leg (Doke et al., 2005). Note that the coefficient C_s (0.31 in m^2) was originally fit to data for subjects with notably longer legs than participants in the current study (0.88 m versus 0.75 m). To account for scaling effects, the coefficient was adjusted using the allometric equation ($y = bx^a$).

$$C_s = bL_{max}^a \tag{4.14}$$

where a = 2 (assuming isometry) and b was solved using Doke et al.'s (2005) fitted coefficient C_s and participant average leg length. The total cost of the model is expressed as the mass-specific cost of transport (CoT, J kg^{-1} m^{-1})—a summation of the cost terms described above.

$$CoT = \frac{f_s}{m_c v}(J + W_s) \quad (4.15)$$

where v is average forward velocity. Note that the cost of transport is normalized to body mass instead of total system mass (body CoM plus load) to distinguish the effect of added cost due to increasing loads.

During the optimization, all variables were non-dimensionalized with the parameters L_{max}, g, and m_t, however all optimization outputs were re-dimensionalized with the appropriate parameter values, as needed. Subject parameter values such as load mass, body mass, maximum allowable leg length, and average forward velocity were used to represent an average study participant as well as individual participants. A summary of these parameter values can be found in Table A.3.

4.2.5 Model simulations

The trajectory optimization procedure was implemented in MATLAB using a sparse nonlinear optimizer program [SNOPT (Gill et al., 2005)] in conjunction with GPOPS-II (Patterson & Rao, 2014) for problem discretization and setup. In order to procure robust solutions, a two-part optimization regime was used (Schroeder & Bertram, 2018). The first part implemented 15 random initial guesses to test for global optimality, and the second perturbed the prevailing optimum 15 times with random noise in order to fine tune the solution's local optimality. This procedure was employed to predict cost of transport of multiple optimal solutions sweeping a wide range of relevant parameter values. Specifically, step frequency (f_s) and damped resonant frequency (via spring constant) of the pole-load (f_{DR}) were systematically varied to probe the cost landscape as a function of relative step frequency (recall, $f_r = \frac{f_s}{f_{DR}}$).

Optimization simulations utilized the vastly underdamped pole characteristics from (Schroeder et al., 2018): $\zeta = 0.013$. Although oscillation amplitudes measured in the empirical data suggest substantially higher levels of pole damping during carrying in practice ($\zeta = 0.172$; Fig. 4.1), the lower damping ratio was still used simply because the oscillation effects are more apparent, and thus, more clearly interpreted. At higher (and perhaps more realistic) damping levels, similar trends emerge, but some nuances are lost. To quantify the empirical damping ratio, a least squares non-linear regression was

performed on equations derived from a basic vibrations analysis assuming a sinusoidal forcing function on a spring-mass system.

$$A_r = \left[\frac{1+(2\zeta f_r)^2}{\left(1-f_r^2\right)^2+(2\zeta f_r)^2}\right]^{0.5} \tag{4.16}$$

$$\phi = tan^{-1}\left[\frac{2\zeta f_r^3}{1-f_r^2+(2\zeta f_r)^2}\right] \tag{4.17}$$

where A_r is the relative amplitude and ϕ is the phase of the load amplitude relative to the forcing function.

The damping ratio resulting from the regression ($\zeta = 0.172$) was used to simulate optimal load interactions and to determine local CoT gradients for individual participants at and around their average preferred step frequencies ($f_{s,avg} \pm 0.20\ Hz$, $0.02\ Hz$ intervals) for both 30 and 50% loading conditions. This was done to relate the local cost gradient to changes in average relative step frequency between rigid and compliant poles.

4.2.6 Statistical analysis

We hypothesized that experienced pole carriers adjust step frequency while carrying a compliant bamboo pole to reduce cost (i.e. CoT). As such, the local gradient of the CoT surface predicted in simulations provides a framework to interpret the consequences of direction and magnitude for changes in relative step frequency between carrying a rigid and a compliant pole.

$$\frac{dCoT}{df_r} \approx \frac{\Delta CoT}{\Delta f_r} \tag{4.18}$$

where $\Delta CoT = CoT_{cmp} - CoT_{rig}$ (predicted cost of carrying a compliant pole minus that of a rigid pole) and $\Delta f_r = f_{r,cmp} - f_{r,rig}$ (participant average relative step frequency used while carrying a compliant pole minus that of a rigid pole). Since the resonant frequency of an ideal rigid pole approaches infinity, the step frequency data measured for the rigid pole condition were normalized by the resonant frequency of the loaded compliant pole instead.

$$f_{r,rig} = \frac{f_{s,rig}}{f_{DR,cmp}} \tag{4.19}$$

This choice scaled the model's data appropriately in the relative frequency domain whilst allowing fair comparisons between the rigid and compliant pole conditions.

A Pearson correlation was performed to test the relationship between the change in relative step frequency and the local gradient of the CoT. We hypothesized that a negative correlation would be found, indicating that participants adjust step frequency to reduce CoT while carrying loads with a compliant pole. This hypothesis is consistent with three specific outcomes: (i) positive CoT slopes associated with negative changes in relative step frequency (Q4 in Fig. 4.7A), (ii) negative CoT slopes associated with positive changes in relative step frequency (Q2 in Fig. 4.7A), and (iii) zero CoT slopes associated with little or no change in relative step frequency. Least squares linear regressions were performed on the data to indicate what proportion of variance could be attributed to the linear relationship.

Linear mixed models were also used to more thoroughly evaluate changes in step frequency due to fixed effects such as loading level and pole type. The mixed model was chosen to control for repeated measures observed among different subjects – where subject was entered as a random effect. The statistical models were developed in JMP (SAS Institute Inc., Cary, NC USA, version 14.1.0) using the restricted maximum likelihood method for parameter estimation and a compound symmetric covariance structure. First, changes in absolute step frequency were evaluated due to load effects with the rigid pole as well as the no load condition (0, 30 and 50% BW). Since walking speed has a known effect on step frequency it was non-dimensionalized ($\tilde{v} = \frac{v}{\sqrt{gL_{max}}}$) and included in the model as a covariate. The relationship between frequency and speed is generally nonlinear [$f_s \propto v^{0.58}$ (Kuo, 2001; Bertram & Ruina, 2001)]. However, a simple linear regression was performed for step frequency versus non-dimensional velocity, and the relationship was deemed sufficiently linear after assessing residuals over the relatively narrow range of speeds chosen by participants.

Another model was used to evaluate changes in relative step frequency, where pole type (rigid versus compliant) and load (30 and 50% BW) were both included as fixed effects. Non-dimensional walking speed was again included in this model as a covariate after confirming linearity with regression and visual assessment of the residuals. Interaction terms relating pole type to load, pole type to $\tilde{v}$ and load to $\tilde{v}$ were also included in the model.

Our optimization model predicts differential subject responses in relative step frequency when carrying the compliant pole versus the rigid pole. Thus, differences in relative step frequency based on the least squares means of each pole type were evaluated for individual subjects with post-hoc t tests and 95% confidence intervals (CI). The significance of our mixed model effects were also evaluated with post-hoc t tests. We adjusted p values (p_{adj}) based on Benjamini and Hochberg's method (1995) to control the false discovery rate during multiple significance testing and considered tests with $p_{adj} < 0.05$ to be significant. Throughout the manuscript, unadjusted p values are reported, and significance is indicated with asterisks. Additional details of the statistical models and general approach can be found in Appendix A.

4.3 Results

4.3.1 Model validation and cost of modulating step frequency

During unloaded walking, there is a trade-off between two cost mechanisms that influence the model: work to swing the leg (costly at high frequencies) and work to extend the support legs (costly at low frequencies). Thus, there exists an optimal intermediate step frequency (1.90 Hz; Fig. 4.3A). This minimum cost solution agrees well with the least squares mean step frequency of participants walking with no load [mean (95% CI): 1.89 (1.83-1.96) Hz]. The optimization model predicts a slight increase in the optimal step frequency to carry non-zero loads, since leg extension work increases (further penalizing low frequencies) while the cost of leg swing remains unchanged. The model's optimal frequency increases to 1.98 Hz (a 4.21% increase) and to 2.02 Hz (a 6.32% increase) with 30 and 50% BW loads, respectively. These compare to mean participant step frequencies of 1.94 (1.88-2.01) Hz (a 2.65% increase, $p < 0.001$*) and 2.02 (1.95-2.08) Hz (a 6.88% increase, $p < 0.001$*; Fig. 4.3B).

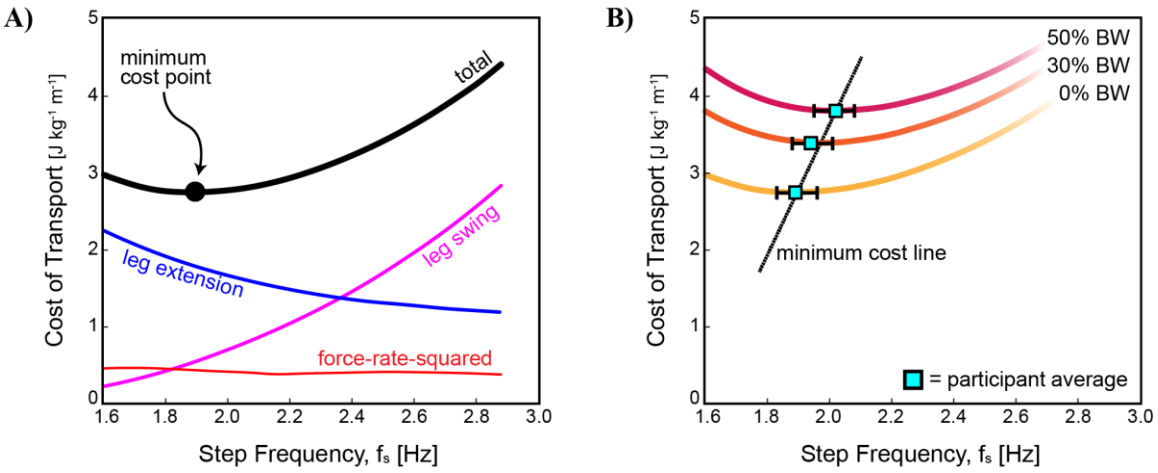

Figure 4.3. Cost of carrying loads on a rigid pole versus step frequency

A) The model's cost of transport (CoT) is shown for zero loading. The total CoT (thick black line) is composed of three components: leg extension work, blue (penalizes lower frequencies); leg swing work, magenta (penalizes higher frequencies); and a modest force rate cost, red. **B)** Total CoT is shown for 0, 30, and 50% body weight (BW) loading levels (light orange, dark orange, and dark red, respectively). Minimum cost increases proportional to load and associated step frequencies are compared to estimates from the linear mixed model (cyan squares). Error bars indicate 95% confidence intervals.

Optimized model outputs were compared to average trials of example subjects walking with varying relative step frequencies and a 50% body weight load carried on compliant poles (Fig. 4.4). Vertical CoM and load position are normalized by participant leg length and plotted alongside outputs of the optimization model used to simulate circumstances appropriate to subject- and condition-specific parameters. The CoM's average height is adjusted to match that of the model curves, and the load's average height is determined such that average spring force matches the weight of the load. Spring force in Figure 4.4 is normalized by body weight. In the examples shown, the model qualitatively matches the empirical trends reasonably well. Phase between the CoM and load positions gradually shifts from very low values ($< 10^o$) at $f_r = 0.76$ (Fig. 4.4A) to $\sim 84^o$ phase at $f_r = 1.12$ (Fig. 4.4D). A more comprehensive comparison between model outputs and participant data can be found in Figure A.1.

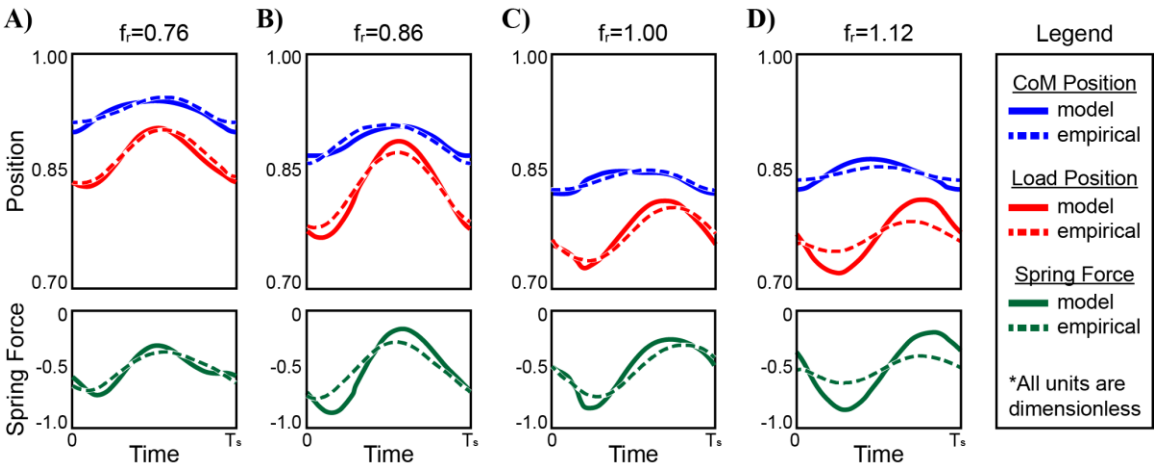

Figure 4.4. Comparing model outputs to empirical data

Average trial data are shown for four example subjects carrying 50% body weight on compliant poles. These data are compared to model outputs: vertical centre of mass (CoM) and load position and spring force. Model simulations used input parameters reflecting individual participant data (e.g. body mass, maximum allowable leg length, average walking speed, etc.; see Table A.3) and $\zeta = 0.172$. Example subjects walking at relative step frequencies: 0.76 **A)**, 0.86 **B)**, 1.00 **C)** and 1.12 **D)**. The model outputs and the empirical data show how phase between the CoM and the load shifts from being mostly in phase at $f_r = 0.76$ to approximately 84^o at $f_r = 1.12$. In general, subjects did not walk at relative step frequencies far above one (perhaps partly due to the poles being tuned to carry larger loads than those provided in the experiments). Figure A.1 shows a more comprehensive comparison of model simulations and subject data.

4.3.2 Model cost from varying pole-load spring constant

Even with constant step frequency, cost still fluctuates per the spring constant – and thus resonance – of the flexible loaded pole; the oscillation's magnitude, phase, and resulting reaction forces transferred to the body are all greatly affected by relative step frequency. Figure 4.5A shows how cost changes when the model takes the same step over a large range of pole spring constants (i.e. absolute step frequency stays constant, but relative step frequency changes due to resonance). The curves in Figure 4.5A show cost for 50% BW loading of an average participant carrying a compliant pole – low damping from (Schroeder et al., 2018) and higher damping from the fit in Figure 4.1. Similar trends were found for 30% BW loading, although the cost fluctuations were more subtle.

The global minimum cost occurs where relative step frequency is slightly above resonance ($f_r = 1.08$ for low damping or $f_r = 1.30$ for high damping) and the maximum just below ($f_r = 0.90$ for low damping or $f_r = 0.85$ for high damping; Fig. 4.5A). In the low

damping curve there is a local minimum that occurs at a relative step frequency of 0.60, just above a 2:1 harmonic, where the load exhibits low magnitude oscillations at twice step frequency (Fig. 4.5C). A 3:1 harmonic is observed where the load oscillates at three times step frequency (Fig. 4.5B). Although the harmonic frequency oscillations are too small to see in the position plot, their effect is visible in the spring force plot. Generally, out-of-phase load oscillations ($90^o \leq \phi \leq 180^o$ at $f_r > 1$) are associated with a lower cost of transport (CoT_{cmp}) relative to carrying a rigid load (CoT_{rig}). Conversely, in-phase load oscillations ($0^o \leq \phi \leq 90^o$ at $f_r < 1$) are associated with an increased CoT_{cmp}, however this increase is slightly reduced at frequencies just above the 2:1 and 3:1 harmonic points ($f_r = 0.60, 0.40$, respectively).

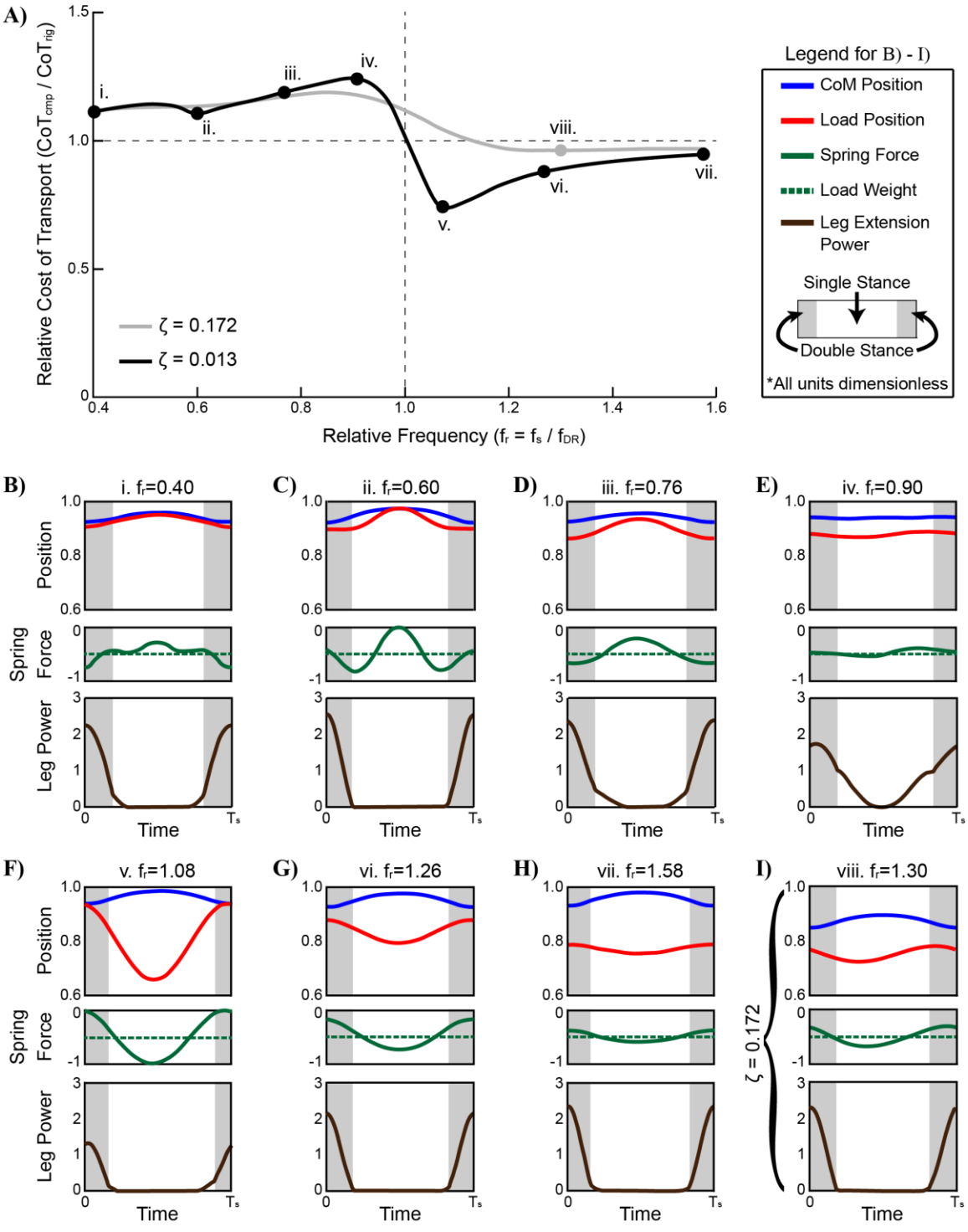

Figure 4.5. Cost of load interaction and various gait solutions presented

A) The model's cost of transport is shown for a 50% body weight load carried on a compliant pole (relative to carrying a rigid pole). Average participant parameters and step characteristics (step frequency, velocity) are used for optimizations associated with a range of pole spring constants resulting in various relative step frequencies (absolute step frequency divided by

the damped resonant frequency of the pole). The cost of transport curve is shown for $\zeta = 0.013$ [low damping from (Schroeder et al., 2018)] and for $\zeta = 0.013$ (higher damping from fit in Fig. 4.1). Note, a relative step frequency equal to one signifies that step frequency is equal to the pole's resonant frequency. Minimum/maximum costs are identified, as well as inflection points and extremes. Although higher damping seems to more accurately characterize the empirical pole carrying data presented, points of interest are mostly chosen from the low damping curve since subtle model predictions are more clearly discerned. **B-H)** Solution variables for points of interest are shown, including: body centre of mass and load positions normalized by leg length (blue and red lines, respectively), spring force and load weight normalized by body weight (solid and dashed green lines, respectively), and absolute value of leg extension power non-dimensionalized with body weight, leg length, and gravitational acceleration (brown line). Shaded regions represent double stance and unshaded regions single stance during a step (0<Time<Ts). **I)** Solution variables for the minimum of the high damping cost of transport curve are shown.

4.3.3 Model total cost of transport

Relative step frequency is the ratio of absolute step frequency to resonant frequency of the pole-load system. In Figure 4.3B, resonant frequency is constant (rigid pole) and the effect of step frequency on cost is explored. In Figure 4.5A, step frequency is constant and the effect of resonant frequency on cost is explored. However, in practice, both parameters have a simultaneous effect, since participants can choose both their step frequency as well as the pole they carry. In particular, spring constant varied from pole to pole, and this likely had a pronounced influence on the subjects' cost landscapes. Figure 4.6 shows how poles with three spring constants (lowest, average, and highest spring constant of poles in our sample) can have a dramatic effect on the shape of the total cost landscape.

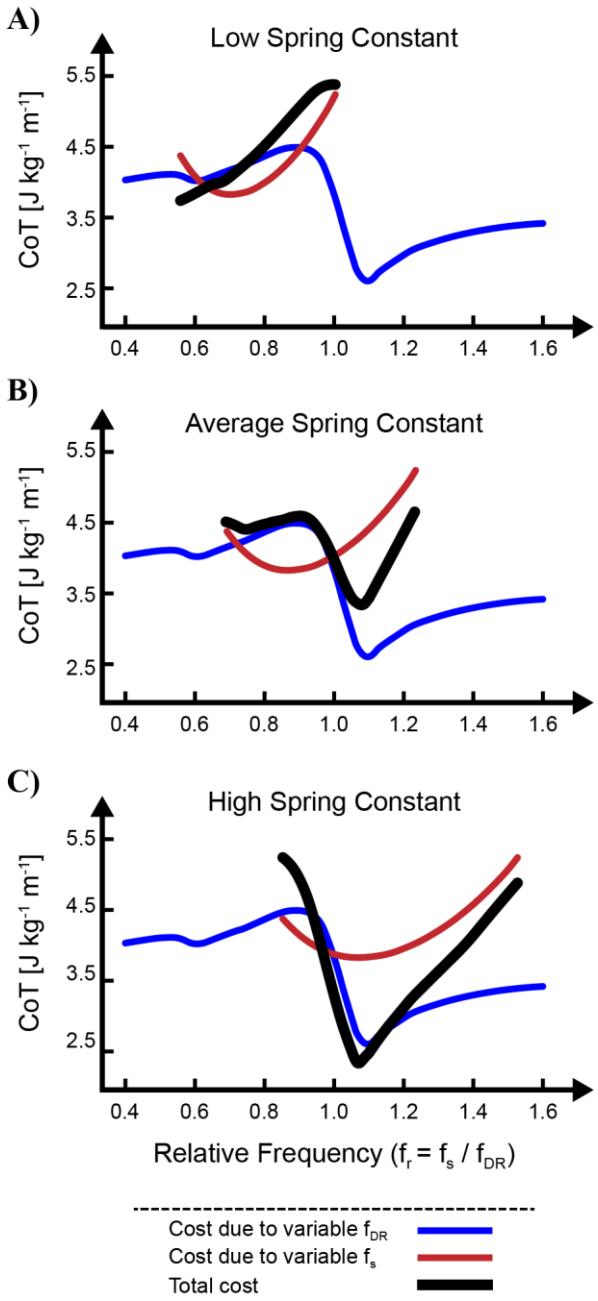

Figure 4.6. Influences on the shape of the total cost of transport

The model's cost of transport is shown for three pole spring constants: **A)** 3.66 kN m^{-1}, **B)** 5.60 kN m^{-1}, and **C)** 8.36 kN m^{-1}. Each figure panel shows how the cost effects of carrying a rigid load (red curve) and a compliant load (blue curve) interact to form the total cost (black curve) for an individual choosing step frequency with a given pole spring constant. The total cost shape varies substantially for spring constants, implying individuals carrying different poles may adopt divergent strategies to minimize cost. Note, both the red and black curves are plotted over a range of step frequencies ($1.60\ Hz \leq f_r \leq 2.88\ Hz$) for each panel.

Each panel in Figure 4.6 has three cost curves. The blue curve indicates cost for carrying a compliant pole over a large range of relative step frequencies. This cost is identical in all three panels since frequency is normalized to pole resonance. The red curve indicates cost for carrying a rigid pole over various step frequencies ($1.60\ Hz \leq f_s \leq 2.88\ Hz$). This cost is also identical in the three panels, although its relative step frequency domain is stretched depending on the resonance of the chosen spring constant. Finally, the black curve indicates how the first two costs interact to influence the total cost curve for an individual with a given pole spring constant and range of step frequencies. Even though the red and blue curves do not change cost in each of the three panels, the shape of the black curve is completely different since the red curve occurs over different segments of the blue curve and this influences the final cost. It is inappropriate to simply sum the two cost curves (i.e. red plus blue equals black), since the cost mechanisms are interdependent and may be optimized simultaneously. However, they can still be conceptualized as two influences that help to shape the total cost surface that a pole carrier navigates.

Individuals navigate different cost landscapes, not only due to differences in body mass and morphology, but also due to properties of the pole they carry. As such, participants may adapt differently depending on the pole, even if energy minimization is the overarching optimization goal.

4.3.4 Step frequency changes at local cost gradients

The effect of pole type and load on relative step frequency was statistically assessed with linear mixed models. Participants as a whole exhibited a slight significant increase in relative step frequency when switching from the rigid pole to the compliant pole [coefficient (95% CI): $\beta = 0.014\ (0.004 - 0.023)$, $p = 0.014$*]. However, when non-dimensional walking speed ($\tilde{v}$) was controlled for, this effect was diminished [$\beta = 0.009\ (\text{-}0.001 - 0.019)$, $p = 0.083$]. Additionally, one interaction term had a significant effect on frequency ($pole\ type\ x\ \tilde{v}$) while two others did not ($load\ x\ \tilde{v}$ and $pole\ type\ x\ load$; see Appendix Table A.1 for full model results). Load was also found to have a strong effect on relative frequency. However, this is unsurprising since load decreases resonant frequency which increases relative step frequency. Given our original hypotheses predict participants should respond differently (e.g. increase/decrease/no change to relative step frequency) depending on the local

slope of their cost curve, we also tested individual responses to pole type (Appendix Table A.2). Shifts in average relative step frequency (Δf_r) were used to quantify gait adaptations of individual participants carrying a compliant pole versus a rigid pole. The direction and magnitude of these shifts are compared to the local gradient, or slope, of each participant's CoT curve in Figure 4.7. A significant negative correlation was found for the 50% loading level ($R = -0.67$, $p = 0.009$*; Fig. 4.7B) with five subjects exhibiting significant changes in relative step frequency (indicated in Fig. 4.7B with magenta-filled diamonds). Specifically, three subjects had a significant positive shift (as in Q2 from Fig. 4.7), two had a significant negative shift (Q3 and Q4) and the rest were not significantly different from zero (red diamonds). This result is consistent with our hypothesis that participants adjust relative step frequency to reduce the CoT predicted by our optimization model when carrying a compliant pole. Slightly under half of the variation could be attributed to the simple linear regression shown in Fig. 4.7B ($y = -0.012x - 0.002$, $R^2 = 0.45$).

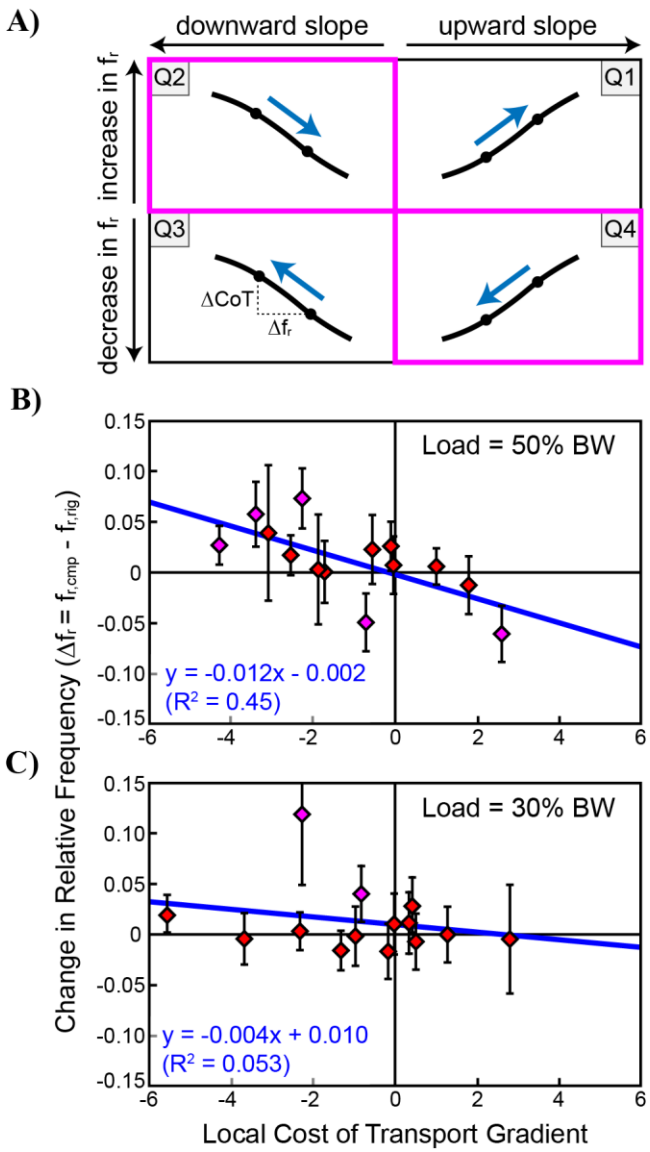

Figure 4.7. Correlation between changes in relative step frequency and local cost gradients

A) Various relationships between relative step frequency shifts (from rigid to compliant pole conditions) and cost slopes are shown. Each quadrant is labelled (Q1-Q4) to indicate either positive or negative slope (black lines) and positive or negative shifts in relative step frequency (blue arrows). It is hypothesized that participants exhibit relative step frequency shifts as illustrated in Q2 and Q4 (outlined in magenta), always pointing downhill to reduce cost. **B)** Changes in relative step frequency are compared to local cost slopes – theoretically predicted by the optimization model – for each participant (N=14) carrying a 50% body weight load. A significant negative correlation was found ($R = -0.67$, $p = 0.009$*) and a linear regression was performed ($R^2 = 0.45$). **C)** For the 30% load, a weak, non-significant negative correlation was found ($R = -0.23$, $p = 0.430$) and a linear regression was performed ($R^2 = 0.053$). Magenta diamonds indicate significant differences in relative step frequency for individual subjects while red diamonds indicate non-significant differences after adjusting p values for multiple testing. Error bars represent 95% confidence intervals.

For the 30% loading level, a weak, non-significant correlation was found ($R = -0.23, p = 0.430$; Fig. 4.7C). Just over 5% of the data's variation could be attributed to the simple linear regression ($y = -0.004x + 0.010$, $R^2 = 0.053$). Notably, changes in relative step frequency were less pronounced than in the 50% loading condition, even though they were associated with a similar range of CoT gradients, and even though two subjects exhibited significant positive shifts in their relative step frequency (magenta diamonds in Fig. 4.7C, Q1 and Q2 from Fig. 4.7A). The average magnitudes of the frequency changes are 0.020 and 0.029 for the 30 and 50% loading conditions, however the 30% condition is largely influenced by an outlier with a particularly large shift (0.119). Without this outlier, the average shift in relative step frequency is only 0.012 for the 30% loading level. For both loading levels, the y-intercepts were not significantly different from zero (95% CI: -0.020 – 0.017 for 50% BW loading, -0.012 – 0.032 for 30% BW loading). These results are consistent with our hypothesis that a zero CoT slope should not motivate a shift in relative step frequency.

4.4 Discussion

4.4.1 Model comparisons

The optimization model predicts many attributes of human gait. E.g. the mass-specific CoT of unloaded walking varies over absolute step frequency as a convex function [i.e. "bowl shape"; (Bertram, 2005)]. However, the minimum CoT (~3 J kg^{-1} m^{-1}) is somewhat higher than that of human metabolic data during walking at a similar velocity and step frequency [closer to 2 J kg^{-1} m^{-1}; (Bertram, 2005; Bastien et al., 2005)]. Although reasons behind the cost shift are unclear, the general trends are qualitatively consistent.

In our model, high step frequencies are dominated by a cost for swinging the leg and low frequencies by a cost to extend the leg (Fig. 4.3A). Previous studies have shown that average mechanical leg power and work increase proportionately to step length raised to the fourth power (Kuo, 2002; Donelan et al., 2002) for constant step frequency. Such models also predict leg work increases non-linearly at lower step frequencies, similar to our model.

Models that consider the cost of leg work and/or frequency-based cost functions for leg swing have been used to explore issues such as the velocity-step-length relationship in walking (Kuo, 2001), the cost of swinging the leg isolated from gait (Doke et al., 2005),

and running in reduced gravity simulations (Polet et al., 2018). In the former two, a force-rate cost has been proposed as a major determinant of energetic cost at higher frequencies, while the latter study indicated that a work-based cost gave more accurate predictions of kinematic outputs. Although more understanding of muscle contraction cost is needed, we opted for a work-based cost of swinging the leg simply so results could be compared more readily with leg extension work. Furthermore, both force rate and work costs give similar predictions at moderate non-dimensional velocities: ~0.38 (Kuo, 2001) and ~0.43 in the current study.

The model predicts CoT for carrying rigid loads. Previous studies have shown that cost increases linearly with load carried (Griffin et al., 2003; Bastien et al., 2005), comparable to the current model (Fig. 4.3B). The optimal frequency is also predicted to increase, since leg extension work increases (i.e. higher penalty on low step frequencies) while leg swinging work is assumed constant. Changes in step frequency were statistically validated by our linear mixed model ($p < 0.001$*), and subjects increase frequency while carrying large loads in other studies (LaFiandra et al., 2003). However, such changes are not always statistically significant (Castillo et al., 2014). A potential for type II errors may exist due to the subtlety of these effects.

4.4.2 Cost mechanisms of load interaction

When step parameters (velocity, step frequency, etc.) are held constant, the model predicts minimal CoT at $1.08 < f_r < 1.30$ (depending on damping). This agrees with work by Castillo et al. (2014) showing that large out-of-phase load oscillations (as in Figure 4.5F) contribute to a minimum CoT at $f_r = 1.21$. At this frequency, metabolic cost was reduced by ~5% when carrying a compliant bamboo pole versus a steel pole. The idea that energetic cost should be reduced at relative step frequencies just above one directly contradicts previous studies suggesting a low spring constant is optimal (Kram, 1991; Ackerman & Seipel, 2014), and that step frequencies near resonance are always most costly (Ackerman & Seipel, 2014; Li et al., 2016A). Although our model predicts maximal cost to occur just below resonance, minimal cost is predicted just above resonance, and this implies the tuning of pole properties such as spring constant can play a critical role in facilitating optimal interactions.

Tuning spring constant was also found to be important for a backpack with elastic load suspension in the fore-aft direction (Li et al., 2016B), where out-of-phase oscillations

were shown to modestly reduce mechanical power calculated from ground reaction forces. Kram (1991) found no difference in the cost of carrying load on a compliant structure made of polyvinyl chloride ($f_r \approx 3$) versus the expected cost of using a backpack with non-compliant straps. This confirms our model's prediction that the cost of carrying a compliant load approaches that of a rigid load at high relative step frequencies (Fig. 4.5A), although this may be a coincidence given Kram studied running, not walking.

Castillo et al. attributed their reduced cost findings to a relatively flat system mass trajectory, where load oscillations cancel out body oscillations. Although our results do not contradict this, we find it more insightful to consider the cost mechanisms in our model. Specifically, leg extension work is largely affected by the loading cycle felt as a force acting on the body. Figure 4.5B-I, shows the spring force of the pole transferred to the shoulder (solid green curves); damping forces are neglected in the underdamped system. These loading cycles indicate periods with relative on-loading and off-loading, where on-loading refers to spring forces more negative than the load weight, effectively heavier, (i.e. solid green line below the dashed green line; Fig. 4.5B-I) and off-loading refers to spring forces less negative than the load weight, effectively lighter (i.e. solid green line above the dashed green line; Fig. 4.5B-I).

Generally, when load oscillations are out of phase, on-loading occurs during single stance and off-loading during double stance ($f_r > 1$; Fig. 4.5F-H) resulting in a reduced CoT (relative to carrying a rigid load). Conversely, when load oscillations are in phase, off-loading occurs during single stance and on-loading during double stance ($f_r < 1$; Fig. 4.5B-D) resulting in an increased CoT. A simple explanation concerns how leg extension work accrues over a step (leg swing cost is unchanged throughout Fig. 4.5A since step frequency is constant). The absolute value of leg extension power is concentrated near double stance, regardless of relative step frequency. This is consistent with the inverted pendulum description of walking – little external mechanical work occurs during single stance and the body moves over the foot as an inverted pendulum with the leg acting as a strut (Cavagna & Margaria, 1966).

Energy loss occurs at the transition from one inverted pendulum to the next and positive leg work is done to make up the loss and maintain steady gait (Donelan et al., 2002; Kuo et al., 2001; Lee et al., 2013). Since most external work is done during double stance, leg extension cost is sensitive to loading during this transition. This helps explain why

the in-phase/out-of-phase relationship is so well correlated to cost. When on-loading occurs during double stance, the leg bears the extra load while doing work on the system mass, and this is energetically expensive. When on-loading occurs during single stance, the leg simply bears the extra load isometrically at zero work cost (there is still a force rate accommodation, but this cost is small).

For higher damping, cost is minimized even though load oscillations are only partially out of phase ($\Phi = 135^o$, Fig. 4.5I). This is because fully out-of-phase oscillations at higher damping require a much higher relative frequency (Fig. 4.1B), far removed from resonance where the amplitude is dwindling. As a result, the minimum cost solution compromises on a relative frequency that is high enough to move the oscillations somewhat out of phase but low enough (i.e. closer to resonance) to garner meaningful amplitude such that off-loading during double stance can still affect cost. Although participants in our study carried loads with oscillations mostly in-phase (Fig. 4.4, Fig. A.1), positive shifts in relative step frequency likely increased phase away from 0^o, thus reducing the amount of off-loading during double stance and contributing to a lower cost (negative cost slope: magenta diamonds in Q2 of Fig. 4.7B,C). It is unclear why subjects did not increase frequency more in order to fully converge on optimal phase relationships. Other studies have suggested physiological noise as a limitation on individuals learning gait parameters minimizing energetic cost (Simha et al., 2019).

There are a few surprising nuances that arise from the low damping solutions in Figure 4.5. Although an in-phase relationship is observed for most relative step frequencies below one, a local minimum occurs just above the 2:1 harmonic frequency ($f_r = 0.60$, Fig. 4.5C). This minimum occurs since the harmonic frequency cancels out some of the on-loading felt by the in-phase, fundamental oscillation. In Figure 4.5B, a relative step frequency slightly above the 3:1 harmonic occurs ($f_r = 0.40$). In this case, both the step frequency and the harmonic frequency are in phase with the body. The harmonics have less influence on overall cost as they occur further away from the fundamental resonant frequency, and magnitude diminishes. However, they provide an interesting subtlety to the interpretations of load oscillations and consequences for associated cost mechanisms.

Another interesting result can be found at the maximum cost point ($f_r = 0.90$; Fig. 4.5E). The oscillations of the CoM and load appear quite flat, despite their vicinity to resonance.

In fact, the load amplitude is quite large (~3.3 times that of the body; see Fig. 4.1A). At the same time, leg extension power continues well into the single stance portion of the step (unlike other solutions shown). This is consistent with a gait sometimes called "Groucho walking" (Bertram et al., 2002) characterized by a flat body trajectory and compliant legs. Groucho walking is energetically costly due to work done to excessively flex/extend the leg and reduce vertical body oscillations (Ortega & Farley, 2005; Gordon et al., 2009; Kim & Bertram, 2018). Although this solution indicates maximal cost on the curve, it is energetically minimal for the particular relative step frequency, so this is the strategy selected by the optimization model. Our interpretation is that in-phase load oscillations near resonance are so costly for leg extension work that it is cheaper to employ a flat, Groucho-like gait to avoid the excessive oscillations. A more modest example of this strategy is observed at $f_r = 0.76$ (Fig. 4.5D), providing evidence of a trade-off between costly load oscillations just below resonance and costly leg extension work associated with a flat gait. Foissac et al. (2009) observed similar gait in subjects carrying a flexible backpack load, where vertical trunk excursion was reduced at walking speeds stimulating resonance and energetic cost increased.

Although Groucho walking is one way to avoid costly large amplitude in-phase oscillations near resonance, another strategy is to simply reduce relative step frequency. Even though such adjustments bring phase even closer to zero, they reduce oscillation amplitudes mostly in phase anyway and this reduces cost (positive cost slope: $f_r < 0.9$, Fig. 4.5A). It appears that most subjects did not use this strategy to reduce cost; however, one subject significantly reduced relative step frequency on a positive cost slope (Fig. 4.7B: magenta diamond in Q4).

4.4.3 Relative step frequency shifts in response to cost gradients

Relative step frequency shifts at local cost gradients are summarized in Figure 4.7. A significant correlation was found for 50% BW loading, but not for 30%. Given that CoT is generally higher for increased loading levels, it is possible that this plays a role in the sensitivity of individuals to adapt gait. However, our hypothesis was that participants follow the gradient downhill, regardless of cost. In other words, if there are cost savings available, why do experienced pole carriers not take advantage of them at 30% BW load?

It is likely that individuals—even experienced pole carriers—are only sensitive to cost savings at a certain threshold. Indeed, many participants walked at relatively flat cost gradients and did not adjust frequency much. It is unclear if participants recognized there were no lower cost solutions nearby, or if they were simply insensitive to shallow gradients. There are also examples of large CoT gradients where participants exhibited little response. The simple regression slope can be conceptualized as the sensitivity of the participant sample to their CoT gradient. However, it is likely that individuals have varying sensitivities to such gradients, characterized by individual slope values. A study with larger load levels or longer carrying durations might have clearer results. We were reluctant to overload participants even though many were used to carrying much greater loads (sometimes their own body weight or more) for substantial distances (kilometers). Indeed, for an average participant carrying a 100% BW load, our model predicts energy savings of approximately 18% (3.92 J kg^{-1} m^{-1} with a compliant pole versus 4.79 J kg^{-1} m^{-1} with a rigid pole).

Alternatively, the model may not account for all relevant costs associated with carrying a compliant bamboo pole during walking: e.g. costs to steady swaying load baskets or for balancing the pole on the shoulder (Li et al., 2019B). We assumed experienced pole carriers are adept and that such costs are secondary to the work-based costs implemented in the model. Using a rigid pole for comparison to the compliant pole, as opposed to a load rigidly fixed to the body (backpack), helped account for such potential extra costs.

Experienced pole carriers are likely not only trying to optimize energetic costs. Individuals might choose to carry loads with a compliant suspension system to reduce peak reaction forces felt at the shoulder (Rome et al., 2005; Rome et al., 2006; Kram, 1991). Such reaction forces were approximated with kinematic data from our participants. On average, participants did see a reduction in peak shoulder forces when carrying the compliant pole versus the rigid pole (for 50% loading: 18.0%, or -75 N; for 30% loading: 12.7%, or -31 N). It is unclear how much these changes were influenced by shifts in relative step frequency. Our model predicts changes in the peak shoulder reaction force due to shifts in relative step frequency alone. For the case of 50% BW loading, an average reduction of -4.5 N (1.2%) was found, however this average was largely dominated by two participants, without whom a slight increase in the reaction force was found: 0.4 N. For the case of 30% BW loading, only a -0.6 N (0.3%) reduction

was found. Although shifts in relative step frequency had little influence on this effect for either load condition, participants likely experienced a sizeable reduction in peak shoulder forces when switching from rigid to compliant pole.

4.4.4 Limitations

We hypothesized that changes in step frequency correlate with theoretical cost gradients predicted by a work-minimizing model. However, there are many reasons why step frequency changes occur. Stability is one alternative, since step frequency changes are often associated with destabilizing perturbations (McAndrew et al., 2010; Hak et al., 2012). Recent studies exploring coupled-oscillator models have shown that walking stability is decreased with lower spring constants (Ackerman & Seipel, 2011A). At the same time, it is unclear what strategies, if any, experienced pole carriers use to stabilize load oscillations. The natural carrying style of resting a hand on top of the pole may be an effective stabilizing strategy, thus eliminating the need to adjust step frequency to avoid instability. Although the current study did not formally evaluate stability, there were no obvious examples of instability during trials. Further empirical studies are needed to investigate this complicating issue.

Another gait feature highly associated with changes in step frequency is walking speed. One goal of the study was to measure experienced bamboo pole carriers in a more ecological setting (i.e. not artificially in a laboratory); as such, subjects were not constrained to walk at fixed speeds, etc. However, we did attempt to control for speed variation in our statistical models. Non-dimensional walking speed ($\tilde{v}$) had a strong significant effect on relative step frequency [$\beta = 0.447\ (0.253 - 0.640)$, $p < 0.001$*], and the inclusion of this covariate diminished the effect of pole type on frequency. However, an interaction between pole type and $\tilde{v}$ was also found to have a strong effect [$\beta = 0.285\ (0.147 - 0.424)$, $p < 0.001$*]. Our interpretation is that individuals vary walking speed as a means to economically change relative step frequency when switching pole type from rigid to compliant. In other words, it is less costly to increase step frequency at higher speeds than it is to do so at a constant speed (and vice versa). This is supported by studies showing that the metabolic cost of walking is minimized when speed covaries with frequency for a given task constraint (Bertram, 2005).

There are numerous simplifying assumptions that may affect the results in this study. Morphology complexities were neglected in favor of a reductionist model. A telescopic

leg replaced complicated flexion/extension of the knee and ankle during walking [e.g. soleus and gastrocnemius contraction toward the end of stance (Winter, 1991)]. Hip actuators could also have applied torque during stance and swing phases. This cost was somewhat accounted for in the model proposed by Doke et al. (2005) where torque work was derived from pendular motions (see Methods for details). Other simplifying factors include a point mass body (zero mass moment of inertia), no distribution of the load along the length of the pole, non-slip foot contacts, and planar sagittal motion only. Although each of these issues has the potential to influence system dynamics and its energetic cost, there are no obvious indications that such considerations are vital to the topic. More complicated models can be used to probe such issues in future studies.

A practical limitation was access to equipment in the field. Metabolic measurements of energy consumption would provide more robust evidence of cost reductions supporting our hypotheses. Without direct measurements, all inferences regarding energy cost are theoretical. Although a primary goal of the study was to allow experienced pole carriers to walk “naturally” (i.e. minimal experimental constraints), this limited the capacity to control for confounding variables and other complications. Future experiments could test learning strategies with more clear cost incentives in a controlled protocol.

4.5 Conclusions

We developed a trajectory optimization model to determine the theoretical CoT for individuals carrying compliant and rigid bamboo poles. We used the model to explore energetic consequences of carrying a rigid pole with various loads over a range of step frequencies. We also explored the energetic consequences of carrying poles with varying spring constants and relative step frequencies. The model considers costs due to leg extension work, leg swing work, and a force-rate-squared cost. This mechanistic perspective was used to interpret reduced costs associated with the alignment of force on-loading and off-loading the body at different portions of the gait cycle. Since the majority of leg extension power is performed during double stance, it is beneficial to be off-loaded during this time, and this occurs most notably in a range of relative step frequencies slightly above resonance where the load and CoM oscillate out-of-phase. Higher order harmonics also affect the CoT, although these effects are modest. Finally, the model predicted changes in relative step frequency as a means for reducing energetic costs associated with the task. Pearson correlations revealed a significant

negative correlation between the change in relative step frequency and the local CoT gradient with 50% BW loads. A weak, non-significant negative correlation was also found for 30% BW loads.

Ultimately, direct evidence of gait adaptation associated with empirical reductions in metabolic cost are required. Such experiments will provide additional validation to the cost mechanisms identified here. Regardless, a theoretical framework for understanding optimal body-pole-load interactions has been proposed that can explain various aspects of gait adaptation during load carriage with a flexible pole.

CHAPTER 5

Human-machine Coupled Oscillations: Cost, Sensitivity and Limits to Entrainment

5.1 Introduction

Human locomotion is an oscillating system, where components of the body and the body itself exhibit cyclical motions. In particular, step frequency and step length are two parameters that fundamentally characterize the oscillation. The former refers to the frequency with which foot contacts are made in time and the latter to the distance the body's centre of mass (CoM) travels during a step. There is direct empirical evidence that humans choose particular combinations of step frequency and step length that minimize the metabolic cost per distance, or cost of transport (Bertram & Ruina, 2001; Kuo, 2001; Bertram, 2005). Furthermore, there is emerging evidence that individuals can adapt gait characteristics and optimize energetic exertion in real time. For example, individuals wearing a knee exoskeleton can adapt their step frequency in response to variable resistance at the joint and reduce metabolic consumption (Selinger et al., 2015; Selinger et al., 2019). The same research group has shown similar results with an actuator system that applies gradual pulling forces in the fore-aft direction to provide either metabolic penalties (pulling backward) or rewards (pulling forward) to elicit gait adaptation that results in metabolic energy reductions (Simha et al., 2019).

These studies utilized systems providing quasistatic perturbations that gradually encouraged individuals to adjust their movement patterns, evidently to minimize energy spent on the task. Although it is true that humans mostly tend to interact with static environments in the real world (e.g. a sidewalk or a staircase, etc.), it would be useful to explore gait adaptations of individuals in more dynamic environments as well. Here, we used a machine oscillator system to provide periodic forces to the trunks of human subjects via a body harness attached to a pulley-cable system and two linear servomotors. The coupling of an oscillating human, who rises and falls with every step, with a machine that pulls up and down with periodic actions constitutes a coupled oscillator system. Humans have been shown to respond to coupled oscillator systems before, albeit more commonly in passive systems; for example, individuals exhibit spontaneous entrainment (i.e. synchronization) with one another when walking on an

undulating flexible pedestrian bridge (Dallard, et al., 2001), just as children learn to adjust the timing of their jumping on a trampoline, so as to increase time in the air. Similarly, infants can learn over time to bounce at the resonant frequency of an elastic harness (Goldfield et al., 1993). Other researchers have found that elastic suspension systems have the potential to improve gait by reducing metabolic cost and/or peak interaction forces in individuals carrying loads in a backpack (Rome et al., 2005; Rome et al., 2006; Li et al., 2016B; Martin & Li, 2018; Li et al., 2019A), on a flexible pole (Kram, 1991; Castillo et al., 2014), or in a hand held load carriage device (Ackerman et al., 2015).

Similar to pedestrians entraining their steps on a flexible bridge, previous studies have used treadmills actuated with controlled oscillations in mediolateral (Peters et al., 2012) and vertical directions (Nessler et al., 2017; Tackett, 2018). These studies showed various levels of entrainment and intermittent phase-locking with the dynamic substrate. Vertical oscillations were associated with higher levels of entrainment when compared to gait synchronization observed in individuals walking on treadmills placed side by side (78.7±8.3% versus 59.2±17.4% of a trial's duration, respectively; Nessler et al., 2017). When high-amplitude noise (i.e. variability; >15%) was added to the time period of the treadmill's oscillation, subject entrainment was significantly degraded (Tackett, 2018).

Exoskeletons have also been used to encourage gait adaptation in coupled oscillator systems. Ahn and Hogan (2010, 2012) used an ankle exoskeleton to provide periodic torque profiles at the ankle joint independent of the subject's actions. Overtime, subjects learned to entrain to the periodicity of the exoskeleton and align their own push off forces with that of the artificial system. Although this study showed that human subjects can entrain to periodic force profiles, it remains unclear what mechanisms motivate such entrainment patterns and why the interactions are chosen as they are. For example, entrainment with a periodic signal can be accomplished by aligning forces anywhere in the gait cycle; in other words, phase is unconstrained, even when two periodic signals become entrained. In this work, we explored the phase interactions chosen by subjects as well as some motivations for why particular interactions might have been preferred over others. We also quantified metabolic energy consumption and mechanical work from interactions with the environment to ultimately inform a discussion regarding the link between mechanics, physiology and locomotor control.

To help contextualize the results of experiments performed in this study, a reductionist trajectory optimization model was used to make predictions about optimal phase relationships and interactions between the human and the machine oscillator system. Such models have had recent success in predicting gait features that minimize energy consumption: e.g. step-length-velocity combinations associated with walking and running gaits (Srinivasan & Ruina, 2006), characteristics of locomotion on gradients (Hasaneini et al., 2013), strategies of bipeds navigating a shaking platform (Joshi & Srinivasan, 2015), velocity profiles of a rimless wheel model navigating rough terrains (Darici et al., 2018) and even manoeuvres associated with the urban sport parkour (Croft et al., 2019). In the current study, predictions by the optimization model were compared to strategies employed by human subjects interacting with the real-world oscillation system.

The experiments were designed to systematically define a basin of entrainment (i.e. parameter space where entrainment occurs) described herein. To do this, we impart forces to subjects over a broad range of parameters (amplitude, frequency) in order to characterize the boundaries of the entrainment basin and the sensitivity of subjects to that basin. Three experiments were conducted on two samples of human participants. Experiment 1 was designed to test if individuals choose to adapt their stepping characteristics by entraining to the motor frequency prescribed in various testing conditions. Metabolic measurements were collected to test if reductions in energetic exertion are associated with entrainment and the particular interaction chosen by participants. Experiments 2 and 3 systematically varied oscillation parameters (e.g. motor frequency, amplitude) gradually over time to characterize a region of circumstances that lead to gait entrainment (i.e. basin of entrainment). Experiments 2 and 3 used a different sample of subjects than the first, in order to limit undesired exposure to the system prior to testing.

As opposed to a machine strapped to a single joint (e.g. ankle), the oscillation system in this work is used to interact directly with the trajectory of the body CoM – arguably the most fundamental aspect of the task of locomotion (Croft et al., 2017) – to directly assess locomotor control strategies driving interactions within a dynamic environment.

5.2 Methods

5.2.1 Machine oscillator system

A custom pulley-cable system (see Fig. 5.1) was built to connect a person wearing a body harness to two linear servomotors (Nippon Pulse America Inc., Radford, Virginia USA; model: S320T). Each actuator was activated to create varying tension in the system (one pulling up on the individual, one pulling down). The harness tension acted as a periodic perturbation applied to subjects walking on a treadmill. The cable pulling upward was attached to the body harness via a padded aluminum bar with straps attached at the sides of the subject but with enough space for the arms to swing freely (Fig. 5.1). The cables pulling downward were connected to the body harness near the waist at oblique angles in the frontal plane (approximately 75˚ from horizontal, depending on the waist height of the subject; Fig. 5.1). Thus, horizontal components of the tension vectors largely cancelled out; any net mediolateral forces due to asymmetry were neglected. All three cables (one pulling up, two pulling down obliquely) were redirected via pulleys mounted on carts that could roll in the fore-aft direction so the subject could drift slightly on the treadmill without altering the loading direction.

Even when the motors were inactive, their weight created a small tension in the cables. Due to motion coupling between the individual and the actuators, subjects also experienced added inertia in the vertical direction while walking in the system. The mass of each actuator and its associated hardware was approximately 2.2 kg (~3.3% of an average subject's body mass) and so contributed to an increased inertial resistance in the vertical direction. The motors were mounted to aluminum plates supported by ball-bearing linear guides (Chieftek Precision Co., LTD., Chino, California USA) so as to fix motion in the vertical direction. The actuators were controlled by a duel-axis motion controller (Galil Motion Control, Inc., Rocklin, California, USA; model: DMC-4123) with sinusoidal amplifiers (model: D3520). Additionally, a direct current power supply (Advanced Motion Controls, Camarillo, California, USA; model PS16L80) was used to power the actuators.

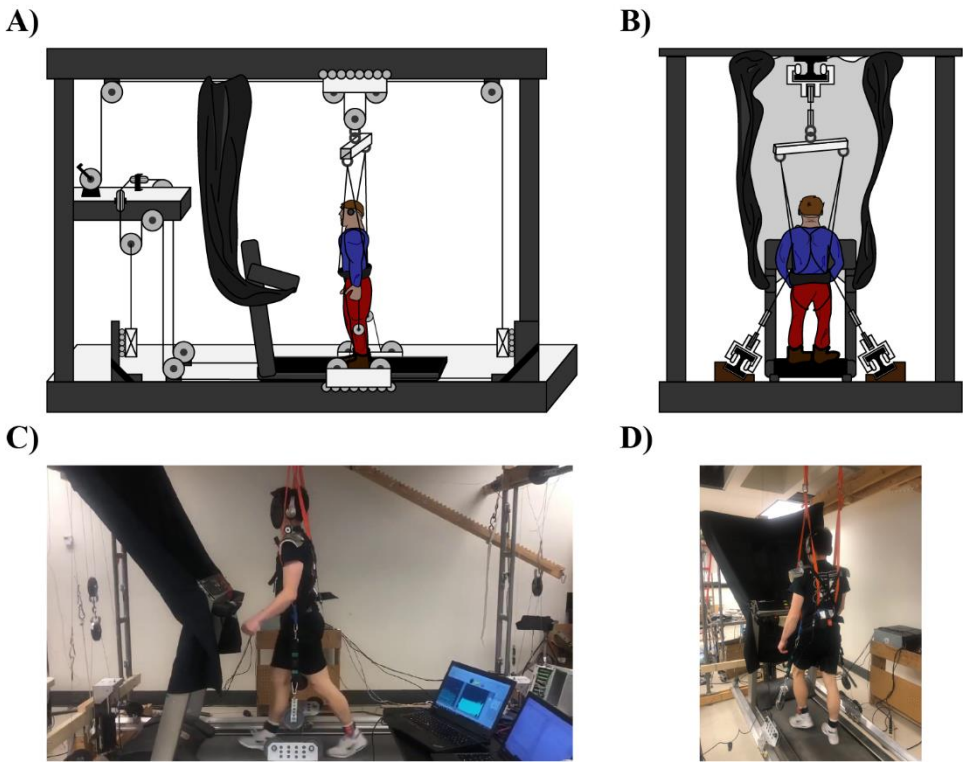

Figure 5.1 Oscillator system schematic and images

The oscillator system is depicted as a schematic from a side view **A)**, and from behind **B)**. Images of a subject walking in the system during a trial, from a side view **C)** and from behind **D)**. A curtain was used to blind the subject from any motion of the oscillators, and headphones were used to play ambient noise so as to block out rhythmic sounds from the system. The headphones were also used to play a metronome beep during portions of one of the experiments.

5.2.2 Current motor control

The motion controller was programmed to send a sinusoidal current signal, $I(t)$, to the motors as desired.

$$I(t) = I_m \cos(2\pi f_m t) \tag{5.1}$$

where I_m is the amplitude of the prescribed current signal, f_m is the motor frequency and t is time. The commanded signal was distributed between both motors (one pulling up, one pulling down – motors B and A, respectively). For example, when an upward force was desired, the sinusoidal signal was prescribed to motor B while a constant current (I_{nom}) was prescribed to motor A to maintain nominal tension in the pulley-cable system. When a downward force was desired, the motors switched roles.

$$I(t) = I_B(t) - I_A(t) \tag{5.2}$$

$$I_B(t) = \begin{cases} I(t) + I_{nom} & , \quad I(t) \geq 0 \\ I_{nom} & , \quad I(t) < 0 \end{cases} \tag{5.3}$$

$$I_A(t) = \begin{cases} I_{nom} & , \quad I(t) \geq 0 \\ -I(t) + I_{nom} & , \quad I(t) < 0 \end{cases} \tag{5.4}$$

where $I_B(t)$ is the current prescribed to motor B (pulls up) and $I_A(t)$ is the current prescribed to motor A (pulls down), both as time-varying functions. Current amplitude was prescribed in units of body weight force (BW) after multiplying by the motor force constant (K_f) and dividing by the subject's BW.

$$A_m = \frac{I_m K_f}{m_c g} \tag{5.5}$$

where m_c is the subject's body mass and A_m is the current amplitude in units of BW. The desired current signal was prescribed with an open loop control. Force feedback was not implemented for simplicity; however, tension forces in the pulley-cable system were monitored throughout all experiments.

5.2.3 Optimization model

The reductionist trajectory optimization model was inspired by previous models used to simulate human locomotion (Srinivasan & Ruina, 2006; Srinivasan, 2011; Hasaneini et al., 2013; Croft et al., 2019). It utilized a point mass to represent the human body (i.e. CoM) and two massless telescoping legs that can extend to perform positive work on the CoM or actively resist compression to perform negative work (Fig. 5.2). The inertia of each motor was modelled as a point mass, and the dynamics of the oscillator system were approximated with a spring-damper mechanism connecting each motor to the CoM, one with tension pulling up and one with tension pulling down (Fig. 5.2).

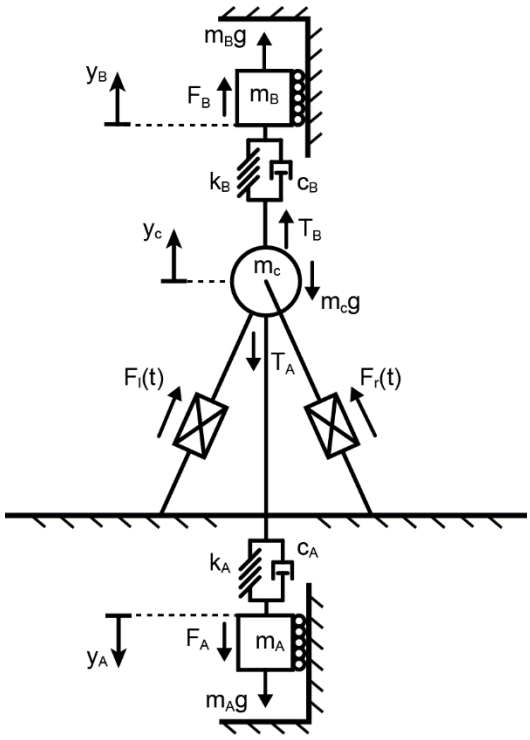

Figure 5.2. Optimization model schematic

The figure shows two massless telescopic leg actuators and a point mass body connected to two mass-spring-damper elements representing the actuators in the oscillator system. Gravity acts down on m_c, the centre of mass (CoM), and down on the mass of motor m_A but *up* on motor m_B in this schematic. In reality, motor m_B hung from a cable in the pulley system, but its weight and motor forces pulled up on the CoM. Thus, its weight vector is pointing up here to reflect this. Motor m_A is shown, oriented in the natural direction where its weight vector points down.

The parameters of the spring and damper elements were determined through independent tests of the system (see Appendix B.1 for more details). Additionally, external forces were applied to the motor point masses as a simplified representation of actuation force due to armature current. A cosine waveform force profile was prescribed in the system similar to Eqs. (5.1-5.4).

$$F_m(t) = A_m \cos(2\pi f_m t + \phi) \tag{5.6}$$

where $F_m(t)$ is the motor force as a function of time, A_m is the amplitude of motor force, f_m is the motor frequency and ϕ is the motor phase (zero phase is aligned with the middle of double stance, approximately at peak ground reaction force). The motor force profile was distributed between both actuators in time. While one actuator pulled with

force from the cosine waveform, the other performed a constant nominal force ($F_{nom} = 10\%\ BW$) to keep the system taut.

$$F_m(t) = F_B(t) - F_A(t) \tag{5.7}$$

$$F_B(t) = \begin{cases} F_m(t) + F_{nom} & , \quad F_m(t) \geq 0 \\ F_{nom} & , \quad F_m(t) < 0 \end{cases} \tag{5.8}$$

$$F_A(t) = \begin{cases} F_{nom} & , \quad F_m(t) \geq 0 \\ -F_m(t) + F_{nom} & , \quad F_m(t) < 0 \end{cases} \tag{5.9}$$

The equations of motion for the system are shown below.

$$\begin{bmatrix} m_c\ddot{x}_c \\ m_c\ddot{y}_c \\ m_B\ddot{x}_B \\ m_B\ddot{y}_B \\ m_A\ddot{x}_A \\ m_A\ddot{y}_A \end{bmatrix} = \begin{bmatrix} \sum_{(i=l,r)} F_i \left(\frac{x_c - x_{fi}}{L_i}\right) \\ \sum_{(i=l,r)} F_i \left(\frac{y_c}{L_i}\right) + T_c - m_c g \\ 0 \\ F_B + m_B g - T_B \\ 0 \\ F_A + m_A g - T_A \end{bmatrix} \tag{5.10}$$

where m_c is body mass, F, L and x_f are leg forces, instantaneous leg length and foot contact positions for the left (l) and right (r) legs, x and y refer to horizontal and vertical position of point masses for the body and the two motors (subscripts c, B, and A), T_c refers to the net harness tension felt by the body ($T_c = T_B - T_A$), T_B is the tension force pulling the CoM up, T_A is the tension force pulling the CoM down, F is the actuator force for motors A and B (subscripts), and g is gravitational acceleration ($9.81\ m\ s^{-2}$). All dot accents refer to time derivatives of their respective variables. Tension forces are the summation of spring and damping forces for each motor.

$$T_B = k_B(y_B - y_c) + c_B(\dot{y}_B - \dot{y}_c) \tag{5.11}$$

$$T_A = k_A(y_A + y_c) + c_A(\dot{y}_A + \dot{y}_c) \tag{5.12}$$

where k and c are the spring constant and damping coefficient, respectively, for motors A and B. Net mechanical work transferred to the CoM from the harness tension was calculated.

$$W_c = \int_0^{T_s} T_C \dot{y}_c \, dt \tag{5.13}$$

Instantaneous leg length (L) and its time rate were derived with kinematic variables.

$$L = \sqrt{\left(x_c - x_f\right)^2 + y_c^2} \tag{5.14}$$

$$\dot{L} = \frac{(x_c - x_f)\dot{x}_c + y_c \dot{y}_c}{L} \tag{5.15}$$

The model optimizes the leg forces over a single step (assuming left and right steps are symmetrical). The body begins at $x_c = 0\ m$ and ends at $x_c = d_s$, where step length is defined as the total distance the body CoM travels over a single step: $d_s = \frac{v}{f_s}$. Here, v is the average forward velocity, and f_s is step frequency. To enforce a given velocity, time begins at $t = 0s$ and ends at $t = T_s$, where T_s is the inverse of step frequency. Foot contact positions were defined for the left (l), the right (r), and the left leg again, for the next step (n): $\begin{bmatrix} x_{fl} \\ x_{fr} \\ x_{fn} \end{bmatrix} = \begin{bmatrix} -0.5 \\ 0.5 \\ 1.5 \end{bmatrix} d_s$. These foot contact positions define the initial position of the body CoM to begin at the middle of double stance (i.e. dual contact phase) at $t = 0\ s$.

In addition to initial and final conditions associated with the optimization of a step, multiple constraints were imposed on the model. For example, a path constraint was used to ensure that leg length never exceeded a maximal value while it produced force.

$$F(L_{max} - L) \geq 0 \tag{5.16}$$

Additionally, leg forces were only allowed to be positive (i.e. extension forces only); however, no constraints were placed on simultaneous leg forces (i.e. double stance was allowed). Other constraints were applied to enforce that final states (position, velocity, etc.) equaled initial states. This was done to ensure that only steady state gaits were considered. Boundaries were set for the vertical position of the CoM to prevent penetration with the ground.

$$y_c > 0 \tag{5.17}$$

The optimization modulated leg forces until it was satisfied the cost function was minimized. The cost function (J) comprised of the absolute value of mechanical work due

to extension forces from the legs (W_e), where positive and negative work were divided by the differential efficiency of muscle during concentric and eccentric contraction (Margaria, 1976), and also a force-rate-squared cost term (FRS), used to penalize extremely impulsive forces, summed for both legs.

$$J = \int_0^{T_s} \left(\dot{W}_e + FRS \right) dt \tag{5.18}$$

$$\dot{W}_e = F\dot{L} \tag{5.19}$$

$$FRS = \epsilon \dot{F}^2 \tag{5.20}$$

where $\dot{W}_e$ is the mechanical power of leg extension, F and $\dot{F}$ is the telescopic leg force (the control variable in the model) and its time rate, respectively, $\dot{L}$ is the contraction velocity of the leg and ϵ is an arbitrary small number used to scale the force-rate-squared cost term. The positive and negative components of mechanical leg power were summed to get the absolute value of power ($\dot{W}_e = \dot{W}_e^+ - \dot{W}_e^-$) and $\epsilon_o \dot{W}_e^+ \dot{W}_e^-$ was added to the cost function, where ϵ_o is an arbitrarily small number. The addition cost term did not contribute to overall cost since it was always driven to zero in all optimization; however, it ensured that positive and negative power could not be performed unrealistically by the same leg at the same time.

Including the FRS term in the cost function smoothens out leg forces that would otherwise be extremely impulsive – both physiologically unrealistic and numerically challenging for the optimization. As such, its implementation is mostly practical. However, there is emerging evidence that some form of this cost does indeed exist, perhaps as a consequence of energy required during sarcoplasmic reticulum ATPase activity (i.e. calcium transport) during muscle contraction (Dean & Kuo, 2011; Doke & Kuo, 2005; Doke & Kuo, 2007). Other gait optimization models have utilized similar costs in their objective functions (Rebula & Kuo, 2015; Handford & Srinivasan, 2018). In optimizations performed here, the scaling constant of the FRS term was hand-tuned so that peak CoM accelerations approximately matched data from humans performing natural, unperturbed walking.

Optimizations were conducted over a range of motor oscillation parameters, including motor phase ($-180^o \leq \phi \leq 180^o$, increments of 45^o) and amplitude ($A_m = 10, 30\%\ BW$).

Another optimization was conducted where motor phase was not prescribed, but rather was included in the model as a decision variable to determine optimal phase. Motor frequency was matched to that of an average subject's preferred step frequency, so all solutions illustrated interactions associated with an entrained gait. An additional optimization was conducted where zero motor force was applied, although tension fluctuations could still be experienced due to the motors' inertia connected to the spring-dampers. Other parameters of the model (e.g. body mass, maximum allowable leg length, etc.) were matched to values measured in subjects that performed the experiments. All variables and equations were non-dimensionalized with the average body mass and leg length of subjects, as well as with gravitational acceleration ($9.81\ m\ s^{-2}$).

The trajectory optimization procedure was implemented in MATLAB using a sparse nonlinear optimizer program [SNOPT (Gill et al., 2005)] in conjunction with GPOPS-II (Patterson & Rao, 2014) for problem discretization and setup. In order to procure robust solutions, a two-part optimization regime was used. The first part implemented fifteen random initial guesses to test for global optimality, and the second perturbed the prevailing optimum fifteen times with random noise in order to fine tune the solution's local optimality. This procedure was employed for every optimization performed.

5.2.4 Participants

A convenience sample of ten healthy university students (five males, five females) were recruited for Experiment 1 with the machine oscillator system including metabolic testing. The mean [± 1 standard deviation (SD)] height of subjects in this sample was 1.71 ± 0.07 m, leg length was 0.91 ± 0.06 m, weight was 65.7 ± 12.2 kg, and age was 26.2 ± 2.9 years. A second sample of eleven healthy university students (six males, five females) were recruited for Experiments 2 and 3 with the machine oscillator system (sensitivity and limits to entrainment tests). One participant was unable to complete the experimental protocol due to a scheduling conflict and was thus, excluded from the analysis. The mean (± 1 SD) height of the remaining ten subjects in the second sample was 1.72 ± 0.07 m, leg length was 0.90 ± 0.03 m, weight was 67.1 ± 7.70 kg, and age was 25.8 ± 4.4 years. Full subject data can be found in Table B.1.

Exclusion criteria for the experiments included any previous or ongoing musculoskeletal injuries or neurological conditions affecting gait or the ability to carry sizable loads in a

conventional backpack. All participants in both samples provided informed consent to participate, and these studies were approved by an ethics review board at the University of Calgary (REB16-1517).

5.2.5 Measurements and analysis

Inertial measurement units, or IMUs (Xsens Technologies B.V., Enschede, The Netherlands) were placed along the body, one just above each ankle and one at the lower lumbar region of the back. The ankle sensors were used to detect signal peaks and calculate step frequency as the inverse of the time period between peaks. The sensor at the back was used to approximate motion of the centre of mass (CoM). These data were integrated twice over time to get velocity and displacement, and a moving average filter (window set to the time period of the oscillations) was subtracted from the raw signals to adjust for any drift offset in the sensors. All IMUs logged data at an acquisition rate of 100 Hz. Step frequency measurements were smoothed with a moving average filter (averaging window of ±5 steps on each data point) to more clearly illustrate step frequency trends over time. Additionally, step frequency (f_s) was reported relative to the subject's preferred cadence (f_p) measured in a baseline trial at the beginning of data collection (see Baseline trials section for more details).

$$f_r = \frac{f_s}{f_p} \tag{5.21}$$

Custom in-line tension transducers were built with strain gauges (Micro-Measurements CEA-06-125UW-350, Wendell, NC, USA) configured in half-bridge circuits. The strain gauges were epoxied to C-shaped steel hooks and were used to measure tension applied to the body harness from the pulley-cable system (Fig. 5.1). One transducer measured tension pulling down and another measured tension pulling up. The strain gauge signal was passed to a strain conditioning amplifier (National Instruments, SCXI-1000 with SCXI-1520 eight-channel universal strain gauge module connected with SCXI-1314 terminal block, Austin, Texas USA), digitized (NI-USB-6251 mass termination) and acquired in a custom virtual instrument in LabVIEW (National Instruments) at an acquisition rate of 100 Hz. The tension transducers were calibrated with a known set of weights before every testing session, and a linear regression was performed to quantify the conversion factor from volts into Newtons force.

At the beginning of each trial, a few seconds of data were collected where the subject stood still before starting the treadmill. During this time, the transducer signals measured force from the motors' weight in the system plus nominal tension from the motors pulling the system taut. This initial tension was averaged over a five second interval and subtracted from the subsequent signal in the trial.

Next, the force data were multiplied by the vertical velocity processed from the CoM IMU to calculate mechanical power provided to subjects in real time. Vertical oscillation cycles were distinguished by identifying peaks in the vertical acceleration channel of the CoM IMU throughout every trial. Tension forces, kinematics and mechanical power were all segmented into blocks of data comprising every step cycle identified in all trials. These data were interpolated at regular intervals matching the average resolution of the raw data collection (typically around 55 data points per step cycle, or approximately 0.01 s). This allowed the signals to be averaged over the step cycle whilst maintaining the original resolution of the raw data collection. Since step cycles were bounded to the peak vertical acceleration of the CoM, this meant that time zero in the step cycle occurred at around the middle of double stance.

Furthermore, the motion controller driving the actuators was programmed to send a pulse signal to the National Instruments data acquisition system at the initiation of every current cycle to the motors. This allowed for accurate data synchronization between the two systems as well as with the Xsens system, since the LabVIEW virtual instrument was programmed to initiate data collection in the IMUs at the beginning of each trial. The motor phase (ϕ) in the gait cycle was also calculated by subtracting the timing of each pulse signal from the timing of peak vertical CoM acceleration, dividing by the time period of the CoM oscillation and multiplying by 360^o.

$$\phi_i = \frac{t_{p,i} - t(\max(\ddot{y}_C)^-)}{T_{s,i}} 360^o \tag{5.22}$$

where ϕ_i is the phase associated with an individual pulse signal, $t_{p,i}$ is the timing of that pulse indicating the initiation of motor current in the cosine waveform, $t(\max(\ddot{y}_c)^-)$ is the timing of a vertical CoM acceleration peak occurring just before $t_{p,i}$ and $T_{s,i}$ is the time period of the current step. Due to dynamics of the system, there was often a slight delay from when current was driven to the motors to when tension force spiked in the harness. The average duration of the delay was calculated for individual subjects and trials and

phase data were shifted for each as appropriate. Plots including phase data in this manuscript indicate when this shift was applied. When no shift was applied, no indication is given.

Oxygen consumption and carbon dioxide elimination rates were measured using a commercial metabolic analysis system (TrueMax 2400, ParvoMedics, Salt Lake City, UT, USA) during Experiment 1. A ten-minute baseline measurement was taken for subjects standing quietly and still. All trial conditions were designed to last for at least five minutes of data collection. This allowed the metabolic data to reach a steady state before calculating mean and SD values on the remainder of the trial (typically the last two minutes of the trial condition being tested). The oxygen consumption rate in $ml\ O_2\ s^{-1}$ was multiplied by a factor of 20.1 to convert to SI units in Watts and the baseline quiet standing measurement was subtracted from the gross measurement of each trial condition. Net metabolic power was then non-dimensionalized by dividing belt speed and subject BW (sometimes referred to as non-dimensional cost of transport). During all metabolics testing, the data were deemed acceptable if the respiratory exchange ratio (or RER) remained below a value of 1.0.

Metabolic data were *not* collected during the sensitivity and limits to entrainment tests since actuation parameters were always changing and thus, a steady state measurement was deemed inappropriate. All participants confirmed that they had fasted for at least three hours prior to any metabolic testing performed over the course of the study.

5.2.6 Test protocol

Experiment 1 was conducted with all participants from the first sample (see Table B.1) and all trial conditions were tested in a three-hour period for each subject. Experiments 2 and 3 were conducted with the second sample. These two tests were performed over the course of one or two days, depending on the subject's availability. However, all trial-conditions associated with each test were always completed on the same day and usually lasted about three hours. Experiment 2, which tested subject sensitivity to entrainment, was always performed first in order to prioritize subject inexperience with the oscillation system. Within each experiment, trial conditions were randomized to minimize any ordering effects.

5.2.6.1 Baseline trials

During the first baseline trial, the subject walked on the treadmill freely (i.e. not wearing the body harness) for a five-minute duration. The treadmill speed was prescribed so as to give the subject a non-dimensional speed of 0.4 – a moderate walking speed.

$$v_b = \tilde{v}\sqrt{gL_{max}} \tag{5.23}$$

where v_b is the belt speed of the treadmill ($1.19\ m\ s^{-1}$ on average), $\tilde{v}$ is non-dimensional speed, g is Earth's gravitational acceleration ($9.81\ m\ s^{-2}$) and L_{max} is the maximal leg length of the subject from the ground to the approximate location of their greater trochanter while standing straight with shoes on. The actual belt speed used in the experiment was rounded to the nearest tenth of a km/hour, per the treadmill's available resolution.

During the second baseline trial, the subject walked on the treadmill at the same belt speed as before, but now outfitted with the body harness connected to the pulley-cable system and for a ten-minute duration. Both actuators provided a constant nominal tension force (approximately 10% BW) to eliminate excessive slack in the system, but the average net force on the body was zero since one tension line pulled up while the others pulled down (Fig. 5.1, 5.2). At the same time, the subject experienced added resistance from the system due to inertia of the motors and hardware coupled to the subject, as well as friction and damping in the system due to back electromotive force (emf). During this baseline trial, the subject's preferred step frequency (f_p) was assessed while walking in the system and motor frequencies prescribed in testing conditions were decided relative to this baseline. Baseline conditions with and without the harness system were conducted in order to test for any effect on metabolic output in Experiment 1. Only the second baseline trial with the subject walking in the harness was tested during Experiments 2 and 3, since no metabolic data were collected.

5.2.6.2 Experiment 1: Cost of Entrainment

After both baseline trials were conducted (walking on the treadmill with and without the harness and no oscillations), the Cost of Entrainment test was performed. This test involved walking on the treadmill for two minutes with constant nominal forces from the actuators to avoid excess slack in the cables. Next, oscillations of electrical current were commanded to the motors at a constant frequency and amplitude and the subject was

allowed to walk on the treadmill in any way they felt appropriate ("free entrainment" phase of the test). After five minutes, the oscillations continued with the same parameters as before, but now a metronome beep was fed through a pair of headphones worn during the test. The metronome cadence was programmed to the subject's preferred step frequency predetermined in the second baseline test and the subject was directed to initiate heel contact with the ground on each metronome beat ("constrained non-entrainment" phase of the test). After another five minutes, the oscillations and the metronome ceased, and the subject was allotted fifteen additional seconds to regain their baseline gait and prepare to stop the treadmill (Fig. 5.3). Metabolic data was collected throughout this test so as to compare oxygen consumption during the free entrainment phase and the constrained non-entrainment phase. This test was performed for six trial conditions associated with various oscillation amplitudes ($A_m = 10, 30\%\ BW$) and motor frequencies displaced from preferred step frequency (f_p) measured in the second baseline test ($\Delta f_m = 0, \pm 6\%$; see Table 5.1).

$$\Delta f_m = \frac{f_m - f_p}{f_p} 100\% \tag{5.24}$$

In the case of trial conditions where $\Delta f_m = 0\%$, no constrained non-entrainment phase was conducted and the trial ended after the free entrainment phase.

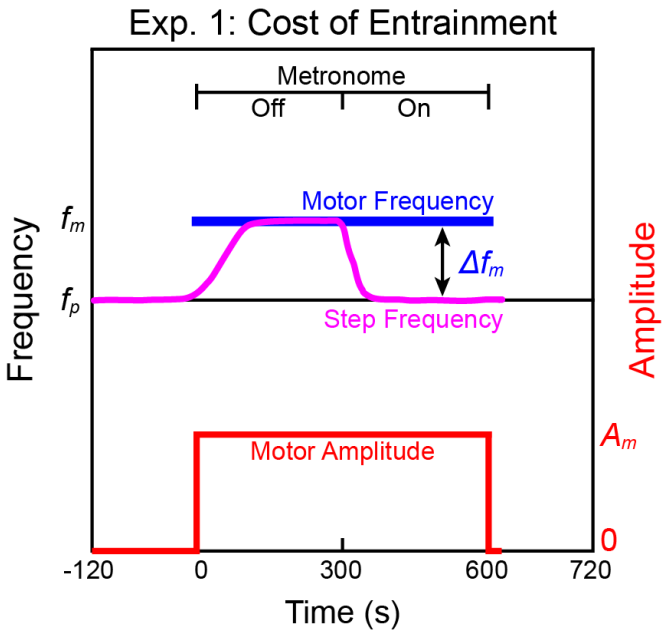

Figure 5.3. Experiment 1 diagram

This figure depicts a generic trial condition with simulated step frequency data (magenta) over time, constant motor frequency (blue) and constant motor amplitude (red). There are no oscillations during the first two minutes of the test. Motor oscillations begin when time equals zero, but with no metronome. These five minutes are called the "free entrainment" phase since subjects are free to interact with the system as they please. During the next five minutes, the metronome is turned on at preferred step frequency (f_p) and subjects are directed to follow its cadence. These five minutes are called the "constrained non-entrainment" phase of the experiment. Finally, there are an extra fifteen seconds after the oscillations and the metronome have been terminated. Oscillation parameters for this experiment are $\Delta f_m = 0, \pm 6\%$ and $A_m = 10, 30\%$ body weight (see Table 5.1).

5.2.6.3 Experiment 2: Sensitivity to Entrainment

After the baseline trial was conducted (walking on the treadmill with the harness and no oscillations), the Sensitivity to Entrainment test was performed. This test involved walking on the treadmill for two minutes with constant nominal forces from the actuators to avoid slack in the cables. Next, current oscillations were commanded to the actuators beginning with low amplitude and ramping up in stepped increments until reaching a maximal amplitude and sustaining for several cycles. The prescribed current amplitude ranged $1 \geq A_m \geq 30\%\ BW$ and increased in increments of $1\%\ BW$ per step (Fig. 5.4). Each stepped increment was sustained for sixteen cycles and the maximal amplitude was extended by 120 cycles. Afterwards, the oscillations were terminated, and participants continued to walk for two additional minutes with only constant nominal tension from the motors. This test was performed for six trial conditions associated with

various motor frequencies displaced from preferred step frequency measured in the second baseline test ($\Delta f_m = \pm 3, \pm 6\ and\ \pm 9\%$; see Table 5.1).

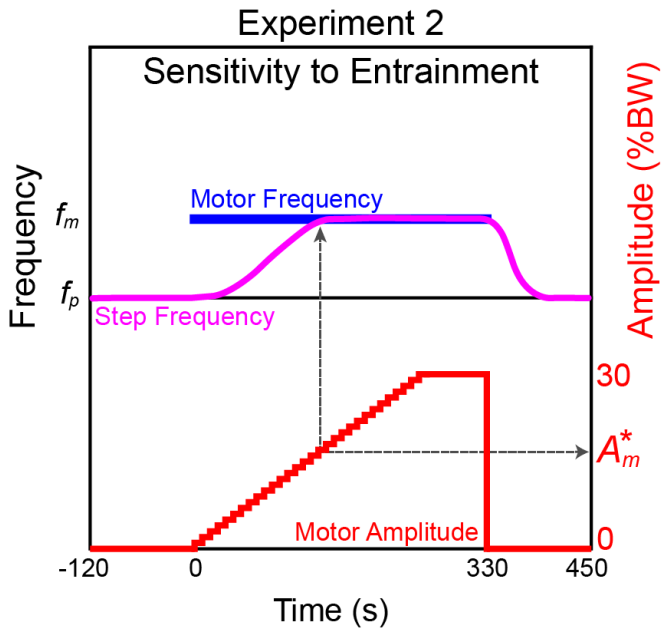

Figure 5.4. Experiment 2 diagram

This figure depicts a generic trial condition with simulated step frequency data (magenta) over time, constant motor frequency (blue) and increasing motor amplitude (red). There are no oscillations during the first two minutes of the test. Motor oscillations begin when time equals zero. Subjects are free to respond to the system as motor amplitude gradually increases over time. The motor amplitude present when the subject initially entrains to the oscillations is referred to as their sensitivity to entrainment (A_m^*). Eventually, motor amplitude maxes out at 30% body weight and sustains for several cycles. Finally, the oscillations cease, and the trial extends for two more minutes while the subject returns to baseline conditions. Oscillation parameters for this experiment are $\Delta f_m = \pm 3, \pm 6\ and\ \pm 9\%$ (see Table 5.1).

5.2.6.4 Experiment 3: Limits to Entrainment

If Experiment 3 was performed on a different day from Experiment 2 due to scheduling, then the baseline condition was repeated on the second day and all subsequent analyses utilized data from the appropriate day of testing. Otherwise, the baseline test was replaced with a few minutes of walking in the system (nominal tension only) to allow for a brief refamiliarization and assessment of preferred step frequency. The test involved walking on the treadmill for two minutes with constant nominal tension, as with the other experiments. Next, current oscillations were commanded to the actuators at a constant amplitude and a motor frequency matching the subject's preferred step frequency (measured during baseline). This was done to place subjects in a state of

immediate entrainment, and 120 cycles were allocated to the subject in order to acclimate to the imposed oscillations. After these cycles, the motor's frequency was programmed to slowly drift away from the subject's preferred step frequency in stepped increments (either higher or lower) and brought back again to preferred. The subject then walked for two additional minutes after the oscillations had ceased (Fig. 5.5). This test was repeated for six trial conditions associated with $\Delta f_m = \pm 10\%$ (increments of 0.01 Hz) and $A_m = 10, 20 \; and \; 30\% \; BW$ (see Table 5.1).

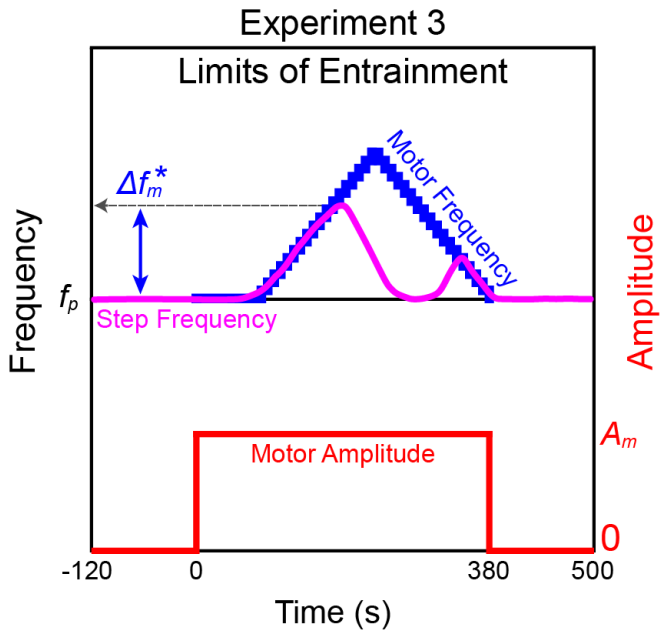

Figure 5.5. Experiment 3 diagram

This figure depicts a generic trial condition with simulated step frequency data (magenta) over time, drifting motor frequency (blue) and constant motor amplitude (red). There are no oscillations during the first two minutes of the test. Motor oscillations begin when time equals zero. Subjects are free to respond to the system as motor frequency gradually drifts away from preferred step frequency (f_p) and back again. The first frequency where subjects reject entrainment is referred to as the limit of entrainment (Δf_m^*). Eventually the oscillations cease, and the trial extends for two more minutes while the subject returns to baseline conditions. Oscillation parameters for this experiment are $A_m = 10, 20 \; and \; 30\%$ body weight with motor frequencies drifting into either higher or lower frequencies, depending on the trial (see Table 5.1).

In all experiments, the subject was blinded to any motion of the actuator system via a curtain placed in front of the treadmill (Fig. 5.1). Furthermore, ambient noise was played through headphones to block out rhythmic sounds of the oscillator system that might otherwise influence the subject's chosen step frequency. When the test required a metronome to set cadence, a beeping sound was played through the headphones in

addition to the ambient noise. For all experiments, each subject was directed to walk in whatever manner felt most natural and/or took the least amount of effort. However, subjects were encouraged to explore different aspects of their gait, including stride length.

Table 5.1. Oscillation parameters for all trials during experiments

Experiment 1: Cost of Entrainment			Experiment 2: Sensitivity to Entrainment			Experiment 3: Limits of Entrainment		
Trial	Δf_m **(%)**	A_m **(% BW)**	**Trial**	Δf_m **(%)**	A_m **(% BW)**	**Trial**	Δf_m **(%)**	A_m **(% BW)**
BL 1	-	-						
BL 2	-	-	BL 2	-	-	BL 2	-	-
1	0	10	1	3	1 to 30	1	0 to 10	10
2	0	30	2	6	1 to 30	2	0 to 10	20
3	6	10	3	9	1 to 30	3	0 to 10	30
4	6	30	4	-3	1 to 30	4	0 to -10	10
5	-6	10	5	-6	1 to 30	5	0 to -10	20
6	-6	30	6	-9	1 to 30	6	0 to -10	30

This table details oscillation parameters associated with every trial condition for all experiments. BL1 refers to the baseline condition where subjects walk on the treadmill without the harness and BL2 refers to the baseline condition where subjects walk on the treadmill with the harness. In Experiment 2, A_m ranges from 1 to 30% BW over the course of each trial. In Experiment 3, Δf_m ranges from 0 to 10% or from 0 to -10% depending on the trial. The trial numbers do not refer to chronological order, since trial order was randomized for every subject.

5.2.7 Defining entrainment

The condition of entrainment was defined with somewhat arbitrary thresholds. A subject was determined to be in a state of entrainment if their step frequency was within ±3 SDs (~±0.02 Hz) of the prescribed motor frequency for at least sixteen out of twenty consecutive steps, or 80%. The entrainment threshold used the average SD of all subjects during the last minute of the second baseline trial (walking on the treadmill with the harness on). During the Cost of Entrainment test, two metrics were formulated to quantify the level of entrainment of a subject in a given trial condition. The first – entrainment step ratio (ESR) – was simply the ratio of entrained steps to total steps taken during the free entrainment phase of the experiment. The second – the average duration

of entrainment ($\Delta\bar{t}_e$) – was used to quantify an average duration of entrainment due to the fact that subjects sometimes drifted in and out of the motor's frequency.

During the Sensitivity to Entrainment test, the entrainment condition was used to determine the oscillation amplitude where entrainment first occurred (A_m^*). This value was considered a metric of subject sensitivity and plotted as a function of $|\Delta f_m'|$.

$$|\Delta f_m'| = \left|\frac{f_m - f_p'}{f_p}\right| 100\% \tag{5.25}$$

where, as opposed to Eq. (5.24), f_p' was the preferred frequency of subjects in the first two minutes of each trial (instead of at baseline). This adjustment was made to control for the fact that subjects sometimes exhibited slightly different preferred step frequencies at the beginning of individual trials. In the Limits to Entrainment test, the entrainment condition was used to determine the first motor frequency where subjects deviated from entrainment ($|\Delta f_m^*|$). This was considered a metric of the subject's limit to entrainment. If subjects regained entrainment as the motor frequency returned closer to the subject's f_p, then this frequency was also recorded as a second limit to entrainment to test for hysteresis between entraining to frequencies drifting away from preferred and frequencies drifting back toward preferred.

5.2.8 Statistical analysis

Step frequency was always reported relative to preferred step frequency from the baseline trial [i.e. $f_r = \frac{f_s}{f_p}$, see Eq. (5.21)]. After filtering the data, each subject's relative frequency over time was interpolated at equal time intervals reflecting the data acquisition of the raw data collection. The median value of the interpolated data was taken across all subjects who entrained at least once in the trial and at each time point, to more accurately represent distributions that were often skewed. Quartiles were used to represent the spread of the distribution for each time point at 25% and 75% levels.

Linear mixed models were used to test how well subjects entrained and under what conditions, for all three experiments. The mixed model was chosen to control for repeated measurements among subjects participating in multiple trials each; subject was included in the models as a random effect. All statistical models were developed and evaluated in JMP (SAS Institute Inc., Cary, NC USA, version 14.1.0) using the restricted

maximum likelihood method for parameter estimation and a compound symmetric covariance structure.

In the linear mixed models used to assess data from Experiment 1, the motor frequency (Δf_m) and amplitude (A_m) as well as an interaction between the two ($\Delta f_m \; x \; A_m$) were added as fixed effects to test if the oscillation parameters contributed significantly to the various outcomes.

The first two models tested the effect of oscillation parameters on entrainment step ratio (ESR) and average entrainment duration ($\Delta \bar{t}_e$) – two metrics characterizing the level of entrainment under circumstances of various trial conditions. A third model used a *post-hoc*, Tukey's Honestly Significant Difference (HSD) test to detect differences in all metabolic conditions ($\alpha = 0.05$), including baseline trials, and to control for Type I error. A separate model was used to test for an effect of net mechanical work done by the harness tension forces on non-dimensional metabolic power. This model also included *ESR* as a covariate to control for the level of entrainment in each trial. $\Delta \bar{t}_e$ was excluded to avoid collinearity. Finally, another model tested effects of motor phase (ϕ) and vertical amplitude of the subject's CoM (A_c) to account for trends of net mechanical work done by the harness tension forces during entrainment. Although it is not expected that motor phase actually has a linear relationship to mechanical work, given its cyclic nature, the phase data collected showed that the vast majority of observations (~95%) were found approximately between 0 and 135^o and the data were deemed sufficiently linear over this range. However, three outlier phase measurements were removed since they were well beyond the phase of other subjects and in other trial conditions. Work and vertical amplitude of the CoM were normalized by a combination of body weight and leg length for an average subject in the relevant models. Δf_m was excluded from this model since there is a correlation between frequency and A_c.

An additional linear mixed model was used to test data from Experiment 2. It aimed to characterize whether any of the following had an effect on the amplitude where initial entrainment occurred in the trial (A_m^*): motor frequency ($|\Delta f_m|$), whether the motor frequency was higher or lower than preferred step frequency [$sgn(\Delta f_m)$; "sgn" is the signum function indicating whether Δf_m is positive or negative], and an interaction between the two [$|\Delta f_m| \; x \; sgn(\Delta f_m)$].

Finally, one more linear mixed model was used to test data from Experiment 3. This model tested the effect of oscillation amplitude (A_m), whether the range of motor frequencies was higher or lower than preferred step frequency [$sgn(\Delta f_m)$], whether the limit of entrainment had any hysteresis as motor frequency drifted away and then returned ($Hysteresis$), as well as interactions between them. The dependent variable in this model was the entrainment limit frequency ($|\Delta f_m^*|$).

The significance of fixed model effects was evaluated with 95% confidence limits (CL) and *post-hoc* t tests where p values were adjusted (p_{adj}) using the Bonferroni correction depending on how many tests were performed in each model. Tests were considered significant if $p_{adj} < 0.05$. Throughout the manuscript, unadjusted p values are reported, and significance is indicated with asterisks. A full summary of all the statistical models implemented can be found in Appendix B.

5.3 Results

5.3.1 Optimization model outputs

Ground reaction forces outputted from the model are shown in Figure 5.6. In the plot on the left, the solution is shown for no oscillation forces – analogous to the second baseline trial (walking on the treadmill while wearing the harness). Net tension in the harness (magenta) is characterized by small fluctuations in force that do a minute amount of net negative work on the CoM ($W_c = -0.09\ J$). Otherwise, the ground reaction forces resemble the familiar "double-humped" profile associated with natural human walking. In the plot on the right, trial conditions are optimized where Δf_m is matched to step frequency, $A_m = 30\%\ BW$ and the phase of the motor forces is optimized in the model. A phase that aligns peak upward motor forces slightly after the middle of double stance (approximately with the force hump from heel strike) is found to minimize cost. In this solution, the harness forces do modest net positive work ($W_c = 2.56\ J$) and thus, the legs do net negative work to compensate and maintain a steady gait. The total ground reaction forces are reshaped from the baseline solution, largely to accommodate the extra oscillation forces. Force during double stance is substantially reduced (from ~1.5 to ~1.15 BW), while forces during the middle of single stance are increased (from ~0.85 to just under 1.20 BW). Overall, cost is lowered by the optimal interaction with the oscillation forces: 0.247 versus 0.343 (non-dimensional cost), a cost reduction of about 28%.

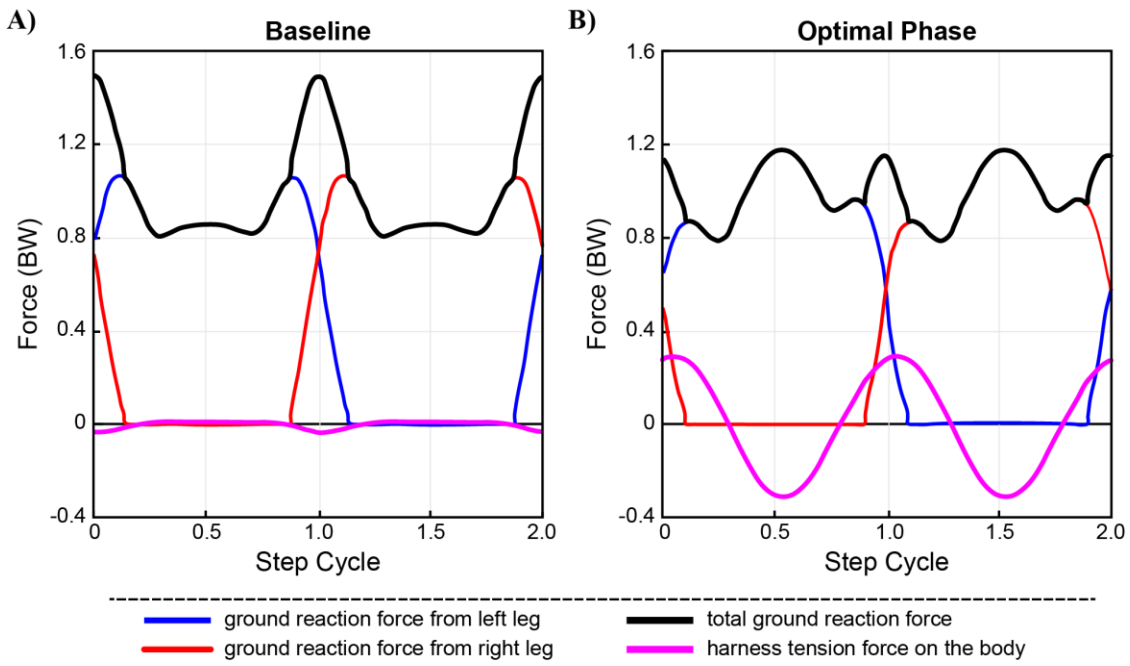

Figure 5.6. Optimization model outputs

This figure shows optimal ground reaction forces: left leg in blue, right leg in red, total ground reaction force in black, and net tension forces from the harness in magenta. One solution is shown for a simulation of the second baseline (walking on the treadmill in the harness but with no oscillation forces) **A)** and another is shown for the case of $\Delta f_m = 0$, $A_m = 30\%\ BW$ where motor phase is a free variable optimized in the model **B)**.

5.3.2 Experiment 1: Cost of Entrainment

5.3.2.1 Entrainment performance

During Experiment 1, there was a wide range of subject responses, including individuals who only entrained in two trials as well as those who entrained in five out of six total trials. The likelihood of subject entrainment largely depended on the oscillation parameters prescribed in the trial condition. For example, all ten subjects entrained when $\Delta f_m = 0, -6\%$ and $A_m = 30\%\ BW$. Conversely, zero subjects entrained when $\Delta f_m = 6\%$ and $A_m = 10\%\ BW$. It should be clarified that subject entrainment does not mean the subject completely entrained throughout the trial, but rather they met the threshold defined previous (i.e. >80% of 20 steps within ±3 SDs of the motor frequency) at least once during the trial. Figure 5.7 shows the median relative step frequency (magenta) as well as 25% and 75% quartiles (grey shaded region) for individuals who entrained at least once during the indicated trial condition. Entrainment in conditions with higher motor frequencies and low amplitude was less stable and more variable. In fact, no data are shown in the low-amplitude-high-frequency trial since no subjects entrained.

Note, the trial data for $\Delta f_m = 0$ cut off early since there was no constrained non-entrainment phase during these trials. However, it is clear that individuals largely followed the metronome well in other trials, as the median data quickly converged on a relative frequency of one at approximately 300 s into the trial.

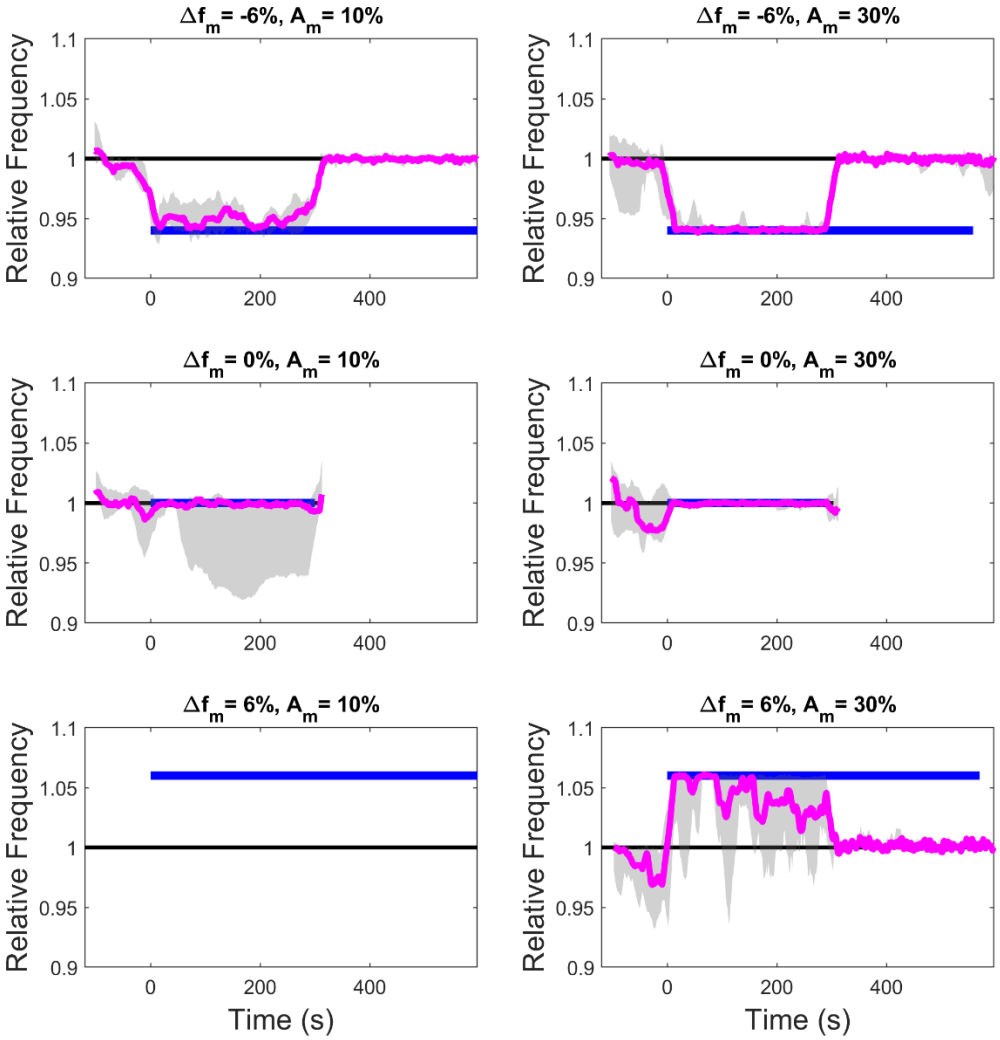

Figure 5.7. Experiment 1 entrainment results

The median relative step frequency (f_r: step frequency divided by preferred step frequency measured during the baseline trial; magenta) is plotted over time as the oscillation amplitude and prescribed motor frequency (blue) are both held constant. 25% and 75% quartiles are used to show relative step frequency variation over time (grey shaded area). All trial conditions are shown, including $\Delta f_m = -6, 0 \; and \; 6\%$ (top, middle and bottom rows, respectively) $A_m = 10, 30\% \; BW$ (left and right columns, respectively). The oscillations began at $Time = 0 \; s$ and ended at approximately $Time = 600 \; s$ (or ten minutes). During the first five minutes of oscillations, subjects were free to respond as they preferred: "free entrainment" phase. During the next five minutes of oscillations, subjects were directed to follow the cadence of a metronome at their predetermined preferred step frequency: "constrained non-entrainment" phase. There was no constrained non-entrainment phase in trial conditions where $\Delta f_m = 0$

and thus, these experiments ended after around 300 s. Note, data are only shown for individuals who entrained at least once throughout the trial. In the trial condition where $\Delta f_m = 6\%$ and $A_m = 10\%\ BW$, no data are shown since no subjects ever entrained.

In many instances, subjects exhibited transient entrainment – meaning that step frequency would drift in and out of the motor's frequency throughout the trial (Fig. 5.8A). To better characterize how well subjects entrained their gait in the various trial conditions, two metrics were considered: entrainment step ratio (ESR) and average entrainment duration ($\Delta\bar{t}_e$; see Fig. 5.8B,C). The entrainment ratio is simply the proportion of steps within ±3 SDs of the motor frequency during the free entrainment phase of the experiment. However, because this metric does not consider how bouts of transient entrainment are distributed throughout the trial, $\Delta\bar{t}_e$ tells the average time duration of all bouts in a given trial, divided by the total time of the free entrainment phase of the experiment (300 s).

A multiple linear mixed model indicated that higher oscillation amplitudes increased both ESR [fitted coefficient (95% confidence limits): $\beta = 2.267\ (1.482, 3.052)$, $p < 0.001$*] and $\Delta\bar{t}_e$ [$\beta = 1.737\ (0.958, 2.517)$, $p =< 0.001$*] while increases in motor frequency led to decreases in the entrainment metrics: [$\beta =$ -3.005 (-4.607, -1.402), $p < 0.001$*] and [$\beta =$ -2.712 (-4.302, -1.121), $p = 0.001$*], respectively. An interaction between motor frequency and oscillation amplitude was not significant ($p = 0.273$). In fact, this interaction was not significant in any of the models tested. As Figure 5.8 shows, there is a wide range of entrainment performance employed by different subjects. However, subjects clearly had a higher entrainment step ratio at larger amplitudes and at lower motor frequencies. This was also the case for the average entrainment duration.

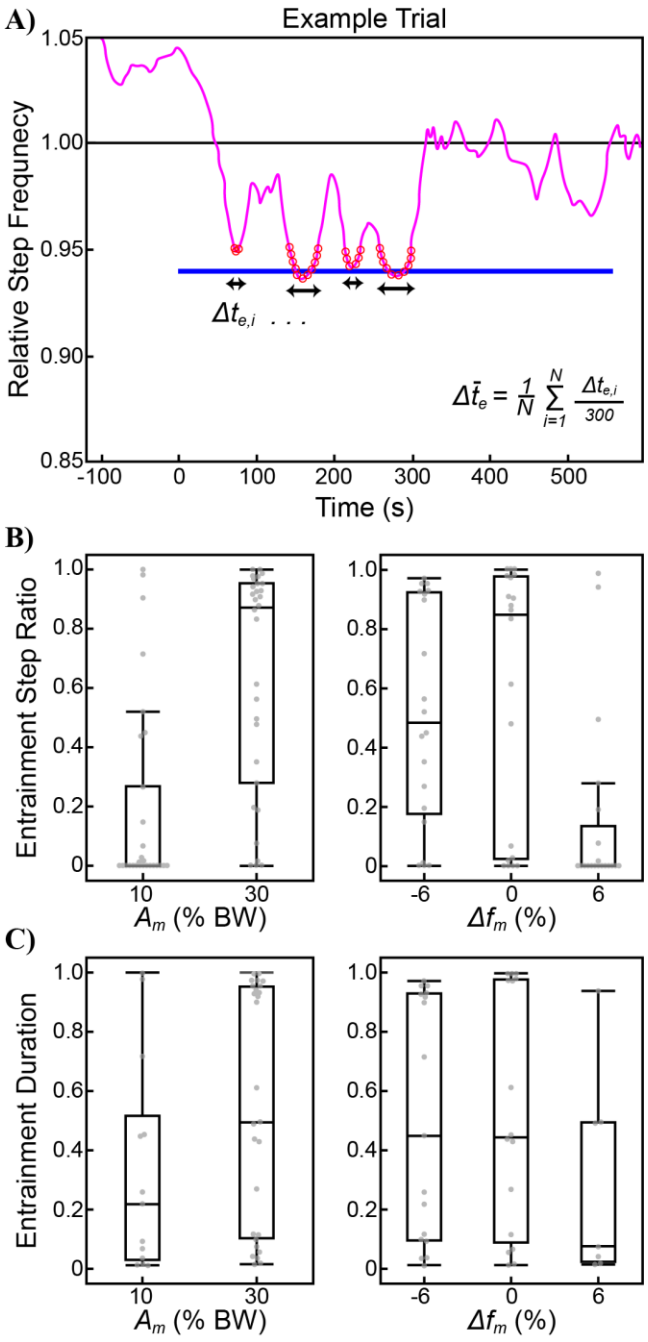

Figure 5.8. Level of entrainment during Experiment 1

A) Data from an example subject illustrates transient entrainment where relative step frequency (step frequency divided by preferred step frequency; magenta) oscillates towards and away from the motor frequency (blue). Data in red indicate when the subject is entrained with the oscillator system. **B)** The entrainment step ratio (ESR; ratio of entrained steps to total steps taken during the free entrainment phase of the experiment) and **C)** the average entrainment duration ($\Delta \bar{t}_e$; average time duration for bouts of entrainment) are shown as a function of oscillation amplitude and motor frequency. Linear mixed models were used to statistically test the effects of trial conditions on both entrainment metrics shown here (see Table B.2 for full results).

5.3.2.2 Metabolic cost of entrainment

A major objective of this test was to compare the metabolic expenditure of individuals during free entrainment (metronome is off) to expenditure during the constrained non-entrainment phase (metronome is on). Metabolic measurements during these experimental phases were compared for every trial condition as well as with baseline conditions (walking on the treadmill with and without the harness, but with no oscillations). Metabolic expenditure was found to increase by 25.8% ($p < 0.001$*) when subjects walked on the treadmill with the harness versus without the harness (Fig. 5.9). However, no significant differences were found when comparing any of the other experimental conditions, with an exception: the condition where $\Delta f_m = -6\%$ and $A_m = 30\%\ BW$ was metabolically more costly for subjects during free entrainment than all other trials and baselines. However, metabolic cost of this condition during free entrainment was not significantly different from that of the constrained non-entrainment phase (Fig. 5.9). No other conditions were significantly different from one another. Surprisingly, the condition that was metabolically more expensive was also one of the conditions where subjects entrained the most consistently and the most robustly. To understand what drove cost in the experiment (since apparently entrainment did not), mechanical variables characterizing the preferred interaction during entrainment were explored.

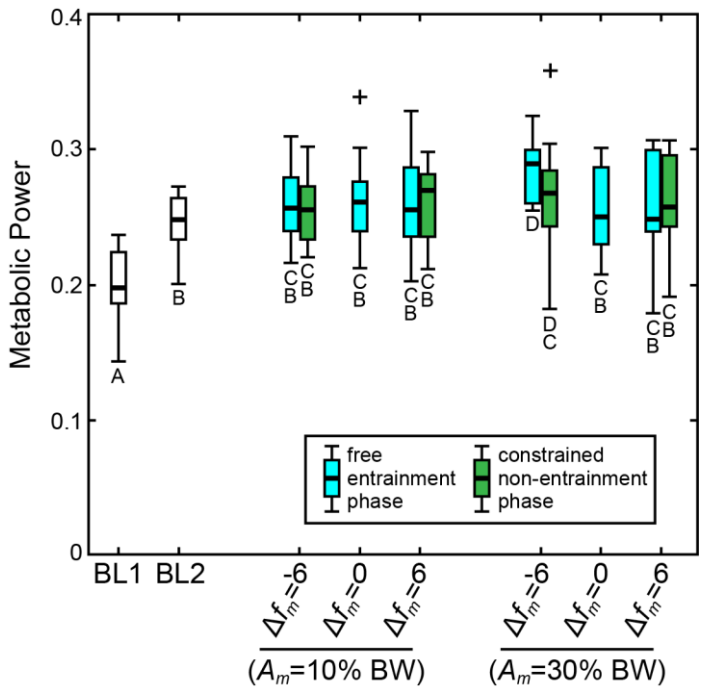

Figure 5.9. Metabolic power during Experiment 1

Non-dimensional metabolic power compared over all trial conditions and baseline tests in Experiment 1. The metabolic cost of every trial condition and baseline test are compared. A *post-hoc* Tukey Honestly Significant Difference (HSD) test was performed on least squares mean values for all conditions. Box plots are labelled with letters connecting conditions where no significant difference was found. Two data points were outliers to the box plots and are marked with "+". See Table B.3 for full results. BL1 is the first baseline test (walking without the harness), and BL2 is the second baseline test (walking with the harness). The free entrainment phase occurred during the first five minutes of oscillations where the subject responded to the system in whichever way they felt most natural. The constrained non-entrainment phase occurred during the second five minutes of oscillations where a metronome guided subjects at a cadence not equal to the oscillation frequency. This allowed for metabolic cost comparisons between entrained and non-entrained gait.

5.3.2.3 Coupled oscillator strategy during entrainment

During entrainment, individuals converged on a stable interaction with the oscillator system. On average, subjects aligned peak motor current approximately a quarter cycle after peak vertical CoM acceleration (i.e. $\phi = 93.8 \pm 55.1^o$, red distribution in middle-right panel of Fig. 5.10). Although the dynamics of the pulley-cable-harness system meant that there was a small delay from the time of peak current to the time of peak tension force felt by the person, this phase relationship indicated that subjects were largely choosing to align upward motor forces (Fig. 5.10: peak T_B occurring just before 0.5) with peak upward CoM velocity, consistent with increased positive mechanical power of the motor forces felt as tension in the harness. Although the motors increase harness

tension when they pull on the subject, the subject can also increase tension as they pull on the motors' inertia. Thus, actual tension measured is the superposition of these two effects. In observing the upward tension in Figure 5.10 (red T_B, in upper-right panel), there are two force humps – one occurring slightly after peak current to the motor (the motor pulling on the subject) and one occurring later in stance at around 80% of the gait cycle (the subject pulling on the motors). The latter force hump is functionally similar to the tension force signal seen in the baseline data (Fig. 5.10: upper left panel). Even though subjects aligned peak motor forces with their CoM vertical velocity (expected to produce positive power), net negative mechanical work was incurred by the tension force for an average subject. This effect was exaggerated (more net negative work) by an increase in vertical velocity amplitude during entrainment compared to baseline.

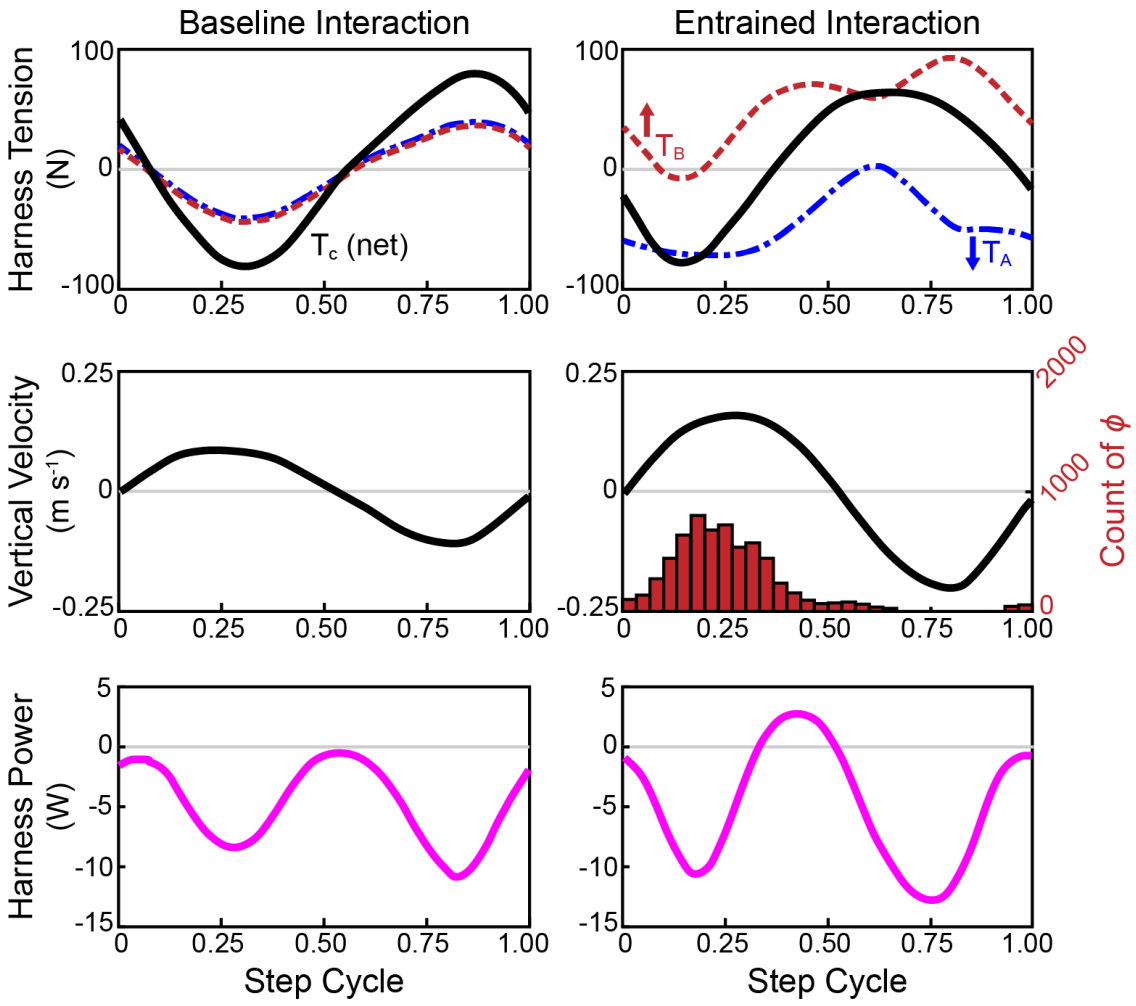

Figure 5.10. Average subject interaction chosen during entrainment

Harness tension forces (top row of plots), vertical centre of mass velocity (middle row), and mechanical power (bottom row) from the harness tension forces are averaged over all subjects during the second baseline test (i.e. while wearing the harness; left column of plots) and during all other trial conditions (right column) for Experiment 1. The tension force plots show net tension (T_c; black) as well as tension from the pulley system pulling up (T_B; red) and from the pulley system pulling down (T_A; blue). A histogram (red) is shown in the entrainment velocity plot, indicating the alignment of peak current sent to the motors (ϕ) during every step for all subjects, where the mode occurs approximately a quarter cycle through the step ($\phi = 0^o$ represents peak upward CoM acceleration, or around the middle of double stance).

5.3.2.4 Determinants of metabolic cost

Although subjects interacting with the oscillator system experienced net negative mechanical work on average, variation on the gait strategy chosen during entrainment illustrated a range of net mechanical work [approximately -0.018 – 0.005 (non-dimensional values)] and a linear mixed model found a strong negative effect of net work

on metabolic cost in individual subjects and trial conditions [$\beta =$ -4.201(-4.960, -3.442), $p < 0.001$*; see Fig. 5.11]. In other words, more net positive work done by the harness tension force meant a lower metabolic cost for subjects and more net negative work meant a higher metabolic cost. The oscillation amplitude also had a strong effect on metabolic power [$\beta = 0.088$ (0.051, 0.125), $p < 0.001$*], showing an increase in cost at higher amplitudes, despite there being generally more entrainment at higher amplitudes. In fact, the level of entrainment was controlled for by including ESR as a covariate in the model, and yet, this variable did not have a significant effect on metabolic power [$\beta =$ -0.004 (-0.013, 0.006), $p = 0.488$]. The motor frequency and an interaction between it and oscillation amplitude were also found to be insignificant after controlling for multiple testing (see Table B.2 for full results).

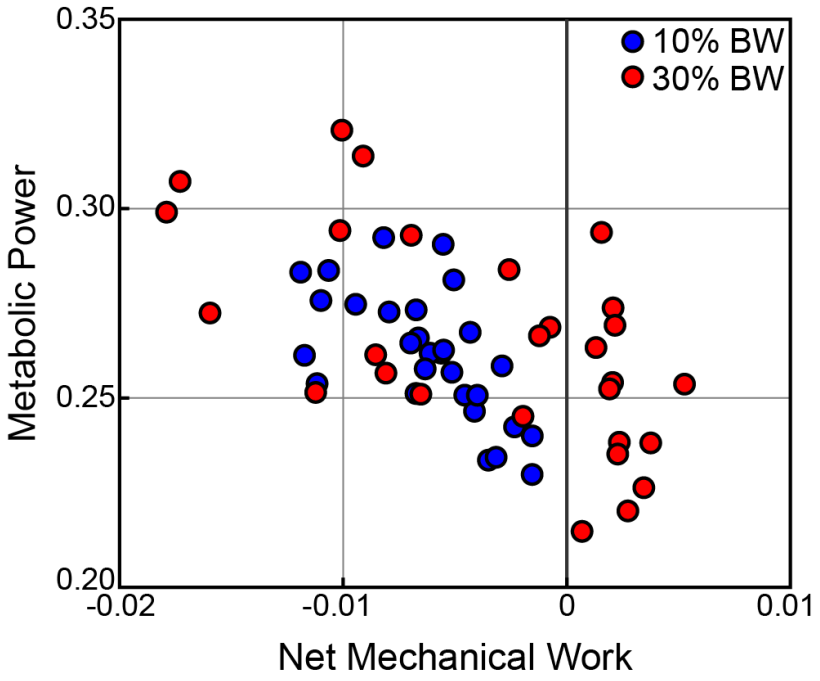

Figure 5.11. Determinants of non-dimensional metabolic power

Average data are shown for each subject in each trial condition during the free entrainment phase of Experiment 1. A linear mixed model was used to assess the effect of net mechanical work (non-dimensional) from harness tension forces on metabolic power (see results in Table B.2).

5.3.2.5 Determinants of net mechanical work by the harness

In Figure 5.12, the average tension force, CoM vertical velocity and mechanical power are shown for three example subjects in trial conditions chosen to illustrate entrainment

strategies resulting in moderate net positive work (left column of plots), moderate net negative work (middle column) and substantial net negative work (right column). One of the largest distinctions between these subject data is the phase alignment of the motor forces. In the left column, the subject aligns the motor phase just after zero (median phase = 27.5°, or 7.6% in the gait cycle), and distinctive motor force humps are observed shortly thereafter (~23.5% in the gait cycle). Due to this alignment, the net tension signal is mostly shaped by motor forces and is approximately aligned with CoM velocity, thus resulting in net positive work ($W_c = 4.127\ J$). In the middle column, phase is increased (64.3°, or 17.9%). Although the resulting motor force hump is still relatively distinct, it is not enough to overcome resistive forces due to inertia and damping in the system, and net negative work accumulates over the step ($W_c = -6.178\ J$). In the right column, motor phase occurs relatively late (114.0°, or 31.7%), and forces out of phase with the CoM velocity are exaggerated. Substantial net negative work occurs in this example ($W_c = -11.595\ J$).

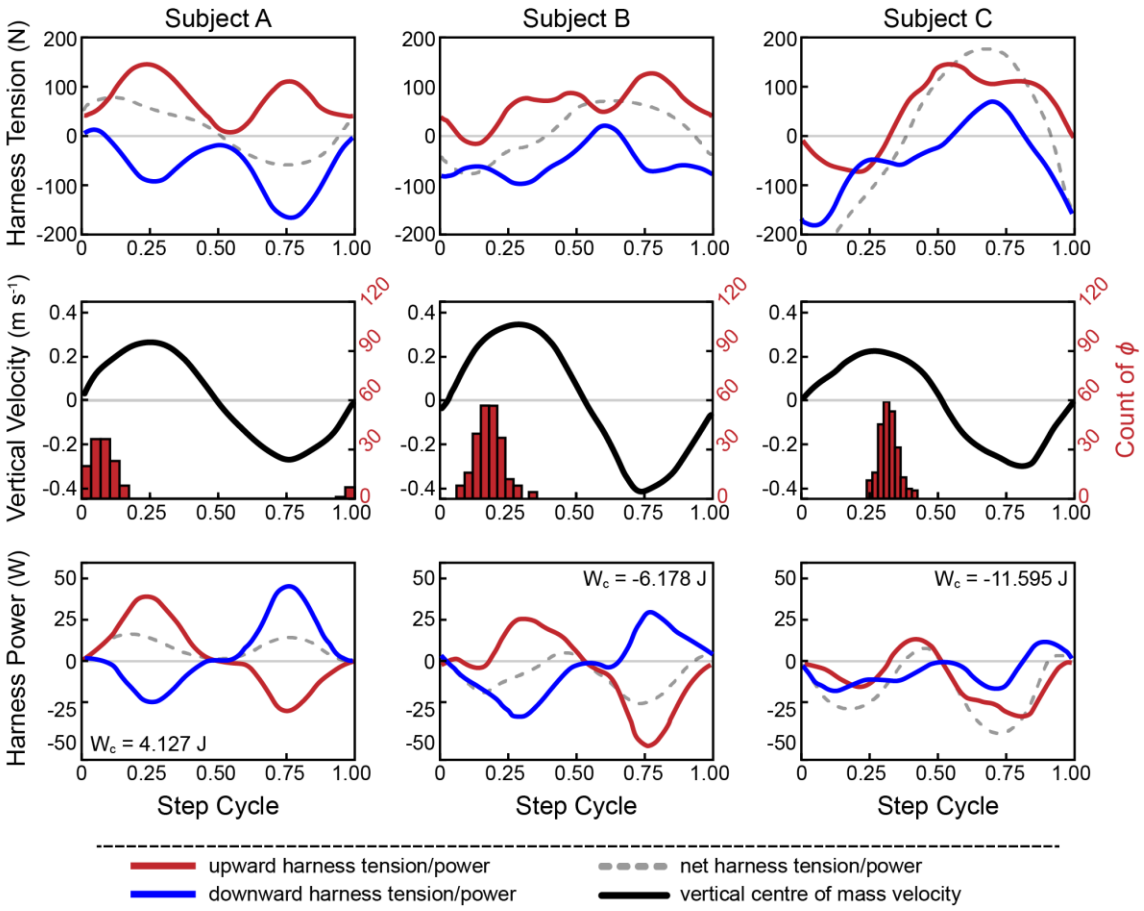

Figure 5.12. Chosen entrainment strategy for three example subjects

Three subjects were chosen to display data at various trial conditions illustrating different entrainment strategies during Experiment 1. Average data for subject A ($\Delta f_m = 6\%$, $A_m = 30\%\ BW$) are shown in the left column of plots, where motor phase alignment occurs at $\phi = 7.6\%$ of the gait cycle. This strategy aligns peak tension forces with the centre of mass (CoM) vertical velocity and thus, results in net positive work ($W_c = 4.127\ J$). Average data for subject B ($\Delta f_m = -6\%$, $A_m = 30\%\ BW$) are shown in the middle column, and motor phase alignment occurs at $\phi = 17.9\%$ of the gait cycle. Since peaks in tension due to motor forces occur slightly later, positive power is relatively lower and net negative work occurs ($W_c = -6.178\ J$). Average data for subject C ($\Delta f_m = -6\%$, $A_m = 30\%\ BW$) are shown where $\phi = 31.7\%$ of the gait cycle and mechanical power from the harness tension forces is dominated by resistive inertial forces, thus leading to substantial net negative work on the CoM ($W_c = -11.595\ J$).

From the examples in Fig. 5.12, it is clear that motor phase has a large effect on the net mechanical work done on the person by the oscillator system. A linear mixed model validates this observation numerically; motor phase had a strong negative effect on net mechanical work [β = -0.064, (-0.089, -0.040), $p < 0.001$*]. Due to its cyclical nature, the relationship between phase and net mechanical work is certainly not linear, despite its implementation in the model. However, most subjects consistently entrained at phase

relationships ranging from approximately 60-180^{o} (after shifting to represent peak force instead of motor current; see Methods of Chapter 5) where a clear, quasi-linear trend is apparent (Fig. 5.13B). Three outlier data points are marked in the plot, each with a yellow “x”, to indicate that they were excluded from the linear model. As such, the model should only be considered relevant over the range of data found in this study. The full, nonlinear relationship between net mechanical work and phase will be discussed in later sections.

The amplitude of vertical CoM oscillations also had a significant effect on net mechanical work [$\beta = -0.427, (-0.724, -0.129), p = 0.009$*; Fig. 5.13A]. This may be due to the fact that resistive inertial and damping forces in the system are increased with larger oscillations while the motor forces are less affected since they are largely determined by the current driven to the motors. Both oscillation amplitude (A_m) and an interaction between amplitude and phase seemed to have a slight effect on net work as well; however, they were found to be insignificant after correcting for multiple testing (see Table B.2 for full results).

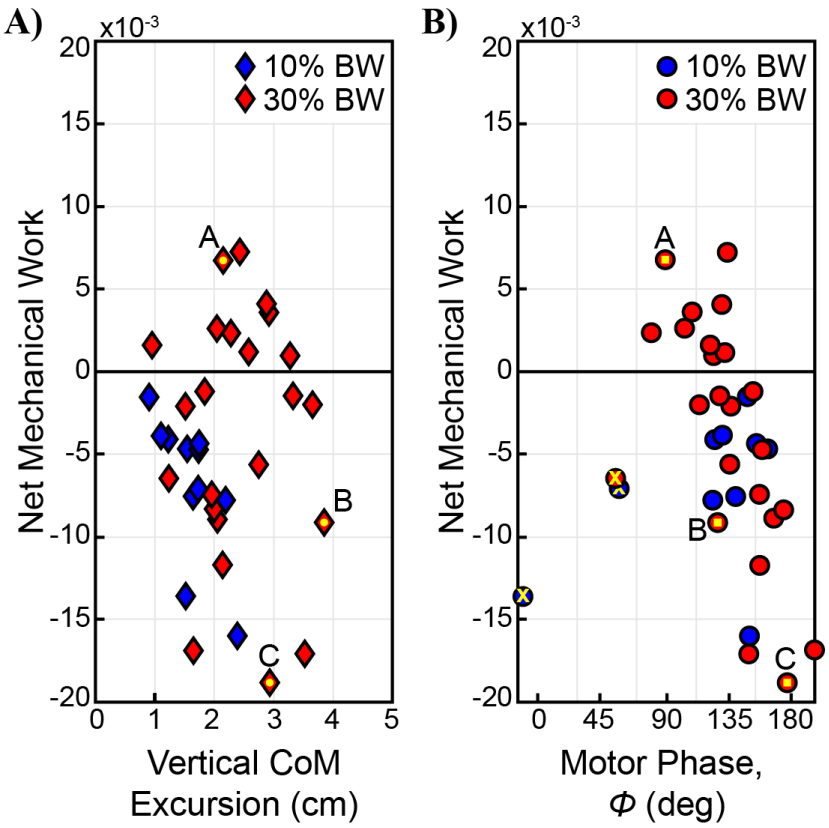

Figure 5.13. Determinants of net mechanical work

The plots show how the net mechanical work done on subjects by harness tension forces (W_c) trends as a function of two variables: vertical centre of mass (CoM) excursion **A)** and phase of peak tension due to motor forces **B)**. These trends were tested statistically with linear mixed models (results of the model shown in Table B.2). Average data are shown for all subjects in all trial conditions where entrainment occurred during the free entrainment phase of Experiment 1. The averages only include data where subjects are entrained with the motor frequency. Three outliers are marked in the phase plot, each with a yellow "x". The outliers were not included in the linear model. Three additional data points are labelled with letters A-C to indicate example data associated with columns from the previous figure (Fig. 5.12).

5.3.3 Experiment 2: Sensitivity to Entrainment

In Figure 5.14, the median relative step frequency (magenta) is shown for the Sensitivity to Entrainment test, alongside 25% and 75% quartiles of the distribution at every time point (grey shaded area). Subjects exhibited successful entrainment at least once throughout the trial in most cases, ranging from all subjects when $\Delta f_m = 3\%$ to seven out of ten subjects when $\Delta f_m = 6,9\%$. However, there was less stable entrainment in motor frequencies further away from preferred step frequency and at lower amplitudes. In general, the distribution of relative step frequency was skewed toward the direction of

preferred step frequency, since some subjects entrained more quickly than others, and subjects almost never overshot the motor frequency.

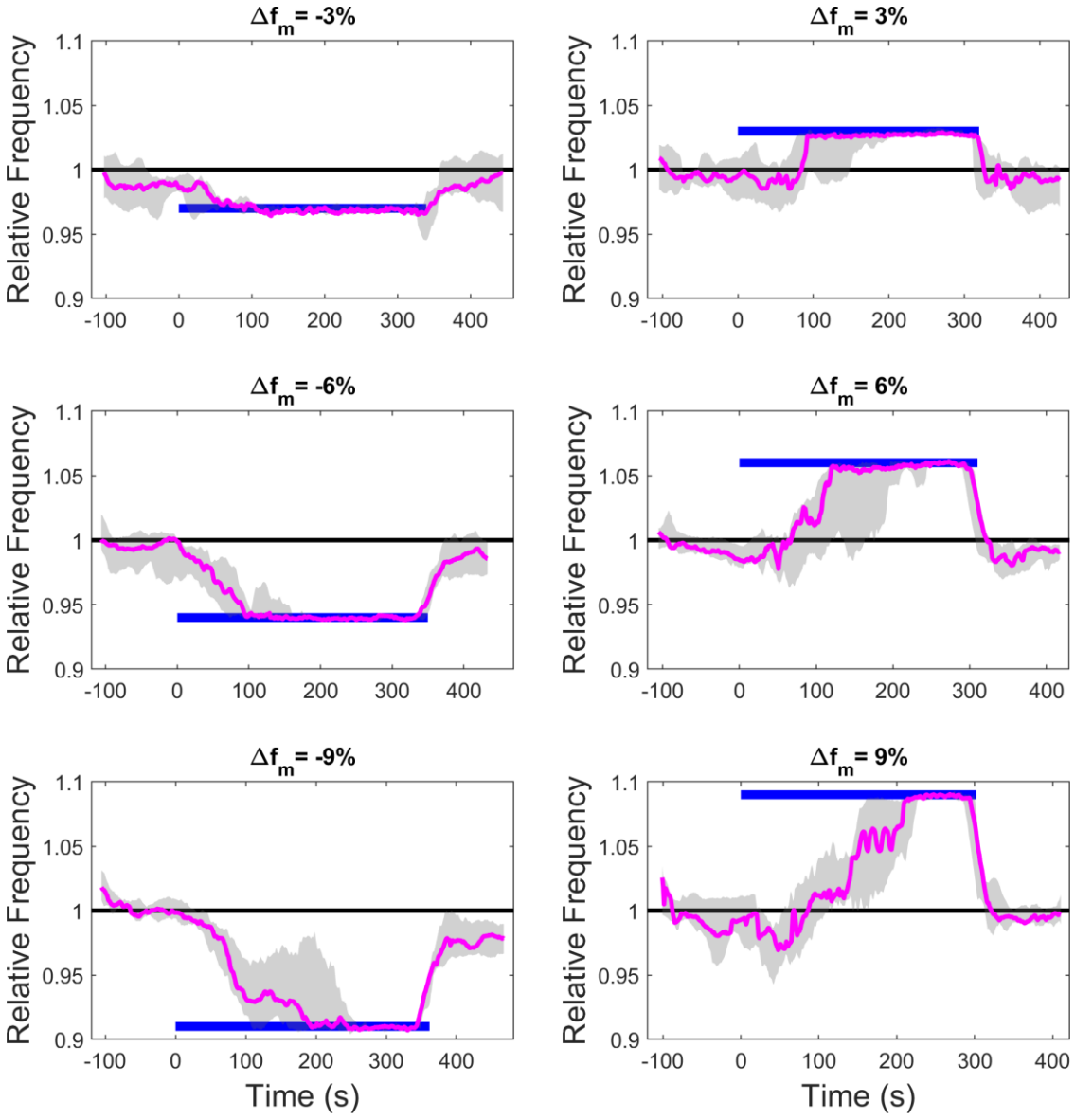

Figure 5.14. Experiment 2 entrainment results

The median relative step frequency (f_r: step frequency divided by preferred step frequency measured during the baseline trial; magenta) is plotted over time as the oscillation amplitude gradually increases and prescribed motor frequency (blue) is held constant. 25% and 75% quartiles are used to show relative step frequency variation over time (grey shaded area). All trial conditions are shown, including $\Delta f_m = \pm 3, \pm 6 \; and \; \pm 9\%$ (top, middle and bottom rows of plots, respectively) and direction of the motor frequency relative to preferred step frequency (lower than preferred in the left column and higher than preferred in the right column). Note, data are only shown for individuals who entrained at least once throughout the trial.

The linear mixed model indicated that subjects required a larger oscillation amplitude to initiate entrainment at motor frequencies further away from their preferred step frequency [$\beta = 1.754, (0.573, 2.935), p = 0.005$*]. The model also suggested individuals require larger amplitudes to entrain when $\Delta f_m > 0$, independent of magnitude, i.e. $|\Delta f_m|$ [$\beta = 0.061\ (0.019, 0.104), p = 0.006$*]. This is shown in Figure 5.15, where the slope of the blue line is shallower than the slope of the red line. However, an interaction between the two effects just described was not significant (see Table B.4 for full results).

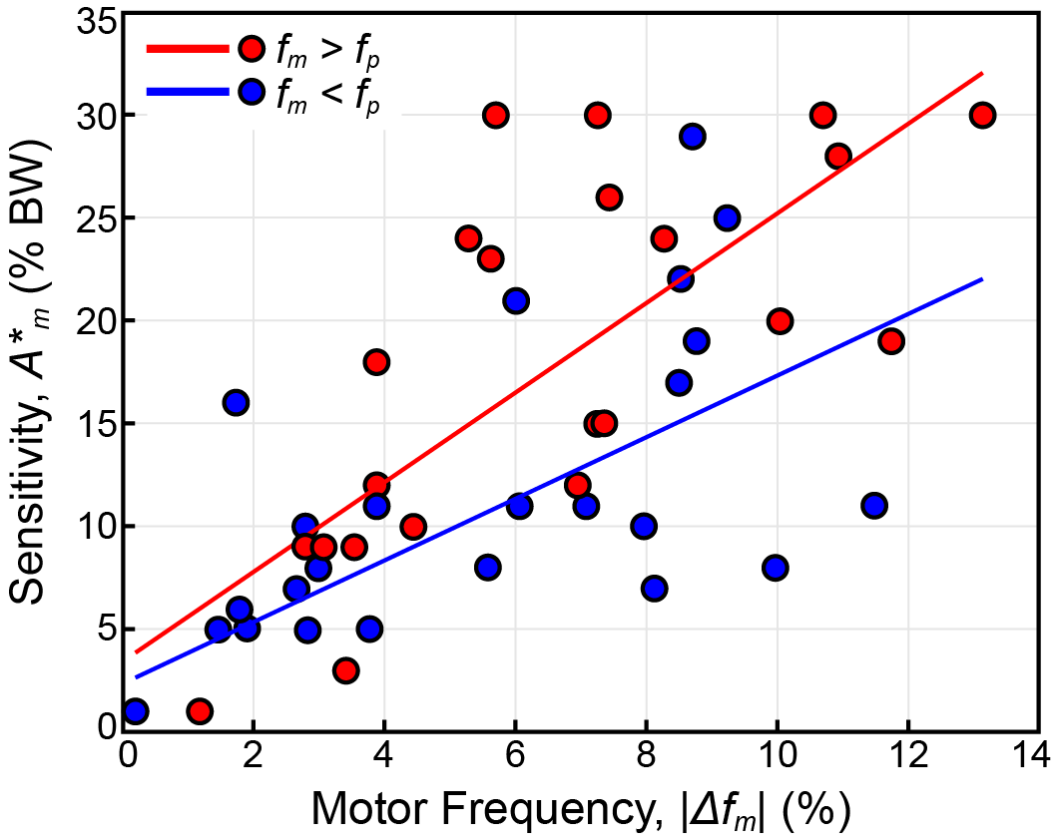

Figure 5.15. Sensitivity to entrainment

This plot indicates the oscillation amplitude where subjects first initiated entrainment, depending on how far away the motor frequency was from preferred step frequency in a given trial. Data are shown for trials where the motor frequency is higher than preferred (red) and lower than preferred (blue).

5.3.4 Experiment 3: Limits to Entrainment

In Figure 5.16, the median relative step frequency (magenta) is shown with 25% and 75% quartiles (grey shaded area) for the Limits to Entrainment test, as with the other two experiments. In every trial condition, nearly all subjects initiate entrainment almost

immediately as the oscillations begin at the subject's preferred frequency. However, as motor frequency drifts away from preferred, many subjects begin to reject entrainment. As the motor frequency begins to drift back toward preferred, a number of individuals re-entrain their gait and follow it the rest of the way. Overall, entrainment is more consistent for subjects at higher oscillation amplitudes and motor frequencies drifting lower than preferred.

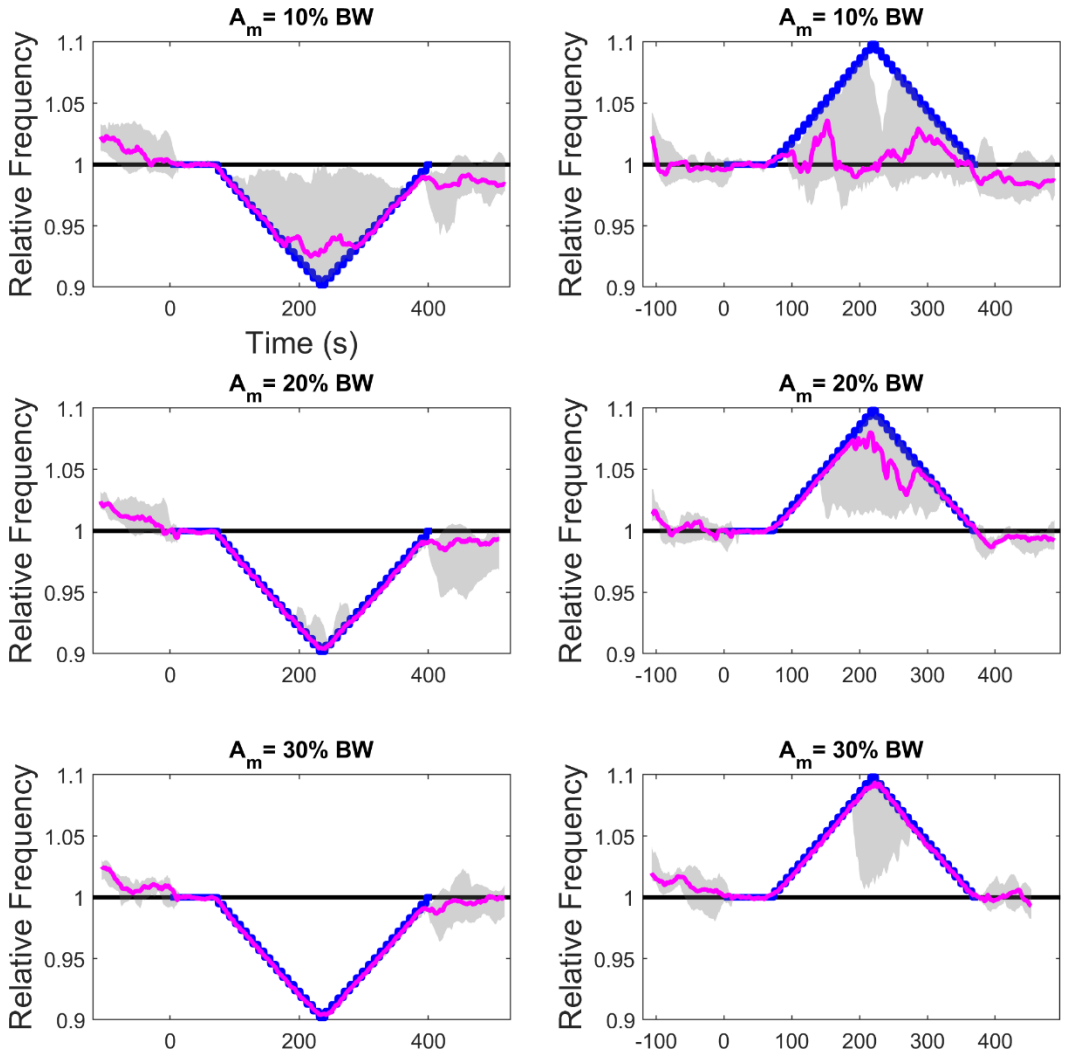

Figure 5.16. Experiment 3 entrainment results

The median relative step frequency (f_r: step frequency divided by preferred step frequency measured during the baseline trial; magenta) is plotted over time as the motor frequency (blue) drifts away and then returns to preferred. 25% and 75% quartiles are used to show relative step frequency variation over time (grey shaded area). All trial conditions are shown, including 10, 20 and 30% BW oscillation amplitudes (top, middle and bottom rows of plots, respectively) and motor frequencies drifting into lower or higher regions (left and right columns, respectively). Note, data are only shown for individuals who entrained at least once throughout the trial.

Figure 5.17 shows how the limit of entrainment (Δf_m^*) increases at larger oscillation amplitudes, and this is supported by the linear mixed model [$\beta = 0.128, (0.052, 0.203), p = 0.001$*]. The direction of the motor frequency drift was also found to have a significant effect on the limit of entrainment, with subjects entraining at frequencies further away from preferred when $\Delta f_m < 0$ [β = -0.024 (-0.032, -0.015), $p < 0.001$*]. However, hysteresis between Δf_m^* as motor frequency drifted away versus when it drifted back was not found to be significant [$\beta = 0.000$ (-0.006, 0.006), $p = 0.914$]. No interactions between any of the effects were deemed significant either (see Table B.5 for full results).

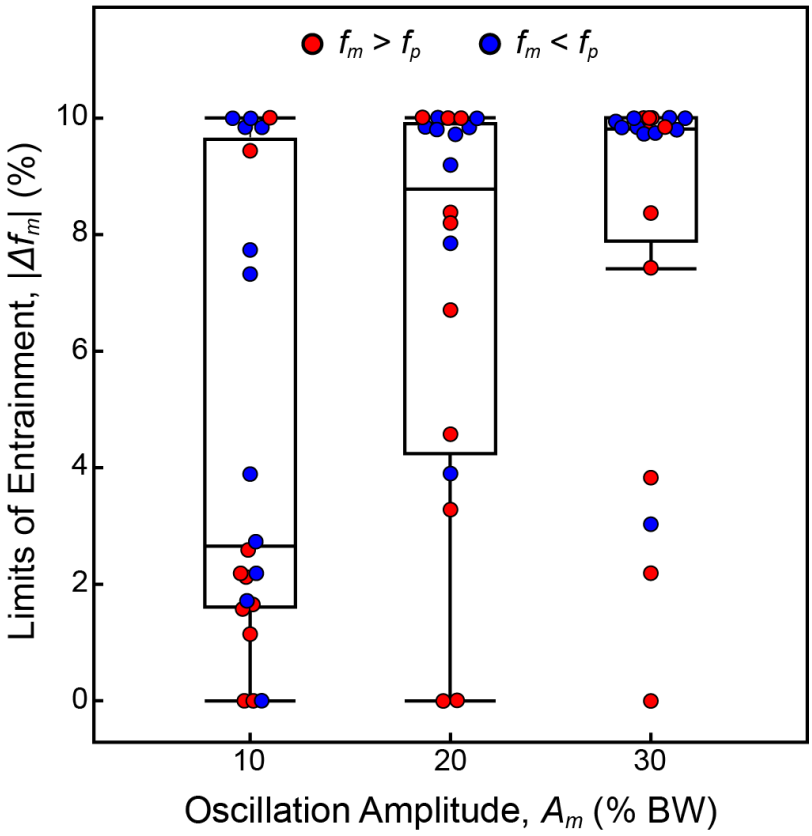

Figure 5.17. Limits of entrainment

This plot indicates the most extreme frequencies that subjects entrained to as the motor frequency drifted away from and returned to preferred step frequency over time. Box plots are shown for the limits of entrainment at 10, 20 and 30% BW trial conditions. Data are shown when the motor frequency drifts to frequencies higher than preferred (red) and lower than preferred (blue).

5.4 Discussion

5.4.1 Basin of entrainment

Overall, most subjects entrained to motor frequencies over a wide range of oscillation parameters. For example, in the Sensitivity to Entrainment test, some individuals entrained at amplitudes as low as 5% BW (or ~33 N) and sometimes at motor frequencies as far away as 13% from their preferred frequency measured at the beginning of the trial. In the Limits of Entrainment test, there were some subjects that were able to follow the motor frequencies to their most extreme drift ($\Delta f_m = \pm 10\%$), even at the lowest amplitude tested ($A_m = 10\%\ BW$). It is possible that these subjects would have entrained at even more extreme frequencies and thus, true limits of entrainment are still unknown for them. Although the magnitude of step frequency adaptations may not sound very impressive, they represent gait adjustments on the high end of the spectrum; e.g. other studies have shown gait adaptations ranging from approximately ±2–8% from preferred step frequency (Selinger et al., 2015; Selinger et al., 2019; Simha et al., 2019; Wong et al., 2019). On the other hand, there were subjects who struggled to entrain with the oscillator system at even the most modest frequencies and with large amplitudes. Similar subject variability has been found in other studies (Selinger et al., 2019). Regardless, clear trends were identified. Subjects displayed the most robust and stable entrainment during trials with low motor frequencies and high amplitudes; in some instances, subjects even entrained more easily with frequencies *below* preferred compared to motor frequencies *matched* to preferred (i.e. no change in step frequency required to entrain). However, this was not a systematic trend.

Overall, subjects exhibited entrainment most easily during Experiment 3 (Limits of Entrainment). This is largely by design, as initial oscillation frequencies were chosen to initiate entrainment by default (assuming subjects maintain step frequency when the oscillations begin). The slow, gradual drift of the oscillation frequencies over time was intended to provide a gentle motivation for subjects to follow along until they preferred to reject entrainment at more extreme frequencies. Indeed, entrainment was so strong that the 25% and 75% quartiles were, at times, not visible (Fig. 5.16: e.g. lower-left panel). On the other end of the spectrum, Experiment 1 (Cost of Entrainment) was the most challenging experiment for subjects to entrain in, even at comparable frequencies and amplitudes. This was true even though the experiment employed unchanging oscillation parameters throughout the test. During Experiment 2 (Sensitivity to Entrainment),

subjects had greater success at entrainment than with Experiment 1. There may be some benefit to the gradual increase in amplitude that eases subjects into an entrained response. At first, oscillations are not strong enough for subjects to notice or perhaps care. Eventually, the oscillations do begin to have an influence. With every few steps, there is a reminder that the oscillations are cycling through a range of interactions, some more favorable than others, and the reminder becomes more prominent over time, as amplitude increases. This may be a gentler way of "nudging" individuals to search for strategies that stabilize the interaction appropriately. On the other hand, in Experiment 1, there is more of a shock to the system, where full amplitude is engaged immediately. Perhaps subjects who do not find immediate entrainment discover that they can manage the perturbations varying from step to step and are therefore, less motivated to find a way to stabilize the interaction.

For all experiments, metrics of entrainment should only be interpreted within the context of the experiment protocol. In particular, the time of exposure to oscillations was not explicitly tested. However, it undoubtedly plays an implicit role in determining how entrainment occurs and under what circumstances. Thus, all results showing levels of entrainment, sensitivity to entrainment, or limits of entrainment, should be considered relevant only within the context of exposure time provided per the specific experiment.

5.4.2 Entrainment at frequencies below and above preferred frequency

A key finding in all experiments was the fact that subjects had an easier time entraining to motor frequencies below their preferred step frequency. In the linear mixed models used to assess Experiments 2 and 3, this effect was found to be significant ($p = 0.006$*, $p < 0.001$* respectively). Furthermore, the entrainment step ratio and the average entrainment duration were both found to be negatively affected by motor frequency ($\beta =$ -3.005 and -2.712, respectively) – meaning lower frequency conditions were associated with more consistent and robust entrainment and higher frequency conditions were associated with less consistent and robust entrainment. It is unclear why lower frequencies should be easier to entrain to. However, there are a few possibilities.

One option is that humans use information at the tissue level rather than the whole-body level (e.g. metabolic power) when making motor control decisions about coordinating gait. This concept relies on the fact that different muscles are used during different portions of the gait cycle and for different functions. During double stance, the triceps

surae is largely engaged to perform simultaneous negative and positive work between the legs and redirect the CoM from falling downward to rising upward again during the step-to-step transition (Donelan et al., 2002A). Furthermore, the mechanical power of these muscles has been shown to increase with step length raised to the fourth power (Donelan et al., 2000B) and thus, increases in metabolic power at lower step frequencies are largely driven by the dramatic increases in leg work. At the same time, these are the muscles that are most likely offloaded when the oscillation forces are aligned appropriately. Therefore, it may be possible that individuals feel more comfortable entraining at lower step frequencies, since the extra work normally required could now be alleviated with work done by the oscillator system.

When entraining to higher step frequencies, the same offloading occurs for the same muscles, but given the shorter step length, less work is required to manage the step-to-step transition. At the same time, metabolic power increases as the leg swings at a higher frequency (Kuo, 2001; Bertram, 2005; Doke et al., 2005; Doke & Kuo, 2007), yet the hip flexors largely responsible for these actions are not necessarily offloaded by entraining with the oscillator system. One interpretation is that humans prefer to avoid overloading individual muscles, sometimes at the expense of other relevant variables such as metabolic cost; researchers have shown that human subjects sometimes prioritize different costs over metabolic exertion, for example various functions of muscle activity (McDonald et al., 2019; Rubenson, 2019). Furthermore, individuals do not adjust gait in exchange for higher levels of oxygen concentration fed to them through an air tube, even as they consciously acknowledge perceiving an increased effort to maintain gait patterns (Wong et al., 2017).

Perhaps reducing step frequency (and increasing step time) is a default reaction when learning to coordinate effective gait in environments characterized by high uncertainty. Since leg forces peak near double stance, there is likely more time between bursts of muscle activity when step time is increased. The relatively “quiet” nature of longer steps could be useful since it reduces signal interference with mechanosensors that provide crucial feedback giving clues about the nature of the environment. There is some evidence of subjects reducing step frequency as a first response to oscillations in lieu of immediate entrainment. For example, Figure 5.7 (middle-left panel) shows increased variability in relative frequencies below preferred, but little to no variation in relative frequencies above preferred, for the trial where $\Delta f_m = 0\%$ and $A_m = 10\%\ BW$.

Conversely the trial where $\Delta f_m = -6\%$ and $A_m = 10\%\ BW$ shows relatively robust entrainment even though the motor frequency is displaced from preferred. Future studies could explicitly test for this response.

5.4.3 Metabolic cost of oscillator interaction strategies

Metabolic power was not well explained by the level of gait entrainment (e.g. ESR) but was instead strongly related to net mechanical work done on the subject's CoM by the harness tension force. Specifically, net negative work was found to increase cost, while net positive work decreased cost. This result seems reasonable in light of the fact that positive muscle work costs more metabolic energy than negative muscle work. For example, individuals walking up a steep slope will consume approximately 4.8 times more metabolic energy than when they walk down that same slope (Margaria, 1976). Since net mechanical work on the CoM must always equal zero in a steady periodic gait, net negative work by the harness tension must be balanced out with net positive work from the legs. Conversely, if the harness tension does net positive work on the CoM, the subject must compensate with net negative work from the legs. Since negative work is less metabolically costly, it is more economical to receive positive work from the harness tension than the other way around. However, this relies on the assumption that no additional work is needed to compensate for extra force on the body, other than the net negative work needed to manage the energy balance.

Ideally, the subject learns a strategy to receive positive work from the oscillator system and uses it to replace positive work that the legs would normally need to produce anyway (e.g. Gordon & Ferris, 2007). In fact, a substantial amount of positive work is typically done by the trailing leg during push off in natural walking. The push off force redirects the orientation of the CoM velocity vector from pointing down to pointing straight ahead, and the force of the leading leg contacting the ground during heel strike does negative work but continues to reorient the velocity vector until it points up at approximately the same magnitude as before push off. In this context, push off serves two roles in human walking: (1) perform positive work on the CoM to overcome energy losses from negative muscle work and collisions with the ground at heel strike and (2) reorient the CoM velocity vector so that the projection of heel strike forces onto the CoM velocity reduces negative work. If a subject wants to use forces from the harness tension to do some of the positive work that push off typically does, then it is important to recognize that this force has a purely vertical orientation, *unlike* that of the push off force.

The vertical orientation means that the harness can only do positive work by aligning motor forces with the vertical velocity vector of the CoM (i.e. peak upward force at $\phi \approx 90^o$), and this is similar to what many subjects did in the experiments.

Unfortunately, there are two consequences to this strategy. Although it allows the harness force to do some of the positive work that push off normally does, it fails to reorient the velocity vector before heel strike since the upward tension force comes too late in stance. In fact, it worsens the problem, since aligning peak upward force with peak upward velocity just after double stance also aligns peak downward force with peak downward velocity toward the end of single stance. The positive work done by the actuator toward the end of stance essentially drives the subject into the ground, likely increasing collision losses (and negative work) substantially in the process. This strategy may ultimately end up being more expensive than having no oscillation forces at all. Indeed, during Experiment 1, subjects in 42 out of 59 trials (~71.2%) expended higher metabolic power than in their baseline trial while wearing the harness, while subjects in 56 out of 59 trials (~94.9%) expended higher metabolic power than in their baseline trial walking without the harness on the treadmill. On the other hand, this also meant that subjects in 17 out of 59 trials (~28.8%) and 3 out of 59 trials (~5.1%) actually experienced *lower* metabolic power than in their baseline trials with and without the harness, respectively. Although metabolic cost was found to be higher overall in trials versus baseline tests without the harness (Fig. 5.9, Table B.3), there were apparently individual subjects who learned to leverage the oscillation system under certain experimental circumstances and reduce cost beyond that of normal walking.

It is possible that a compromise of positive power from the tension forces can alleviate some of the negative consequences while still helping to improve cost overall. If instead of aligning peak upward tension force with peak upward velocity, the subject modulates the alignment of motor force so that it occurs just *slightly* after the middle of double stance, then the beginning of the upward force hump can help to reorient the velocity vector before heel strike while the end of the force hump can replace some of the positive work associated with push off. This realignment also shifts peak downward force back earlier in time so that it occurs more towards the middle of single stance where the leg can bear the extra force isometrically.

The strategy described above is consistent with the solution presented by the trajectory optimization model, where peak upward forces minimize leg work at $\phi \cong 10^o$, or just slightly after the middle of double stance (Fig. 5.6B). However, in order for the optimal strategy to minimize cost, it requires the downregulation of push off forces and muscle activity[2] so that the harness forces can replace positive muscle work [similar to findings by Gordon & Ferris, (2007)]. Yet subjects substantially increased the vertical excursion of their CoM when they entrained to motor oscillations versus at baseline (an increase of 58.2% or 125.5% for $A_m = 10\%$ or $30\%\ BW$, respectively). The increased body oscillation during entrainment is likely evidence that subjects did not downregulate their push off. Instead, along with the relatively late motor phase, it seems that subjects preferred to increase positive power from the harness forces by aligning motor forces approximately with vertical CoM velocity (Fig. 5.10, 5.18D). Contrary to the optimization model, subjects that leveraged the most positive power from the oscillations had the lowest metabolic cost (local minimum at around $\phi = 100^o$). These results, however, should be treated with caution. Experiments presented here did not explicitly control the motor phase, but rather, the phase variation depicted in Figure 5.18B represents subject preferences during the free entrainment phase of Experiment 1. Since subjects did not sample phase closer to the minimum cost solution predicted by the optimization model ($\phi \cong 10^o$), it is unclear if chosen phase values surround a global optimum or merely a local optimum. The grey dashed line in Figure 5.18B indicates a sine wave fit to the data, under the assumption of a cyclical cost over phase. However, it is unclear how accurate this fit might be over such a narrow range of data. Thus, extrapolation beyond the data range is labelled with a question mark to indicate uncertainty of the trend.

[2]Downregulation of muscle activation during repetitive actions when movement error is small is sometimes referred to as “slacking” (Reinkensmeyer et al., 2009)

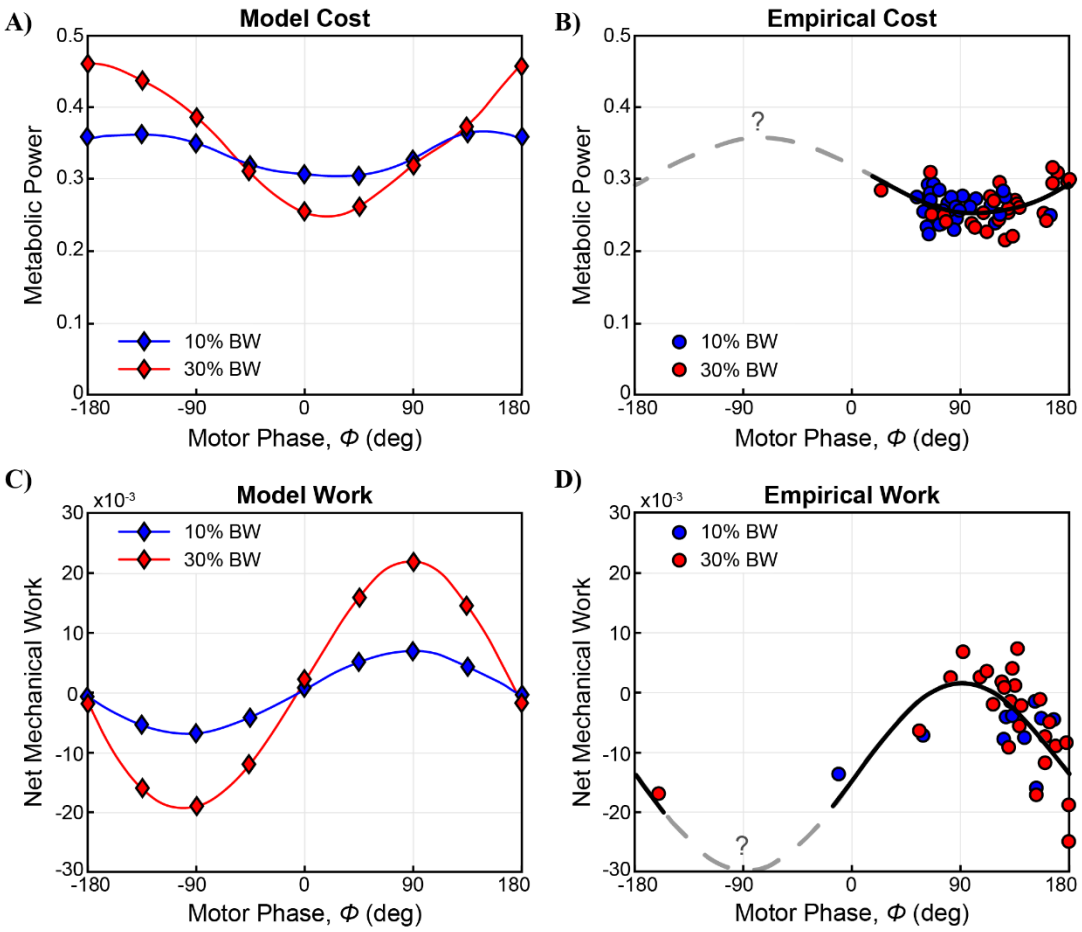

Figure 5.18. Optimization model predictions compared to subject data

Model outputs [**A)** and **C)**] are compared with empirical data from Experiment 1 [**B)** and **D)**]. Non-dimensional metabolic power is shown in **A)** and **B)**, whereas non-dimensional net mechanical work from the harness tension is shown in **C)** and **D)**. Both 10% and 30% BW oscillations (blue and red, respectively) are indicated in all plots. Model data in **A)** and **C)** are shown for a spline interpolation of phase optimized at 45^o intervals. Empirical data in **B)** and **D)** are fitted with sine functions to indicate how cost potentially extrapolates over the full range of phase (extrapolation indicated with grey dashed line, outside the range of data). The minima of both metabolic power curves from the model occur slightly after $\phi = 0^o$ **A)** where net mechanical work is slightly positive **C)**. Minimum metabolic power is observed in the empirical data near $\phi = 90^o$ **B)**, approximately where net positive work is maximal **D)**.

If subject phase data do, in fact, represent a global metabolic power minimum, one explanation as to why the optimization model does not predict the correct phase is that it neglects collisions and other forms of passive energy dissipation. Instead, the model purely uses leg forces (as well as the oscillation forces) to do negative work on the CoM. Although negative work is already discounted in the model by the efficiency of eccentric muscle contraction, having the ability to dump energy passively may improve the cost of

an interaction where more net positive work is received from the oscillation forces (larger motor phase), since it is even cheaper to dump this extra energy.

Another difference between the optimization model outputs and the empirical data is that the curves for net mechanical work in the model tend to average at around zero, whereas the data show net negative work over most of the phase domain. This discrepancy may partially be explained by the increased vertical oscillations of the CoM while subjects are entrained. As was shown with the linear mixed model, increases in vertical oscillations of the CoM are associated with an increase in net negative work done since the motors' inertia are coupled to these oscillations via the dynamics of the pulley-cable-harness system which imparts resistive forces on the CoM. Importantly, the optimization model does not predict an increase in vertical oscillations of the CoM, and this difference likely helps to optimize cost. Subjects in the real system may choose to maximize positive mechanical power from the system in part to reduce resistive forces from the dynamics of the system.

5.4.4 Interactions with other active devices

It is possible that the motor control system uses mechanical and/or physiological variables as a proxy for energetic cost, as other researchers have previously suggested (Snaterse et al., 2011). In this case, it appears that subjects prefer to maximize positive mechanical power from the oscillations. However, it is unclear if humans prefer to maximize power from all mechanical device interactions or if this is a phenomenon relevant to the specific system used in the experiments discussed here. Ahn and Hogan (2010, 2012) found that subjects aligned ankle torques at push off with those from an ankle exoskeleton. This example may or may not support our findings. On the one hand, this is a simple alignment of joint torques. On the other hand, the function of ankle torques during push off is to generate positive power on the CoM, and thus, one could argue that this alignment allows the actuator to maximize positive power on the CoM.

Another example is a study by Selinger et al. (2015) that used a knee exoskeleton to provide damping forces at the joint as a means to penalize high or low step frequencies and motivate individuals to adjust step frequency in the opposite direction to minimize metabolic exertion in real time. Since this device can *only* do negative work on subjects, it provides an interesting comparison. While subjects could not leverage any positive mechanical power from this device, they could, however, lessen negative mechanical

power by adjusting their step frequency. It is possible that subjects in the current oscillator studies were also attempting to minimize negative mechanical power from the harness forces. However, this seems unlikely, since subjects increase vertical CoM oscillations and this increased resistive forces in the system and ultimately, net negative work. There seems to be a disconnect between the preference of positive mechanical work from the motor forces and increased negative work from large vertical oscillations of the CoM.

Sánchez et al. (2019) investigated gait adaptation of subjects walking on a split-belt treadmill (a treadmill that contains separate belts moving at different speeds for each leg). In the study, they used a conceptual model to predict that subjects should employ a positive step length asymmetry (steps onto the fast belt should be longer than steps onto the slow belt) in order to gain net positive mechanical power from the treadmill and reduce metabolic output. Subjects were first guided through a range of step asymmetry options, in part to expose them to different gait strategies but also to measure metabolic cost as a function of step asymmetry. Next, subjects were allotted ten minutes to adapt on the split-belt treadmill in any way that felt natural. By the end of the ten minutes, subjects had, in fact, converged on the positive step asymmetry predicted in the study. This gait strategy was associated with decreased positive work done by the legs (i.e. down regulation) and reduced metabolic cost.

These examples provide evidence of preferred subject interactions that involve either reducing net negative work or increasing net positive work from dynamic external devices. This strategy is consistent with results seen in the experiments here, where subjects align motor forces with vertical CoM velocity to maximize mechanical power. However, in the case of the knee exoskeleton and the split-belt treadmill adaptations, both strategies were also aligned with minimal energetic exertion. Thus, it is unclear if the motivation was to increase positive mechanical power or to decrease metabolic cost. In experiments presented here, a solution that maximizes net mechanical power does not simultaneously minimize energetic cost (per the optimization model's prediction); however, there does appear to be a cost minimum at approximately the average motor phase chosen by subjects. A more controlled testing of motor phase is required to validate predictions by the optimization model and to verify energetic optimality of preferred subject interactions.

5.4.5 Entrainment stabilizes interactions for internal gait control models

Given that the majority of subjects learned to entrain under a large range of oscillation parameters, perhaps the biggest takeaway is that individuals prefer a stable interaction with the environment. This could be interpreted as further evidence in support of a feedforward gait control mechanism, since unpredictability makes feedforward control more difficult. If instead, the interaction with the environment is relatively stable, then this allows the motor control system more opportunity to rely on feedforward models, in particular when exposed to uncertain environments.

Various studies have shown evidence of a dual-part locomotor control process, including a rapid response to external stimuli (i.e. a feedforward control) and a slower, more gradual, fine-tuning of the response (Snaterse et al., 2011; O'Connor & Donelan, 2012; Pagliara et al., 2014). The authors interpreted their findings as evidence of an internal model used to make quick predictions (within seconds) regarding energetic cost based on state estimations. This approach was deemed reasonable under the assumption that direct optimization of energy consumption might last on the order of tens of seconds (i.e. slow response). In these studies, the fast response dominated the gait adjustment while the slower response more subtly adjusted the adaptation. Mawase et al. (2013) proposed that feedforward and feedback control mechanisms also play a role during gait adaptation to split-belt treadmills. Feedforward mechanisms were further associated with learned gait adaptations in experiments where a perturbation system was used to either stabilize and destabilize the lateral balance of individuals with and without incomplete spinal cord injury (Wu et al., 2017).

The experiments presented in the current study describe subject interactions that can be relatively volatile, at least before subjects converge on entrainment. In particular, inexperience with the oscillation system may require a three-part locomotor control process, where the dual-part control described previous is preceded by a "stabilizing" phase. Here, stability does not necessarily refer to fall avoidance or balance, but rather to a state of consistency, where interactions with the environment are sufficiently repeatable over subsequent steps. A relatively stable interaction may be required before a feedforward or a feedback control can be successfully implemented, and entrainment could provide that stability. Koban et al. (2019) explained a similar perspective in a slightly different context, with regards to interpersonal synchronization (e.g. individuals entrain gait when walking side by side). They proposed that theories of neural

computation such as predictive coding or the Free Energy Principle could explain the phenomenon. The idea was brought forth that “Each brain minimizes coding costs by reducing the mismatch between the representations of observed and own motor behavior. Continuous mutual prediction and alignment result in an overall minimization of free energy, thus forming a stable attractor state.” It is easy to see how such a principle might be translated to entrainment opportunities with the mechanical oscillator system presented here. In lieu of a direct metabolic motivation for entrainment, it may be possible that the brain is attempting to minimize coding costs by stabilizing the environment so as to make feedforward predictions more precise and actionable.

5.5 Conclusions

In this manuscript, we have shown that individuals prefer to entrain with oscillation forces as part of an interacting coupled oscillator system. Entrainment interactions occurred over a wide range of oscillation parameters, including frequency ($-10\% < \Delta f_m < 10\%$) and amplitude ($5\% < A_m < 30\%\ BW$). During entrainment, subjects preferred to align motor forces approximately with the vertical velocity of their CoM, thus maximizing mechanical power transferred to them from the system. Entrainment is also associated with large increases in the vertical oscillation of their CoM, which likely increases the amount of negative power done by resistive forces from the system dynamics. Linear mixed models were used to show that entrainment metrics are significantly increased at lower motor frequencies (below preferred step frequency) and higher oscillation amplitudes. No significant differences were found in metabolic power overall, except that baseline trials where individuals walked freely on the treadmill indicated less metabolic power and a low-frequency-high-amplitude trial condition was associated with higher metabolic power output. Still, entrainment seemed to have no bearing on metabolic measurements, except to the extent that net positive work by the harness forces was associated with reduced cost relative to net negative work. Motor phase significantly contributed to the net mechanical work done by the system.

Overall, the results suggest human subjects prefer interactions with the oscillator system that increase positive mechanical power (harness forces aligned with vertical CoM velocity). This interaction could be interpreted as evidence that the motor control system utilizes mechanical proxies to estimate energetic exertion, particularly when interacting with an uncertain environment (dynamic perturbing oscillations). However, it is possible

that this principle extends to feedforward modelling responsible for gait control in many other circumstances as well. Indeed, the relatively slow response of whole-body metabolic processes (usually delayed by tens of seconds or minutes) may provide the motor control system with motivation to use additional information to make predictions about cost and guide more urgent gait decisions before direct cost information is received.

CHAPTER 6

Discussion and Conclusions

6.1 The Energetic Cost of Human Walking

This thesis set out to describe human locomotion as an oscillating system where the individual interacts with their environment to accomplish the task while optimizing cost – in this case, energetic consumption. In Chapter 2, a review was conducted listing important insights into features of human gait – walking in particular – that contribute to energy efficient locomotion. Much of this insight stems from a perspective that recognizes energy exchange between the organism and the environment (through collision losses, etc.; Kuo, 2002; Kuo et al., 2005; Ruina et al., 2005; Srinivasan & Ruina, 2006; Lee et al., 2011; Bertram & Hasaneini, 2013; Lee et al., 2013) is often more revealing than energy exchange within the organism – e.g. fluctuations and transduction between kinetic and potential energy (Cavagna et al., 1977; Cavagna et al., 2002).

In walking, the heel of the foot contacts the ground just before the contralateral foot leaves the ground (i.e. double stance). The body's centre of mass (CoM) rises over the remaining contact leg in an arced trajectory (i.e. single stance), where the leg maintains roughly constant length, and gravity passively redirects the body from rising to falling late in stance. Since the leg does not change length during this time, little to no mechanical work is done on the CoM. This is the classical description of human walking as an inverted pendulum (Cavagna & Margaria, 1966; Alexander, 1980). As the body continues to fall toward the ground, the stance leg (now trailing the CoM) begins to deviate from its constant arc length, and the ankle plantarflexes to push off the ground. The impulse from push off imparts positive power and reorients the CoM velocity vector from pointing down to straight ahead in the direction of travel just as the heel of the next foot collides with the ground and energy is lost (Kuo, 2002; Ruina et al., 2005; Bertram & Hasaneini, 2013; Lee et al., 2013). Assuming a steady, periodic gait, positive work must always equal negative work done per step on average. Still, even though net mechanical work may balance out to approximately zero, both the positive and negative components of muscle work done by the legs are associated with metabolic energy consumed by the individual (Margaria, 1976; Hesser et al., 1977).

6.2 Optimization Modelling as a Simulation of Energy Minimization

Since a large proportion of mechanical work in walking is utilized to redirect the CoM from falling to rising in the step-to-step transition (Donelan et al., 2002A; Donelan et al., 2002B), it provides a useful framework for developing hypotheses regarding the cost of locomotion and its relationship to interactions with the environment. In Chapter 2, trajectory optimization was used to test whether a linear actuator driving a load vertically off the CoM of a bipedal model could reduce cost when its forces were optimized. The idea was for the actuator to generate an upward reaction force on the CoM and help facilitate the step-to-step transition at a reduced cost. When work done by the additional actuator was not included in the cost function, the model did indeed leverage the actuator using this strategy. In fact, it was able to manage the step-to-step transition entirely, allowing work by the legs to plummet almost to zero. However, when work done by the actuator was included in the cost function, the model chose to only leverage isometric forces from the actuator, and the solution was dynamically equivalent to bipedal walking with additional load coupled to the CoM. The optimization was rerun multiple times with the cost of actuator work weighted from zero to one, to evaluate solutions with intermediate actuator contributions. It became clear that although the vertical actuator could perform all the work needed to redirect the CoM during the step-to-step transition, this strategy was far more costly.

The legs can manage the transition much more efficiently due to the geometry involved. The angle between the trailing leg force and the CoM velocity vector during push off is much closer to orthogonal compared to that of the vertical actuator, and thus, projection of push off forces onto velocity in the form of mechanical power is much less costly. A similar geometry occurs for the leading leg performing negative work as the velocity vector points up and forward. Even though the vertical actuator is quite inefficient, it can still be used as a manipulation of the cost of human walking when the cost of the actuator is not considered, e.g. an external oscillation coupled to the biped. Indeed, this case study premises the main objective of this thesis, which is to understand how experienced and inexperienced individuals learn to interact within coupled oscillator systems, and what drives them to choose the interactions that they choose.

Two coupled oscillator systems were chosen to complement and contrast one another. The first system was passive in nature and investigated load-carrying strategies that

Vietnamese farmworkers use to carry extremely heavy loads on flexible bamboo poles during fieldwork (Chapter 4). The second system placed human subjects in a controlled machine oscillation environment while they walked on a treadmill in laboratory experiments (Chapter 5).

6.3 Quantifying Properties of Bamboo Poles as a Passive Oscillating System

Before exploring the coupled oscillator systems, Chapter 3 was used to characterize properties of the bamboo pole itself, whilst considering design features that may be important to the energetics of carrying loads in this fashion. Several basic mechanical properties were identified based on the assertion that in order for the flexibility of the pole to have meaningful influence on the cost of gait, the damped resonant frequency would likely need to be tuned approximately within range of step frequencies associated with natural walking. Thus, properties such as spring constant, damping ratio and second moment of area were directly measured in order to calculate Young's modulus and resonance with classical beam theory.

Load-deflection tests were used to quantify spring constant and calculate Young's modulus, while resonance tests were used to characterize damping ratio from logarithmic decay of free vibrations. These data were then used to predict resonant frequency as a function of load and were compared to direct measurements of the damped resonant frequency during free vibration. This procedure was conducted on four bamboo poles purchased from local farmworkers in Vietnam and brought back to the lab for testing. The results were compared to testing data performed on ten additional bamboo poles on site in Vietnam. Resonant frequencies generally ranged from around 2-4 Hz in the field-tested poles, though slightly lower in the lab-tested poles, for loads as high as 20.5 kg at each end. Thus, the low end of this frequency range approached relevant step frequencies at a reasonable walking speed. Values for damping ratio were extremely low ($\zeta < 0.02$), as they were for hysteresis in the load-deflection curves. A full evaluation of the pole properties indicated that the bamboo poles were well-tuned to affect the energetics of gait when bearing very heavy loads (20 kg and more).

6.4 Subtle Gait Adjustments in Experienced Pole Carriers

The pole properties were implemented in trajectory optimization procedures during Chapter 4. The optimization was directed to minimize energetic cost for a biped model with a point mass load suspended from a spring-damper mechanism representing the flexible pole. Optimizations were used to sample a large parameter space along dimensions of step frequency, pole stiffness, two load levels and two damping coefficients. The results of the model were used to map cost landscapes encompassing the different variables. At the same time, experiments were carried out with experienced pole carriers in Vietnam. Subjects were asked to walk with 30 and 50% body weight (BW) loads on two different pole types (rigid and compliant). Step frequency was measured with accelerometers to detect adjustments in cadence when switching from the rigid to the compliant pole, or from low loads to high loads. These shifts in step frequency were then compared to local gradients of the cost functions predicted by the optimization model. It was hypothesized that subjects would increase their step frequency when operating on a negative cost gradient, decrease their frequency when operating on a positive cost gradient and maintain their frequency when operating on a zero gradient. When comparing shifts in frequency to the cost gradient, a negative correlation ($R = -0.67, p = 0.009$*; asterisk indicates significance after controlling for multiple significance testing) was found supporting the hypotheses when carrying heavy loads of 50% BW. Still, the results were far more ambiguous when subjects carried 30% BW loads ($R = -0.23, p = 0.430$), at least as a group. However, there were subjects who appeared more sensitive and did exhibit significant frequency shifts consistent with expectations based on their individual cost gradients.

Overall, changes in step frequency due to pole type were found to be significant ($p = 0.014$*). However, when the statistical model included non-dimensional walking speed as a covariate, this effect decreased ($p = 0.083$). On the other hand, a significant interaction between pole type and walking speed ($p < 0.001$*) indicated that subjects may have used changes in speed as a means to increase or decrease frequency when switching from the rigid pole to the compliant pole. This interpretation is supported by empirical data showing that metabolic cost is reduced when step frequency increases/decreases are correlated with speed increases/decreases (Bertram & Ruina, 2001; Bertram, 2005).

6.5 Mechanics and Cost of Interactions with a Loaded Bamboo Pole

The optimization model predicted cost to be minimized when step frequency is slightly higher than the damped resonant frequency of the loaded pole (by a factor of 1.08-1.30, depending on the level of damping on the load). Step frequencies in this region were associated with decreased loading during double stance and increased loading near the middle of single stance (load oscillations out of phase with the CoM). This oscillation pattern was consistent with the optimization model in Chapter 2, which found cost to be minimized when the actuator provided upward force during double stance. The reason this interaction is less costly is because mechanical power is proportional to force, and the legs were offloaded during double stance – a period of time associated with peak power. On the other hand, the increased loading during single stance could be supported by isometric leg forces (i.e. no effect on power since contraction velocity is zero). Oscillations with increased loading during double stance were most costly (load oscillations in phase). This interaction occurred at step frequencies just below the damped resonant frequency of the loaded pole: a factor of 0.85-0.90 times resonance).

6.6 Consequences of Damping Properties

Although Chapter 3 revealed extremely low damping ratio measurements for the poles (average $\zeta = 0.013$), this parameter drastically overpredicted load oscillation amplitudes during trials where subjects carried the poles in practice. As such, a regression was used to fit damping ratio to the oscillation amplitude data from experimental trials with subjects. The fit yielded a different damping ratio ($\zeta = 0.172$), still underdamped, but an order of magnitude higher than the property when characterized with direct measurements of the poles. At higher damping values, the effect of cost based on phase of the loading fluctuations was complicated by the fact that phase changed more gradually near resonance; thus, there were fewer frequencies that allowed a favorable phase of the oscillation (step frequency >> resonance) while at the same time providing a meaningful oscillation amplitude able to influence cost (step frequency ≈ resonance), since load oscillations decreased at higher step frequencies.

It is possible that the loaded pole experiences more energy loss in practice for several different reasons. For example, there is likely increased wind velocity (thus, drag) when individuals carry their poles over ground versus when they are tested in a fixed position. It also seems likely that increased damping occurs when the pole is rested on the

shoulder, as soft tissues in the human body can contribute to energy losses in the system. Another possibility is that experienced pole carriers may utilize an active strategy to intentionally damp out energy from oscillations to improve stability and/or exercise control over the pole; specifically, the natural carrying style of experienced pole carriers is observed to support the bamboo over a single shoulder and rest the hand over the top of the pole. It is possible that experienced carriers use the resting hand as an active damping mechanism.

6.7 Resolving Inconsistent Findings in the Literature

There are many seemingly conflicting results in the literature comparing the cost of carrying loads with compliant devices. Kram (1991) explained that a very compliant pole can repeatedly flex as the carrier's body oscillates up and down during gait, and this allows the load to maintain a relatively flat horizontal trajectory. It was thought that the carrier would not need to do work to lift the load with repeated steps and thus, the carrying cost should be decreased. When Kram measured the metabolic output of westerners carrying compliant poles made from polyvinyl chloride (PVC), he found that cost increased similar to that expected when carrying the same load in a conventional backpack, even though the trajectory of the load was indeed flatter with the compliant pole. It was acknowledged that the flexing pole still transmitted forces to the body and may have sabotaged any potential cost savings. The optimization model in Chapter 4 predicts that the cost of carrying a compliant pole approaches that of carrying a rigid pole (or using a backpack) when spring constants are very low – this despite differences in loading profiles: constant force for a compliant load, and in-phase oscillations for the rigid load. Still, constant loading from a low-stiffness load may affect mechanical power over a larger duration than loading from a rigid load (relatively impulsive) and thus, the cumulative effect on cost may be approximately the same. It is true that Kram's experiments (1991) studied running instead of walking, and this distinction cannot be ruled out as making any interpretation based on the walking optimization model invalid.

Despite Kram's study showing no difference in cost between carrying loads on a very compliant pole versus a backpack, recent modelling results have indicated low stiffness to be optimal (Ackerman & Seipel, 2014) and stiffness with resonance near step frequency to be most costly (Ackerman & Seipel, 2014; Li et al., 2016A). The optimization modelling results in Chapter 4 directly challenge these assertions since cost

is shown to be minimized at step frequencies only slightly higher than resonant frequencies (not when step frequency >> resonance). The modelling results presented in this thesis not only suggest that cost is most-affected at frequencies near resonance, but also that slight deviations from resonance (either higher or lower) can determine the difference between minimum cost and maximum cost. Results from a study using a backpack with a compliant suspension system (Foissac et al., 2009) found that cost was increased at walking speeds where step frequency was slightly lower than resonance. They also found that subjects reduced the vertical excursion of the body. This result is precisely what the optimization model predicts in this range of frequencies. Although reducing vertical excursion typically leads to a higher cost since more work is performed due to increased leg compliance (Ruina et al., 2005; Ortega & Farley, 2005; Gordon et al., 2009), this strategy is still cheaper when the alternative is to bear very large load oscillations in phase with the body at resonance.

Rome et al. (2005, 2006) found that a compliant backpack suspension device significantly decreased metabolic cost. Although spring constant of the device was not reported, they identified load oscillations out of phase with the body, consistent with predictions of minimized cost by the optimization model. Another group studying walking with bamboo poles found that subjects consumed approximately 5% less metabolic energy when carrying the compliant pole at appropriate frequencies compared to a rigid steel pole. The authors explained that high-amplitude out-of-phase load oscillations explained the cost savings since they cancelled out oscillations of the body, thus leading to a flatter system trajectory. Although their results were consistent with the optimization model's predictions, it is unclear why a flat system trajectory should be less costly generally. Consider that the cost of walking is greatly increased when individuals increase leg compliance to minimize vertical excursion of the body (Kim & Bertram, 2018; Ortega & Farley, 2005; Gordon et al., 2009). Although this type of gait is also characterized with a flat system trajectory, cost is greatly increased. On the other hand, when one considers work done by the legs to overly flex in such a crouched position, it is easy to see why such a gait might lead to increased metabolic cost.

6.8 Future Directions on Pole Carrying Studies

In previous studies, researchers used novice participants (i.e. Westerners) to carry compliant poles in experiments. However, it is possible that any benefits associated with

the strategy of carrying a bamboo pole requires substantial experience and/or training [e.g. pole balance (Li et al., 2019B)]. Thus, study participants were recruited in Chapter 4 only after confirming ample experience using such devices during farm work in Vietnam. A main objective of the study was to allow experienced pole carriers to use the device in as natural a setting as possible (i.e. minimal experimental constraints, testing done in the field, etc.). Although the goal was to observe natural carrying styles without interference, one drawback was reduced experimental control over the relevant variables. For example, subjects used whatever pole they felt comfortable with and whichever gait parameters they preferred (speed, frequency, etc.). This meant that different subjects displayed different responses when switching from the rigid pole to the compliant pole, even though the variety of responses may have all been appropriate, given the circumstances for each subject.

Future experiments might benefit from a more controlled approach. Specifically, a pole capable of variable stiffness could be useful. Such a pole might consist of multiple wooden slats pinned together at the ends, but with a power screw threaded through the top layer. An actuator could drive the power screw to spread the slats apart to increase the second moment of area, and thus, stiffness, in real time. A variable-stiffness pole could be useful for adjusting resonance without having to change load. Ultimately, this benefit would allow for experiments where initial conditions of the pole's stiffness are controlled to place a subject on a steep cost gradient, and test for the same response in all subjects (e.g. increased step frequency over time). A slightly different experiment could be conducted where a subject is given a controller to adjust stiffness during experiments in real time. This would allow subjects to explore different interactions with the loaded pole without having to alter their own gait. Future experiments conducted in the lab would benefit from additional equipment to measure important biomechanical and physiological variables (e.g. ground reaction forces, metabolic power, etc.). Electromyography could also be used to measure activation in various muscles of the arm to provide evidence of active damping strategies used to steady oscillations.

6.9 Gait Interactions with Machine Oscillations

Although bamboo pole carrying is a great system to study ecological interactions within coupled oscillator systems, there are fundamental limitations. Given the passive quality of the oscillating load, many aspects of the interaction are constrained. For example,

phase and amplitude of the load's oscillation (relative to the person) are fundamentally dependent on step frequency. Due to this dependence, it is difficult to isolate the different variables and their contribution to gait choices made by individuals.

In Chapter 5, subject responses to a machine oscillator were tested, and the system was programmed to simultaneously control parameters such as amplitude and frequency, independently. Three experiments were conducted; in Experiment 1 (also called the Cost of Entrainment test), subjects were exposed to oscillations of constant amplitude and frequency for a ten-minute duration. During the first five minutes, subjects were free to respond as they preferred ("free entrainment" phase of the experiment). During the second five minutes, a metronome was used to guide the subject's cadence at a frequency not matched to that of the motors ("constrained non-entrainment" phase of the experiment). Metabolic power was measured throughout all trials and compared between both phases of the experiment. In Experiment 2 (also called the Sensitivity to Entrainment test), subjects were exposed to oscillations of constant frequency, starting with a very small amplitude that gradually increased over time. The amplitude where subjects initially entrained was referred to as their sensitivity to entrainment (A_m^*) and was recorded for multiple motor frequencies. In Experiment 3 (also called the Limits of Entrainment test), subjects were exposed to oscillations of constant amplitude, and starting with a motor frequency matched to their own preferred step frequency. However, the motor frequency gradually drifted away from preferred and then returned to preferred over time. The frequency where subjects first rejected entrainment was referred to as their limit to entrainment (Δf_m^*) and was recorded for multiple amplitudes and motor frequencies that drifted into higher or lower ranges.

6.10 Predicting Energy-minimizing Interactions with the Oscillator

In addition to the experiments, a trajectory optimization model was used to make predictions regarding energy-minimizing interactions in the system. The output solution of the model indicated that energy is minimized when the interaction provides peak upward force just after the middle of double stance – approximately aligned with the force hump due to heel strike. This interaction extracts net positive mechanical work from the oscillations since upward force overlaps with positive aspects of centre of mass (CoM) velocity more than negative aspects. In the model, leg work was differentially scaled by the inverse of concentric and eccentric muscle efficiency (for positive and

negative work, respectively). By allowing the oscillations to do net positive work on the CoM, this allowed the legs to downregulate force (and thus, power) during the step-to-step transition. Overall, net negative leg work was required to compensate for net positive work from the oscillator forces, since the optimization was constrained to steady periodic gaits only (i.e. net work must equal zero). However, less leg work was done overall. The bias towards positive power was modest, and overall, forces were mostly aligned with double stance.

6.11 Entrainment with Static Oscillation Parameters

In Experiment 1, subjects tended to entrain to motor frequencies more consistently and robustly at higher amplitudes ($A_m = 30\%\ BW$) and at frequencies lower than preferred step frequency. In fact, no subjects ever entrained in the trial condition with parameters: $\Delta f_m = 6\%$ and $A_m = 10\%$ (i.e. high frequency, low amplitude). Two metrics were devised to indicate levels of entrainment for subjects during different experimental conditions. Entrainment step ratio (ESR) was defined as the ratio of entrained steps to total steps taken during the free entrainment phase of the experiment, and $\Delta\bar{t}_e$ was the average time duration of entrainment bouts, since sometimes subjects only entrained for a few steps at a time. Motor frequency was found to have a significant effect on these metrics ($p < 0.001$* for both metrics), where higher frequencies were associated with lower levels of entrainment. Conversely, higher amplitudes were associated with higher levels of entrainment ($p < 0.001$*, again for both metrics).

6.12 The Link between Mechanics and Metabolic Energy

Non-dimensional metabolic power was compared over all trial conditions tested. Subjects had a higher metabolic output when they walked on the treadmill wearing the harness system versus without. Additionally, subjects had a higher metabolic power in the trial condition associated with the oscillation parameters: $\Delta f_m = -6\%$ and $A_m = 30\%$ body weight (BW). No significant differences were found between metabolic power during the free entrainment and the constrained non-entrainment phases of the experiment. Furthermore, the entrainment step ratio (ESR) had no effect on metabolic cost ($p = 0.488$). These results, when taken together, suggest that metabolic cost did *not* play a direct role in motivating entrainment. However, net mechanical work from the harness tension forces did have a strong effect on metabolic power ($p < 0.001$*).

Although most subjects received net negative work, those who had less negative work (or more positive work) consumed less metabolic power.

Certain variables were found to play a large role in determining the net mechanical work done on subjects by the harness forces. Net mechanical work was maximal when peak tension forces occurred at ~100° (or about a quarter of a cycle after the middle of double stance) and decreased until about 200° ($p = 0.009$*). Vertical CoM velocity also peaked at around 100°, and since power is the product of force and velocity, this phase resulted in positive net mechanical work. Furthermore, metabolic cost was minimized at this phase value. The amplitude of the vertical CoM oscillation also contributed to the amount of net mechanical work done on the subject, where larger oscillations were associated with more net negative work and vice versa ($p = 0.009$*). This is likely due to a coupling between the subjects' body mass and the mass of the motors, via the pulley-cable system. Due to this coupling, not only did the motors increase harness tension when pulling on the subject, but the subject also increased harness tension by pulling on the motors, and the latter created a resistive inertial effect that resulted in increased negative work on subjects.

6.13 Paradoxical Subject Actions during Entrainment

As a group, subjects consistently made two prominent adjustments when converging on entrainment with the oscillator system. (1) They aligned peak tension due to motor forces approximately with fluctuations in vertical CoM velocity, thus increasing net *positive* power from the system. (2) They also drastically increased the vertical oscillation amplitude of their CoM (by 58.2% and 125.5% when $A_m = 10$ and $30\%\ BW$, respectively), thus increasing net *negative* power from the system. In general, these two effects ran contrary to one another. However, subjects who were able to maximize the effect of (1) and mitigate the effect of (2) tended to have lower metabolic power.

6.14 Discrepancies between the Model and Empirical Entrainment

In Chapter 2, a trajectory optimization model showed that upward force from a coupled oscillator mechanism could assist the legs in redirecting the CoM from falling to rising during double stance. In doing so, the legs were able to manage the step-to-step transition with less work overall, while accommodating extra downward force isometrically near the middle of single stance. However, when modelling the oscillator

system described in Chapter 5, mechanical work was scaled by the inverse of efficiency associated with positive and negative muscle work. The result was a very similar solution, albeit biased slightly to allow peak upward force to occur during peak heel strike forces (just after the middle of double stance, approximately 10° phase). This slight shift highlights the efficiency of gaining modest net positive work from the oscillator system, compensating with net negative leg work, and reducing scaled leg work overall to lower cost.

If it is cheaper to receive positive power from the oscillator system, then why not exaggerate the strategy by completely aligning positive forces with positive velocity (e.g. phase closer to 100° instead of 10°)? Indeed, this is approximately what subjects did on average during entrainment. In the model, such a strategy may increase positive power at the trade-off of a less efficient step-to-step transition. If oscillation forces occur after double stance, then downregulated push off will not be effective at reorienting the vertical CoM velocity in order to reduce collisions at heel strike (i.e. more energy dissipation; Kuo, 2002). Ultimately, this means that push off downregulation cannot take place to the same degree, since the extra negative work must be offset by enough positive work. The problem is exacerbated at this phase since peak downward forces occur a quarter cycle before the middle of double stance, i.e. just before heel strike. Essentially, these downward forces drive the CoM into the ground and exaggerate energy losses. Thus, it is optimal to maintain the bulk of upward force during double stance to help manage redirection of the CoM during the step-to-step transition, yet also take advantage of modest net positive work and gain a slight efficiency boost. This is not what subjects did.

It is unclear why subjects did not, on average, adopt this strategy. One explanation is that the model is wrong, or perhaps oversimplified, and does not sufficiently represent the reality of the subjects' interactions with the oscillator system. Certainly, the model is extremely simplified; it only maintains the most crucial elements needed to describe human walking. Furthermore, the mass-spring-damper elements also likely oversimplify the dynamics of the pulley-cable-system, which in reality has friction, inertia beyond that of the motors, gearing due to the configuration of the pulleys, and other features that complicate the dynamics. Still, there is some evidence that the average subject chose a locally optimal interaction with the system, if not a globally optimal solution. Natural variation between individuals and trial conditions shows that the average subject chose a

phase relationship minimizing metabolic power. However, caution should be exercised when interpreting this evidence. The study design did not systematically control for phase, and furthermore, only a small range of phase was sampled due to natural variation of subject-preferred interactions. It is unclear if subjects could reduce metabolic power at different phases underexplored in the experiments.

If the model is correct, and subjects chose a suboptimal phase interaction with the system, why might this be? Perhaps subjects are attempting to maximize positive mechanical power from phase with the motor forces as a means to overcome net negative power resulting from increased CoM amplitude. It would seem that increased oscillation amplitudes imply a lack of force downregulation from push off and heel strike during double stance. This interpretation of the results, if correct, would contrast studies showing that subjects learn to downregulate push off forces in the presence of an ankle exoskeleton (Gordon & Ferris, 2007). It might be more difficult for the motor control system to functionally connect upward forces at the trunk with push off forces at the periphery. This may hint at sensory feedback from mechanosensors more local to the tissues involved during plantarflexion.

6.15 Defining the Basin of Entrainment

During Experiment 2, subjects initiated entrainment over a range of frequencies displaced from their preferred step frequency (either higher or lower). The amplitude where individuals first initiated entrainment (sensitivity to entrainment, A_m^*) was increased when larger frequency adjustments were required to entrain ($p = 0.005$*). Furthermore, subjects required larger amplitudes to entrain at motor frequencies higher than their preferred and lower amplitudes at frequencies lower than their preferred, regardless of the overall magnitude of the adjustment. In other words, subjects seemed to be more sensitive to entrainment in lower frequency ranges.

During Experiment 3, subjects followed the motor frequencies as they drifted away from their preferred step frequency, but eventually rejected entrainment at motor frequencies that were too extreme (limits of entrainment, Δf_m^*). Subjects were willing to maintain entrainment with frequencies much farther away from preferred at higher oscillation amplitudes ($p = 0.001$*). Furthermore, subjects entrained to oscillation frequencies much farther away from preferred for frequencies below their preferred step frequency ($p <$

0.001), similar to results in Experiment 2. When the motor frequencies drifted back towards preferred, subjects often re-entrained with the oscillations and followed them the rest of the way. However, there was no statistical difference between the limits of entrainment as motor frequencies drifted away versus when they drifted back ($p = 0.914$), i.e. no hysteresis was observed.

Throughout all three experiments, subjects entrained over a wide range of oscillation parameters. In some instances, subjects entrained to oscillations with amplitude as low as 5% BW (or ~33 N) and at motor frequencies as far away as 13% from their preferred step frequency. In the Limits to Entrainment test, some subjects were able to follow the motor frequencies to their most extreme drift point ($\Delta f_m = \pm 10\%$), even at the lowest amplitude tested ($A_m = 10\%\ BW$). These results represent large step frequency adaptations not commonly seen experimentally. Other studies have shown adaptations between approximately ±2–8% (Selinger et al., 2015; Selinger et al., 2019; Simha et al., 2019; Wong et al., 2019). Still, there were many subjects that struggled to learn entrainment at the most modest motor frequencies and the strongest oscillation amplitudes.

6.16 On Differential Subject Responses

It is still unclear why some subjects entrain, and others do not. One option is that individuals have different levels of physical intelligence. This could mean that some subjects were attempting to entrain, but had a hard time accomplishing the task – i.e. learning what they needed to adjust in order to converge on the correct solution. This explanation might apply to individuals who exhibited particularly transient entrainment, where they moved in and out of synch with the oscillations. Another option is that subjects are simply unaware that entrainment is even an option. This may result from a lack of sensitivity to signals that stimulate entrainment. In past studies, researchers have shown that subjects sometimes require a “guided exploration” where they are led through a range of options available to them in an experiment before they are able to spontaneously converge on appropriate responses (Sellinger et al., 2015; Sellinger et al., 2019; Simha et al., 2019). In the experiments described here, no guided exploration was conducted, and most individuals were still able to discover entrainment as a possible gait interaction. Part of the reason for this is that non-entrainment naturally provides exploration to subjects; non-entrainment requires that interactions between the

oscillator and the human are always changing with every step, since two non-entrained signals create a lower frequency oscillation of the interaction. Still, this form of exploration requires that subjects recognize the appropriate entrainment interaction as it passes them by, and this may be how physical intelligence plays a role. Other researchers have attempted to use natural variation in the environment to facilitate learning of gait adaptations to optimize energy expenditure in an exoskeleton (Wong et al., 2019). However, in this example, subjects failed to learn the appropriate adjustments.

One final option explaining differential subject responses is that perhaps individuals were fully aware that entrainment was an option, and yet they decided against it. Indeed, it seems reasonable to assume that individuals may have different perceptions on what constitutes an appropriate interaction with a machine as well as different preferences based on comfort levels, state of mind, etc.

There were two subjects that rarely entrained during Experiments 2 and 3, and their examples may provide interesting case studies for some of the explanations described. In each example, the respective subject took a drastically different approach to interacting with the system. One subject simply maintained their preferred step frequency in almost all trial conditions. Step frequency variation increased somewhat during oscillations, but there was never any hint of real entrainment. After the data collection was finished, the subject made a comment that they felt they were “really adapting well” to how the system was interacting with them. This inherent disconnect may be an example of someone unaware that entrainment is even an option. Alternatively, it could be an example of someone who has a very different perception on what their interaction should be.

The other subject who rarely entrained chose to exaggerate their step frequency wildly and somewhat unpredictably. For example, in Experiment 3, they would sometimes increase their frequency, presumably to avoid entrainment at the beginning of the trial. When the motor frequency began to increase as well, the subject would increase their frequency even more, apparently in an attempt to outrun the motor frequencies. The end result was an exhausting display of one’s refusal to interact with the system meaningfully for more than a step or two. After the data collection was finished, I asked the subject why they responded as they did. Their response indicated that entraining with the

system gave them a sense of anxiety, almost as if the system was in control of their movements more than their own body. Thus, to preserve autonomy, the individual chose to expend a lot of energy “running” away from the motor frequencies. In the context of interactions quantified in Experiment 1, what the subject was saying made a lot of sense. When subjects entrain, they align the motor forces with their CoM vertical velocity, and these forces produce positive power. Perhaps this subject was uncomfortable allowing the machine oscillations to do too much work on their body, since it provided an experience of lacking personal control and/or autonomy of their own body motions.

The anecdotal evidence of these two subjects’ informal testimony prompts an intriguing and fundamental question: what is the role of conscious perception in gait control decisions? Common experience tells us that we do not typically think about walking in our daily lives. However, the experiments involved interacting in an environment that was likely very much outside the realm of daily experience for most subjects. It may be possible that individuals consciously monitor their gait and/or posture when navigating unusual or tricky environments (Yogev-Seligmann et al., 2008; Huffman et al., 2009). This is analogous to the novice golfer focusing attention on their golf swing during a lesson with a trainer (Guadagnoli et al., 2010); the immediate outcome may not be impressive, but it may be helpful for individuals to consciously focus on technique until they have learned an effective motor control strategy given the task goal (Masters & Maxwell, 2008).

6.17 Future Directions on Studies Exploring Machine Oscillations

Future studies investigating the interactions of human subjects in coupled oscillator systems should attempt to quantify a more thorough relationship between metabolic cost and phase of the oscillator forces on the CoM. In the studies described here, natural variation of individuals during various testing conditions indicated a local minimum in metabolic cost where phase of peak motor forces relative to the middle of double stance was approximately 100°, more or less aligned with peak vertical CoM velocity. However, it is unclear how energetic cost varies in other regions of phase. In particular, it would be useful to test if phase near double stance results in higher or lower cost than that preferred by subjects on average. Such studies could utilize a metronome signal, visual feedback or a combination of the two to regulate frequency and phase of subjects for time durations long enough to measure metabolic cost.

At the same time, such studies could gather additional relevant data, including electromyography signals from relevant muscles to test for downregulation or the lack thereof, during entrainment with oscillations. Ground reaction forces could also provide opportunities to calculate leg work to compliment measurements of work done by harness forces. Motion capture could also be used for a more detailed accounting of work done at the joint level, as well as subtle adjustments in the kinematic patterns of various body segments during phase interactions. Force feedback could be implemented in the oscillator system, in order to achieve a greater degree of control over the interactions subjects experience in various tests. Finally, learning studies could also be conducted to test for changes in motor control strategies after repeated training sessions in the system.

6.18 Conclusions

Although bamboo pole carrying may appear more different than similar to a mechatronics system that pulls on people as they walk on a treadmill, the fundamental dynamics interactions are quite analogous. In one case, the flexing of the pole bears down on the carrier in alternating periods of on-loading and off-loading. In the other, tension cables provide alternating periods of upward and downward forces to the individual in the system. Of course, with bamboo poles, carriers have more control over the oscillations of the suspended load and can therefore, assert their intentions more freely on the system. Furthermore, entrainment is given since the forcing function drives the oscillation frequency of the load. At the same time, variables such as phase and relative magnitude are highly dependent on the step frequency taken and its proximity to resonance in the system. Meanwhile, parameters of oscillations in the mechatronics system are prescribed by the controller operating the actuators, although subjects can affect some aspects of their interaction to a certain degree. In many cases, subjects expressed suspicion that the oscillations were changing from cycle to cycle, even when parameters were held constant. This often occurred when subjects had not learned to entrain in the system, and thus, the phase interaction was indeed changing with every step, although not due to the programming of the motors. It was not clear that any subjects in the pole carrying study ever felt that they were not in control of their own pole.

Still, both examples provide opportunities to explore humans interacting within dynamic external environments. Such interactions can help provide important insights on motor control regimes that determine successful integration of the organism with its environment. Certainly, part of what influences that success is how well the organism can manage crucial resources needed to survive. It is clear that energy is one such resource, and many locomotory behaviors appear to be motivated in order to limit its expenditure. At the same time, energy's role in shaping movement patterns and motor behaviors in real time is convoluted by sensory-motor noise, inter- and intra-personal variability, perception of task, and athletic capability. It is true that human locomotion is fundamentally just an oscillation, but it is an oscillation driven by intelligence, both conscious and subconscious. Only by continuing to probe fundamental aspects of motor behavior will we be able to sustain continued progress toward uncovering mechanical, physiological and neurological principles underlying gait control.

Bibliography

Abram, S. J., Selinger, J. C., & Donelan, J. M. (2019). Energy optimization is a major objective in the real-time control of step width in human walking. *Journal of Biomechanics*. *91*(25), 85-91. doi: 10.1016/j.jbiomech.2019.05.010

Ackerman, J., & Seipel, J. (2011A). Coupled-oscillator model of locomotion stability with elastically-suspended loads. *Proceedings of the ASME 2011 International Design Engineering Technical Conference & Computers and Information in Engineering Conference*. August 28-31, Washington, DC, USA.

Ackerman J, & Seipel J. (2011B). Energetics of bio-inspired legged robot locomotion with elastically-suspended loads. *Proceedings of the 2011 IEEE/RSJ International Conference on Intelligent Robots and Systems*; 2011 September 25-30, San Francisco, CA, USA.

Ackerman, J., & Seipel, J. (2014). A model of human walking energetics with an elastically-suspended load. *Journal of Biomechanics*. *47*(8), 1922-1927. doi: 10.1016/j.jbiomech.2014.03.016

Ackerman, J., Kelley, K., & Seipel, J. (2015). Dynamics of carrying a load with a handle suspension. *Journal of Biomechanics*. *48*(6), 1084-1091. doi: 10.1016/j.jbiomech.2015.01.025

Ahn, J., & Hogan, N. (2010). Feasibility of dynamic entrainment with ankle mechanical perturbation to treat locomotor deficit. *Proc. IEEE Ann. Int'l Conf. Eng. in Medicine and Biology Soc. (EMBC)*. August 31-September 4, Buenos Aires, Argentina.

Ahn, J. & Hogan, N. (2012). Walking is not like reaching: Evidence from periodic mechanical perturbations. *PLoS ONE*. *7*(3): e31767. doi: 10.1371/journal.pone.0031767

Alexander, R. McN. (1976). *"Mechanics of Bipedal Locomotion" in Perspectives in Experimental Biology 1.* P. S. Davies, ed., Oxford, Pergamon.

Alexander, R. McN. (1980). Optimum walking techniques for quadrupeds and bipeds. *Journal of Zoology*. *192*(1), 97-117. doi: 10.1111/j.1469-7998.1980.tb04222.x

Alexander, R. McN. (1992). A model of bipedal locomotion on compliant legs. *Philosophical Transactions of the Royal Society B-Biological Science*. *338*(1284), 189-198. doi: 10.1098/rstb.1992.0138

Amada, S., & Lakes, R. S. (1997). Viscoelastic properties of bamboo. *Journal of Materials Science*. *32*(10), 2693-2697. doi: 10.1023/A:1018683308211

Athans, M., & Falb, P. L. (1969). *Optimal control*. New York, NY: McGraw Hill.

Baker, W. E., Woolam, W.E., Young, D. (1967). Air and internal damping of thin cantilever beams. *International Journal of Mechanical Sciences*. *9*(11): 743–766. doi: 10.1016/0020-7403(67)90032-X

Banks, H. T., & Inman, D. J. (1991). On damping mechanisms in beams. *Journal of Applied Mechanics*. *58*(3): 716-723. doi: 10.1115/1.2897253

Bastien. G. J., Willems, P. A., Schepens, B., & Heglund, N. C. (2005). Effect of load and speed on the energetic cost of human walking. *European Journal of Applied Physiology*. *94*(1–2), 76–83. doi: 10.1007/s00421-004-1286-z

Benjamini, Y., & Hochberg, Y. (1995). Controlling the false discovery rate: A practical and powerful approach to multiple testing. *Journal of the Royal Statistical Society B-Methodological*. *57*(1), 289-300. doi: 10.1111/j.2517-6161.1995.tb02031.x

Bertram, J. E. A. (2005). Constrained optimization in human walking: cost minimization and gait plasticity. *Journal of Experimental Biology*. *208*(6), 979–991. doi: 10.1242/jeb.01498

Bertram, J.E.A. (2016A). *Concepts through time: Historical perspectives on mammalian locomotion. Ch. 1. In: Understanding mammalian locomotion: Concepts and applications* (1st ed.). Wiley-Blackwell, Hoboken, USA, pp.1-25.

Bertram, J. E. A. (2016B). *Considering gaits: Descriptive approaches. Ch. 2. In: Understanding mammalian locomotion: Concepts and applications* (1st ed.). Wiley-Blackwell, Hoboken, USA, pp.27-50.

Bertram, J.E.A. (2016C). *Concepts in locomotion: Wheels, spokes, collisions and insight from the center of mass. Ch. 5. In: Understanding mammalian locomotion: Concepts and applications* (1st ed.). Wiley-Blackwell, Hoboken, USA, pp. 111-141.

Bertram, J. E. A., & Ruina, A. (2001). Multiple walking speed-frequency relations are predicted by constrained optimization. *Journal of Theoretical Biology*. *209*(4), 445–453. doi: 10.1006/jtbi.2001.2279

Bertram, J. E. A., D'Antonio, P., Pardo, J., & Lee, D. V. (2002). Pace length effects in human walking: "Groucho" gaits revisited. *Journal of Motor Behavior*. *34*(3), 309-318. doi: 10.1080/00222890209601949

Bertram, J. E. A., & Hasaneini, S. J. (2013). Neglected losses and key costs: Tracking the energetics of walking and running. *Journal of Experimental Biology*. *216*(6), 933-938. doi: 10.1242/jeb.078543

Bertram, J. E. A., Gutmann, A., Randev, J., & Hulliger, M. (2014). Domestic cat walking parallels human constrained optimization: optimization strategies and the comparison of normal and sensory deficient individuals. *Human Movement Science*. *36*, 154-166. doi: 10.1016/j.humov.2014.05.008

Bonnard, M., & Pailhous, J. (1993). Intentionality in human gait control: Modifying the frequency-to-amplitude relationship. *Journal of Experimental Psychology: Human Perception and Performance*. *19*(2), 429-443. doi: 10.1037/0096-1523.19.2.429

Bourke, P. (1988, July). Calculating the area and centroid of a polygon. Retrieved from http://paulbourke.net/geometry/polygonmesh/

Brandão, M., Hashimoto, K., Santos-Victor, J., & Takanishi, A. (2015). Optimizing energy consumption and preventing slips at the footstep planning level. *Proceedings of the 15th IEEE/RAS International Conference on Humanoid Robots*. Nov. 3-5. Seoul, South Korea.

Bregler, C., Malik, J., & Pullen, K. (2004). Twist based acquisition and tracking of animal and human kinematics. *International Journal of Computer Vision*. *56*(3), 179-194. doi: 10.1023/B:VISI.0000011203.00237.9b

Browning, R. C., Modica, J. R., Kram, R., & Goswami, A. (2007). The effects of adding mass to the legs on the energetics and biomechanics of walking. *Medicine and Science in Sport and Exercise*. *39*(3): 515-525. doi: 10.1249/mss.0b013e31802b3562

Buzsáki, G., & Draguhn, A. (2004). Neuronal oscillations in cortical networks. *Science*. *304*(5679), 1926-1929. doi: 10.1126/science.1099745

Castillo, E. R., Lieberman, G. M., McCarty, L. S. & Lieberman, D. E. (2014). Effects of pole compliance and step frequency on the biomechanics and economy of pole carrying during human walking. *Journal of Applied Physiology*. *117*(5), 507-517. doi: 10.1152/japplphysiol.00119.2014

Cavagna, G. A., & Margaria, R. (1966). Mechanics of walking. *Journal of Applied Physiology*. *21*(1), 271-278. doi: 10.1152/jappl.1966.21.1.271

Cavagna, G. A., Heglund, N. C., & Taylor, C. R. (1977). Mechanical work in terrestrial locomotion: two basic mechanisms for minimizing energy expenditure. *American Journal of Physiology*. *233*(5), R243-R261. doi: 10.1152/ajpregu.1977.233.5.R243

Cavagna, G. A., & Franzetti, P. (1986). The determinants of the step frequency in walking in humans. *Journal of Physiology*. *373*(1), 235-242. doi: 10.1113/jphysiol.1986.sp016044

Cavagna, G. A., Willems, P. A., Legramandi, M. A., & Heglund, N.C. (2002). Pendular energy transduction within the step in human walking. *Journal of Experimental Biology*. *205*(21), 3413-3422.

Cavagna, G. A., & Legramandi, M. A. (2015). Running, hopping and trotting: tuning step frequency to the resonant frequency of the bouncing system favors larger animals. *Journal of Experimental Biology*. *218*(20), 3276-3283. doi: 10.1242/jeb.127142

Charteris J. (1998). Comparison of the effects of backpack loading and of walking speed on foot-floor contact patterns. *Ergonomics*. *41*(12), 1792–1809. doi: 10.1080/001401398185974

Cikajlo, I., & Matjačić, Z. (2007). The influence of boot stiffness on gait kinematics and kinetics during stance phase. *Ergonomics*. *50*(12), 2171-2182. doi: 10.1080/00140130701582104

Collins, S., Ruina, A., Tedrake, R., & Wisse, M. (2005). Efficient bipedal robots based on passive dynamic walkers. *Science*. *307*(5712), 1082-1085. doi: 10.1126/science.1107799

Croft, J. L., Schroeder, R. T., & Bertram, J. E. A. (2017). The goal of locomotion: Separating the fundamental task from the mechanisms that accomplish it. *Psychonomic Bulletin and Review*. *24*(6), 1675–1685. doi: 10.3758/s13423-016-1222-3

Croft, J. L., Schroeder, R. T. & Bertram, J. E. A. (2019A). Determinants of optimal leg use strategy: horizontal to vertical transition in the Parkour wall climb. *Journal of* Experimental Biology. 222(1), jeb190983. doi: 10.1242/jeb.190983

Croft, J. L., Schroeder, R. T., & Bertram, J. E. A. (2019B). The landscape of movement control in locomotion: Cost, strategy, and solution. *Frontiers in Psychology*. *10*(716). doi: 10.3389/fpsyg.2019.00716

Cunningham, C. B., Schilling, N., Anders, C., & Carrier, D. R. (2010). The influence of foot posture on the cost of transport in humans. *Journal Experimental Biology*. *213*(5), 790-797. doi: 10.1242/jeb.038984

Dallard, P., Fitzpatrick, A. J., Flint, A., Le Bourva, S., Low, A., Ridsdill Smith, R. M. & Willford, M. (2001). The London Millennium Footbridge. *The Structural Engineer*. *79*(22), 17-33.

Darici, O., Temeltas, H., & Kuo, A. D. (2018). Optimal regulations of bipedal walking speed despite an unexpected bump in the road. *PLoS ONE*. *13*(9): e0204205. doi: 10.1371/journal.pone.0204205

Dean, J., & Kuo, A. D. (2011). Energetic costs of producing muscle work and force in a cyclical human bouncing task. *Journal of Applied Physiology*. *110*(4), 873-880. doi: 10.1152/japplphysiol.00505.2010

de Langre E. (2008). Effects of wind on plants. *Annual Review of Fluid Mechanics*. *40*(1), 141–68. doi: 10.1146/annurev.fluid.40.111406.102135

Dilão, R. (2009). Antiphase and in-phase synchronization of nonlinear oscillators: The Huygens's clocks system. *Chaos: An Interdisciplinary Journal of Nonlinear Science*. *19*(023118). doi: 10.1063/1.3139117

Dixon, P. C., Bowtell, M. V., & Stebbins, J. (2014). The use of regression and normalisation for the comparison of spatio-temporal gait data in children. *Gait and Posture*. *40*(4), 521-525. doi: 10.1016/j.gaitpost.2014.06.009

Doke, J., Donelan, J. M., & Kuo, A. D. (2005). Mechanics and energetics of swinging the human leg. Journal of Experimental Biology. 208(3), 439-445. doi: 10.1242/jeb.01408

Doke, J., & Kuo, A. D. (2007). Energetic cost of producing cyclic muscle force, rather than work, to swing the human leg. *Journal of Experimental Biology*. *210*(13), 2390-2398. doi: 10.1242/jeb.02782

Donelan, J. M., Kram, R., & Kuo, A. D. (2001). Mechanical and metabolic determinants of preferred step width in human walking. *Proceedings of the Royal Society B-Biological Sciences*. *268*(1480). doi: 10.1098/rspb.2001.1761

Donelan, J. M., Kram, R., & Kuo, A. D. (2002A). Simultaneous positive and negative external mechanical work in human walking. *Journal of Biomechanics*. *35*(1), 117-124. doi: 10.1016/S0021-9290(01)00169-5

Donelan, J. M., Kram, R., & Kuo, A. D. (2002B). Mechanical work for step-to-step transitions is a major determinant of the metabolic cost of human walking. *Journal of Experimental Biology*. *205*(23), 3717-3727.

Floria, P., Sanchez-Sixto, A., Ferber, R., & Harrison, A. J. (2017). Effects of running experience on coordination and its variability in runners. *Journal of Sports Science*. *36*(3), 272-278. doi: 10.1080/02640414.2017.1300314

Foissac, M., Millet, G. Y., Geyssant, A., Freychat, P., & Belli, A. (2009). Characterization of the mechanical properties of backpacks and their influence on the energetics of walking. Journal of Biomechanics. 42(2), 125-130. doi: 10.1016/j.jbiomech.2008.10.012

Garcia, M., Chatterjee, A., & Ruina, A. (1998). Speed, efficiency, and stability of small-slope 2D passive dynamic bipedal walking. *Proceedings of the 1998 Conference on Robotics and Automation*. May 20. Leuven, Belgium.

Gellman, K. S., & Bertram, J. E. A. (2002). The equine nuchal ligament 2: passive dynamic energy exchange in locomotion. *Veterinary and Comparative Orthopaedics and* Traumatology. 15(1), 7-14. doi: 10.1055/s-0038-1632706

Gill, P. E., Murray, W., & Saunders, M. A. (2005). SNOPT: An SQP algorithm for large-scale constrained optimization. *Society for Industrial and Applied Mathematics Review*. 47(1), 99-131. doi: 10.1137/S0036144504446096

Godsiff, D.T., Coe, S., Elsworth-Edelsten, C., Collett, J., Howells, K., Morris, M., & Dawes, H. (2018). Exploring the metabolic and perceptual correlates of self-selected walking speed under constrained and un-constrained conditions. *Journal of Sports Science Medicine*. *17*(1), 1-6.

Goldfield, E. C., Kay, B. A., & Warren, W. H. Jr. (1993). Infant bouncing: the assembly and tuning of action systems. *Child Development*. *64*(4), 1128-1142. doi: 10.1111/j.1467-8624.1993.tb04191.x

Gordon, K. E., & Ferris, D. P. (2007). Learning to walk with a robotic ankle exoskeleton. *Journal of Biomechanics*. *40*(12), 2636-2644. doi: 10.1016/j.jbiomech.2006.12.006

Gordon, K. E., Ferris, D. P., & Kuo, A. D. (2009). Metabolic and mechanical energy costs of reducing vertical center of mass movement during gait. *Archives of Physical Medicine and Rehabilitation*. *90*(1), 136-144. doi: 10.1016/j.apmr.2008.07.014

Gottschall, J. S., & Kram, R. (2005). Energy cost and muscular activity required for leg swing during walking. *Journal of Applied Physiology*. *99*(1), 23-30. doi: 10.1152/japplphysiol.01190.2004

Grieve, D. W., & Gear, R. J. (1966). The relationship between length of stride, step frequency, time of swing and speed of walking for children and adults. *Ergonomics*. *9*(5), 379-399. doi: 10.1080/00140136608964399

Griffin, T. M., Roberts, T. J., & Kram, R. (2003). Metabolic cost of generating muscular force in human walking: insights from load-carrying and speed experiments. *Journal of Applied Physiology*. *95*(1), 172-183. doi:10.1152/japplphysiol.00944.2002.

Guadagnoli, M., Holcomb, W., & Davis, M. (2010). The efficacy of video feedback for learning the golf swing. *Journal of Sports Sciences*. *20*(8), 615-622. doi: 10.1080/026404102320183176

Gutmann, A., Jacobi, B., Butcher, M. T., & Bertram, J. E. A. (2006). Constrained optimization in human running. *Journal of Experimental Biology*. *209*(4), 622-632. doi: 10.1242/jeb.02010

Hak, L., Houdijk, H., Steenbrink, F., Mert, A., van der Wurff, P., Beek, P. J. & van Dieën, J. H. (2012). Speeding up or slowing down?: Gait adaptations to preserve gait stability in response to balance perturbations. *Gait and Posture*. *36*(2), 260-264. doi: 10.1016/j.gaitpost.2012.03.005

Handford, M. L., & Srinivasan, M. (2018). Energy-optimal human walking with feedback-controlled robotic prostheses: A computational study. *IEEE Transactions on Neural* Systems and Rehabilitation Engineering. 26(9), 1773-1782. doi: 10.1109/TNSRE.2018.2858204

Hasaneini, S. J., Macnab, C. J. B., Bertram, J. E. A., & Leung, H. (2013). The dynamic optimization approach to locomotion dynamics: human-like gaits from a minimally-constrained biped model. *Advanced Robotics*. *27*(11), 845-859. doi: 10.1080/01691864.2013.791656

Hasaneini, S. J., Bertram, J. E. A., & Macnab, C. J. B. (2015). Energy optimal relative timing of stance-leg push-off and swing-leg retraction in walking. *Robotica*. *35*(3), 654-686. doi: 10.1017/S0263574715000764.

Hedrick, T. L. (2008). Software techniques for two- and three-dimensional kinematic measurements of biological and biomimetic systems. *Bioinspiration and Biomimetics*. *3*(3): 34001-34006. doi: 10.1088/1748-3182/3/3/034001

Hein, T., Schmeltzpfenning, T. Krauss, L., Maiwald, C., Hortstmann, T., & Grau, S. (2012). Using the variability of continuous relative phase as a measure to discriminate between healthy and injured runners. *Human Movement Science*. *32*(1), 683-694. doi: 10.1016/j.humov.2011.07.008

Hesser, C. M., Linnarsson, D., & Bjurstedt, H. (1977). Cardiorespiratory and metabolic responses to positive, negative and minimum-load dynamic leg exercise. *Respiration Physiology*. *30*(1-2), 51-67. doi: 10.1016/0034-5687(77)90021-4

Holt, K. G., Jeng, S. F., & Ratcliffe, R. (1995). Energetic cost and stability during human walking at the preferred stride frequency. *Journal of Motor Behavior*. *27*(2), 164-178. doi: 10.1080/00222895.1995.9941708

Huffman, J. L., Horslen, B. C., Carpenter, M. G., & Adkin, A. L. (2009). Does increased postural threat lead to more conscious control of posture? *Gait and Posture*. *30*(4), 528-532. doi: 10.1016/j.gaitpost.2009.08.001

Johnstone, M. (1995). *Restoration of normal movement after stroke*. New York, NY: Churchill Livingstone Inc.

Joshi, V., & Srinivasan, M. (2015). Walking on a moving surface: energy-optimal walking motions on a shaky bridge and a shaking treadmill can reduce energy costs below normal. *Proceedings of the Royal Society A-Mathematical, Physical and Engineering* Sciences. 471(), 20140662. doi: 10.1098/rspa.2014.0662

Kim, J., & Bertram, J. E. A. (2018). Compliant walking appears metabolically advantageous at extreme step lengths. *Gait and Posture*. *64*, 84–89. doi: 10.1016/j.gaitpost.2018.05.020

Koban, L., Ramamoorthy, A., & Konvalinka, I. (2019). Why do we fall into sync with others? Interpersonal synchronization and the brain's optimization principle. *Social* Neuroscience. 14(1), 1-9. doi: 0.1080/17470919.2017.1400463

Kram, R. (1991). Carrying loads with springy poles. *Journal of Applied Physiology*. *71*(3), 1119-1122. doi: 10.1152/jappl.1991.71.3.1119

Kuo, A. D. (2001). A simple model of bipedal walking predicts the preferred speed-step length relationship. *Journal of Biomechanical Engineering*. *123*(3), 264-269. doi: 10.1115/1.1372322

Kuo, A. D. (2002). Energetics of actively powered locomotion using the simplest walking model. *Journal of Biomechanical Engineering*. *124*(1), 617-619. doi: 10.1115/1.1427703

Kuo, A. D., Donelan, J. M., & Ruina, A. (2005). Energetic consequences of walking like an inverted pendulum: step-to-step transitions. *Exercise and Sport Science Review*. *33*(2), 88-97.

Kurz, M. J., Stergiou, N., Buzza, U. H., & Georgoulis, A. D. (2005). The effect of anterior cruciate ligament reconstruction on lower extremity relative phase dynamics during walking and running. *Knee Surgery, Sports Traumatology, Arthroscopy*. *13*(2), 107-115. doi: 10.1007/s00167-004-0554-0

LaFiandra, M., Wagenaar, R. C., Holt, K. G., & Obusek, J. P. (2003). How do load carriage and walking speed influence trunk coordination and stride parameters? *Journal* of Biomechanics. 36(1), 87-95. doi: 10.1016/S0021-9290(02)00243-9

Lakkad, S. C., & Patel, J. M. (1981). Mechanical properties of bamboo, a natural composite. *Fibre Science and Technology*. *14*(4): 319–22.
doi: 10.1016/0015-0568(81)90023-3

Lee, D. V., Bertram, J. E. A., Anttonen, J. T., Ros, I. V., Harris, S. L., & Biewener, A. A. (2011). A collisional perspective on quadrupedal gait dynamics. *Journal of the Royal Society Interface*. *8*, 1480-1486. doi: 10.1098/rsif.2011.0019

Lee, D. V., Comanescu, T. N., Butcher, M. T., Bertram, J. E. A. (2013). A comparative collision-based analysis of human gait. *Proceedings of the Royal Society B-Biological Sciences*. *280*(1771), 20131779. doi: 10.1098/rspb.2013.1779

Lewis, C. L., & Ferris, D. P. (2011). Invariant hip movement pattern while walking with a robotic hip exoskeleton. *Journal of Biomechanics*. *44*(5), 789-793.
doi: 10.1016/j.jbiomech.2011.01.030

Li, D., Li, T., Li, Q., Liu, T., & Yi, J. (2016A). A simple model for predicting walking energetics with elastically-suspended backpack. *Journal of Biomechanics*. *49*(16), 4150-3153. doi: 10.1016/j.jbiomech.2016.10.037

Li, T., Li, Q., Liu, T., Yi, J., & Gong, G. (2016B). Development of a novel elastic load-carrying device: Design, modeling and analysis. *IEEE/ASME International Conference on Advanced Intelligent Mechatronics*. July 12-15. Banff, AB, Canada.

Li, T., Li, Q., Liu, T., and Yi, J. (2019A). How to carry loads economically: Analysis based on a predictive biped model. *ASME Journal of Biomechanical Engineering*. doi: 10.1115/1.4044505.

Li, T., Li, Q., & Liu, T. (2019B). Understanding the mechanics and balance control of the carrying pole through modeling and simulation. *PLoS ONE*. *14*(6), e0218072. doi: 10.1371/journal.pone.0218072

Lotrič, M. B., & Stefanovska, A. (2000). Synchronization and modulation in the human cardiorespiratory system. *Physica A: Statistical Mechanics and its Applications*. *283*(3-4), 451–461. doi: 10.1016/S0378-4371(00)00204-1

Lythgo, N., Wilson, C., & Galea, M. (2011). Basic gait and symmetry measures for primary school-aged children and young adults. II. Walking at slow, free and fast speed. *Gait and Posture*. *33*(1), 29-35. doi: 10.1016/j.gaitpost.2010.09.017.

Malcolm, P., Derave, W., Galle, S., & De Clercq, D. (2013) A simple exoskeleton that assists plantarflexion can reduce the metabolic cost of human walking. *PLoS ONE*. *8*(2): e56137. doi: 10.1371/journal.pone.0056137

Maloiy, G. M. O., Heglund, N. C., Prager, L. M., Cavagna, G. A., & Taylor, C. R. (1986). Energetic costs of carrying loads: have African women discovered an economic way? Nature. 319, 668-669. doi: 10.1038/319668a0

Mansfield, A., Schinkel-Ivy, A., Danells, C. J., Aqui, A., Aryan, R., Biasin, L., DePaul, V. G., & Inness, E. L. (2017). Does perturbation training prevent falls after discharge from stroke rehabilitation? A prospective cohort study with historical control. *Journal of Stroke and Cerebrovascular Diseases*. *26*(10), 2174-2180. doi: 10.1016/j.jstrokecerebrovasdis.2017.04.041

Margaria, R. (1976). *Biomechanics and Energetics of Muscular Exercise*. Oxford, England: Clarendon Press.

Margaria, R., Cerretelli, P., Aghemo, P., & Sassi, G. (1963). Energy cost of running. *Journal of Applied Physiology*. *18*(2), 367-370. doi: 10.1152/jappl.1963.18.2.367

Martin, J. P., & Li, Q. (2018). Altering compliance of a load carriage device in the media-lateral direction reduces peak forces while walking. *Scientific Reports*. *8*(13775). doi: 10.1038/s41598-018-32175-x

Masters, R., & Maxwell, J. (2008). The theory of reinvestment. *International Review of Sport and Exercise Psychology*. *1*(2), 160-183, doi: 10.1080/17509840802287218

Mawase, F., Haizler, T., Bar-Haim, S., & Karniel, A. (2013). Kinetic adaptation during locomotion on a split-belt treadmill. *Journal of Neurophysiology*. *109*(8), 2216-2227. doi: 10.1152/jn.00938.2012

McAndrew, P. M., Dingwell, J. B., & Wilken, J. M. (2010). Walking variability during continuous pseudo-random oscillations of the support surface and visual field. *Journal of* Biomechanics. 43(8), 1470-1475. doi: 10.1016/j.jbiomech.2010.02.003

McDonald, K. A., Hieronymi, A., Cusumano, J. P., & Rubenson, J. (2019). Optimization in human walking: Decoupling whole-body energetics and local muscle effort. *Abstract presented at the 43rd Annual Meeting of the American Society of Biomechanics*. August. Calgary, AB. Abstract retrieved from https://www.dropbox.com/s/7xrlez4mcpjjn3z/isb2019_abstracts_all.pdf?dl=0.

McGeer, T. (1990). Passive dynamic walking. *International Journal of Robotics Research*. *9*(2), 62-82. doi: 10.1177/027836499000900206

Meinders, M., Gitter, A., & Czerniecki, J. M. (1998). The role of ankle plantar flexor muscle work during walking. *Scandinavian Journal of Rehabilitation Medicine*. *30*(1), 39-46. doi: 10.1080/003655098444309

Miller, L. A. (2005). Structural dynamics and resonance in plants with nonlinear stiffness. *Journal of Theoretical Biology*. *234*(4): 511–524. doi: 10.1016/j.jtbi.2004.12.004

Minetti, A. E., & Alexander, R. McN. (1997). A theory of metabolic costs for bipedal gaits. *Journal of Theoretical Biology*. *186*(4), 467-476. doi: 10.1006/jtbi.1997.0407

Mochon, S., & McMahon, T. A. (1980). Ballistic walking. *Journal of Biomechanics*. *13*(1), 49-57. doi: 10.1016/0021-9290(80)90007-X

Mooney, L. M., Rouse, E. J., & Herr, H. M. (2014). Autonomous exoskeleton reduces metabolic cost of human walking during load carriage. *Journal of NeuroEngineering and Rehabilitation*. *11*(80), . doi: 10.1186/1743-0003-11-80

Néda, Z., Ravasz, E., Brechet, Y., Vicsek, T., & Barabási, A.-L. (2000). The sound of many hands clapping. *Nature*. *403*, 849-850. doi: 10.1038/35002660

Nessler, J. A., Heredia, S., Belair, J., & Milton, J. (2017). Walking on a vertically oscillating treadmill: Phase synchronization and gait kinematics. *PLoS ONE*. *12*(1), e0169924. doi: 10.1371/journal.pone.0169924

O'Connor, S. M., & Donelan, J. M. (2012). Fast visual prediction and slow optimization of preferred walking speed. J*ournal of Neurophysiology*. *107*(9), 2549-2559. doi: 10.1152/jn.00866.2011

Ortega, J. D., & Farley, C. T. (2005). Minimizing center of mass vertical movement increases metabolic cost in walking. *Journal of Applied Physiology*. *99*(6), 2099-2107. doi: 10.1152/japplphysiol.00103.2005

Pagliara, R., Snaterse, M., & Donelan, J. M. (2014). Fast and slow processes underlie the selection of both step frequency and walking speed. *Journal of Experimental Biology*. *217*(16), 2939-2946. doi: 10.1242/jeb.105270

Patterson, M. A., & Rao, A. V. (2014). GPOPS-II: A MATLAB software for solving multiple-phase optimal control problems using hp-adaptive Gaussian quadrature collocation methods and sparse nonlinear programming. *ACM Transactions on* Mathematical Software. 41(1), 1–37. doi: 10.1145/2558904

Perry, J., & Burnfield, J. M. (2010). *Gait analysis. Normal and pathological function*. Thorofare, NJ: Slack Inc.

Peters, B. T., Brady, R. A., & Bloomberg, J. J. (2012). Walking on an oscillating treadmill: Strategies of stride-time adaptation. *Ecological Psychology*. *24*(4), 265-278. doi: 10.1080/10407413.2012.702637

Polet, D. T., Schroeder, R. T., & Bertram, J. E. A. (2018). Reducing gravity takes the bounce out of running. *Journal Experimental Biology*. *221*(3), jeb162024. doi: 10.1242/jeb.162024

Potwar, K., Ackerman, J., & Seipel, J. (2015). Design of compliant bamboo poles for carrying loads. *ASME Journal of Mechanical Design*. *137*(1), 1-14. doi: 10.1115/1.4028757.

Prentice, S. D., Hasler, E. N., Groves, J. J., & Frank, J. S. (2004). Locomotor adaptations for changes in the slope of the walking surface. *Gait and Posture*. *20*(3), 255-265. doi: 10.1016/j.gaitpost.2003.09.006

Rebula, J. R. & Kuo, A. D. (2015). The cost of leg forces in bipedal locomotion: A simple optimization study. PLoS ONE. 10(2), e0117384. doi: 10.1371/journal.pone.0117384

Reinkensmeyer, D. J., Akoner, O. M., Ferris, D. P., & Gordon, K. E. (2009). Slacking by the human motor system: Computational models and implications for robotic orthoses. *In*

Engineering in Medicine and Biology Society. EMBC 2009 Annual International Conference of the IEEE. September 3-6. Minneapolis, MN, USA.

Rome, L. C., Flynn, L., Goldman, E. M., & Yoo, T. D. (2005). Generating electricity while walking with loads. Science. 309(5741), 1725-1728. doi: 10.1126/science.1111063

Rome, L. C., Flynn, L. and Yoo, T. D. (2006). Rubber bands reduce the cost of carrying loads. Nature. 444, 1023-1024. doi: 10.1038/4441023a

Rubenson, J. (2019). *Decoupling the metabolic and neuromuscular control of human walking*. Poster presented at the *Neuromechanics Satellite Meeting*. August. Calgary, AB.

Ruina, A., Bertram, J. E. A., & Srinivasan, M. (2005). A collisional model of the energetic cost of support work qualitatively explains leg sequencing in walking and galloping, pseudo-elastic leg behavior in running and the walk-to-run transition. *Journal of Theoretical Biology*. *237*(2), 170-192. doi: 10.1016/j.jtbi.2005.04.004

Russ, D. W., Elliott, M. A., Vanderborne, K., Walter, G. A., & Binder-Macleod, S. A. (2002). Metabolic costs of isometric force generation and maintenance of human skeletal muscle. *American Journal of Physiology*. *282*(2), E448-E457. doi: 10.1152/ajpendo.00285.2001

Sawicki, G. S., & Ferris, D. P. (2008). Mechanics and energetics of level walking with powered ankle exoskeletons. *Journal of Experimental Biology*. *211*(9), 1402-1413. doi: 10.1242/jeb.009241

Sawicki, G. S., & Khan, N. S. (2016). A simple model to estimate plantarflexor muscle-tendon mechanics and energetics during walking with elastic ankle exoskeletons. *IEEE Transactions on Biomedical Engineering*. *63*(5): 914-923. doi: 10.1109/TBME.2015.2491224.

Schäfer, C., Rosenblum, M. G., Kurths, J., & Abel, H. H. (1998). Heartbeat synchronised with ventilation. Nature. 392(6673), 239–240. doi: 10.1038/32567

Schroeder, R. T., & Bertram, J. E. A. (2018). Minimally actuated walking: Identifying core challenges to economical legged locomotion reveals novel solutions. *Frontiers in Robotics and AI*. *5*(58). doi: 10.3389/frobt.2018.00058

Schroeder, R. T., Croft, J. L., Ngo, G. D., & Bertram, J. E. A. (2018). Properties of traditional bamboo carrying poles have implications for user interactions. *PLoS ONE. 13*(5), e0196208. doi: 10.1371/journal.pone.0196208

Schroeder, R. T., Bertram, J. E. A., Son Nguyen, V., Vin Hac, V., & Croft, J. L. (2019). Load carrying with flexible bamboo poles: Optimization of a coupled oscillator system. *Journal of Experimental Biology*. *222*(23), jeb203760. doi: 10.1242/jeb.203760

Schwartz, M. H., Rozumalski, A., & Trost, J. P. (2008). The effect of walking speed on the gait of typically developing children. *Journal of Biomechanics*. *41*(8), 1639-1650. doi: 10.1016/j.jbiomech.2008.03.015

Selinger, J. C., O'Connor, S. M., Wong, J. D., & Donelan, J. M. (2015). Humans can continuously optimize energetic cost during walking. *Current Biology*. *25*(18), 2452-2456. doi: 10.1016/j.cub.2015.08.016

Selinger, J. C., Wong, J. D., Simha, S. N., & Donelan, J. M. (2019). How humans initiate energy optimization and converge on their optimal gaits. *Journal of Experimental Biology*. *222*(19), jeb198234. doi: 10.1242/jeb.198234

Simha, S. N., Wong, J. D., Selinger, J. C., & Donelan, J. M. (2019). A mechatronic system for studying energy optimization during walking. *IEEE Transactions on Neural Systems and Rehabilitation Engineering*. *27*(7), 1416-1425. doi: 10.1109/TNSRE.2019.2917424

Snaterse, M., Ton, R., Kuo, A. D., & Donelan, J. M. (2011). Distinct fast and slow processes contribute to the selection of preferred step frequency during human walking. *Journal of Applied Physiology*. *110*(6), 1682-1690. doi: 10.1152/japplphysiol.00536.2010

Srinivasan, M. (2011). Fifteen observations on the structure of energy-minimizing gaits in many simple biped models. *Journal of the Royal Society Interface*. *8*(54), 74-98. doi: 10.1098/rsif.2009.0544

Srinivasan, M. & Ruina, A. (2006). Computer optimization of a minimal biped model discovers walking and running. *Nature*. *439*, 72-75. doi: 10.1038/nature04113

Srinivasan, M., & Ruina, A. (2007). Idealized walking and running gaits minimize work. *Proceedings of the Royal Society A-Mathematical, Physical and Engineering Sciences*. *463*(2086), 2429-2446. doi: 10.1098/rspa.2007.0006

Stefanovska, A. (2007). Coupled oscillators: Complex but not complicated cardiovascular and brain interactions. *IEEE Engineering in Medicine and Biology Magazine*. 26(6): 25-29. doi: 10.1109/EMB.2007.907088

Stefanovska, A., Haken, H., McClintock, P. V. E., Hožič, M., Bajrović, F., & Ribarič, S. (2000). Reversible transitions between synchronization states of the cardiorespiratory system. Physical Review Letters. 85(22), 4831–4834. doi: 10.1103/PhysRevLett.85.4831

Strang, K. T., & Steudel, K. (1990). Explaining the scaling of transport costs: the role of stride frequency and stride length. *Journal of Zoology*. *221*(3), 343-358. doi: 10.1111/j.1469-7998.1990.tb04006.x

Tackett, E. (2018). The effect of noise on gait synchronization to a vertical oscillating treadmill (Master's thesis). California State University San Marcos. Retrieved from http://csusm-dspace.calstate.edu/handle/10211.3/205427?show=full

Takahashi, K. Z., Lewek, M. D., & Sawicki, G. S. (2015). A neuromechanics-based powered ankle exoskeleton to assist walking post-stroke: a feasibility study. *Journal of NeuroEngineering and Rehabilitation*, *12*(23). doi: 10.1186/s12984-015-0015-7

Taylor, C. R., Schmidt-Nielsen, K., & Raab, J. L. (1970). Scaling of energetic cost of running to body size in mammals. *American Journal of Physiology*. *219*(4), 1104-1107.

Tran V. (2010). Growth and quality of indigenous bamboo species in the mountainous regions of Northern Vietnam. (Ph.D thesis). Georg-August-Universität Göttingen, Göttingen, Germany. 2010. Retrieved from http://citeseerx.ist.psu.edu/viewdoc/download?doi=10.1.1.427.7372&rep=rep1&type=pdf

Tucker, V. A. (1970). Energetic cost of locomotion in animals. *Comparative Biochemistry and Physiology*. *34*(4), 841-846. doi: 10.1016/0010-406X(70)91006-6

Umberger, B. R. (2010). Stance and swing phase costs in human walking. *Journal of the Royal Society Interface*. *7*(50), 1329-1340. doi: 10.1098/rsif.2010.0084

Usherwood, J. R. (2010). Inverted pendular running: A novel gait predicted by computer optimization is found between walk and run in birds. *Biology Letters*. *6*, 765-768. doi: 10.1098/rsbl.2010.0256

Usherwood, J. R. (2016). *Reductionist models of walking and running. Ch. 4. In: Understanding mammalian locomotion: Concepts and applications* (1st ed.). Wiley-Blackwell, Hoboken, USA, pp.143-172.

Winter, D. A. (1991). *The Biomechanics and Motor Control of Human Gait: Normal, Elderly and Pathological* (2nd ed). Waterloo, Canada, Waterloo Biomechanics.

Winter, D. A. (2009). *Biomechanics and motor control of human movement* (4th ed). Wiley.

Winter, D. A., & Robertson, D. G. E. (1978). Joint torque and energy patterns in normal gait. *Biological Cybernetics*. *29*(3): 137-142. doi: 10.1007/BF00337349

Witte, K. A., Fatschel, A. M., & Collins, S. H. (2017). Design of a lightweight, tethered, torque-controlled knee exoskeleton. *In 2017 International Conference on Rehabilitation Robotics (ICORR)*. July17-20. London, UK.

Wong, J. D., O'Connor, S. M., Selinger, J. C., & Donelan, J. M. (2017). Contribution of blood oxygen and carbon dioxide sensing to the energetic optimization of human walking. *Journal of Neurophysiology*. *118*(2), 1425-1433. doi: 10.1152/jn.00195.2017

Wong, J. D., Selinger, J. C., & Donelan, J. M. (2019). Is natural variability in gait sufficient to initiate spontaneous energy optimization in human walking? *Journal of Neurophysiology*. *121*(5), 1848-1855. doi: 10.1152/jn.00417.2018

Wu M. M., Brown G., & Gordon, K. E. (2017). Control of locomotor stability in stabilizing and destabilizing environments. *Gait and Posture*. *55*, 191-198. doi: 10.1016/j.gaitpost.2017.04.021.

Yogev-Seligmann, G., Hausdorff, J. M., & Giladi, N. (2008). The role of executive function and attention in gait. *Movement Disorders*. *23*(3), 329-342. doi: 10.1002/mds.21720

Zelik, K. E., & Adamczyk, P. G. (2016). A unified perspective on ankle push-off in human walking. *Journal Experimental Biology*. *219*(23), 3676-3683. doi: 10.1242/jeb.140376.

Zhang, J., Fiers, Pieter, Witte, K. A., Jackson, R. W., Poggensee, K. L., Atkeson, C. G., & Collins, S. H. (2017). Human-in-the-loop optimization of exoskeleton assistance during walking. *Science*. *356*(6344), 1280-1284. doi: 10.1126/science.aal5054

Appendix A (additional materials for Ch. 4)

This section includes additional materials associated with content from Chapter 4.

A.1 Full Results from Statistical Models

This section details results from statistical models referred to in Chapter 4.

A.1.1 Linear Mixed Model Results

Table A.1. Statistics model results from Chapter 4

	Absolute Step Frequency [Hz]				
Model Description	Term	β	Lower CL	Upper CL	p
1.) Rigid pole data only	Intercept	1.111	0.897	1.325	<0.001*
	Load [30 – 0]	0.053	0.032	0.075	<0.001*
	Load [50 – 30]	0.074	0.053	0.096	<0.001*
	$\tilde{v}$	1.830	1.352	2.308	<0.001*
	Relative Step Frequency				
Model Description	Term	β	Lower CL	Upper CL	p
2.) Simple model	Intercept	0.645	0.578	0.712	<0.001*
	Pole Type	0.014	0.004	0.023	0.014*
	Load	0.238	0.228	0.248	<0.001*
	Pole Type x Load	-0.002	-0.016	0.011	0.832
3.) Simple model plus covariate & interactions	Intercept	0.458	0.356	0.560	<0.001*
	Pole Type	0.009	-0.001	0.019	0.083
	Load	0.232	0.222	0.242	<0.001*
	Pole Type x Load	-0.008	-0.022	0.006	0.249
	$\tilde{v}$	0.447	0.253	0.640	<0.001*
	Pole Type x $\tilde{v}$	0.285	0.147	0.424	<0.001*
	Load x $\tilde{v}$	0.004	-0.132	0.141	0.950

This table summarizes the repeated measures mixed linear models used during analysis in the Chapter 4. Model 1.) includes data from individuals carrying the rigid pole as well as data from the no load condition. Absolute step frequency was fit to load level (0, 30 and 50% subject body weight) while controlling for non-dimensional walking speed ($\tilde{v}$). Interaction terms between the covariate and the fixed effect were not included since they were not found to be significant. In model 2.), the main fixed effects – load level (30 and 50% body weight) and pole type (rigid and compliant) – were used to fit relative step frequency data for all conditions except the no load condition. Non-dimensional walking speed was not included since interactions were found to be significant. However, an expanded version of the model is labelled 3.) in the table. It includes non-dimensional walking speed and related interactions. All three models included subject as a random variable with compound symmetric covariance

structures. All confidence limits (CL) are set to a level of 95% and p values are marked with an asterisk to indicate significance after controlling for multiple testing.

A.1.2 Subject Step Frequency Changes due to Pole Type

Table A.2. Effect of pole type on individual relative step frequency in Chapter 4

Subject (N=14)	Load (%)	Δf_r	Lower CL	Upper CL	p
A	30	0.020	0.001	0.039	0.044
B	30	-0.002	-0.031	0.027	0.901
C	30	0.000	-0.027	0.028	0.988
D	30	0.003	-0.015	0.022	0.726
E	30	-0.007	-0.035	0.021	0.618
F	30	0.029	0.001	0.058	0.046
G	30	-0.004	-0.031	0.022	0.743
H	30	-0.016	-0.036	0.005	0.133
I	30	-0.016	-0.045	0.012	0.262
J	30	0.011	-0.020	0.043	0.475
K	30	0.011	-0.021	0.042	0.506
L	30	0.041	0.013	0.070	0.005*
M	30	-0.004	-0.058	0.049	0.875
N	30	0.123	0.052	0.194	<0.001*
A	50	0.028	0.009	0.048	0.004*
B	50	0.007	-0.022	0.035	0.636
C	50	-0.065	-0.093	-0.037	<0.001*
D	50	0.006	-0.012	0.024	0.493
E	50	-0.049	-0.077	-0.020	<0.001*
F	50	-0.012	-0.040	0.017	0.408
G	50	0.026	0.002	0.051	0.032
H	50	0.018	-0.002	0.037	0.078
I	50	0.001	-0.030	0.031	0.967
J	50	0.023	-0.011	0.057	0.181
K	50	0.058	0.026	0.090	<0.001*
L	50	0.074	0.045	0.104	<0.001*
M	50	0.004	-0.050	0.058	0.882
N	50	0.040	-0.027	0.106	0.243

This table summarizes differences in the least squares means of relative step frequency between the rigid and compliant pole conditions for individual subjects at both loading levels (30 and 50% body weight) using model 2.) from Table A.2 (results from data in Chapter 4). p values are assessed for significance (marked with asterisks) using Benjamini and Hochberg's method for multiple comparisons testing (1995). All confidence limits (CL) are set to a level of 95%.

A.2 Additional Materials and Results

This section details additional materials and results from Chapter 4.

A.2.1 Model Versus Empirical Data for Every Subject

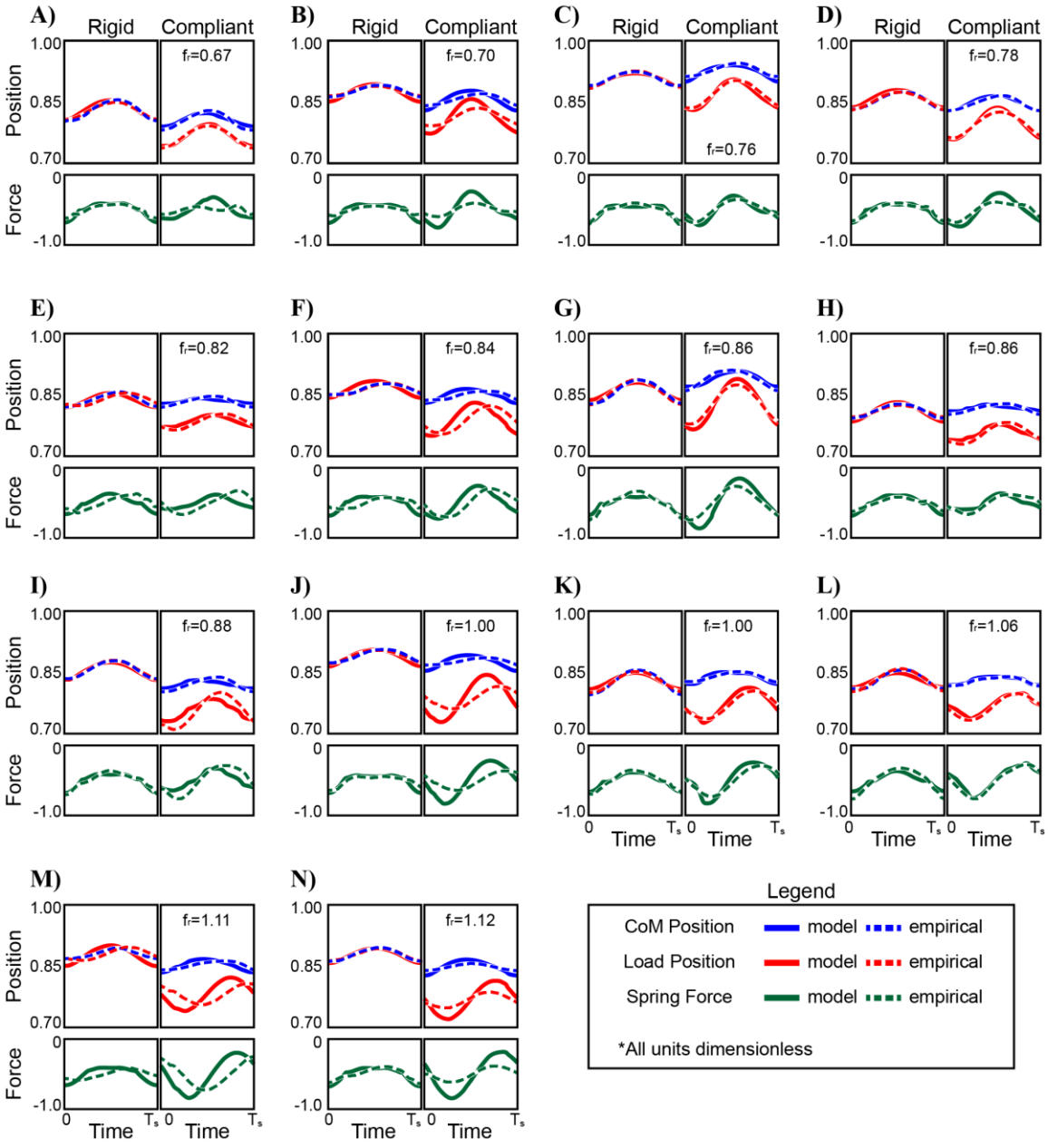

Figure A.1. Comparing model outputs to empirical data from Chapter 4

Average trial data are shown for all subjects [N=14, panels **A-N**] carrying 50% body weight loads on both rigid and compliant poles (left and right columns in each panel, respectively). These data are compared to various model outputs, including vertical centre of mass (CoM) position, vertical load position and spring force calculated from the difference in position times the spring constant of the pole used. The model simulations use input parameters reflecting

each subject's data (e.g. body mass, maximum allowable leg length, average forward speed, etc.; see Table A.3 for all input parameters). The subjects are arranged in panels **A**-**N** in ascending order with respect to their relative step frequency with the compliant pole.

A.2.2 Table of model inputs

Table A.3. Optimization model input parameters for simulations in Chapter 5

Subject (N=14)	Body Mass [kg]	Leg Length [m]	Forward Speed [m s^{-1}]					Step Frequency [Hz]					Pole Stiffness [kN m^{-1}]
			C, 0%	R, 30%	C, 30%	R, 50%	C, 50%	C, 0%	R, 30%	C, 30%	R, 50%	C, 50%	
A	50.0	0.754	1.22	1.11	1.20	1.18	1.31	1.88	1.77	1.84	1.85	1.93	8.36
B	39.5	0.659	0.96	0.96	1.03	0.98	1.06	1.91	1.96	1.96	2.01	2.03	6.84
C	49.0	0.837	1.05	1.01	1.01	0.95	0.88	1.80	1.80	1.80	1.83	1.69	5.00
D	46.0	0.741	1.06	1.03	1.08	1.14	1.14	1.86	1.85	1.86	1.96	1.97	5.98
E	49.0	0.749	1.14	1.39	1.22	1.39	1.32	1.88	2.07	2.04	2.24	2.11	6.56
F	44.5	0.667	1.07	1.01	1.03	1.07	1.08	1.91	1.93	2.02	2.10	2.07	5.50
G	56.5	0.848	1.32	1.31	1.27	1.26	1.22	1.75	1.76	1.75	1.79	1.84	5.32
H	49.5	0.761	1.23	1.26	1.21	1.29	1.30	1.94	1.91	1.86	1.93	1.97	5.30
I	49.0	0.684	1.15	1.10	1.09	1.11	1.20	1.87	2.00	1.95	2.06	2.06	5.50
J	46.0	0.698	0.99	0.90	1.02	0.95	0.97	1.88	1.89	1.92	1.94	1.98	3.66
K	53.0	0.766	1.44	1.31	1.29	1.33	1.38	2.03	2.03	2.06	2.04	2.16	5.00
L	52.0	0.742	1.42	1.38	1.36	1.40	1.47	2.03	2.06	2.18	2.24	2.41	5.50
M	54.0	0.752	1.01	1.06	1.10	1.16	1.30	1.93	2.14	2.13	2.35	2.36	5.00
N	64.5	0.786	1.22	1.08	1.46	1.17	1.26	1.87	1.91	2.21	2.11	2.18	5.00
mean	50.2	0.746	1.16	1.14	1.17	1.17	1.21	1.90	1.93	1.97	2.03	2.06	5.61

Input parameters used for the optimizations detailed in Chapter 4. These parameters match the average values measured for each subject during experiment trials for pole type (R=Rigid Pole, C=Compliant Pole) and loading level (0, 30 and 50% body weight) conditions. The optimizations shown in Fig. A.1 use the parameters indicated for a 50% loading level, where the letter under the "Subject" column corresponds to the figure panel in Fig. A.1.

Appendix B (additional materials for Ch. 5)

This section includes additional materials associated with content from Chapter 5.

B.1 Methods and Results of Oscillator System Dynamics Testing

The oscillator system described in Chapter 5 was characterized by two forced mass-spring-damper elements (each element representing a motor and the pulley-cable system it was connected to; motor B pulled up, motor A pulled down; see Fig. 5.2). In order to determine parameters such as spring constant and damping coefficient, independent tests were conducted. In one such test, a subject was fitted with the body harness and instructed to stand still in the system throughout the duration of the test. Both motors were commanded to increase tension in their respective pulley systems in graduated steps of equal amplitude; each step was sustained for five seconds while tension transducers measured force (after calibration with known weights) and optical encoders measured deflection. The five second time duration was deemed long enough for transient effects to fully decay and measurements were averaged over the last 2.5 seconds of each step. Simple least squares linear regressions were used to characterize the force-deflection data, and the resulting slopes were considered the spring constants for the pulley systems associated with each motor. This test was repeated two additional times to ensure repeatability of the results. Compliance in the system is assumed to come from pulley attachments that are not ideally rigid as well as from some flexibility in the body harness. The resulting spring constants of the system (with 95% confidence limits) were $k_A = 2.031\ (1.954, 2.114)\ kN\ m^{-1}$ and $k_B = 1.272\ (1.198, 1.356)\ kN\ m^{-1}$ for motors A and B, respectively.

In a second test, a subject was again fitted with the body harness and instructed to stand still throughout the duration of the test. The motors were commanded to provide a constant tension in the system, beginning with nominal tension due to the weight of the motors suspended from cables. Simple least squares regressions were used to fit damping coefficient parameters of the mass-spring-damper model, where spring constant values were used from the first test. This test was performed for three step magnitudes over a range relevant to that used in the experiments of Chapter 5. The output parameters of the regressions were averaged and considered the damping coefficients of the system. Energy dissipation in the system was largely assumed to

come from back electromotive force in the motors. The resulting damping coefficients of the system (with 95% confidence limits) were $c_A = 216.3\ (213.0, 219.6)\ N\ s\ m^{-1}$ and $c_B = 168.2\ (167.4, 168.9)\ N\ s\ m^{-1}$ for motors A and B, respectively. Damping ratio was calculated for each pulley system based on the parameter estimates from the regressions: $\zeta_A = 1.70$ and $\zeta_B = 1.67$. These results indicated an overdamped system.

B.2 Summary of Subject Data

Table B.1. Summary of subject data

Subject	Experiment	Sex	Age	Body Mass (kg)	Height (m)	Leg Length (m)	Belt Speed (m s^{-1})
1	1	male	22	69.7	1.69	0.86	1.17
2	1	female	24	51.9	1.70	0.89	1.19
3	1	male	31	72.9	1.75	0.94	1.22
4	1	male	21	83.8	1.87	0.97	1.22
5	1	male	29	83.9	1.75	0.98	1.25
6	1	female	27	64.1	1.62	0.88	1.17
7	1	female	27	48.0	1.60	0.79	1.11
8	1	female	27	66.4	1.68	0.98	1.25
9	1	female	27	50.0	1.68	0.87	1.17
10	1	male	27	66.0	1.77	0.96	1.22
mean			**26.2**	**65.7**	**1.71**	**0.91**	**1.20**
(SD)			**(3.0)**	**(12.8)**	**(0.08)**	**(0.06)**	**(0.04)**
1	2, 3	male	37	73.0	1.74	0.87	1.17
2	2, 3	male	26	73.4	1.70	0.91	1.19
3	2, 3	male	23	67.7	1.73	0.89	1.19
4	2, 3	male	18	81.2	1.86	0.94	1.22
5†	2	male	28	67.1	1.81	0.95	1.22
6	2, 3	female	25	56.0	1.70	0.89	1.19
7	2, 3	female	24	61.2	1.59	0.83	1.14
8	2, 3	female	27	62.0	1.66	0.88	1.17
9	2, 3	female	24	62.9	1.69	0.90	1.19
10	2, 3	female	27	57.8	1.67	0.90	1.19
11	2, 3	male	25	76.3	1.78	0.93	1.19
mean			**25.8**	**67.1**	**1.72**	**0.90**	**1.19**
(SD)			**(4.6)**	**(8.0)**	**(0.07)**	**(0.03)**	**(0.02)**

This table summarizes subject data and indicates which experiments each individual participated in. Experiment 1 refers to the Cost of Entrainment test, Experiment 2 refers to the Sensitivity to Entrainment test and Experiment 3 refers to the Limits of Entrainment test. †Note, subject 5 could not complete the test protocol for Experiment 3 and was thus, excluded from all analysis. SD is the standard deviation of the sample.

B.3 Full Results from Statistical Models

This section details results from statistical models referred to in Chapter 5.

B.3.1 Models Results from Experiment 1

Table B.2. Statistics model results from the Cost of Entrainment test in Chapter 5

Model Description	Dependent Variable	Independent Variables	β	Lower CL	Upper CL	*p*
1.) Entrainment step ratio versus trial conditions	ESR	Intercept	-0.042	-0.230	0.146	0.656
		Δf_m	-3.005	-4.607	-1.402	<0.001*
		A_m	2.267	1.482	3.052	<0.001*
		$\Delta f_m \; x \; A_m$	-8.838	-24.862	7.185	0.273
2.) Average time duration of entrainment versus trial conditions	$\Delta \bar{t}_e$	Intercept	-0.030	-0.227	0.166	0.756
		Δf_m	-2.712	-4.302	-1.121	0.001*
		A_m	1.737	0.958	2.517	<0.001*
		$\Delta f_{\mathrm{m}} \; x \; A_m$	-12.269	-28.174	3.637	0.127
3.) Metabolic power versus net mechanical work	P_{met}	Intercept	0.329	0.308	0.351	<0.001*
		Δf_m	0.098	0.025	0.172	0.009
		A_m	0.088	0.051	0.125	<0.001*
		$\Delta f_m \; x \; A_m$	0.845	0.176	1.513	0.013
		ESR	-0.004	-0.013	0.006	0.488
		W_c	-4.201	-4.960	-3.442	<0.001*
4.) Determinants of net mechanical work	W_c	Intercept	0.012	0.004	0.020	0.005*
		A_m	0.026	0.006	0.046	0.012
		ϕ	-0.064	-0.089	-0.040	<0.001*
		A_c	-0.427	-0.724	-0.129	0.009*
		$A_m \; x \; \phi$	-0.427	-0.834	-0.021	0.040

This table summarizes linear mixed models used for analysis in Experiment 1: Cost of Entrainment. Models 1.) and 2.) test metrics for the entrainment level of subjects in all trial conditions. The third model tests variables that explain subject-trial variation in the net metabolic power, and the fourth model quantifies determinants of net mechanical work on subjects from the harness force. Δf_m is the difference in motor frequency from preferred step frequency and normalized by preferred (expressed as a decimal, not a percentage). A_m is the oscillation amplitude of current sent to the motors (expressed as a fraction of subject body weight). ESR is the entrainment step ratio, or the ratio of steps in entrainment to total steps taken and $\Delta \bar{t}_e$ is the average time duration of bouts of entrainment, both during the free entrainment phase of the experiment. W_c is the net mechanical work done on the subject by the harness tension forces and ϕ is the phase of the motor current relative to the gait cycle (divided by 360°), where zero is aligned with peak centre of mass

acceleration in the vertical direction (approximately the middle of double stance). P_{met} is the metabolic power of subjects and A_c is the vertical oscillation amplitude of the centre of mass. All variables are non-dimensionalized, confidence limits (CL) are set to a level of 95% and p values are marked with an asterisk to indicate significance after controlling for multiple testing.

B.3.2 Tukey's HSD Results from Experiment 1

Table B.3. Tukey's HSD results for metabolic data of Cost of Entrainment test in Chapter 5

Level 1 (L1)				Level 2 (L2)							
dfm	Am	Met.	Exp. Type	dfm	Am	Met.	Exp. Type	L1-L2	Lower CL	Upper CL	*p*
-6	30	off	CoE	0	0	off	BL1	0.089	0.071	0.107	<0.001*
-6	30	on	CoE	0	0	off	BL1	0.075	0.056	0.094	<0.001*
0	10	off	CoE	0	0	off	BL1	0.067	0.049	0.085	<0.001*
6	30	on	CoE	0	0	off	BL1	0.063	0.044	0.082	<0.001*
6	30	off	CoE	0	0	off	BL1	0.062	0.044	0.080	<0.001*
6	10	off	CoE	0	0	off	BL1	0.061	0.043	0.079	<0.001*
6	10	on	CoE	0	0	off	BL1	0.061	0.043	0.079	<0.001*
-6	10	off	CoE	0	0	off	BL1	0.061	0.043	0.078	<0.001*
0	30	off	CoE	0	0	off	BL1	0.060	0.042	0.078	<0.001*
-6	10	on	CoE	0	0	off	BL1	0.060	0.042	0.078	<0.001*
0	0	off	BL2	0	0	off	BL1	0.051	0.033	0.069	<0.001*
-6	30	off	CoE	0	0	off	BL2	0.038	0.020	0.056	<0.001*
-6	30	off	CoE	-6	10	on	CoE	0.029	0.011	0.046	<0.001*
-6	30	off	CoE	0	30	off	CoE	0.029	0.011	0.046	<0.001*
-6	30	off	CoE	-6	10	off	CoE	0.028	0.011	0.046	<0.001*
-6	30	off	CoE	6	10	on	CoE	0.028	0.010	0.045	<0.001*
-6	30	off	CoE	6	10	off	CoE	0.028	0.010	0.045	<0.001*
-6	30	off	CoE	6	30	off	CoE	0.026	0.009	0.044	<0.001*
-6	30	off	CoE	6	30	on	CoE	0.026	0.007	0.044	<0.001*
-6	30	on	CoE	0	0	off	BL2	0.024	0.005	0.043	0.002*
-6	30	off	CoE	0	10	off	CoE	0.021	0.004	0.039	0.004*
0	10	off	CoE	0	0	off	BL2	0.016	-0.002	0.034	0.112
-6	30	on	CoE	-6	10	on	CoE	0.015	-0.003	0.033	0.250
-6	30	on	CoE	0	30	off	CoE	0.015	-0.004	0.033	0.283
-6	30	on	CoE	-6	10	off	CoE	0.014	-0.004	0.033	0.322
-6	30	off	CoE	-6	30	on	CoE	0.014	-0.005	0.033	0.362
-6	30	on	CoE	6	10	on	CoE	0.014	-0.005	0.032	0.370
-6	30	on	CoE	6	10	off	CoE	0.014	-0.005	0.032	0.401
-6	30	on	CoE	6	30	off	CoE	0.012	-0.006	0.031	0.568
6	30	on	CoE	0	0	off	BL2	0.012	-0.007	0.031	0.628
-6	30	on	CoE	6	30	on	CoE	0.012	-0.008	0.031	0.742
6	30	off	CoE	0	0	off	BL2	0.011	-0.007	0.029	0.669
6	10	off	CoE	0	0	off	BL2	0.010	-0.008	0.028	0.782
6	10	on	CoE	0	0	off	BL2	0.010	-0.008	0.028	0.792
-6	10	off	CoE	0	0	off	BL2	0.010	-0.008	0.027	0.839
0	30	off	CoE	0	0	off	BL2	0.009	-0.009	0.027	0.877

Table B.3. (cont. from last page)

Level 1 (L1)				Level 2 (L2)							
Δf_m	A_m	Met.	Exp. Type	Δf_m	A_m	Met.	Exp. Type	L1-L2	Lower CL	Upper CL	p
-6	10	on	CoE	0	0	off	BL2	0.009	-0.009	0.027	0.891
0	10	off	CoE	-6	10	on	CoE	0.007	-0.010	0.025	0.960
-6	30	on	CoE	0	10	off	CoE	0.007	-0.011	0.026	0.978
0	10	off	CoE	0	30	off	CoE	0.007	-0.010	0.025	0.972
0	10	off	CoE	-6	10	off	CoE	0.007	-0.011	0.024	0.981
0	10	off	CoE	6	10	on	CoE	0.006	-0.011	0.024	0.989
0	10	off	CoE	6	10	off	CoE	0.006	-0.011	0.024	0.992
0	10	off	CoE	6	30	off	CoE	0.005	-0.013	0.023	0.999
0	10	off	CoE	6	30	on	CoE	0.004	-0.015	0.023	1.000
6	30	on	CoE	-6	10	on	CoE	0.003	-0.015	0.022	1.000
6	30	on	CoE	0	30	off	CoE	0.003	-0.016	0.022	1.000
6	30	on	CoE	-6	10	off	CoE	0.003	-0.016	0.021	1.000
6	30	off	CoE	-6	10	on	CoE	0.002	-0.015	0.020	1.000
6	30	on	CoE	6	10	on	CoE	0.002	-0.016	0.021	1.000
6	30	off	CoE	0	30	off	CoE	0.002	-0.015	0.020	1.000
6	30	on	CoE	6	10	off	CoE	0.002	-0.017	0.021	1.000
6	30	off	CoE	-6	10	off	CoE	0.002	-0.016	0.019	1.000
6	30	off	CoE	6	10	on	CoE	0.001	-0.016	0.019	1.000
6	10	off	CoE	-6	10	on	CoE	0.001	-0.016	0.018	1.000
6	30	off	CoE	6	10	off	CoE	0.001	-0.017	0.019	1.000
6	10	on	CoE	-6	10	on	CoE	0.001	-0.016	0.018	1.000
6	10	off	CoE	0	30	off	CoE	0.001	-0.016	0.018	1.000
6	30	on	CoE	6	30	off	CoE	0.001	-0.018	0.020	1.000
6	10	on	CoE	0	30	off	CoE	0.001	-0.016	0.018	1.000
-6	10	off	CoE	-6	10	on	CoE	0.001	-0.016	0.018	1.000
6	10	off	CoE	-6	10	off	CoE	0.001	-0.017	0.018	1.000
6	10	on	CoE	-6	10	off	CoE	0.000	-0.017	0.018	1.000
-6	10	off	CoE	0	30	off	CoE	0.000	-0.017	0.018	1.000
0	30	off	CoE	-6	10	on	CoE	0.000	-0.017	0.017	1.000
6	10	off	CoE	6	10	on	CoE	0.000	-0.017	0.017	1.000

This table summarizes the results of Tukey's HSD test for data in Experiment 1 (Chapter 5). Each row indicates significance of the difference between least squares means associated with trial conditions in Level 1 (L1) and Level 2 (L2). There are three levels of motor frequency ($\Delta f_m = 0, \pm 6\%$), two levels of oscillation amplitude ($A_m = 10,\ 30\%\ body\ weight$), two experimental phases where the subject is either allowed to freely entrain to the oscillations (i.e. Met. = off; $0 < time < 300\ s$) or is instructed to follow the metronome (i.e. Met. = on; $300 < time < 600\ s$), and three experiment types: baseline trial 1 (BL1: the subject walks freely on the treadmill with the harness off), baseline trial 2 (BL2: the subject walks freely on the treadmill with the harness on), and a typical trial (CoE, where the subject interacts with the system at constant frequency and constant amplitude). All confidence limits (CL) are set at 95% and p values are marked with an asterisk to indicate significance after controlling for multiple testing.

B.3.3 Model Results from Experiment 2

Table B.4. Statistics model results from the Sensitivity to Entrainment test in Chapter 5

Model Description	Dependent Variable	Independent Variables	β	Lower CL	Upper CL	*p*
1.) Sensitivity to Entrainment	A_m^*	Intercept	0.010	-0.064	0.085	0.783
		$\|\Delta f_m\|$	1.754	0.573	2.935	0.005*
		$sgn(\Delta f_m)$	0.061	0.019	0.104	0.006*
		$\|\Delta f_m\| \; x \; sgn(\Delta f_m)$	0.284	-1.415	1.983	0.736

This table summarizes the linear mixed model used for analysis in Experiment 2: Sensitivity to Entrainment (Chapter 5). Model 1.) indicates how trial conditions affect the amplitude where initial entrainment occurs. $|\Delta f_m|$ is the distance between the normalized motor frequency and preferred step frequency (expressed as a decimal, not a percentage), and $sgn(\Delta f_m)$ uses the signum function to indicate whether the motor frequency is higher or lower than preferred step frequency. All confidence limits (CL) are set at 95% and p values are indicated significant with an asterisk after correcting for multiple comparisons.

B.3.4 Model Results from Experiment 3

Table B.5. Statistics model results from the Limits of Entrainment test in Chapter 5

Mode Description	Dependent Variable	Independent Variables	β	Lower CL	Upper CL	*p*
1.) Limits to Entrainment	$\|\Delta f_m^*\|$	Intercept	0.054	0.032	0.076	<0.001*
		A_m	0.128	0.052	0.203	0.001*
		$sgn(\Delta f_m)$	-0.024	-0.032	-0.015	<0.001*
		Hysteresis	0.000	-0.006	0.006	0.914
		$A_m \; x \; sgn(\Delta f_m)$	0.065	-0.041	0.171	0.228
		$A_m \; x$ Hysteresis	0.013	-0.041	0.066	0.642
		$sgn(\Delta f_m) \; x$ Hysteresis	-0.002	-0.011	0.007	0.649

This table summarizes the linear mixed model used for analysis in Experiment 3: Limits to Entrainment (Chapter 5). Model 1.) indicates how trial conditions affect the motor frequency where subjects first abandon entrainment. A_m is the oscillation amplitude (expressed as a decimal, not a percentage), $sgn(\Delta f_m)$ uses the signum function to indicate whether the motor frequency drifts higher or lower than preferred step frequency and Hysteresis tests whether there is an effect on the limit of entrainment when it is measured as the motor frequency drifts away from preferred or returns to preferred. All confidence limits (CL) are set at 95% and p values are indicated significant with an asterisk after correcting for multiple comparisons.

Appendix C (copyright permissions)

The following are letters and/or policies indicating permission to use publication content in this thesis. Additionally, the following coauthors have given explicit consent to use publication content in this thesis: John E.A. Bertram, James L. Croft, Giang D. Ngo and Van Son Nguyen.

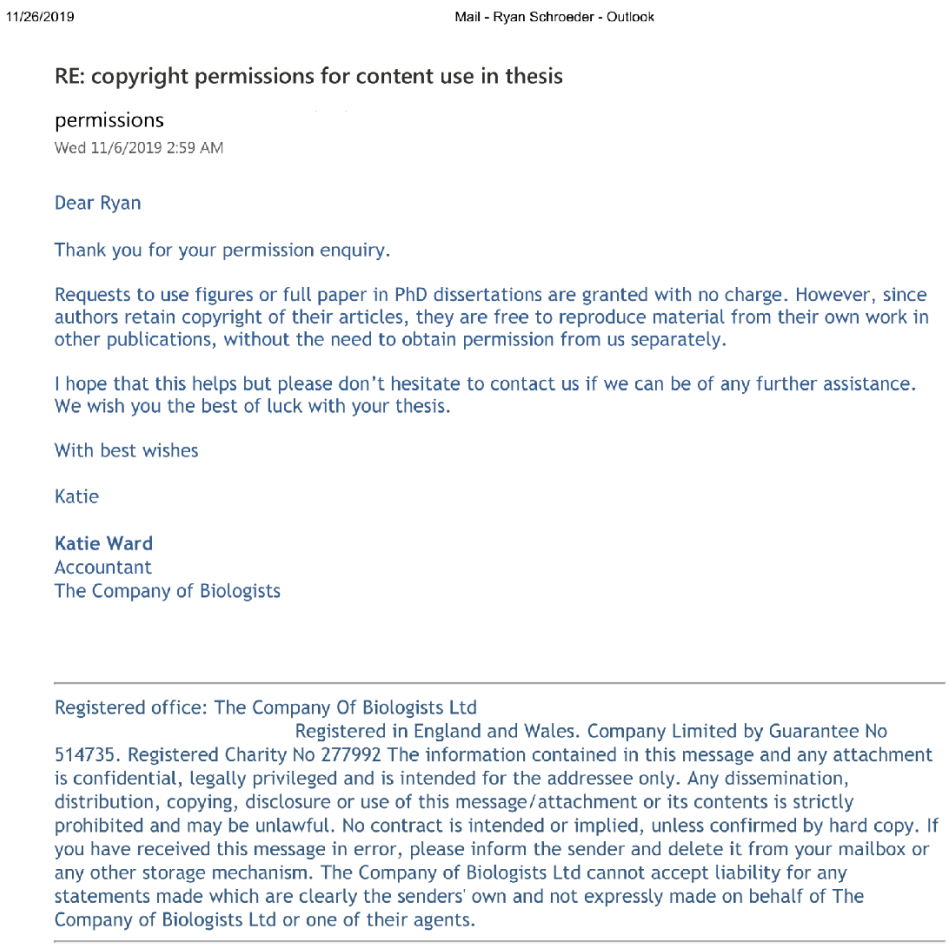

11/26/2019 Mail - Ryan Schroeder - Outlook

RE: copyright permissions for content use in thesis

permissions
Wed 11/6/2019 2:59 AM

Dear Ryan

Thank you for your permission enquiry.

Requests to use figures or full paper in PhD dissertations are granted with no charge. However, since authors retain copyright of their articles, they are free to reproduce material from their own work in other publications, without the need to obtain permission from us separately.

I hope that this helps but please don't hesitate to contact us if we can be of any further assistance. We wish you the best of luck with your thesis.

With best wishes

Katie

Katie Ward
Accountant
The Company of Biologists

Registered office: The Company Of Biologists Ltd
Registered in England and Wales. Company Limited by Guarantee No 514735. Registered Charity No 277992 The information contained in this message and any attachment is confidential, legally privileged and is intended for the addressee only. Any dissemination, distribution, copying, disclosure or use of this message/attachment or its contents is strictly prohibited and may be unlawful. No contract is intended or implied, unless confirmed by hard copy. If you have received this message in error, please inform the sender and delete it from your mailbox or any other storage mechanism. The Company of Biologists Ltd cannot accept liability for any statements made which are clearly the senders' own and not expressly made on behalf of The Company of Biologists Ltd or one of their agents.

Frontiers Copyright Statement

All content included on Frontiers websites (including Loop), such as text, graphics, logos, button icons, images, video/audio clips, downloads, data compilations and software, is the property of Frontiers if created by Frontiers, or of the person or entity who or which owned it prior to submission to Frontiers. If not owned by Frontiers, it is licensed to Frontiers Media SA (Frontiers) or its licensees and/or subcontractors.

The copyright in the text of individual articles (including research articles, opinion articles, book reviews, conference proceedings and abstracts) is not the property of Frontiers, and its ownership is not affected by its submission to or publication by Frontiers. Frontiers benefits from a general licence over all content submitted to it, and both Frontiers and its users benefit from a Creative Commons CC-BY licence over all content, as specified below.

Images and graphics not forming part of user-contributed materials are the property of or are licensed to Frontiers may not be downloaded or copied without Frontiers' explicit and specific permission or in accordance with any specific copyright notice attached to that material.

The combination of all content on Frontiers websites, as well as the design and the look and feel of the Frontiers websites, and the copyright and all other rights in such content and combination, are the sole property of Frontiers.

As an author or contributor you grant permission to others to reproduce your articles, **including any graphics and third-party materials supplied by you**, in accordance with the Frontiers Terms and Conditions. The licence granted to third parties over all contents of each article, **including third-party elements**, is a Creative Commons Attribution ("CC BY") licence. The current version is CC-BY, version 4.0, and the licence will automatically be updated as and when updated by the Creative Commons organisation.

You may include a requirement to reproduce copyright notices in materials contributed by you, but you may not restrict the right to reproduce the entire article, including third-party graphics. This means that you must obtain any necessary third-party consents and permissions to reproduce third-party materials in your articles submitted to Frontiers.

E-books are subject to the same licensing conditions as the articles within them.

Articles published prior to the effective date of this notice: Please note that reproduction of third-party graphics and other third-party materials contained in articles published prior to the effective date of this notice may be subject to third-party notices prohibiting their reproduction without permission. You must comply with those notices.

Articles published prior to July 2012: The licence granted for these articles may be different and you should check the pdf version of any article to establish what licence was granted. If an article, dating from before July 2012, carries only a non-commercial licence and you wish to obtain a commercial licence, please contact Frontiers at **editorial.office@frontiersin.org**.

All software used on this website, and the copyright in the code constituting such software, is the property of or is licensed to Frontiers and its use is restricted in accordance with the **Frontiers Terms and Conditions**. All copyright, and all rights therein, are protected by national and international copyright laws.

This Copyright Statement comes into effect on **25th May, 2018**.

License